REPORT DOCUMENTATION PAGE

Form Approved OMB No. 0704-0188

1. REPORT DATE *(DD-MM-YYYY)*	2. REPORT TYPE	3. DATES COVERED *(From – To)*
20-10-2003	Conference Proceedings	15 July 2002 - 18 July 2002

4. TITLE AND SUBTITLE

Thermochemical Processes in Plasma Aerodynamics

5a. CONTRACT NUMBER
F61775-02-WF060

5b. GRANT NUMBER

5c. PROGRAM ELEMENT NUMBER

6. AUTHOR(S)

Conference Committee

5d. PROJECT NUMBER

5d. TASK NUMBER

5e. WORK UNIT NUMBER

7. PERFORMING ORGANIZATION NAME(S) AND ADDRESS(ES)

Leninetz Holding Company, NIPGS
212, Moskovsky Prospekt
St. Petersburg 196066
Russia

8. PERFORMING ORGANIZATION REPORT NUMBER

N/A

9. SPONSORING/MONITORING AGENCY NAME(S) AND ADDRESS(ES)

EOARD
PSC 802 BOX 14
FPO 09499-0014

10. SPONSOR/MONITOR'S ACRONYM(S)

11. SPONSOR/MONITOR'S REPORT NUMBER(S)
CSP 02-5060

12. DISTRIBUTION/AVAILABILITY STATEMENT

Approved for public release; distribution is unlimited.

20040920 082

13. SUPPLEMENTARY NOTES

14. ABSTRACT

The Final Proceedings for Thermochemical Processes in Plasma Aerodynamics, 15 July 2002 - 18 July 2002

This is an interdisciplinary conference. Topics to be covered include 1) Active thermal protection on the basis of endothermic reactions; 2) The problem of catalysis at the conversion of hydrocarbon fuel; 3) Burning of a modified hydrocarbon fuel; 4) Non-equilibrium kinetics with hydrocarbon components participation; 5) Plasma aerodynamics of flows.

15. SUBJECT TERMS

EOARD, Magnetohydrodynamic (MHD), Combustion, Plasma Aerodynamic

16. SECURITY CLASSIFICATION OF:			17. LIMITATION OF ABSTRACT	18. NUMBER OF PAGES	19a. NAME OF RESPONSIBLE PERSON
a. REPORT	b. ABSTRACT	c. THIS PAGE			WAYNE A. DONALDSON
UNCLAS	UNCLAS	UNCLAS	UL		19b. TELEPHONE NUMBER *(Include area code)* +44 (0)20 7514 4299

Holding company "LENINETZ"

International workshop

Thermochemical and plasma processes in aerodynamics

Saint-Petersburg
15 – 19 July, 2002

Holding company "LENINETZ"
212 Moskovsky pr., St. Petersburg, 196066, Russia

Organized:
Holding company "LENINETZ"
In co-operation and sponsorship by:
HSRI
AFOSR
EOARD
JLHT SPSU and HC "LENINETZ"

CONTENTS

CATALYTIC TECHNOLOGIES IN NEW AREAS OF ENGINEERING.

A. L. Kuranov, A. V. Korabelnikov, B. V. Formakovskiy, T. S. Vinogradova***

**Hypersonic Systems Research Institute*
"Leninetz" Holding Company
Moskovskiy pr., 212, Saint-Petersburg, Russia
*** Central Scientific and Research Institute of constructional materials "Prometey"*
Shpalernaya Str., 49, Saint-Petersburg, Russia

It is known the role of catalyst in the development of chemical and oil-refining industry. At the present time about 80% of all chemical production is being made with the help of this method.[1]. Catalysts allow one to intensify chemical processes due to the change of the reaction rate, direct them towards the formation of certain desirable product. In this case catalysts are practically not expended.

The application of catalysis is constantly being spread including such areas as missile and airspace technique, energetics and ecology. For example, it is well known catalytic decomposition of hydrazine as an energy source for missile technique [2]:

$$3N2H4=4(1-x)NH4+(1+2x)N2+6xH2, \quad (1)$$

where x - is degree of ammonia decomposition ($0 \leq x \leq 1$). The required degree of ammonia decomposition in catalytic reactor is defined by its purpose and reached by application of certain catalyst. The activity of metal catalysts in this reaction changes in the following consequence: Ir>Ru>Rh>Ni> ...>Pt>Pd. On the base of hydrazine the various types of micro-engines and gas generators are developed, which are used in control systems and as board energy sources on unmanned and manned space vehicles.

Now the projects of hypersonic hydrocarbon-fuelled flight vehicles are being developed very intensively [3-7]. "Ajax" project is the most energy integral one. The various approaches are organically connected in this conception: the first – utilization of heat losses and transformation on its basis of hydrocarbon fuel into the most energy qualitative fuel; the second-control of ionized air flow in the engine in order to increase its thrust-economic performances and transform a part of air kinetic energy into electric one; and at last, energetic influence on the ram airflow with the purpose of improving aerodynamic characteristics of the flying vehicle.

Endothermic processes of hydrocarbon fuel conversion can be divided into thermal and catalytic one. Thermal processes (cracking, pyrolysis) can be realized easier than the catalytic ones. But they are exceeded on a number of important characteristics by catalytic processes. Application of catalysis allows one to control rate and depth of reaction, that influences greatly on the reaction heat, composition of products and finally on density of absorbed heat flux and the qualitative composition of new fuel. Among the existing catalytic reactions hydrocarbon steam reforming has been considered by us in a wide range of temperature (300 –900C):

$$aCnHm+bH2O \rightarrow \{H2, CH4, CO, CO2\} \quad (2)$$

Activity of catalysts in steam reforming is decreasing in the following line: Pt>Pd>Ni>Co>... This reaction exceeds in several times non-catalytic thermal processes of hydrocarbon decomposition by its thermal effect, rate and quantity of

obtained hydrogen. This reaction is the candidate to be conducted onboard of flying vehicle. In fig.1 the element of heat-protection of this vehicle is shown. The developed system of chemical heat regeneration and fuel conversion and its basic elements in the form of catalytic thermochemical reactors allows one to create active heat protection (heat flux $q \approx 1MW/m^2$ and to increase cooling resource of initial hydrocarbon fuel to 5-10 MJ/kg.

If on hypersonic flying vehicle as a heat source to conduct an endothermic reaction serves an aerodynamic heating and heat of power installation, but for stationary and transport gas turbines of various purposes as a heat source serves a heat of exhausted gases. In fig. 2 the scheme of the gas turbine with steam injection and chemical regeneration of heat on the base of steam reforming of methane is shown.

$$CH_4 + H_2O \leftrightarrow 3H_2 + CO \qquad (3)$$

Additional heat absorption can be obtained by utilization of heat which is leaving through the walls of combustion chamber. The application of chemical regeneration of heat allows one to increase efficiency of the turbines by 15-20% and decrease a cost of power energy in the case of using them at the electric power station.

The inexhaustible sources of the prime energy such as a nuclear power and the sun energy have also undoubted interest [8]. Direct use of these kinds of energy is difficult, but they should be transformed to the convenient form for consumers. One of the ways of such transformation is use of reversible catalytic chemical processes as the reaction (3). In [9,10] chemothermal method of conversion, accumulation and energy transformation at the distance known under the name of catalytic technology EVA-ADAM is described (fig. 3). It is based on the sequential realization of endothermic reaction of steam methane reforming in the place of energy production, heat transportation by the cool energy carrier in the chemical bounded condition and the reverse exothermal reaction of hydrogenation of carbon oxides to methane in the place of energy consumption. Instead of the nuclear reactor in fig. 3 the heat source can be represented by the concentrator of sun energy.

Optimisation of fuel combustion processes and decreasing of atmosphere pollution by the harmful substance have such importance as the utilization of heat and the use of nontraditional energy source. Catalyst can help here. Catalytic combustion differs principally from combustion in the traditional understanding since fuel oxidizes on the surface of solid catalysts without flame formation [1]. It is classified low-temperature catalytic combustion (300-700°C) and high-temperature catalytic combustion (900-1300°C). Low-temperature catalytic combustion is applied in catalytic heat generators to heat the industrial area and the houses, transport vehicles as well as to combust harmful organic compounds in exhausted gases of chemical industry. High-temperature catalytic combustion is considered as perspective method for application in combustion chamber of gas turbines (fig. 4). Catalytic combustion allows one to increase completeness of combustion of hydrocarbon fuel excluding formation of CO and carcinogenic hydrocarbon. Reduction of combustion temperature allows one to decrease many times the release of NOx . At t<800°C Pt and Pd are used as a catalyst on aluminium oxide. For high-temperature combustion perovskites as ABO_3, where A=(La, Nd, Sm), B=(Al, Co, Cr) are being studied.

Catalysis has also obtained a wide spreading to solve other energy problems. The catalytic properties of electrodes have the main importance in the creation of fuel cells. At the present time high-temperature fuel cells on the solid oxide electrolytes which are working at t=850 –1000°C are considered as the most perspective ones.

These types of fuel cells allow one to use usual natural kinds of fuel such as natural gas, gasoline and etc. They can work at the regime of joint production not only of electricity but also of some valuable chemical products [8].

The brief review of conditions of catalyst application in a various areas of technique shows that industrial catalysts do not meet the severe requirements of the exploitation in new conditions. The necessity of search and study of new high-temperature catalysts and carriers having the developed specific surface, strength, heat resistance, capability of keeping these characteristics under the unfavourable conditions of chemical, thermal and mechanic influence is appeared. The development of scientific principles of catalyst preparation helps to apply new methods of purposeful synthesis of active structures, the regulation of porous structures and the distribution of an active component as well as to develop mathematical models of technological operations. The development of the technology of gradient functional catalytic coating with the established chemical compound and structure is the example of this catalyst design. Such technology allows one to create constructions of thermal catalytic devices with low hydraulic resistance, increased mechanical strength and improved exploitation characteristics.

The essence of this technology consists in sequential covering a metal substrate with layers of materials having different properties and performing different functions. In this case the methods of plasma, magnetron and ion-plasma spraying are used. Development of complex oxide catalytic systems, the active part of which consists of oxygen-containing compounds of two or more elements, could be considered as example of application of this technology. Such complex oxide systems are very active in reactions of catalytic combustion of the fuel. Considering the process of catalytic combustion of the fuel, the specific attention should be paid to thermal stability of transition metals oxides (Table).

Table

Maximum values of thermal stability for some oxides

Oxide	Maximum temperature, ° C
Co_3O_4	900-950
CoO	1795
ThO_2	2800
CeO_2	2500
Cr_2O_3	2266
Al_2O_3	2050
Fe_3O_4	1594
Mn_3O_4	1564
MnO	1785

In the course of research the most perspective modifying additives have been discovered which could slow down the speed of phase conversion of aluminum oxide. First of all the rare-earth metals oxides (La, Ce, Nd) are considered as such kind of compounds. It is known that stabilization of transition forms of the aluminum oxide is possible up to T=1200 °C.

There is a range of activity of catalytic materials, the maximum corresponding to the metals of platinum group – Pt, Pd having activity exceeding activities of other oxides by two orders of magnitude. As well, the most active oxides of transition metals are the following: Co_3O_4, MnO_2, CuO and Cr_2O_3.

In order to create a gradient-functional porous catalytic material taking into consideration the composition of used catalysts, the following systems are the most reasonable to be used for plasma spraying: for adhesive layer – Al, Ni/Al_2O_3 system, for intermediate layer – $Al_2O_3/CeO_2/La_2O_3$ system, for catalytic layer – $Al_2O_3/CuO/Cr_2O_3$; $Al_2O_3/CuO/MnO_2$; Al_2O_3/Co_3O_4 systems.

The initial powder materials have been analyzed in order to perform preliminary selection of the main components of porous oxide composition. The phase, chemical and granulometric composition and physical-and-mechanical properties of transition and rare-earth metals powder have been determined including bulk density, humidity, as well as mixing quality control and determination of optimal rate at dosage of powder materials.

Influence of added rare-earth elements oxides of the transition metals on coating structure in the range of concentration of stabilizing element from 0,01 to 2% in the form of oxide under plasma spraying conditions has been studied. Possibility of stabilization of the aluminum gamma oxide up to 950° C is confirmed.

Composition of modified powders in order to obtain catalytically active materials of the system by the plasma spraying method has been developed as following:

- for adhesive layer the summary contain of Al, Ni is from 1 to 5%;
- for intermediate layer the summary contain of CeO_2, La_2O_3, NdO is up to 2%;
- for catalytic layer the summary contain of CuO, Cr_2O3; CuO, MnO_2; $Al2O_3$, Co_3O_4 is from 2 to 10%.

Technology of high-speed plasma spraying of catalytic carrier on a metal substrate is well in line with the modern methods of activator applying such as magnetron and ion-plasma methods as well as various methods of reactive impregnation that allows one to obtain high-active micro-crystal and amorphous materials.

In order to obtain a catalytic material combination of the following methods is the most reasonable:

- plasma spraying in inert and oxidized medium;
- ion-plasma or magnetron spraying;
- chemical applying of activator.

Technology of plasma spraying allows the following:

- to create durable adhesive layer;
- to conduct stabilization of low-temperature aluminum oxide;
- to provide high porosity of secondary carrier;

- to provide introduction of catalytically active transition metals oxides as well as a catalytic activity of the material.

Technology of evaporative condensation including ion-plasma and magnetron spraying has a specific feature such as , the first, use of the cathode system that makes possible to have stekhiometric composition of coating , and , the second, use of the focusing system and deflection of heterophase flow that eliminates formation of dropping phase.

Technology of ion-plasma and magnetron spraying allows the following:

- to create amorphous and micro-crystal structure of coating;
- to make the sequent applying of activators, increasing considerably a catalytic activity of material in comparison with a carrier;
- to apply coating of 2-5 μm thickness, not decreasing dynamic characteristics of material.

Technology of chemical applying of activator allows the following:

- to increase considerably concentration of active components;
- to apply on a catalytic material, if necessary, compounds which are not economically to use at other methods of applying;
- to decrease considerably consumption of activators.

To prepare a catalytic material on the base of thermally stable oxide compositions the following sequence of technological procedures have been developed (fig. 5):

- preparation of initial materials including chemical and ultra-sound treatment of the surface of metal carrier; grinding by means of disintegration equipment, drying and dissemination of initial powdered materials; mechanical-and-chemical synthesis of the catalytically active oxide powdered composition on the base of transition and rare-earth metals;
- high-speed plasma spraying of powdered composition on the metal carrier;
- activation (magnetron or ion-plasma spraying or chemical impregnation) of the surface of catalitically active composition;
- formation of catalytic element including profiling of catalytically active material, assembly and thermal treatment.

The considered technology of applying of the gradient-functional catalytic coatings could be used as well for a steam conversion of fuel in systems of heat utilization and obtaining of hydrogen.

In conclusion, it is useful to mark that a brief review of catalysis application means that new catalytic technologies have a great practical potential. Obviously, they shall be applied intensively in the nearest future in transport power plants of ground, sea and air basing, as well as in power devices intended for conversion and accumulation of nuclear and sun energy.

References

1. Г. К. Боресков. Гетерогенный катализ – М.: Наука, 1988.
2. Т. П. Гайдей, В. Н. Новгородов, И. Я. Тюряев. Каталитическое разложение гидрозина как источник энергии. ЖПХ, 1997, т .70 вып. 7.
3. D. H. Petley. Thermal management for Mach 5 cruise aircraft using endothermic fuel. AAIA 90-284-CP
4. R. M. Zubrin. The methane-acetylene cycle aerospace plane: a promising candidate for Earth to orbit transportation. AAIA 92-0688
5. A. Korabelnikov, A. Kuranov, Thermochemical conversion of hydrocarbon fuel under the concept "AJAX", AIAA-99-4921
6. A. Siebenhaar, F. F. Chen, M. Karpuk et al. "Engineering scale titanium endothermic fuel reactor for hypersonic scramjet engine" AIAA 99-4909
7. Ю. М. Шихман, В. Е. Шлякотин и др. Исследования высокоскоростных и высокотемпературных ВРД, использующих топлива повышенного хладоресурса. Фундаментальные и прикладные проблемы космонавтики., №4, 2000г.
8. Chemistry for the Energy Future. A. Bridgwater and D. O. Hall (Eds.), Oxford, 1999.
9. H. Fedders, R. Harth, B. Höhlein. Experiments for combining nuclear heat with methane steam reforming process. Nucl. Eng. and design. 1975. №34.
10. Э. К. Назаров, Н. А. Дубяга, Л. В. Семенова. Физико-химические основы процессов хемотермического метода передачи энергии на дальние расстояния. Атомно-водородная энергетика, 1986, вып. 7.

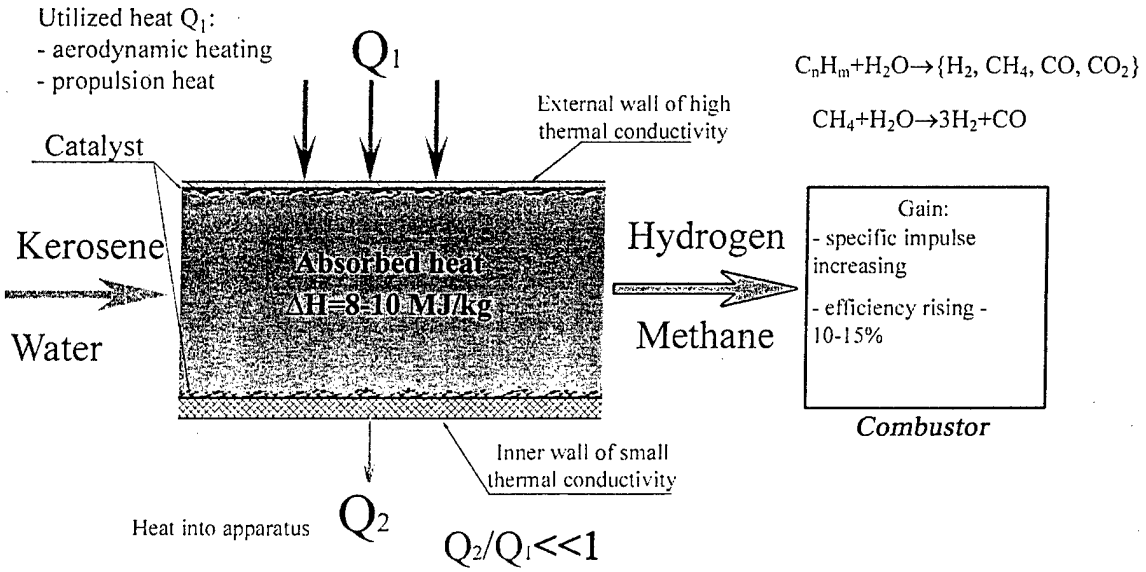

Fig. 1 Heat protection element – catalytic heat exchanger-reactor

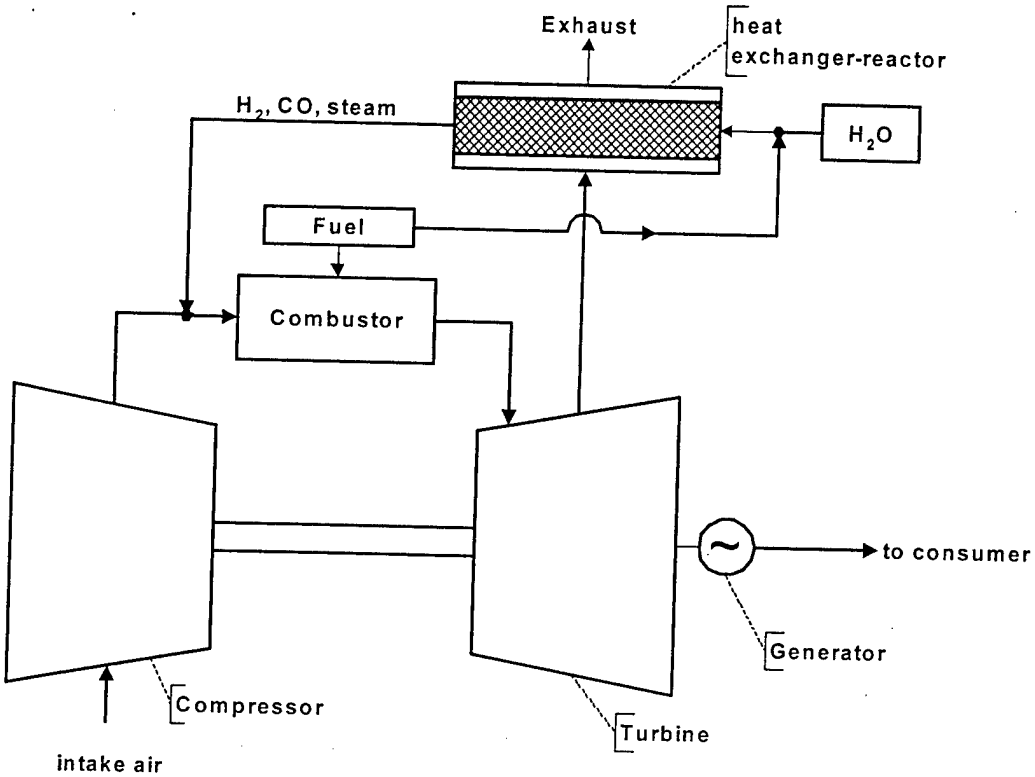

Fig. 2 Gas turbine with injected steam and chemical heat regeneration

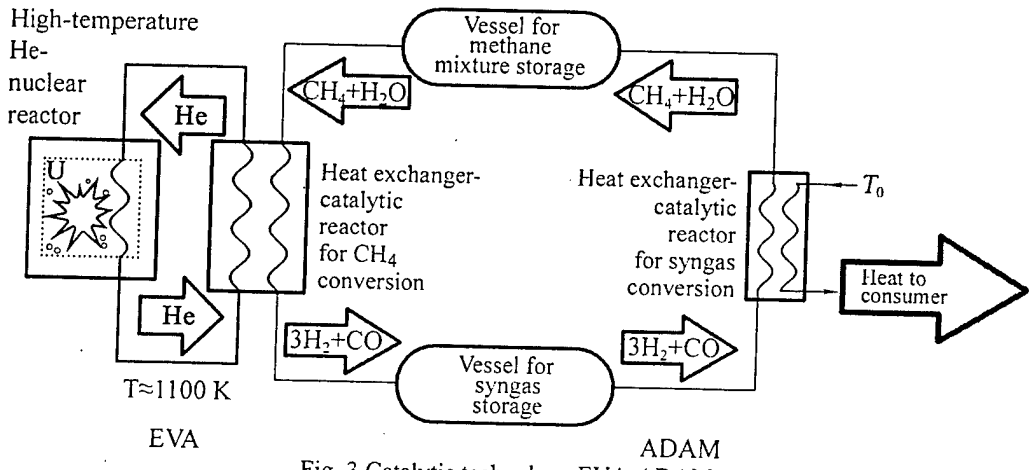

Fig. 3 Catalytic technology EVA-ADAM

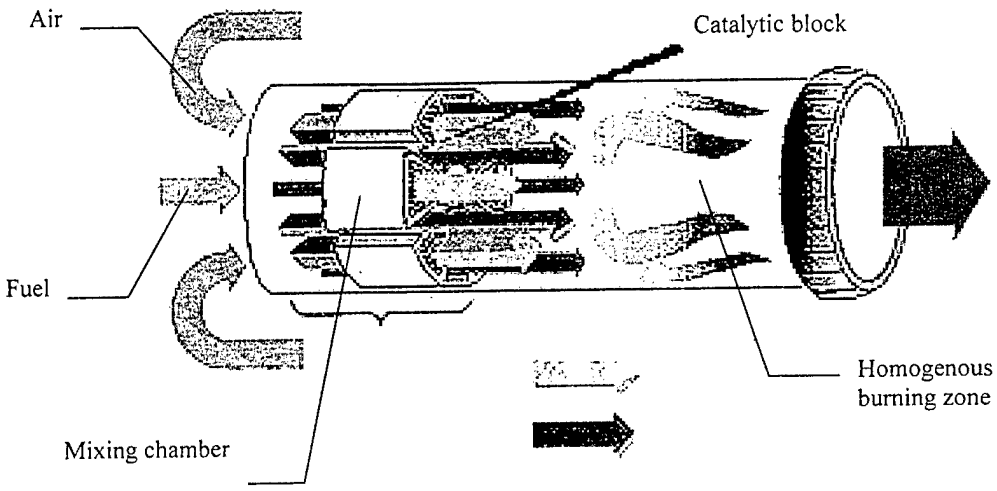

Fig. 4 Catalytic combustion chamber

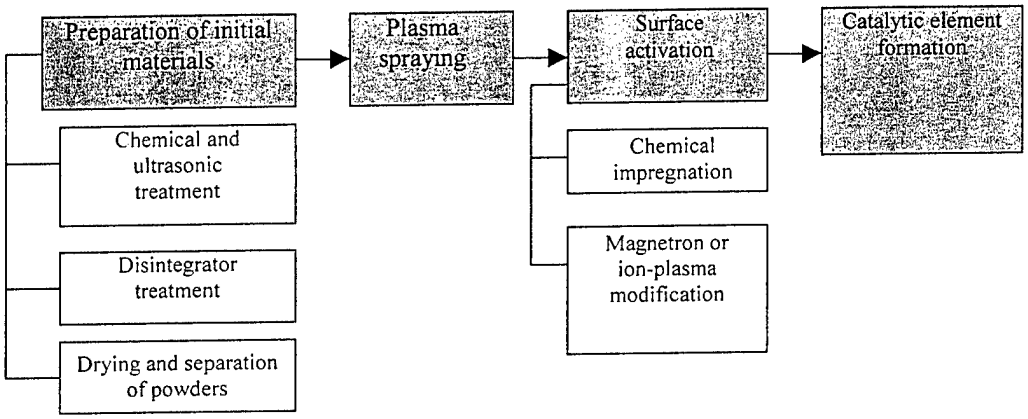

Fig. 5 Technological procedure of preparing catalytic material

PLASMA METHODS OF HIGH-SPEED AIR STREAM CONTROL AND FEATURE OF PLASMA FORMATIONS CREATION

Kuranov A.L., Kuchinsky V.V.*, Sukchomlinov V.S.***

This paper is devoted to the problems of aerodynamic characteristics control of the bodies at streamlining them by high-speed airflow by the creation of artificial plasma formations. We limit to the case of airflows. Low temperature plasma of gas discharge will be observed as a method of the influence. The more complete survey including laser methods of energy addition in flow is given in the paper [1]. The given report is continuation of work [1].

Research of low-temperature plasma influence of shock waves parameters in weakly ionized gas were carried out by the big number of authors [1-27]. The increase in shock speed, the expansion and the deformation of shock wave, intensity contractions are at the entrance in the region of low ionized gas the normal shock wave. The typical research result of shock wave propagation through plasma is submitted on fig. 1 and 2, taken of work [27].

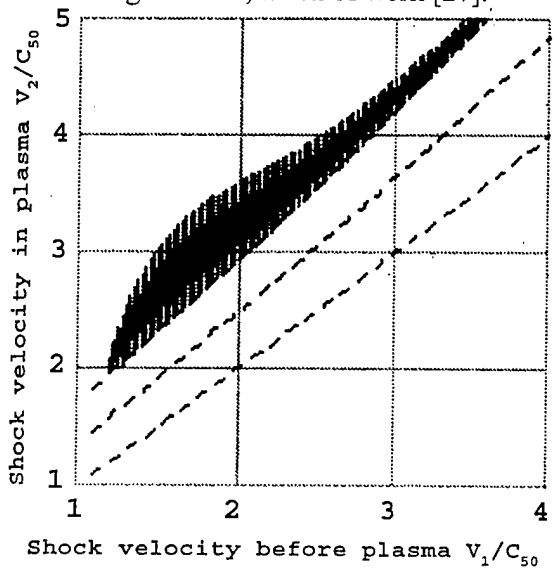

Fig.1.

The authors of work [2] used interference instrumentation to determine density distribution in shock front for some characteristic of the discharge. At the pressure more than 3 Torr and E/P=6-8 V/cm-Torr the shock wave increases its width in 10 times and takes the form of dual-frequency profile which components are called as precursor and residual wave. For the case with the discharge where the pressure doesn't exceed 3 Torr and E/P=20-40 V/cm- Torr, the three wave system appears at which leader adds to precursor.

In works [3] microwave interferometer is used to measure electron concentration in the region of distribution of normal shock wave in low ionized plasma, created by impulse discharge. It was shown that decomposition of electron density after turning of impulse matches to density decomposition due to dissociative recombination in some cases without shock wave. When shock wave distributes through the discharge after impulse the distribution of electron density changes and is accompanied by sharp increasing concentration of electrons in shock wave front.

In works [4-5] the measurements of photo refraction are used to show that speed of precursor is lower than residual wave that leads to expansion of shock profile at passage through discharge. When shock wave leaves the area of discharge the reconstruction of shock intensity is observed.

The measurement of shock wave in decomposed air plasma showed that anomalous dynamic qualities remain further than it was predicted by kinetics of

recombination. The first drew attention to this event the authors of the works [6]. They showed that anomalous dynamic qualities disappeared approximately at 0.020 s. The results of measurement of parameters of shock wave in a small shock tube with axled electric field are shown in work [7]. It is shown that observed modifications in characteristics of shock wave do not appear after plasma formation but only after enough time for plasma formation. The idea of the experiment is that discharge relaxation of low ionized plasma is faster at turning on discharge than temperature relaxation, which appeared due to plasma heating. If the change of parameters of shock wave determinate only by the action of heat mechanism so after turning on discharge and plasma decomposition the conserved heat leads to changing parameters, which are fixed during the discharge burning. These results are proving (on the experiment level) that the gradient temperature area on border plasma-neutral gas arises (because the plasma temperature increases due to heating volume of gas in the discharge) is the main factor in the modification of the parameters of the shock waves for research conditions when shock wave spread in the direction of electric field.

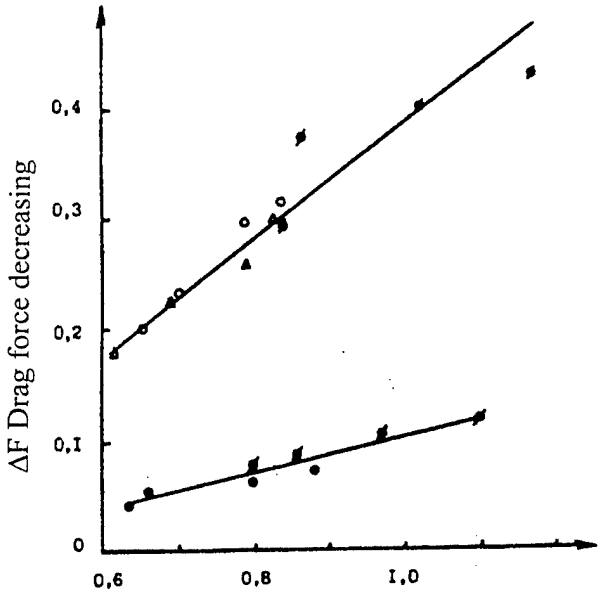

Fig.2.

The existent results of experimental and theoretical researches allow one to suggest the existent of two possible mechanisms of changing characteristics of shock wave at its distribution inside weakly ionized gas: a) the gradient temperature area on border plasma-neutral gas arises because the plasma temperature increases due to heating volume of gas in the discharge and b) local increasing electric field and ionization degree in shock wave that leads to local increasing energy power release.

In works [8] it is found that the distribution of shock wave in electrical field, which are transversely to the direction of shock movement, is conducted by the influence on parameters of the shock wave due to reinforcement of ionization in front of shock wave. These works are detailed analyzed in the paper (the our second paper here). These researches are conducted in the university of John Hopkins (the laboratory of the applied physics) with using shock tube with glow discharge.

Other important problem at which methods of a plasma flow is possible, is the problem of sound impact easing at transition through a sound barrier of passenger and transport heavy supersonic planes. Theoretical research of sonic boom is given in some works, including works [9 and 10]. Pressure that appears on the earth surface as a result of sonic boom can be described by the formula:

$$p - p_\infty = \frac{p_\infty K \gamma M_\infty^2 F(y)}{\sqrt{2\beta h}},$$

where p – static pressure near the earth surface, p - static pressure of surrounding plane environment, K – coefficient of signal reflection, γ –attitude of heat, M - Mach number (but $\beta = \sqrt{M_\infty^2 - 1}$), h – height of flight and $F(y)$ - function:

$$F(y) = \frac{1}{2\pi} \int_0^y \frac{d^2 A}{dx^2} \frac{dx}{\sqrt{y-x}},$$

where x gives the distance from the nose part, $A(x)$ is the section and y is permanent quantity on the characteristic surface.

There are several methods of increasing negative influence of sound impact on a ground surface. The first way (the most evident) is the change of the plane form. As it is shown in work [11] for the optimal dependence of the cut on distance of the nose of the plane $A(x)$ must be proportional to $x^{5/2}$. For the supersonic commercial plane (weight 272 т, Mach number 2.7, height of the flight 18 km) the required length of the plane [10, 12], at which we avoid of building shock wave at the earth surface is 305 m. By the international requirement the maximal length must not be more than 80m.

The second way is to model the plane of the most length due to energy addition in front of the nose of the plane. In work [11] it is shown, that power, which are necessary to obtain time of self-regulation 10 ms for supersonic commercial plane of the length 91.4 m and weight 272 t is 220 MW that is equal to 60% cruising speed of the plane. In works [13,14] the comparative research of this problem is conducted and obtained the greater importance of the required power. The plane flies in the flow of heated air that requires additional measures of heat defense. In work [15] the results of energy addition on the unit of the aerodynamic surface upstream the flow is analyzed. The optimal variants of the influence on wave resistance of power addition and quantities of energy heated the flow are determinated. These designs are conducted for the supersonic commercial plane of length 91.4 m and with the speed M=2.4. In this work significant drag reduction due to moving of the plane in heat wake behind the heat area are obtained. The estimation was given of increasing of useful power (30%) for elimination of the sonic boom.

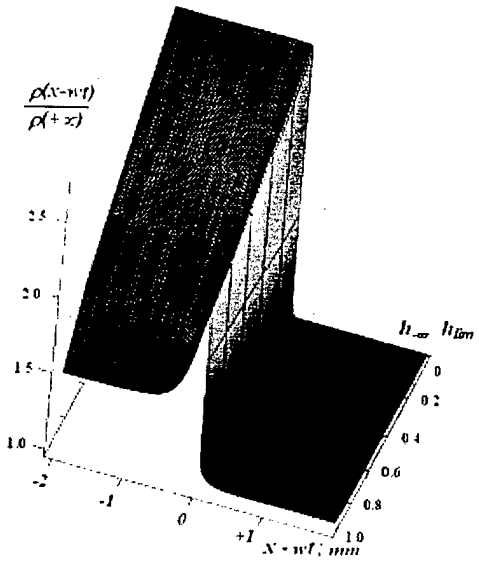

Fig. 3.

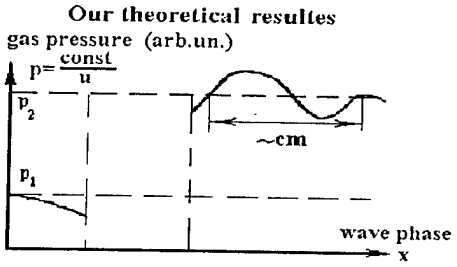

F.10.

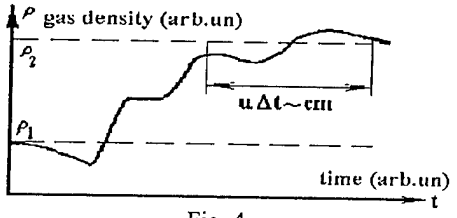

Fig. 4.

temperature peak and the way of the "temperature weak at which energy releases under the plane. In work [16] the concept of off-axes energy addition due to SHF radiation is suggested.

The results of considered above works on reduction of the negative influence of sonic boom can be summarized the next way. There are some problems to solve this problem including technical one and the practical realization without them impossible. It is necessary to optimize space distribution of input energy and the shape of flying vehicle glider (according to its missions). Besides, it is necessary to develop convenient and effective device for energy addition in airflow.

The problem of energy addition in the shock wave is divided into three basic tasks: research of physic mechanisms, which are leading to energy release near the shock front, determination of modification of a shock wave under energy influence; the analysis of the experimental methods and devices, which allow one to realize energy influence [1].

One of the possible mechanisms of appearance of the heat source initiating by shock and acoustic waves passing through plasma is suggested in works [6,7]. According to these works, sharp density enhancement as a result of plasma compression leads to the increase of electrostatic intensity and as a consequence, the rise of heat release. The appearance of the heat source near the shock front leads to a visible modification of a shock wave. The work [7] is devoted to this problem. In particular, this work shows the analytic expressions for the speed, the pressure and the temperature distribution, which are added up as a result of the heat source influence. In fig.3 the example of the design of modification of shock wave density at the various values of power, which is put in the center of shock front, is shown. In this figure the density quantity is normalized on its unperturbed value, energy contribution is normalized on a limit value (from the point of view of the existence of the one-dimensional stationary solution). It is seen the gradual increase of the specific pick in density distribution with increasing the energy contribution.

The display of the specific plasma effects is shown in the conducted experimental research due to influence of the heat mechanism. The influence of the dissipative plasma properties is analyzed in work [19]. In the fig.4 it is shown a qualitative type of shock structure, which is described by the asymptotic expressions, obtained from the solution of the equation of Kortveg-de Vris-Burgers [19]. The middle area fits to the values of the shock phase, where the obtained solutions are wrong. Here in the position data "density – the moment of density registration" density data, obtained by G.I. Mishin, Y.L.Serov and others on the ballistic route in "Physicotechnical Institute of A.F.Ioffe (PTI)". It is obviously, that on this graph a wave phase is proportionate to time on the experimental graph. It is shown, that both these figures are qualitative similar. Some differences are caused by that distribution function differs from Maxwell one in experimental plasma in PTI. Besides, it is considered during writing plasma equitation it is considered that charged particles disappear as a result of ambipolar diffusion, while in the experimental conditions in PTI recombination has the main part in destruction of all particles.

For the more detailed analysis of influence of special plasma properties it is necessary to define data of dissipation parameters in the specific plasma installations. In the present time many plasma installations are tested, with help of which the influence on the shock distribution and formation are realized. Discharge, which has no walls, intended for creating artificial plasma shell near the surface of the flying vehicle is studied in works [18.26]. Discharge (without walls) has some specific properties. Current density depends on an unique parameter, on pressure. The results

of the determination j for all experimental tested cases (various currencies, cathode forms, electrode positional relationship, anode material and etc.) are received. It is possible to consider that with the consideration of the mistake of the determination j all the points lay on the fluently growing dependence [18]:

$$j\left(\mathrm{mA/cm^2}\right) \approx \frac{5}{18} p^{\frac{3}{2}}(\mathrm{Torr})$$

The second important quantity, defined energy addition in gas due to plasma, is covered discharge length of the part cathode surface l, as time is proportionate to l. This quantity doesn't depend on the distance between electrodes, but it depends on air pressure (at the settled currency). The derivative dl/dt increases with reducing pressure. The dependence $l(t)$ changes with modification of the cathode geometric form. Therefore, it is possible to hope that the discharge of such type will have enough fastness and reliability in control that is one of the requirements showed to the onboard plasma generator.

The possibility of practical application of the considered methods is defined by their energy economy, but in a number of cases (e.g. in energy addition for improving conditions of passing over a sound barrier of the air liners such as the "Concorde" and " Tu-144") the requirement of energy economy must be inessential. But this requirement is the main for the basic region of the application of energy methods, for increasing aerodynamic characteristics of the flying vehicles (for reducing drag and increasing aerodynamic quality). In perspective energy methods of influence should be the basis for control of the hypersonic characteristics without inertia and in spite of all difficulties the alternative of these methods is impossible found seemingly.

References

1. Knight D., Kuchinsky V., Kuranov A., Sheikin E. "Aerodynamic Flow Control at High Speed Using Energy Addition. IVTAN, 2002.
2. Klimov, A. I. and Mishin, G. I., "Interferometric Studies of Shock Waves in a Gas Discharge Plasma," Sov. Tech. Phys. Lett., 16(12), Dec. 1990, pp. 960-962.
3. Gorshkov, V. A., Klimov, A. I., Mishin, G. I., Fedotov, A. B., and Yavor, I. P., "Behavior of Electron Density in a Weakly Ionized Nonequilibrium Plasma with Propagating Shock Wave," Sov. Phys. Tech. Phys., 21(10), Oct. 1987, pp. 1138-1141.
4. Ganguly, B. N. and Bletzinger, P., "Shock Wave Dispersion in Nonequilibrium Plasma," AIAA Paper 96-4607, Nov. 1996.
5. Ganguly, B. N. and Bletzinger, P., "Acoustic Shock Wave Propagation in Nonequilibrium Nitrogen and Argon Plasmas," Proceedings of the Workshop on Weakly Ionized gases, June 1997.
6. Klimov, A. I., Koblev, A. N, Mishin, et. al., Sov. Tech. Phys. Lett, 8, 240 (1982).
7. Ionikh, Y. Z., Chernysheva, N. V., Meshchanov, A. V., Yalin, A. P. and Miles, R. B., "Direct Evidence for Thermal Mechanism of Plasma Influence on Shock Wave Propagation," Physics Letters A, 259 (1999), pp. 387-392.
8. Van Wie D.M., Wesner A.L., Gauthier L.R. Shock Wave Characteristics Measured in Gas Discharges. Proceedings of the 3 Workshop on Weakly Ionized gases, AIAA-99-4824, Norfolk 1999
   Van Wie D.M., Gauthier L.R. Shock Propagation in a Weakly Ionized Gas With Transverse Electric Field. Works of II symposium 'Thermochemical processes in plasma aerodynamics. SPB, 2001.

9. G. Whitham. The Behavior of Supersonic Flow Past a Body of Revolution, Far From the Axis. Proceedings of the Royal Society, Series A, 201:89-109, 1950.
10. R. Seebass. Sonic Boom Theory. Journal of Aircraft, 6(3):177-184, May-June 1969.
11. S. Batdorf. On Alleviation of the Sonic Boom by Thermal Means. AIAA Paper No. 70-1323, 1970.
12. F. McLean. Configuration Design for Specific Pressure Signature Characteristics. In Second Conference on Sonic Boom Research, volume NASA SP 180, May 1968.
13. D. Miller and H. Carlson. On the Application of Heat or Force Field to the Sonic Boom Minimization Problem.
14. D. Miller and H. Carlson. A Study of the Application of Heat on Force Fields to the Sonic Boom Minimization Problem. Technical Report TN D-5582, NASA, December 1969.
15. F. Marconi. An Investigation of Tailored Upstream Heating for Sonic Boom and Drag Reduction. AIAA Paper No. 98-0333, 1998.
16. R. Miles, L. Martinelli, S. Macheret, M. Shneider, I. Girgis, S. Zaidi, D. Mansfield, M. Siclari, P. Smereczniak, R. Kashuba, and P. Vogel. Suppression of Sonic Boom by Dynamic Off-Body Energy Addition and Shape Optimization. AIAA Paper No. 2002-0150, 2002.
17. A.L.Kuranov, V.V.Kuchinskyi, V.Yu.Sepman, V.S.Sukhomlinov, Yu.Tolmachev, V.Borzov and A.Yuriev. Flow About Power Control for the AJAX Project. 2nd Weakly Ionized Gases Workshop Norfolk, VA. 1998
18. A.L.Kuranov, V.V.Kuchinsky, V.S.Sukhomlinov, V.Yu.Sepman and Yu.A.Tolmachev Influence of Dispersive Properties of Plasma on Acoustic Wave Propagation AIAA-99-3536, 30th Plasmadynamics and Lasers Conference Norfolk, VA, 1999.
19. V.Yu.Kolosov, V.Yu.Sepman, V.S.Sukhomlinov, Y.A.Tolmachev, A.L.Kuranov, V.V.Kuchinsky, V.A.Shaverev, M.V.Otugen Acoustic Dispersion Effect on the Propagation of a Shock Wave in a Glow Discharge Plasma 9th International Space Planes and Hypersonic Systems and Technologies Conference Norfolk, VA 1999, AIAA 99-4882
20. A. L. Kuranov, V.V. Kuchinskiy, V.S. Sukhomlinov The main features of distribution of shockwaves in nonuniform mediums created with the help discharge plasma. IVTAN, 2000. P. 25-28
21. A.L.Kuranov, V.V.Kuchinskyi, V.Yu.Sepman, V.S.Sukhomlinov, Yu.Tolmachev. Optimization of the Methods of Energy Impact on High Speed Flows/ Workshop «Perspectives of MHD and Plasma technologies in Aerospace Applications». Moscow. IVTAN, 1999. P. 137
22. V. Kuchinsky, V. Suhomlinov, V.Sheverov, and M. Otugen. Influence of Stationary Energy Cart in the Area of Density Jumping on Formation and Parameters of a Shock Wave Around a Body in a Low Temperature Plasma. In *Perceptivities of MHD and Plasma Technologies in Aerospace Application,* pages 307-312, Moscow, 2000. Institute of High Temperatures, Russian Academy of Sciences.
23. V.Y.Golyatin, A.L.Kuranov, V.V.Kuchinsky, V.S.Sukhomlinov, The Mechanism of Influence of Low-Temerature Plasma on Aerodynamic Streamlining. American Institute of Aeronautics and Astronautics, Norfolk, VA, 2001, AIAA-2001-3055
24. V. Kuchinsky and V. Suhomlinov. Optimization of the Methods of Energy Influence on High-Speed Flows and Distribution of Shock Waves in Weakly

Ionized Gas. In *Conference on Fundamental Research for Hypersonic Technologies,* pages 379-381, Moscow, 1998.

25. V.S.Sukhomlinov, V.Yu.Kolosov, V.A.Shaverev, M.V.Otugen. Formation and Propagation of a Weak Shock Wave in a Gas with Temperature Gradient., Norfolk, VA,1999, AIAA-99-4943
26. V. Ivanov and V. Suhomlinov. Plasma Generators of New Types. In Thermochemical Processes in Plasma Aerodynamics, pages 74-78, St. Petersburg, September 2001. Hypersonic System Research Institute, Leninitz Holding Company.
27. Esakov, 1.1., . Grachev, L. P., and Khodataev, K. V., "The Review of Plasmagasdynamic Experiment in Russia" 9th International Space Planes and Hypersonic Systems and Technologies Conference Norfolk, VA 1999, AIAA 99-4821.

ENTROPY & EXERGY METHODOLOGY WITH APPLICATION TO HIGH SPEED VEHICLE ANALYSIS & DESIGN

Charles F. Suchomel, David J. Moorhouse, Jose A. Camberos, Lt. Charlie Hoke

Air Force Research Laboratory, Wright-Patterson AFB, Ohio

Entropy & Exergy Methodology
With Application to High Speed Vehicle
Analysis & Design

Charles F. Suchomel
David J. Moorhouse
Jose A. Camberos
Lt. Charlie Hoke
Air Force Research Laboratory
Wright-Patterson AFB, Ohio

THERMOCHEMICAL PROCESSES IN
PLASMA AERODYNAMICS
16-19 July 2002 Workshop
St. Petersburg, Russia

Exergy Team

AFRL

- Dr. David Moorhouse - Acting Director; Air Vehicle Multidisciplinary Technology Center
- Mr. Charles Suchomel - Program Manager; Research Applications to Flight Systems, Aircraft Thermo-Economics of Energy Usage and Loss
- Dr. Jose Camberos & Lt. Charlie Hoke - CFD &CEM Sciences Center, Exergy - Optimization
- Dr. Richard Rivir - Propulsion Directorate

AFOSR: Sponsor - Dr. John Schmisseur
Exergy Theory, Entropy Generation Minimization, etc

ACADEMIA

- VPI, UM, VT, GT, ... (NIPGS, MIPT, ...)

Outline

- Background
- Vehicle System Design in Exergy Terms
- Exergy Consideration of a Hypersonic Inlet
- Preliminary Development of the MHD Equations, with Entropy Generation
- Future Work

Exergy–Based Design Methods

Develop exergy and thermo-economic methodologies to all aspects of aerospace vehicle design including integrated system of energy systems

Create a methodology to enable the development of revolutionary <u>and efficient</u> aerospace systems based on the second law of thermodynamics

Exergy-Based Design Methods

Energy Consideration is NOT New, BUT Aircraft Uses Have Been Implicit, Disconnected and Indirect

- Energy and Exergy Balance Methods Have Been Used for Ground Power Plants
- "Well Known" in Non-Aerospace Community
- Aerospace Use Studied Only at the Component Level

Explicit Use of Entropy & Exergy Principles:

- Adds a New Term to the Breguet Range Eq.
- Optimum Lift Distribution Is Non-Elliptical
- Synthesis of 1st and 2nd Law

Design Optimization Based on *Exergy* and the Second Law

This Thrust is Developing Design/Analysis Methods Based on 2nd Law:

- Mission Requirements in Work/Exergy Terms Flow Down to Components of an Energy System.
- Computation of Entropy Generation, Structure as an Energy System, etc,
- Each System/subsystem Can be Designed to System-Level Metrics

We Are Assuming This Approach Will Be Mandatory for Revolutionary Concepts

Such as a Plasma-Based Hypersonic Flight Vehicle

Why Entropy & Exergy Methods For Plasma Based Aircraft Design ???

Technology Challenges:

- Accurate prediction/design tools
- Plasma generation at reasonable energy levels
- Control of plasma fields
- Flight weight/small volume magnetic systems
- Integration of airframe & propulsion system
- Energy extraction/power distribution
- Energy conservation only
  - 1st Law Principles
- **Exergy/entropy for design & analysis of entire vehicle**
  - 2nd Law Principles

Exergy equals available work from an energy source

Maximum work potential of a system

Technology Payoffs:

- Economical high speed
- Significantly lower structure temp
- More efficient combustion
- Innovative control
- Extended aircraft range

Outline

- Background
- Vehicle System Design in Exergy Terms
- Exergy Consideration of a Hypersonic Inlet
- Preliminary Development of the MHD Equations, with Entropy Generation
- Future Work

System Level Exergy Methods

Define specific energy as total energy per unit weight: $E = h + \frac{1}{2g}V^2$

Then at each point in the mission:

$\frac{dw_c}{dt} = W_p \frac{dE}{dt} + P$ customer work, which is a requirement.

$\frac{dw_o}{dt} = W \frac{dE}{dt} + DV$ overhead work, which should be minimized !

And the system equation is that the Exergy of the fuel burned must equal the customer + overhead work done through the mission:

$$-\eta H \frac{dW}{dt} = \frac{dw_c}{dt} + \frac{dw_o}{dt}$$

H is energy content of the fuel/weight, η is overall efficiency, $dW/dt < 0$.

System Level Exergy Methods

The Trade-off for any general energy consuming device: e.g., MHD

$\frac{dw_{oM}}{dt} = W_M \frac{dE_w}{dt} + P_M$ is the increment in overhead work

The incremental system equation is:

$$\eta_M H \frac{dW_M}{dt} = \eta H \frac{dW}{dt} - \left[W_M \frac{dE_w}{dt} + P_M - T_M V \right]$$

The Improvement in System Efficiency and Thrust Produced Must Overcome the Additional Overhead Work of the MHD Devise Weight and Power Required

Aerospace Vehicle Design
Exergy as a System-Level Metric

Design Mission Stated in Terms of Work to be Done
How precise does this need to be ?

Comes From the Exergy of the Fuel Consumed

Propulsion System Converts Fuel Into:
Mission Work, Including Power to Drive Mission Equipment
+
Mission Overhead
- Overcome Vehicle Drag
- Power for Other Subsystems
- Power to Lift Itself and Required Fuel
+
Waste due to Inefficiencies in Operation & Thermal Performance

Outline

- Background
- Vehicle System Design in Exergy Terms
- Exergy Consideration of a Hypersonic Inlet
- Preliminary Development of the MHD Equations, with Entropy Generation
- Future Work

Example Subsystem Problem Tailoring of Inlet Shock Position

Using $M \equiv V/a$ and $a = \sqrt{\gamma RT}$

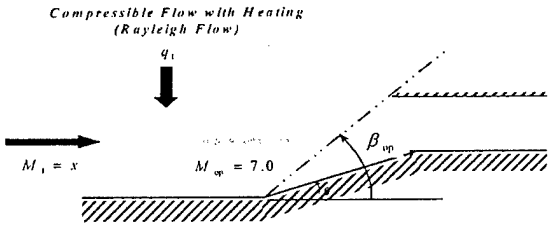

Shock-on-lip condition maximizes engine mass flow without shockwave ingestion problems

Inlet Shock Wave Tailoring – Thermal Energy

- Rayleigh Line Flow
- Add thermal energy to reduce Mach number – achieve shock-on-lip condition
- Approximating a flow control process such as MHD

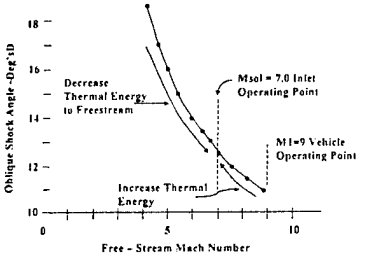

Oblique Shock Angle vs Mach No.

Shock Inlet Tailoring – Rayleigh Line Analysis

- Shock angle is a function of Mach number only

$$\tan\theta = 2\cot\beta\left[\frac{M_1^2\sin^2\beta - 1}{M_1^2(\gamma + \cos 2\beta) + 2}\right]$$ theta-beta-M relationship

- Heat addition required to achieve desired Mach number given by the Rayleigh line analysis

$$q = C_p(T_{02} - T_{01}) \quad \text{where} \quad \frac{T_{02}}{T_{01}} = \left(\frac{1+\gamma M_1^2}{1+\gamma M_2^2}\right)^2\left(\frac{M_2}{M_1}\right)^2\left(\frac{1+\frac{\gamma-1}{2}M_2^2}{1+\frac{\gamma-1}{2}M_1^2}\right)$$

Entropy and Exergy Balance Equations

- **Entropy Generation Rate – Heating Process**

$$\dot{S}_{gen} = \rho_1 V_1(s_2 - s_1) - \frac{\dot{Q}}{T}$$

- **Entropy Equation – Shock**

$$s_2 - s_1 = R\left(\frac{1}{\gamma-1}\ln\left(\frac{T_2}{T_1}\right) - \ln\left(\frac{\rho_2}{\rho_1}\right)\right) = -R\ln\left(\frac{P_{02}}{P_{01}}\right)$$

- **Exergy Destruction**

$$\dot{X}_{destroyed} = T_1\dot{S}_{gen}\Big|_{\dot{Q}} + T_1\dot{S}_{gen}\Big|_{shock}$$

Shock Inlet Tailoring

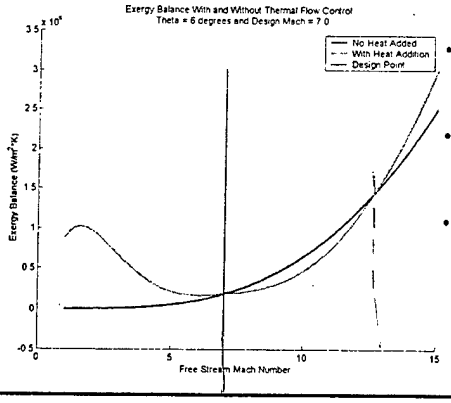

- Region of favorable exergy balance observed
- Occurs when free stream higher than design point
- Aerodynamics only. Benefits for propulsion system still TBD

7

MHD Subsystem Problem
Tailoring of Inlet Shock Position

MHD Inlet Flow Control Instead of

Compressible Flow with Heating (Rayleigh Flow)

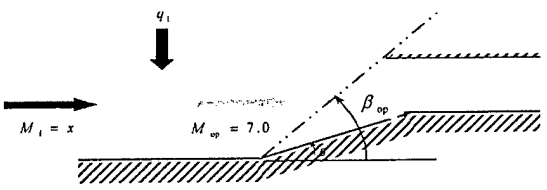

Shock-on-lip condition maximizes engine mass flow without shockwave ingestion problems

Outline

- Background
- Vehicle System Design in Exergy Terms
- Exergy Consideration of a Hypersonic Inlet
- **Preliminary Development of the MHD Equations, with Entropy Generation**
- Future Work

MHD Equations in General

- Amalgamation of equations of fluid motion and Maxwell equations of electromagnetism.
- Assume "single fluid" type to couple effects of electromagnetic fields on fluid motion.
- Flow velocities much smaller than speed of light → non-relativistic.

Classical Physics a Microscopic Level

- Flow length scales much larger than Debye length.
- Flow time scales much larger than reciprocal of plasma frequency.

Assumptions to Develop Equations

- All velocities are small compared with speed of light.
- Electric field is of order $\boldsymbol{U}\times\boldsymbol{B}$; $\boldsymbol{E}$ fields are induced or of that order.
- $\boldsymbol{H} \sim \boldsymbol{H}'$ and $\boldsymbol{B} \sim \boldsymbol{B}'$ → $\boldsymbol{B} = \mu\boldsymbol{H}$ in any frame of reference.
- Displacement current is negligible with compared to $\boldsymbol{J}$
- Ohm's law is $\bar{J} = \sigma\left(\bar{E} + \bar{U}\times\bar{B}\right)$
- Space charge in moving reference frame equals zero.
- Force $\rho_e\boldsymbol{E}$ is negligible compared to $\boldsymbol{J}\times\boldsymbol{B}$; the electric stress and energy is negligible compared with $\boldsymbol{H}\cdot\boldsymbol{B}$.
- For high conductivity, Ohm's law indicates that $\boldsymbol{E} = -\boldsymbol{U}\times\boldsymbol{B}$ and electric current obtained from: $\boldsymbol{J} = \nabla\times\boldsymbol{B}$.

Theoretical Possibility

- Lorentz Force Law: $\bar{F} = q\left(\bar{E} + \bar{U}\times\bar{B}\right)$
  - Non-relativistic, stationary frame, charged particle.
- Generalized Ohm's Law

$$\sigma\left(\bar{E} + \cancel{\nabla p_e / en_e}\right) = \bar{J} + \underbrace{\beta e\left(\cancel{\bar{J}\times\bar{b}}\right)}_{\text{Hall Current}} + \underbrace{\bar{S}_b\times\left(\cancel{\bar{J}\times\bar{b}}\right)}_{\text{Ion Slip}}$$

- Joule Heating $\bar{J}\cdot\left(\bar{E} + \bar{U}\times\bar{B}\right)$
  - Coupling mechanism between electromagnetics and thermodynamics.
  - Alleviates heat load.
  - Can be used to postpone sonic choke for internal flows.

Maxwell Equations

- Faraday's Law: $\dfrac{\partial\bar{B}}{\partial t} + \nabla\times\bar{E} = 0$
- Ampere's Law: $\dfrac{\partial\bar{D}}{\partial t} - \nabla\times\bar{H} = -\bar{J}$
- Coulomb's Law: $\nabla\cdot\bar{D} = \rho_e$
- Gauss' Law: $\nabla\cdot\bar{B} = 0$

Constitutive Relations
Non-Relativistic Motion

- Electric Field Vectors: $\bar{D} = \varepsilon \bar{E}$
- Magnetic Field Vectors: $\bar{B} = \mu \bar{H}$
- Ohm's Law: $\bar{J} = \sigma\left(\bar{E} + \bar{U} \times \bar{B}\right)$
- Electric Charge Density: ρ_e

MHD Balance Equations I

- Continuity: $\dfrac{\partial \rho}{\partial t} + \dfrac{\partial}{\partial x_j}\left(\rho u_j\right) = 0$
  - Single fluid.
- Momentum:

$$\frac{\partial \rho u_i}{\partial t} + \frac{\partial}{\partial x_j}\left\{\rho u_i u_j + p\delta_{ij} - \tau_{ij}\right\} = \bar{f}_{\text{Lorentz}}$$

- Lorentz Force:

$$\bar{f}_{\text{Lorentz}} = \rho_e \bar{E} + \bar{J} \times \bar{B}$$

Imposing MHD Assumptions

- Electromagnetic Momentum Balance:

$$\frac{\partial}{\partial t}\left(\varepsilon \bar{E} \times \bar{B}\right) + \varepsilon \nabla\left(\frac{\bar{E} \cdot \bar{E}}{2}\right) - \left(\bar{E} \cdot \nabla\right)\varepsilon \bar{E} - \varepsilon \bar{E} \nabla \cdot \bar{E}$$
$$+ \nabla\left(\frac{\bar{B} \cdot \bar{B}}{2\mu_m}\right) - \left(\bar{B} \cdot \nabla\right)\frac{\bar{B}}{\mu_m} = -\underbrace{\left(\bar{J} \times \bar{B} + \rho_e \bar{E}\right)}_{\text{Lorentz Force Density}}$$

- Under MHD Assumptions

$$\Rightarrow \quad \bar{F}_{\text{Lorentz}} = \bar{J} \times \bar{B} \cong \left(\bar{B} \cdot \nabla\right)\frac{\bar{B}}{\mu_m} - \nabla\left(\frac{\bar{B} \cdot \bar{B}}{2\mu_m}\right)$$

MHD Balance Equations I:
Mass & Momentum

- Continuity: $\frac{\partial \rho}{\partial t} + \frac{\partial}{\partial x_j}\left(\rho u_j\right) = 0$
- Momentum:

$$\frac{\partial \rho u_i}{\partial t} + \frac{\partial}{\partial x_j}\left\{\rho u_i u_j + p\delta_{ij} - \tau_{ij} - M_{ij}\right\} = 0$$

- Viscous Stress Tensor $\tau_{ij} = \mu\left(\frac{\partial u_i}{\partial x_j} + \frac{\partial u_j}{\partial x_i}\right) + \lambda \frac{\partial u_k}{\partial x_k}\delta_{ij}$

Maxwell Tensor $M_{ij} = \frac{B_i B_j}{\mu_m} - \frac{B^2}{2\mu_m}\delta_{ij}$

MHD Balance Equations II:
Total Energy

- Energy: $\frac{\partial \rho Z}{\partial t} + \frac{\partial}{\partial x_j}\left\{\rho Z u_j + p u_j - \tau_{ji} u_i - M_{ji} u_i + q_j\right\} = 0$
- Total Energy: $Z \equiv \frac{1}{2}u^2 + \frac{p/\rho}{\gamma - 1} + \frac{B^2}{2\rho\mu_m}$
- "Joule Heating":
  - Arises from EM power density: $\dot{P} \equiv \bar{E} \cdot \bar{J}$

$$\frac{\partial \rho e}{\partial t} + \frac{\partial}{\partial x_j}\left\{\rho e u_j + p u_j - \tau_{ji} u_i + q_j\right\} = \dot{P}$$

Illustration for One Dimensional Case
of an Applied Electromagnetic Field in Magneto-Aerodynamics

- Modified Rankine-Hugoniot Conditions
  - Shock jump in x_1 direction.

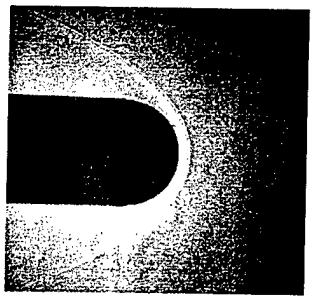

$$[\rho u] = 0$$
$$[p + \rho u_1 u_1] = \int (J_2 B_3 - J_3 B_2) dx$$
$$[\rho u_1 u_2] = \int (J_3 B_1 - J_1 B_3) dx$$
$$[\rho u_1 u_3] = \int (J_1 B_2 - J_2 B_1) dx$$
$$[\rho u_1 h] = \int \left(J_1^2 + J_2^2 + J_3^2\right)/\sigma \, dx$$
$$[B_1] = 0$$
$$[J_2/\sigma - u_3 B_1 - u_1 B_3] = 0$$
$$[J_3/\sigma - u_1 B_2 - u_2 B_1] = 0$$

Thermodynamic Entropy Jump
(One Dimension Case)

- Entropy Balance:

$$\rho u_1 \frac{ds}{dx} = \frac{\rho u_1}{T}\frac{dh}{dx} - \frac{u_1}{T}\frac{dp}{dx}$$

- Entropy Jump

$$\rho u_1 [s] = \int \frac{\kappa}{T^2}\left(\frac{dT}{dx}\right)^2 dx + \int \frac{2\mu+\lambda}{T}\left(\frac{du}{dx}\right)^2 dx + \int \frac{J^2}{\sigma T} dx - \int \frac{u_1 (\bar{J}\times\bar{B})_1}{T} dx$$

Bityurin says this is "work" and doesn't really fit in BGN.

Entropy Generation with MHD

- Transport of Entropy: $\dot{S}_{gen} = \frac{\partial S}{\partial t} + \frac{\partial F_k}{\partial x_k} + \frac{\partial}{\partial x_k}\left(\frac{q_k}{T}\right)$
- Constitutive formula: $\dot{S}_{gen} = \frac{\tau_{ki}}{T}\frac{\partial u_i}{\partial x_k} - \frac{q_k}{T^2}\frac{\partial T}{\partial x_k}$
- Entropy Generation with MHD:

$$\dot{S}_{gen} = \frac{\tau_{ki}}{T}\frac{\partial u_i}{\partial x_k} + \frac{M_{ki}}{T}\frac{\partial u_i}{\partial x_k} - \frac{q_k}{T^2}\frac{\partial T}{\partial x_k}$$

- Exergy Destroyed: $\boxed{\dot{X}_{destroyed} = T_0 \dot{S}_{gen}}$

Outline

- Background
- Vehicle System Design in Exergy Terms
- Exergy Consideration of a Hypersonic Inlet
- Preliminary Development of the MHD Equations, with Entropy Generation
- Future Work

FUTURE WORK

Extensions to the Current Activities:

- Rigorous Theoretical Proof of the MHD Analogy
- Inlet Tailoring by use of MHD
  - efficiency compared to thermal energy tailoring

Long Range Activities:

- Expand the Analysis Approach with Exergy, or Entropy Generation, as the Common Currency for Design Trade-Off
- Develop Methodology for System-Level Optimization

THE BROADER VISION: System-Level Analysis & Optimization

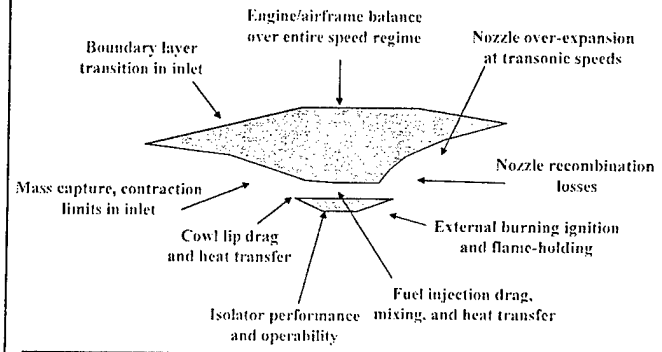

Exergy, Entropy Generation as the 'Common Currency'

2003 EXERGY WORKSHOP

PLACE: TBD

TIME: SPRING / EARLY SUMMER

SPONSOR: EOARD/AFRL/VA

POC: EOARD - WAYNE DONALDSON
USA - CHUCK SUCHOMEL
- DAVE MOORHOUSE
OTHER - TBD

Exergy-Based Design Methods
Products

"The Vision and Need for Energy-Based Design Methods", AIAA Paper no. 2000-4850
RE-WRITTEN AS:"A Proposed System-Level Multidisciplinary Analysis Technique Based on Exergy Methods", submitted to AIAA Journal of Aircraft

"On the Construction of Entropy Balance Equations for Arbitrary Thermophysical Processes", AIAA Paper no. 2001–0815, January 2001.

"Energy-Based Design Workshop", AFRL-VA-TR-2001-3003, January 2001.

"Integrated Wing Design with Active Conformal Control Surfaces," AIAA 2001-1428, April 2001

"The Role of Entropy and The Second Law in Computational Thermofluids", AIAA 2001-2758, June 2001.

"Exergy Methods Applied to the Hypersonic Vehicle Challenge", AIAA-2001-3063, Jun '01

"Entropy and Exergy Balance Equations for MHD Fluid Flow with Application to Hypersonic Vehicle Analysis and Design", AIAA-2002-2183, May 2002

MECHANISMS OF ALKALINE-ATOMIC INHIBITORS OF DECAY OF THE MHD GENERATOR PLASMA

G.V. Zhuvikin, A.L.Kuranov, T.L.Tkachenko

"HSRI" HC "Leninetz", SPb State University

The abstract

The physical mechanisms of alkaline-atomic inhibitors of decay of the MHD generator plasma including ionization-recombination processes, the radiation capture phenomenon, and the conversion of atomic thermal motion into the electron excitation energy by quasi-molecular transitions are analyzed. The problems of the application of these mechanisms to increase the non-equilibrium plasma conductivity are considered.

The power of unit volume of the MHD generator is evaluated as $Q \sim \sigma v^2 B^2$, where σ and v are the flow conductivity and velocity, B - induction of a magnetic field. Variables σ and v determine the main requirements, which are now presented to a working substance of the energetically effective MHD generator: 1) high conductivity; 2) abilities of creation of a flow boosted up to high speed. From all known substances the liquid metals have greatest conductivity ($\sim 10^5$ Om^{-1} cm^{-1}), however their usage in hypersonic aircraft is not obviously possible. At the same time in conditions of the hypersonic flight a high-speed gas flow ($\sim 10^3$ m/s) is appears in the natural way. But the conductivity of such flow produced by the thermal ionization thus appears negligible. To evaluate the conductivity of the weakly ionized gas it is possible to take advantage of a ratio $\sigma=e^2 n_e / m_e n_0 k_s$, where e, m_e and n_e are charge, mass and concentration of electrons, n_0 is the concentration of neutral components, k_s is the rate constant of elastic scattering of electrons. Thus included in conductivity the degree of ionization $\alpha=n_e/n_0$ can be estimated in conditions of thermodynamic equilibrium with use of the approximate Saha formula:

$$\alpha^2 \quad (m_e/h)^{3/2}(kT)^{5/2}(1/p)\, exp(-E_i/kT), \qquad (1)$$

where h is the Planck constant, p is the gas pressure, E_i is the ionization energy of the gas molecules, T - temperature. The ionization energy of some atoms and molecules considered in the given activity, is presented in tab.1. There the values of a dissociation energy of molecules are included as well.

Table 1.

	N_2	O_2	NO	N	O	Na	Na_2
E_i	15.6	12.07	9.26	14.5	13.6	5.11	4.9
D_0	9.76	5.11	6.50	--	--	--	0.737

The estimations show, that reaching a necessary degree of ionization in a pure air flow needs the temperature of the order 7000-8000K, that is unacceptable in conditions of the hypersonic flight. The use of the easily ionizable dopes, for example, sodium, allows to reduce the gas temperature up to 2000-3000K, however this temperature is excessively high as well. Besides, the orientation on the easily ionizable component as on a main working substance, appears to be economically and ecologically unacceptable in conditions of the flight. The problem of technological compatibility of dopes with conditions of hypersonic flight essentially limits a scale of their

application. Thus, in spite of the fact that the idea of the easily ionizable dopes to increase the conductivity of the MHD generator plasma is developing for a long time [1], the process of the thermal ionization in conditions of the hypersonic flight is not expedient neither from the power, nor from an economic point of view. For this reason the study of capabilities of the plasma creation with high non-equilibrium conductivity with use of rather small quantities of the easily ionizable dopes has become the important and actual part of the «AJAX» project.

A number of various physical mechanisms of creation and maintenance of the gas non-equilibrium conductivity is under development and investigation. Irrespective of a particular way of the energy input in a flow, the analysis of interaction of atomic-molecular subsystems of gas medium taken in various combinations, allows essentially to facilitate searching optimum conditions of ionization. The example of such approach is given by researches on the plasma life-time increase after the switching off the external source of ionization. In works [2, 3] it was reported on observation the effect of the decrease of loss of charged particles in the decaying nitrogen plasma in the presence of small (about 0.1 %) amount of sodium vapors. The additional study of elementary processes connected to this phenomenon [4], has shown a capability to increase the efficiency of the gas ionization by the change of the usage character of the easily ionizable dope by means of the influence to the ionization-recombination balance. In conditions of the conducted experiments the main part of ionic components was presented by ions of nitrogen N_2^+. As for ions of the dope, it was shown that the processes

$$N_2(v\ 21) + Na \quad N_2 + Na^+ + e \qquad (2)$$

$$N_2(A^3\Sigma_u^+) + Na \quad N_2 + Na^+ + e \qquad (3)$$

$$N_2^+ + Na \quad N_2 + Na^+ \qquad (4)$$

play the main role in their production

At the same time the contribution of direct ionization of the dope by electron impact

$$Na + e \quad Na^+ + 2e \qquad (5)$$

has appeared to be negligible in comparison with chemoionization (2), ionization (3) and the charge exchange (4).

Also it was shown [4], that the main role in the loss of charged particles belongs to processes

$$N_2^+ + e \quad N + N \qquad (6)$$

$$Na^+ + e + N_2 \quad Na + N_2 \qquad (7)$$

$$Na^+ + e + e \quad Na + e \qquad (8)$$

One can see, that the loss of ions of nitrogen dimers and sodium atoms are of essentially different character. While for nitrogen it is two-particle process, for sodium it is three-particle one. Estimations show, that in conditions of rather low pressure the recombination rate of the sodium ions can be on three orders smaller the recombination rate of nitrogen ions. These estimations are qualitatively confirmed by laboratory experiment in the glow discharge in the mixtures of nitrogen with sodium vapors. The total pressure was 1 to 14 Tor and the sodium doping did not exceed 4 %. The typical curves of the conductivity time dependence in the plasma afterglow illustrate a role of the small additions of alkaline metal as an inhibitor of the plasma decay (fig.1).

The dependence of the effective life-time of the plasma upon the concentration

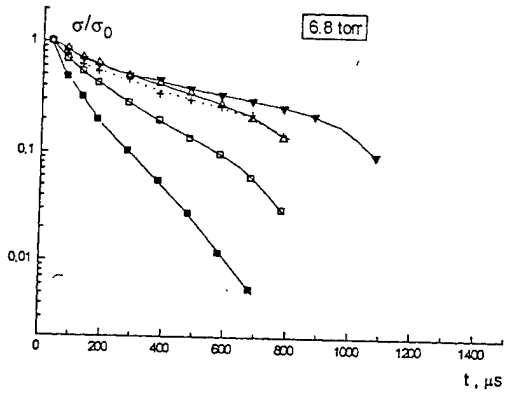

Fig.1. Conductivity of decaying nitrogen-sodium plasma for various values of temperature in the case of initial pressure 6.8 Tor.

of sodium atoms for various pressures of nitrogen is presented on fig.2.

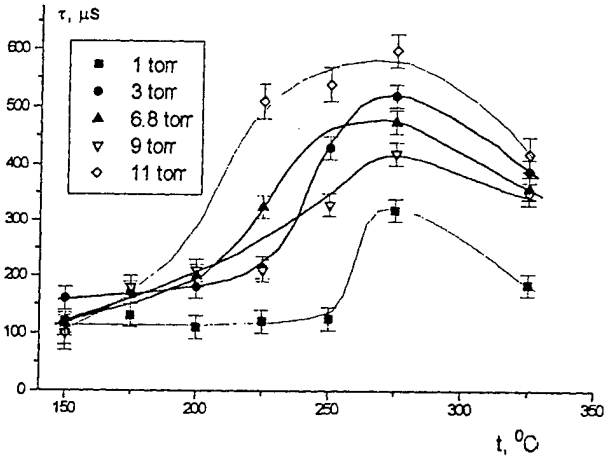

Fig.2. Dependence of effective time of decay of plasma on the temperature for initial pressure 1, 3, 6.8, 9, and 11 Tor.

If $\tau(N)$ is the dependence of the plasma effective life-time on the concentration of the alkaline dope, the time dependent gain in the plasma conductivity is

$$\sigma_N(t)/\sigma_0(t) = e^{(\tau(N)-\tau(0))t} \quad (9)$$

One can conclude, that the use of alkaline inhibitor can be especially effective in the impulse - periodic operational mode of the plasma energization ensuring value of the conductivity within a given range of values ($\sigma_{max} - \sigma_{min}$) (fig.3). Thus the injection of inhibitor in a flow also can be more effective in the impulse - periodic mode, synchronized with cycles of energization.

Table 2.

	NO_2	O_2	NO	OH	O	Na	N_2O	O_3
E_A	2.42	0.44	0.03	1.8277	1.46	0.5479	0.24	2.103

In comparison with the laboratory plasma the real MHD generator plasma may contain a number of new components with large value of the electron affinity E_A (tab. 2). This table can be supplemented as well with more data concerning the numerous products of the fuel combustion. The rather large value of the electron affinity of a number of these molecules belongs to the unfavorable factors, which can be exhibited at transition from laboratory nitrogen-sodium plasma to the air plasma of the MHD generator.

One more unfavorable factors appears from the fact that the growth of the sodium concentration above a certain value, as it is seen from fig.2, is not resulting in the increase the plasma life-time, but results even in acceleration of the plasma decay. The origin of this phenomenon is not finally resolved, the supposition [4] however was already proposed, that this can be promoted by the growth of the sodium dimer Na_2 concentration. The argument is, that the growth of the sodium vapor density, is accompanied with the growth of the concentration of molecular ions Na_2^+ which, as well as in case with ions of nitrogen dimer recombine very fast in the process of two-particle dissociative recombination

$$Na_2^+ + e \quad Na + Na \qquad (10)$$

Let's stay on this moment in more detail, noting, that parameters of plasma in conditions of hypersonic flight essentially differ from parameters of laboratory plasma

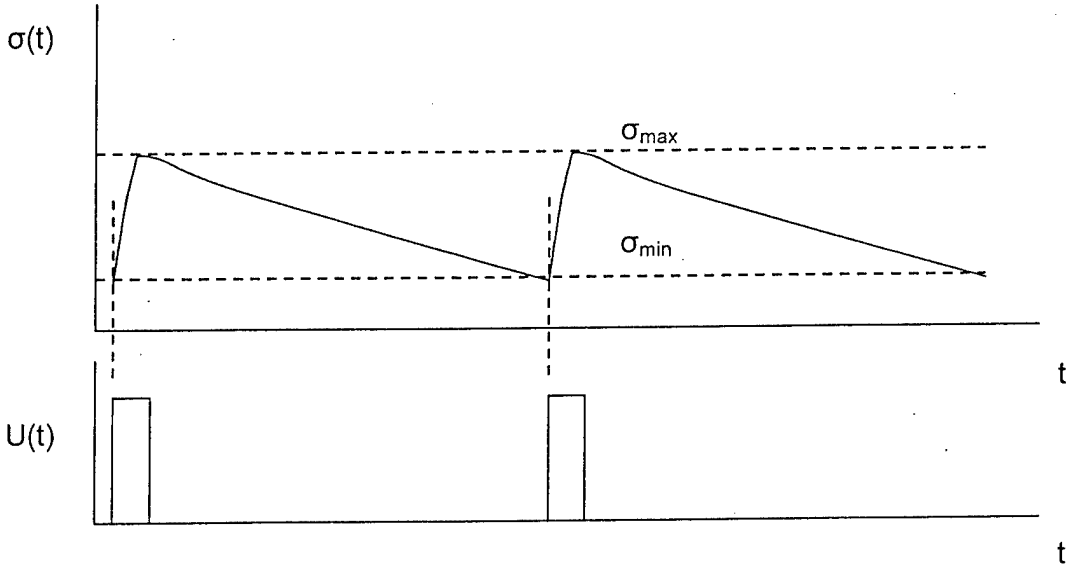

Fig.3. An action of the inhibitor of the plasma decay in impulse - periodic operational mode of the energization source.

of a glowing discharge [2-4], at least in two factors - temperature and geometric sizes of the working medium.

As to temperature relation, that, really, according to tables by Nesmeyanov [5], the concentration of the sodium dimer grows very fast with the temperature increase. However it is correct only in conditions of a saturated vapour in thermodynamic equilibrium with a surface of a liquid metal. Such conditions can be realized, for example, at injection of a jet of dispersed liquid sodium or sodium - potassium eutectic in a flow of the MHD generator channel. If the atomic sodium concentration is small, and the gas temperature is high, the sodium dimers density will be minor because of a dominance of the process of a thermal dissociation. So, if three-particle recombination

$$Na + Na + B \quad Na_2 + B, \tag{11}$$

Is the main mechanism of the sodium dimers formation (B is a particle of the main gas), and main mechanism of its destruction is the collisions with the same particles

$$Na_2 + B \quad Na + Na + B, \tag{12}$$

then the equilibrium concentration of the sodium atoms and dimers will be connected by the relation

$$[Na_2] = (K_1 / K_2)\,[Na]^2 \tag{13}$$

The estimations done for temperature region 1000-2000K and the concentration of sodium atoms of the order $10^{14}cm^{-3}$ show that the presence of the sodium dimers can be neglected.

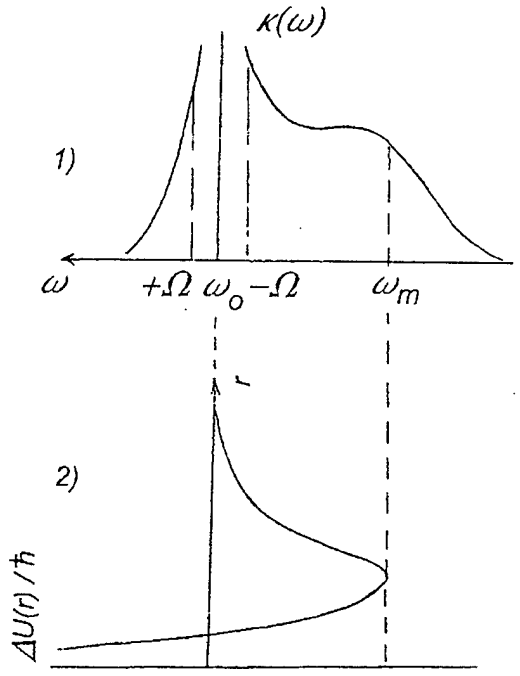

Fig.4. Formation of the absorption coefficient spectral profile near to a resonant line of the optically active atom.

The second factor, the geometric sizes of the medium, introduces into consideration the effect of the radiation capture. In this connection the special interest is represented by results of works [6-8], in which the principal capability of creation of energetically essential non-equilibrium conditions in a two-component gas mixture was investigated.

The optically active component is presented by atoms of a chemical element with a low potential of resonant excitation, for example, by atoms of alkaline metal. The second component is presented by atoms or molecules of the carrier gas. In the result of interaction of these two components the specific optically active quasi-molecular subsystem is formed in the gas mixture. This subsystem makes it possible to increase essentially a degree of the power non-equilibrium in large volume of the gas medium.

The principal mechanisms of the offered technology of the gas mixture energization are: 1) quasi-molecular absorption of the optical radiation in a layer of a moderate optical thickness; 2) the excitation energy transfer from qasi-molecules to atoms of optically active dope; 3) the radiation capture at the frequency of resonant transition of the dope atoms.

The mechanism of the quasi-molecular absorption is illustrated by fig.4. The absorption in the spectral area $|\omega - \omega_0| < \Omega$ is formed at the expense of collisional broadening of a spectral line of the dope atom. A main part of an integral absorption of a spectral line is located here. The relation of an absorption coefficient to frequency in this area is determined by a convolution of the Doppler and Lorentz spectral profiles. Because of a large optical thickness of a layer of absorptive atoms, the radiation of an external source cannot penetrate into the depth of a gas flow on these frequencies.

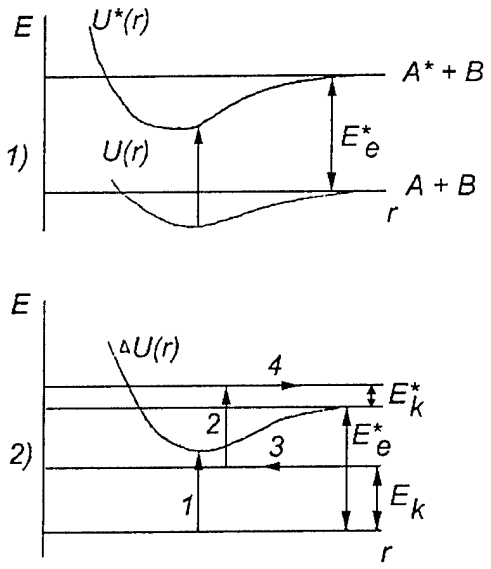

Fig.5. The scheme of the quasimolecule energy conversion into the energy of electron excitation of the atom of optically active component.

The absorption in the spectral region $|\omega - \omega_0| > \Omega$ is formed at the expense of quasistatic broadening as a result of the interaction of atoms of the dope with atoms and molecules of the main gas. The spectral profile of the absorption coefficient here depends on the function $\Delta U(r)=U^*(r)-U(r)$, which is equal to the difference of the interaction potentials of atoms in quasi-molecules A*-B and A-B. Here A* is the atom of an impurity in an excited state (see also fig.5). The absorption coefficient in this spectral area can be on 3-5 orders less the absorption coefficient in the center of a line. This spectral diapason can be used as a channel of the optical energy input into the internal areas of a flow.

The mechanism of the electron energy transfer from quasi-molecule to optically active atom also includes the process of the atomic thermal motion conversion into the energy of electron excitation. The power scheme of such conversion is presented on fig.5 (2). Here terms E_k^* and E_k are kinetic energy of relative motion of atoms in excited and unexcited qausi-molecules respectively, term E_e^* is the electron energy of the free optically active atom. In the process of the atoms approach (arrow 3), absorption of a photon with frequency ω_{ex} (arrows 1, 2) and consequent retraction (arrow 4), the optically active atoms of the dope gain the electron excitation energy

$$E_e^*=E_k^*-E_k+\hbar\omega_{ex} \qquad (14)$$

This energy equals to the energy of a photon with a resonant frequency ω_0 of the atom A. As the radiation with this frequency is located in depth of the medium with a large optical thickness, thereby it is captured by the whole volume of a gas mixture. It is important to underline, that the mechanism of the radiation capture does not depend on a way of obtaining of atoms A in the state of resonant excitation. They can be produced both in the process of optical excitation, and in the result of an action of an external source of ionization, for example, by electronic beam or by the electrical discharge.

The mechanism of the radiation capture by atoms of easy ionizable component increases the effective life-time of τ_{eff} of these atoms in an excited state. The effective time depends on a thickness of an absorptive layer and on the dependence of an absorption coefficient to frequency. To estimate the effective life-time of resonantly exited atoms of an impurity one may use the results of works by T.Holstein for the case, when optical medium has the form of the cylinder with a given radius R (see, for example, [9]). For the aims of estimations the channel of the MHD generator with rectangular cross-section can be approximately replaced with the cylinder one (fig.6). The results of Holstein's calculations look like [9]:

$$\tau_{eff}^{(L)}=(\tau_0/1.12)\,[\pi\, k_0^{(L)}R]^{1/2} \qquad (15)$$

for the case of the Lorentz spectral line profile and like

$$\tau_{eff}^{(D)}=(\tau_0/1.60)\, k_0^{(D)}R\,[\pi \ln(k_0^{(D)}R)]^{1/2} \qquad (16)$$

for the case of the Doppler profile.

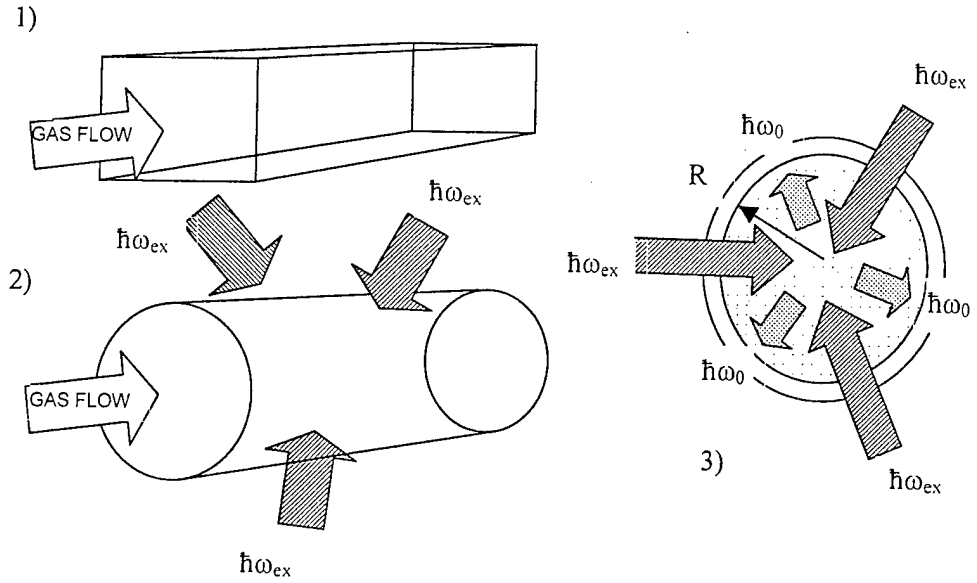

Fig.6. The approximation of rectangular geometry of a working gas medium in the MHD generator channel by the cylinder (1-2) and the scheme of the optical volumetric excitation of alkaline-atomic inhibitor of the plasma decay (3).

The absorption coefficients $k_0^{(L)}$ and $k_0^{(D)}$ at the resonant frequency ω_0 included in expressions (15) and (16), can be found under the formulas given, for example, in [10]. So, for the Doppler spectral line profile, the oscillator strength f_0, the concentration of absorptive atoms N_0, and the temperature T it is possible to write:

$$k_0^{(D)} = 2\,[\ln 2/\pi]^{1/2}\,(\pi e^2/m_e c)\,f_0\,N_0 / (\Delta\omega_D/2\pi) \qquad (20)$$

$$\Delta\omega_D = 2\,(\omega_0 / c)[2\,\ln 2\,R_G\,T / \mu\,]^{1/2} \qquad (21)$$

where R_G -is the universal gas constant, μ is the atomic mass of the dope, e and m_e are charge and mass of electron, and c is the light speed.

In particular, for effective life-time of resonantly exited level of the sodium atom it is obtained

$$\tau_{eff}^{(D)} = 3.6\,10^{-10}\,\tau_0\,N_0\,R / T^{1/2}\,[\ln(3.25\,10^{-10}\,N_0 R / T^{1/2})]^{1/2}, \qquad (22)$$

where variables N_0, R, T are taken in the CGS system.

For $N_0 = 10^{14} cm^{-3}$, $R = 50$ cm, $T = 1000$ K it is found $\tau_{eff}^{(D)} = 1.8\,10^5\,\tau_0$. Taking into account that the radiation life-time of the resonantly exited sodium atom is about 10 ns, the effective life-time for the indicated conditions will be about 1 ms. This value corresponds to the range of life-times of metastable atoms. Besides, the energy of ionization of the sodium atom from this state is about 3 эВ, that essentially improves conditions of the sodium ionization as for the purely thermal mechanism (Saha formula (1)), as for elementary processes (2) - (4).

In conclusion it is necessary to underline two important circumstances.

First, the use of the radiation capture mechanism on the frequency of the resonant transition of atoms of easily ionizable dope allows to increase the efficiency of creation of non-equilibrium conductivity of a gas flow, in addition to other methods of ionization.

Second, the use of the quasimolecular absorption mechanism in far quasistatic wings of a resonant line of the dope atoms allows to create the volume excitation of the dope resonant states, thereby selectively acting on the particular electron

subsystem which is responsible for the inhibition of the decay of non-equilibrium plasma.

References

1. Alferov V.I. Thermal physics of high temperatures, 1979, v.17, p.156.
2. Kuranov A.L., Skoblo I.N., Suleimenov I.E., Chaika M.O. // Physics of low-temperature plasma. The conference proceedings. June 20-26, 1995, Petrozavodsk, V.2, p.236.
3. Kuranov A.L., Skoblo I.N., Suleimenov I.E., Chaika M.O. //Plasma Physics Reports, 1998, v.24, p.1060.
4. Kuranov A.L., Skoblo I.N., Suleimenov I.E., Chaika M.O., Skoblo Yu.E., Ionikh Yu.Z. Influence of small alkaline additives on recombination processes in the glowing nitrogen discharge.
5. Nesmejanov A.N. The vapour pressure of chemical elements. M., 1961.
6. Bezuglov N.N., Zhuvikin G.V., Kuranov A.L., Shubina O.V. Excitation of optically active gas mixture taking into account the radiation capture. // XI All-Union conference on the dynamics of rarefied gases. July 8-13 1991, Leningrad. Leningrad mechanical institute. Book of abstracts, p.39.
7. Borisov E.N., Zhuvikin G.V., Karpenko A.I., Kuranov A.L., Sepman V.Yu. On the quasimolecular mechanism of the gas mixture cooling. // XI All-Union conference on dynamics of rarefied gases. July 8-13 1991, Leningrad. Leningrad Mechanical Institute. Book of abstracts, p.41.
8. Kuranov A.L., Borisov E.N., Zhuvikin G.V., Sepman V.Yu., Karpenko V.N. A method of the plasma generartion. // Patent RU 2035129 (1995).
9. Bezuglov N.N. The radiation transfer. // In book. " Reference book on constants of elementary processes including atoms, ions, electrons, photons". Editor A.G.Zhiglinsky. - SPbSU, 1994, p.312-334.
10. Frish S.E. Determination of concentration of normal and exited atoms and the oscillator strengths by methods of light emission and absorption. In book "Spectroscopy of the gas discharge plasma ". Leningrad, Nauka, 1970, p.7 – 62

NUMERICAL MODELING OF PLASMACHEMISTRY AND DISCHARGE STRUCTURE IN AIR

I. V. Kochetov, A. P. Napartovich

State Science Center of Russia "Troitsk Institute for Innovation and Thermonuclear Research", 142190 Troitsk Moscow region, TRINITI, Russia, E-mail: apn@triniti.ru

Abstract

Results of numerical modeling of the characteristics of various types of the discharges in air and other gases are given. The problems of collection of data of cross sections of electron interactions with atoms and molecules and of the rate constants for reactions, in which the excited and charged particles and radicals are involved, are discussed. The application of developed databases is illustrated by modeling the characteristics of the discharge in nitrogen, oxygen and air within the framework of homogeneous model. The results of simulation of a negative corona in air by 1.5D and 3D models are described.

Introduction

Modeling plasma in air requires knowledge of an electron energy spectrum, kinetic rate constants for reactions of excited and charged particles, and chemically active radicals.

To describe electron kinetics in non-equilibrium plasma, a simplifying assumption of the fixed shape of electron energy distribution function (EEDF) is not applicable. It is known, that the shape of distribution function is rather sensitive to gas mixture composition and both degrees of excitation and ionization. Nowadays, for calculations EEDF numerical solving of the Boltzmann equation is used, allowing taking into account all these factors.

A plenty of the charged and excited components and chemically active radicals require a large number of kinetic equations for these components to be solved. The equation system, as a rule, consists of the nonlinear differential equations with different rate constants.

In the certain conditions, for example corona discharge, the value of an electrical field essentially varies in the discharge gap. In such conditions, it is necessary to use models of the discharge describing spatial distribution of an electrical field and components of plasma.

1. EEDF modeling

Physics of the gas discharge, plasma chemistry and number of other applied sciences deal with low temperature plasma. For modeling physical processes in such plasma, which are taking place in an external electrical field, it is necessary to know the values of following electron kinetic constants: drift velocity of electrons; average energy; diffusion coefficient; rate constants for excitation of molecular vibrations and electronic levels; rate constants for ionization and etc.

Usually, experimental researches on electronic kinetic coefficients are carried out for pure gases, and the detailed information is obtained only for drift velocity, characteristic energy and rate constants of ionization. In this connection, it is very important to have the theoretical model for calculation kinetic coefficients in gas mixtures. All mentioned kinetic coefficients may be calculated by integration EEDF with the appropriate cross sections of electron collision with atoms and molecules. In turn, EEDF may be obtained by the numerical solution of the Boltzmann equation.

Calculated EEDF evidently depends on a used set of the electron collision cross sections. Unfortunately, experimental, and theoretical information about cross sections for various processes (elastic scattering, excitation of molecular rotation, vibration and electronic levels, the ionization) is not

quite complete and even contradictory. To be sure in a correctness of the calculated EEDF, it necessary to carry out some "fitting" of cross sections starting from published ones. The usual procedure of "fitting" for pure gases consists in updating a set of cross sections so that the consent between calculated and experimentally measured electron kinetic coefficients is achieved. In many cases, such a method allows one to reduce uncertainty caused by scatter in experimental data of cross sections. In this way, it is possible to obtain the self-consistent sets of cross sections for pure gases. The term "self-consistent" means, that the calculation with the derived set of cross sections, gives a good consent with experimental data on electron drift velocity, characteristic energy, ionization rate constant and other kinetic coefficients. The obtained self- consistent sets of cross sections for pure gases are used further for calculations of kinetic coefficients for gas mixture.

In the literature, permanently new information about electron scattering cross sections on atoms and molecules appears, which allows improving the theoretical modeling of electron kinetics. Researchers in TRINITI are engaged in these problems since 1980, and the extensive databank is collected, which contains the information about cross sections of such processes, as elastic scattering (transport cross section), excitation of molecular rotation, vibration and electronic levels, ionization, recombination, dissociation, electron attachment. To this day, there are sets of cross sections for H_2, CO, O_2, N_2, CO_2, Kr, He, Ne, Xe, Ar, F_2, Cl_2, CF_4, H_2O, HCl, O, SF_6, NO, N, Na, Cs, CCl_4, BF_3, BCl_3, CH_4, C_2H_6, Hg, NH_3, NF_3.

2. Modeling kinetics of the excited and charged particles

The information about mechanisms of chemical reactions and their rate constants for various conditions, such as gas pressure, temperature, degree of excitation and others is necessary for modeling a plasma chemical system. Considering a number of various chemical species in a system, it is clear that the problem of reliable modeling of any system requires large efforts in collection of information about processes in this system. For any research group, the unique way to have a success is to carry out this work continuously over many years. Of a great importance is also an opportunity to get information directly from researchers interested in having such information. Fortunately, with occurrence of Internet the last problem has become solvable.

The group of TRINITI is engaged in activity of collection the data on rate constant of plasma-chemistry reactions within many years.

In the discharge plasma in electronegative gases, processes of an electron detachment may play the large role. Detachment of the electrons from negative ions may happen in their collisions with neutral particles (molecules and radicals), vibrational excited molecules and electronic excited atoms and molecules. The detachment processes can significantly change the balance of the electrons, in a great degree determine the shape of voltage-current characteristics, and result in development of various kinds of instability of the electrical discharge. The developed database on reactions with heavy particles is constantly supplemented by the data, appearing in the literature, on processes detachment of the electron from negative ions. The special attention was given to processes detachment from ions O^-, O_2^- and O_3^- as in collisions with various molecules and radicals, and with electronic excited molecules such as $O_2(a1\Delta_g)$, $O_2(b1\Sigma+_g)$. These processes are important for simulation of plasma-chemical processes in air and for modeling electrical discharge generators of oxygen in electronic state $O_2(a1\Delta_g)$.

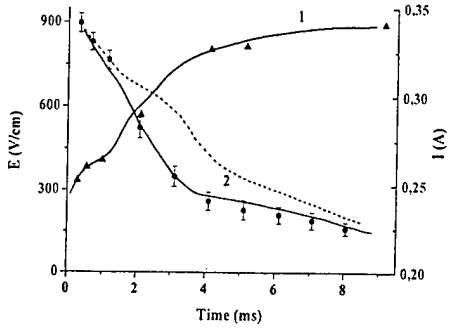

Fig. 1. Comparison of calculated electric field and current for self-sustained discharge in N_2 (line) with experimental data (markers). Dash-line shows results of calculations in a model ignoring processes of energy exchange between vibrational and electronic states [2].

3. Homogeneous model (0D)

The models with the self-consistent solution of the electron Boltzmann equation in parallel with kinetics equations for the excited and charged particles and radicals include up to 50÷300 equations and are to be solved numerically. Modeling of various new media of plasma chemistry reactor may require to do spelling and debugging of the new subroutines having some thousands operators. The basic advantage of the program developed by us, - automatic synthesizing of the necessary subroutines by using the reactions, written in a symbolic form, for electronic, molecular, ion and radiation kinetics, that reduces to a minimum expenses of time on programming and debugging a model of plasma chemical reactor.

In some situations, an energy exchange between vibration and electronic excited levels can be important. The special experiments with the control of uniformity of nitrogen plasma in electric discharge have confirmed a large role of vibrational excited molecules in a mechanism of growth of a discharge current [1]. The kinetic model developed for the nitrogen plasma including mechanisms of associative ionization with collisions electronic and/or vibrational excited molecules, satisfactorily describes experimental data on dynamic behavior of discharge parameters for rather various conditions. In particular, dynamic behavior of parameters for the self-sustained discharge with pressure 50 Torr [2] and instability development time for a discharge controlled by an electron beam, with

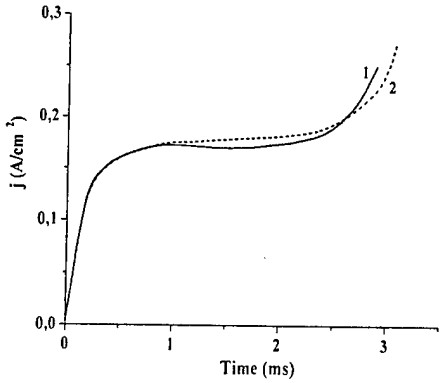

Fig. 2. Experimental (1) and calculated (2) dependence of current density of non-self-sustained discharge on time [3].

pressure 1 bar [3] were described with a high accuracy (fig. 1 - 2).

In work [4] the positive column of the glow discharge in a flow of gas from the chemical generator $O_2(a1\Delta_g)$ was studied. Experimentally it was found that for concentration $O_2(a1\Delta_g)$ 50 % and pressure 1.5 and 2 Torr an electrical field of

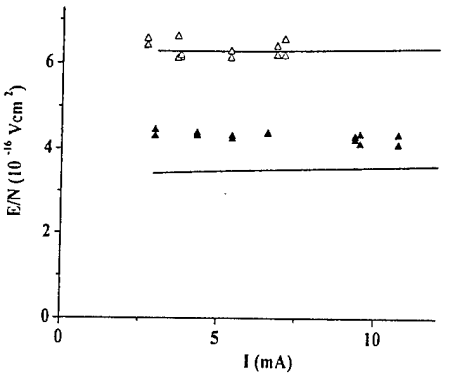

Fig. 3 Comparison between experimental values of the reduced electric field corrected for the gas heating with theoretically predicted values for oxygen at pressure 2 Torr for SDO content 0 (open marker) and 50% (solid marker) [4].

maintenance of the discharge is appreciably reduced in comparison with conditions, when 100 % of oxygen is in the ground state. The theoretical model of the glow discharge, developed by us, gives results well agreeing with an electrical field

reduction, observed in the experiment for the mixture with $O_2(a1\Delta_g)$ (fig. 3).

For modeling plasma-chemical processes taking place in the electrical discharge in dry and humid air with a high pressure P ~ 1 bar, in ref. [5] about 40 reactions with electron and 200 reactions with heavy particles were taken into account. For reactions of detachment and ion-ion recombination an effective temperature of ions plays an important role. It was estimated from the Wannier equation accounting heating of ions by an electric field of the discharge. In fig. 4, there are shown the calculated dependences of discharge voltage and current density (and also of its electronic and ionic components) on time of flight of the gas portion from a

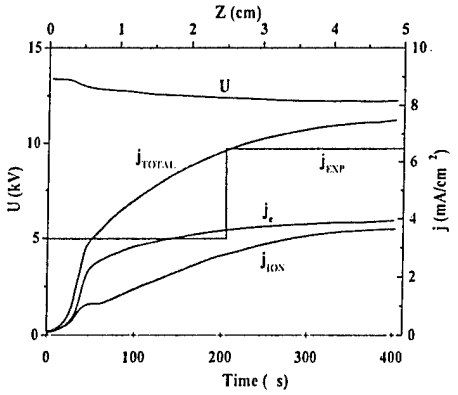

Fig. 4. Calculated electric characteristics of self-sustained discharge and experimentally measured current density on two 2.5-cm cathode sections in humid air [5].

discharge entrance down to an exit [5]. Experimentally measured currents through two identical cathode sections of 2.5 cm length each along gas flow are compared with theory in fig. 4.

4. Modeling a negative corona in air

A negative corona - low current discharge between the cathode (wire or needle) and flat anode is very widely used in an industry. Studying the negative corona between a needle and plane, G. W. Trichel has detected regular pulses of a current [6]. He has given a qualitative explanation to this phenomenon, which included such important feature, as effect of shielding by a cloud of positive ions near to the cathode. The role of negative ions practically was ignored. In the subsequent work [7], it was claimed, that the Trichel pulses exist only in electronegative gases and the role of negative ions, as trigger mechanism was allocated. It was emphasized also, that the time of drift of negative ions to the anode is appreciably longer than period of pulses.

The work [8] is most known, among theoretical discussions and contains the review of the old theories of this phenomenon. By numerical modeling including the solution of the one-dimensional equations of continuity for electrons, positive and negative ions together with the Poisson equation for an electrical field, it was possible to explain the form of a first pulse. The secondary emission under action of positive ions was ignored [8].

4.1. 1.5D model

The basis of the numerical model, created by us for corona discharge in air, form the known equations for a continuity of electron, positive and negative ions fluxes, and also Poisson equation and equation for the electric circuit with experimental parameters. Generally speaking, charged particle kinetics in air plasma is rather complex. Its complete description requires consideration of evolution of a plenty of components. However, earlier a simplified model was formulated [9] based on a complete kinetic model. This simplified model predicts the average characteristics of corona discharge of a thin wire in air at atmospheric pressure satisfactorily.

The key step, which has allowed us numerically to reproduce periodic Trichel pulses, consisted in the account of fast expansion of current channel along distance from the cathode to anode [10] (change of the area of the current channel was more than 10^4 times). The form of the current channel was chosen the same as in the experiment.

The detailed analysis of a nature and mechanisms of Trichel pulses, based on numerical modeling, was absent till publication [10]. 1.5D model for the first time has allowed one to reproduce the established sequence of Trichel pulses.

For the first time, complete dynamics of an establishment of Trichel pulses, starting from the first pulse, was described numerically in [11]. The process of transition of corona discharge to glow discharge was investigated numerically for

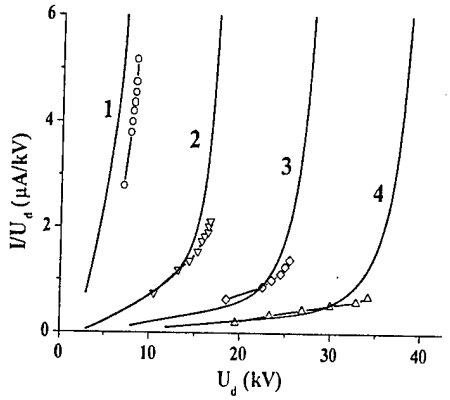

Fig. 5. Reduced voltage-current characteristics calculated and measured (markers) for multiple pin to plane electrode configuration. Pin radius curvature $R_P = 0.006$ cm; discharge spacing h is varied: 1, ○ - $h = 0.5$ cm; 2, ▽ - 1 cm; 3, ◇ - 1.5 cm; 4, △ - 2 cm [12].

two various electrode designs: a pin - plane and multi-pin cathode - plane. Fig. 5 shows comparison of calculated and experimentally measured reduced voltage-current characteristics for discharge with multi-pin cathode in air [12].

4.2. 3D model

The results of numerical modeling in a framework of 1.5D model with the fixed shape of the current channel reproduced not bad experimental data on voltage-current characteristics and repetition frequency, and also on an establishment of pulses in time [10-11]. However, derivation of the equations of 1.5D model is based on the assumptions, which not only cannot be proved, not addressing to exacter model, but also obviously are very approximate. The strict approach requires to use 3D numerical model, which in axi-symmetric geometry can be reduced formally to 2D model in variable radius - distance along a discharge axis.

To satisfy requirements of good discrete approximation calculations were carried out on non-uniform curvilinear grid, border of which was coordinated with a configuration of electrodes. As the form of the cathode can be in a large degree arbitrary, in algorithm the generator of grids, automatically fitting a grid to boundary conditions was applied. The developed numerical algorithm is conservative (keeps a complete current) for anyone curvilinear grid. However, convergence of iterations in above mentioned algorithm is as better, as closer curvilinear grid to the orthogonal one, and, hence, thus is higher speed of calculations [13]. Fig. 6 shows the establishment of a calculated with 3D model sequence of Trichel pulses.

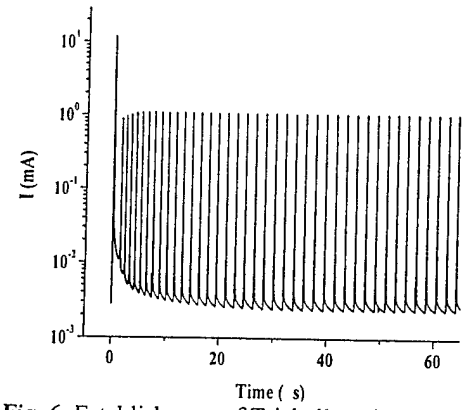

Fig. 6. Establishment of Trichel's pulses [13].

It is instructive to compare results obtained in [13] with results of modeling in framework 1.5D model in [10], where the structure of the current channel was set in advance, and the parameters were fitted so that the numerical results were close to experimental one. The shape of the current channel was supposed to be constant in time. The results of simulations, in which fit parameters are absent, show that, actually, the area of sharp gradients near to pin is much shorter (tens μm instead of hundreds), and the diameter of the current channel significantly changes in time. Nevertheless,

dynamics of the integrated characteristics of corona discharge in both models is similar. In details, however, there is an essential difference: 1.5D model [10] predicts formation of ionization wave along an axis of the discharge resulting in additional peak on the leading edge of a current pulse; 3D the model predicts formation of the cathode layer with the subsequent extension of it

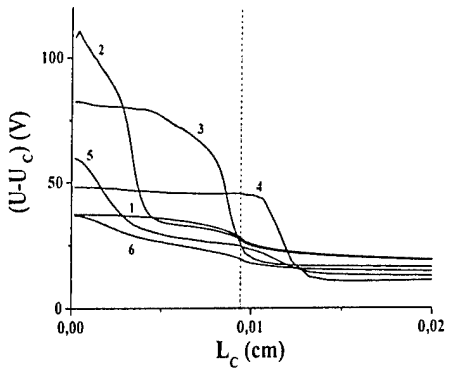

Fig. 7. Distribution potential along the line of numerical grid, lactated at distance 3 μm from cathode surface, at various time [13].

over the surface of the cathode (fig. 7). As in this model no any assumption is used, it is expected, that the scenario of the discharge development by a wave-like expansion of a cathode layer over the surface of the cathode is more correct.

5. Conclusion

The created databases of cross sections of electrons scattering on atoms and molecules, of rate constants for ion-molecule reactions and numerical models for the simulation plasma chemistry processes allow us to describe the characteristics of the homogeneous discharge in nitrogen, oxygen and air. For the first time, with the help of the 1.5D and 3D models it became possible to describe numerically the periodic sequence of current pulses in the negative corona discharge in air.

References

1. Napartovich A. P., Akishev Y. S., 1993, *Proceedings of XXI ICPIG*, **3**, 207, Bochum.
2. Berdyshev A. V., Kochetov I. V., Napartovich A.P., 1988, *Fizika Plazmy*, **14**, 742.
3. Berdyshev A. V., Golovin A. S., Gurashvili V. A. et al, 1989, *Fizika Plazmy*, **15**, 335.
4. Napartovich A. P., Kochetov I. V., Vagin N. P., et al, 2002, *Czechoslovak J. of Phys.*, **52**, A1.
5. Akishev Yu. S., Deryugin A. A., Karal'nik V. B. et al, 1994, *Plasma Phys. Rep.*, **20**, 511.
6. Trichel G. W., 1938, *Phys. Rev.*, **54**, 1078.
7. Loeb L. B., Kip A. F., Hudson G. G. et al, 1941, *Phys. Rev.*, **60**, 714.
8. Morrow R., 1985, *Phys. Rev. A*, **32**, 1799.
9. Akishev Yu. S., Deryugin A. A., Napartovich A. P., et al, Proc. of ICPIG-XXII. New Jersey. USA. 1995. Part 2, 147.
10. Napartovich A. P., Akishev Yu. S., Deryugin A. A., et al, 1997, *J.Phys.D: Appl. Phys.*, **30**, 2726.
11. Akishev Yu. S. Grushin M. Y., Kochetov I. V., et al, 1999, *Plasm. Phys. Rep.*, **25**, 922.
12. Akishev Yu. S., Grushin M. Y., Kochetov I. V., et al, 2000, *Plasm. Phys. Rep.*, **26**, 157.
13. 13. Akishev Yu. S., Kochetov I. V., Loboiko A. I., Napartovich A. P., 1998, *International Symposium on High Pressure, Low Temperature Plasma Chemistry*, Hakone VI, 308.

MHD GENERATOR WITH NONEQUILIBRIUM CONDUCTIVITY TO CONTROL SCRAMJET PERFORMANCE

A.L. Kuranov, E.G. Sheikin

Hypersonic Systems Research Institute, St. Petersburg, Russia

Nowadays "AJAX" concept is a very popular concept of hypersonic aircrafts development. It includes some basic technologies [1], one of which is based on using of MHD systems on the vehicle. It was shown in [2-4] that MHD interaction allows one to increase air mass flow rate at off-design conditions, to increase flow compression in inlet and to increase specific impulse and thrust of scramjet. Here we consider scramjet with MHD control by internal flow which, according to [4, 5], allows us to increase scramjet specific impulse. Quasi-1D approach is used to analyze the MHD interaction effect on scramjet performance. The simplified scheme of the propulsion is shown in the Fig.1. Numerical subindexes used below correspond to cross-sections denoted in the Fig.1. Frequently used names for scramjet with MHD control are the Magneto-Plasma-Chemical Engine (MPCE) (historically the first appellation for the propulsion) [5] and scramjet with MHD-bypass of energy [6].

In order to realize MHD interaction it is necessary to ensure the appreciable electric conductivity of flow. At conditions of scramjet as a rule equilibrium conductivity of a flow upstream the combustion chamber is negligible to produce essential MHD interaction. Thus it is necessary to put some energy into flow to create nonequilibrium flow conductivity. It is evidently that MHD generator with nonequilibrium conductivity can be realized only in that case, when power spent on flow ionization does not exceed power produced by MHD generator. Such operating mode of system including MHD generator and ionizer we name as a self-sustained mode. Power spent on flow ionization depends on the value of conductivity need to be created, gas-dynamic properties of flow and type of ionizer [3, 7]. Power produced by MHD generator depends on the flow conductivity, gas-dynamic properties of flow, MHD parameters and type of MHD generator. Thus conditions at which the self-sustained operational mode can be realized depend upon many factors, such as: location of MHD generator on the vehicle, geometry of scramjet, flight path of the vehicle, MHD parameters, type of ionizer and so on.

MHD generator with nonequilibrium conductivity for scramjet applications was investigated in papers [2,4,7,8]. To analyze scramjet with MHD control we use model of MHD generator from [4] which allows us essentially simplify analysis of the complex system. Regime of MHD flow in the model is determined by ξ parameter which is proportional to static pressure longitudinal gradient. Simple relations for calculation of ionization fraction in air plasma sustained by e-beam from [8] are used for calculation of flow conductivity σ as a function of parameters of flow and the power density spent on flow ionization q_i. In [2,8] it is shown that for a given value of magnetic induction B there is some critical value for power density spent on ionization $q_i=q_{cr}$ at which power density produced by MHD generator q_g is equal to q_i. Self-sustained operational mode for nonequilibrium MHD generator ($q_g \geq q_i$) is realized when $q_i \leq q_{cr}$.

Fig.2 demonstrates relative power characteristics both for Faraday and Hall MHD generators with nonequilibrium conductivity. The factor $\eta_g=W_g/W_0$ is relative power produced by MHD generator (W_g is the power produced by MHD generator, W_0 is the total flow enthalpy). The factor $\eta_{ion}=W_{ion}/W_0$ is the relative power spent on flow ionization (W_{ion} is the power spent on flow ionization). The difference $\eta_g-\eta_{ion}=(W_g-W_{ion})/W_0$ determines

the so-called relative power excess which characterizes real power produced by MHD generator with nonequilibrium conductivity. One can see that at some magnitude of MHD interaction parameter $S_v=\sigma B^2 L/\rho v$ the η_g and η_{ion} values become equal. So, self-sustained operational mode for MHD generator with nonequilibrium conductivity is limited not only by parameters of ionizer and magnetic system, but also by the length of the MHD generator. Points in the Fig.2 mark the limiting values of MHD interaction parameter. As it follows from Fig.2 the limiting MHD interaction parameter for Hall MHD generator is less than for Faraday one.

In the calculations it was supposed that power density q_i spent on ionization is constant in the volume of MHD generator. According to [2] e-beam current density j_b, electron energy E_b and gas density ρ determine q_i value by the ratio: $q_i = (j_b/e)\rho Y(E_b)$, where e is the charge of electron and Y is the electron stopping power. So by varying parameters j_b and E_b along the channel of MHD generator we can realize both any distribution of q_i along the channel length and keep q_i constant if it is necessary.

Fig.3 shows relative power excess produced by Faraday MHD generator with a constant cross-sectional area (a) ($\xi_1=\tilde{\xi}$ which is determined in [4]) and with a constant pressure along the channel (b) (ξ=0). One can see that regime ξ=0 is more preferable regime for power production. While increasing the Mach number at MHD generator entrance the power excess increases too in both regimes. Here we consider two simple regimes for assignment of q_i distribution: q_i=const and j_b=const (E_b is fixed). As it follows from Fig.3a the ionizer with a constant power density spent on ionization provides more power excess than ionizer with a constant e-beam current density in MHD generator with $\xi=\tilde{\xi}$. For MHD generator with $\xi=0$ the tendency is contrary.

To choose preferential regime of flow in MHD generator which implements flow control in scramjet we compare specific impulses of scramjet with MHD control for various values of ξ_1 factor. Model for scramjet with MHD control developed in [4,8] is used in calculations. Relative values of specific impulse for scramjet with MHD control (namely specific impulse of "MHD scramjet" divided by specific impulse of classical scramjet) as a function of the enthalpy extraction ratio are shown in the Fig.4a. One can see that increase of factor ξ_1 causes the scramjet specific impulse to be increased. Fig.4b demonstrates dependency of relative power spent on ionization $r=W_{ion}/W_g$ as a function the enthalpy extraction ratio η_g. While increasing the ξ_1 the factor r rise take place. The flow regime characterized by minimal ξ_1 is preferable if MHD generator with nonequilibrium conductivity is considered as a power source. Requirements for ξ_1 parameter in the case when MHD generator is used for scramjet control are opposite. In this research we consider possibilities of nonequilibrium MHD generator for flow control and so maximal realizable factor ξ_1 is required. Factors $\xi_1>\tilde{\xi}$ correspond to convergent channel and undesirable to avoid additional shock waves. So hereinafter we will consider MHD flows characterized by factor $\xi_1=\tilde{\xi}$, which approximately describes MHD generator with constant cross-sectional area.

Various regimes of power spending on ionization of flow are compared in the Fig.5. One can see that ionization regime with a constant power density spent on ionization gives us opportunity to reach greater values of specific impulse and power excess than the regime with a constant e-beam current density. This tendency is correct both for Faraday and Hall MHD generators. So hereinafter we will consider the regime with a constant power density spent on ionization.

By analyzing the scramjet with MHD control in [8] were obtained analytical relations which impose restrictions on the system parameters at which MHD

interaction increase specific impulse of scramjet. In particular the inequality (1), which is presented below, prescribes the range of variation of subsystems parameters for scramjet with MHD control by using MHD generator with a constant cross-sectional area:

$$\gamma - 1 + \frac{\gamma + 1/\psi}{M_1^2 - 1} > \frac{T_1}{\Delta T} \cdot \left[1 + \frac{\delta}{\psi} \right] \qquad (1)$$

where γ is specific heat ratio, T_1 and M_1 are temperature and Mach number at the entrance of MHD generator, ΔT is the temperature increase in the combustion chamber, $\delta = \left(1 - (1-r)/k_3\right)$, r is relative power density spent on flow ionization, $\psi = 1/k_1 - 1$ for Faraday MHD generator or $\psi = \left(1 + \beta^2 k_1^2\right) / \left(\beta^2 k_1 (1 - k_1)\right)$ for Hall MHD generator, k_1 and k_3 are the load factors for MHD generator and MHD accelerator, β is the Hall parameter.

As a result of the inequality (1) analysis one can obtain limitations on flight Mach number at which MHD interaction causes the scramjet specific impulse to be increased. Fig.6 shows dependencies of maximal flight Mach number upon factor δ for various values of ψ factor. MHD interaction increases specific impulse of scramjet in the case when flight Mach number is less than the maximal flight Mach number: $M_\infty < M_{max}$. The factor δ mainly characterizes relative power spent on flow ionization. In situation when power spent on ionization is equal to zero (initially ionized flow) $\delta = 0$. Factor $\delta = 1$ describes situation for which whole of power produced by MHD generator is spent on flow ionization. It is evidently that while increasing the factor δ the M_{max} is decreasing. Decrease of the total turning angle θ_N causes the maximal Mach number M_{max} to be increased. At small value of δ, minimization of ψ factor provides expansion of range of Mach number at which MHD interaction improves scramjet performance. Contrary at $\delta \approx 1$ increase of ψ factor causes the M_{max} to be increased.

Fig.7 demonstrates how specific impulse of scramjet with Faraday nonequilibrium MHD generator depends on the MHD interaction parameter S_v and on the load factor k_1. It follows from Fig.7 that maximal specific impulse of scramjet with MHD control for considered conditions can be achieved in the range of variation of MHD interaction parameter $0.3 < S_v < 0.7$ and load factor $0.15 < k_1 < 0.45$.

Fig 8 demonstrates relative specific impulse of scramjet with MHD control and power excess produced by MHD generator with nonequilibrium conductivity depending on the magnetic induction and on the power density spent on ionization. One can see that there are optimal values of power density q_i at which required both specific impulse and power excess can be achieved at minimal value of magnetic induction.

As it follows from the Fig.9-10 optimal value of the load factor for specific impulse differ from one for power excess. Maximal power excess is achieved at $k_1 \approx 0.5$ both for case with given power density spent on ionization (Fig.9) and case with given magnetic induction (Fig.10). As for specific impulse its maximal values can be achieved at the load factors, which are essentially less than 0.5.

Obtained results show that MHD generator with nonequilibrium conductivity can be used on hypersonic aircraft both for electric power production and for scramjet specific impulse increasing. Requirements for parameters of the MHD generator depend on its functionality.

Acknowledgements

This work was supported by EOARD, ISTC grant № 2088p.

References

1. Kuranov A.L., Korabelnicov A.V., Kuchinskiy V.V., and Sheikin E.G., Fundamental techniques of the "AJAX" concept. Modern state of research, AIAA paper 2001-1915

2. Brichkin D.I., Kuranov A.L., and Sheikin E.G. MHD-technology for scramjet control, AIAA Paper 98-1642
3. Brichkin D.I., Kuranov A.L., and Sheikin E.G. The potentialities of MHD control for improving scramjet performance, AIAA Paper 99-4969.
4. Kuranov A.L., Kuchinskiy V.V., and Sheikin E.G., Scramjet with MHD control under "AJAX" concept. Requirements for MHD systems, AIAA paper 2001-2881
5. Fraishtadt V.L., Kuranov A.L., and Sheikin E.G. Use of MHD systems in hypersonic aircraft, Technical Physics, 1998,**43**, 1309
6. Park C., Bogdanoff D.W., and Mehta U.B. Theoretical Performance of a Nonequilibrium MHD-Bypass Scramjet, AIAA Paper 2001-0792.
7. Macheret S.O., Shneider M.N., and Miles R.B., Potential performance of supersonic MHD power generators, AIAA paper 2001-0795
8. Kuranov A.L., and Sheikin E.G. MHD control on hypersonic aircraft under "AJAX" concept. Possibilities of MHD generator, AIAA Paper 2002-0490

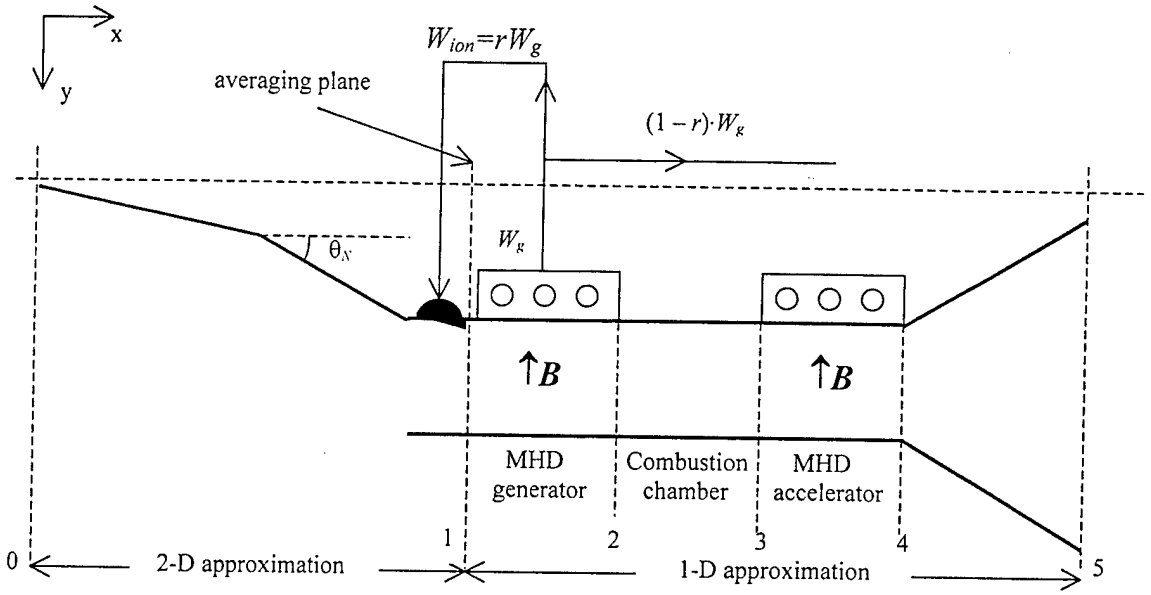

Fig.1. The simplified scheme of scramjet with MHD control by internal flows for investigation in quasi-1D approach.

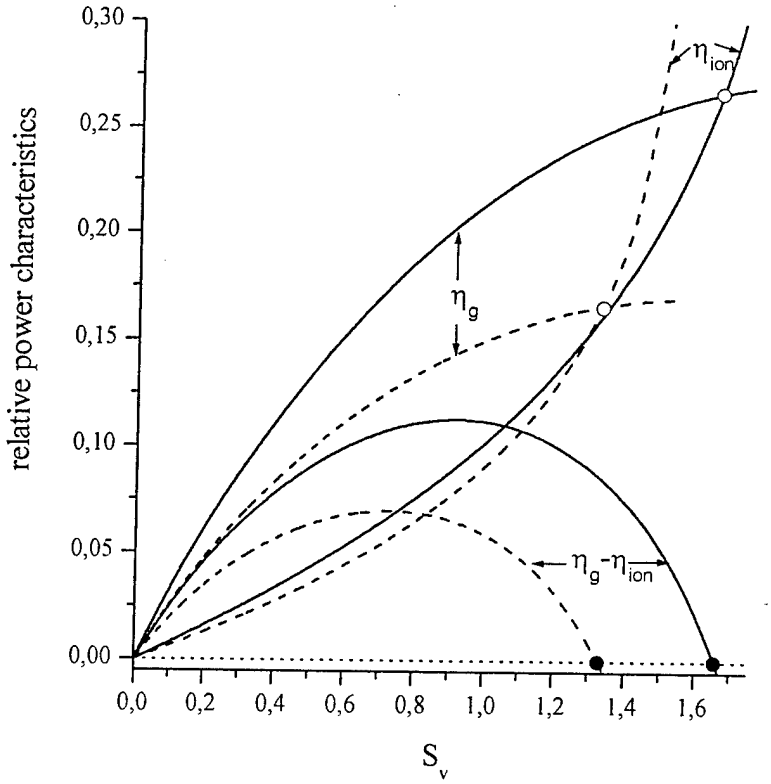

Fig.2 Relative power characteristics of MHD generator with nonequilibrium conductivity as a function of MHD interaction parameter. Solid curves for Faraday MHD generator and dashed curves for Hall MHD generator with β=2. M_i=3.3, (q_i – constant) q_i/q_{cr}=0.05, ξ=0.5, k=0.5.

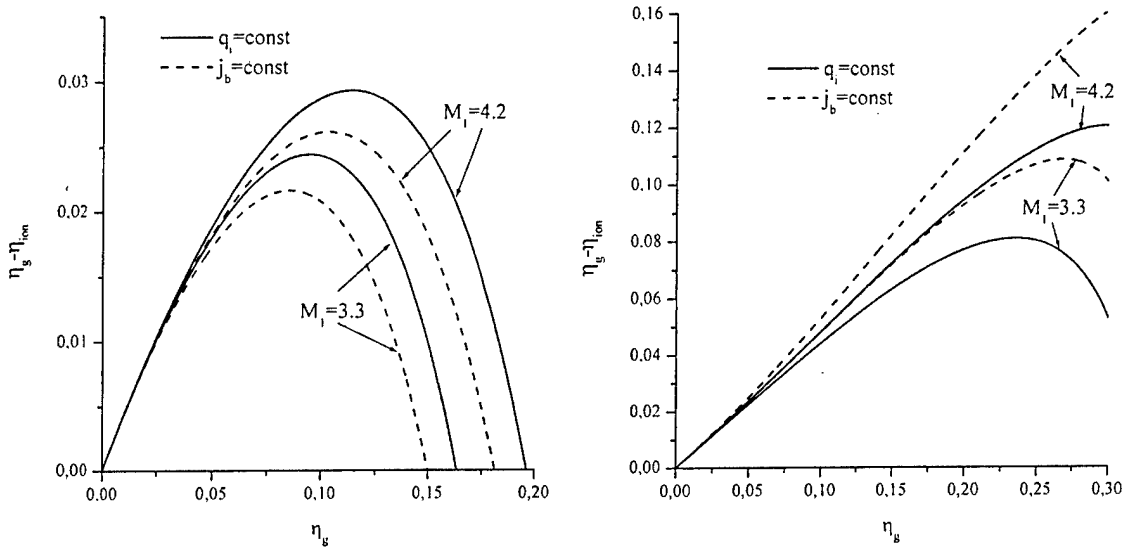

a) b)

Fig.3 Relative power excess produced by Faraday MHD generator with nonequilibrium conductivity: k=0.5, q_i=const for solid lines j_b=const for dashed lines. Mach number at MHD generator entrance is shown near the curves, q_1/q_{cr}=0.3. a) $\xi = \tilde{\xi}$, b) ξ=0

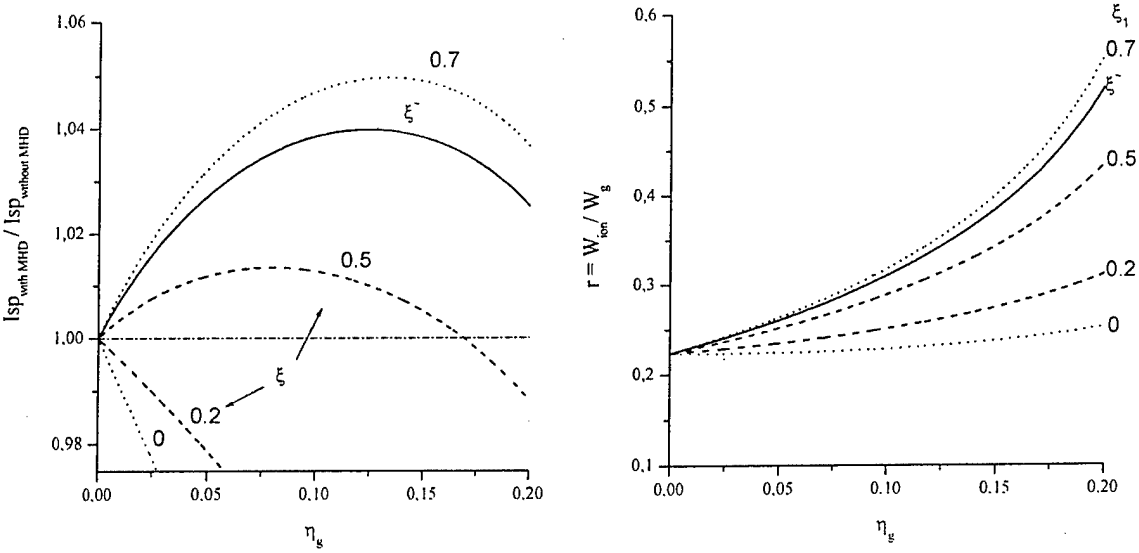

a) b)

Fig.4 Relative specific impulse (a) and relative power spent on ionization (b) for MHD generator with various parameters ξ_1. θ_N=15°, M_d=10, F_{th}=0.12, M_0=6, q_i/q_{cr}=0.05, power density q_i is constant in MHD generator volume.

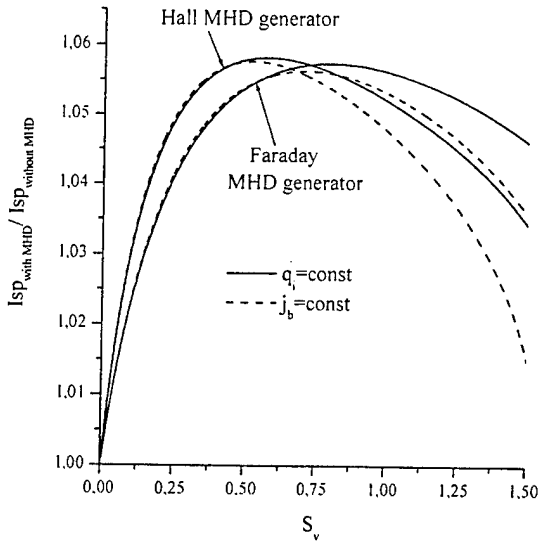

a)

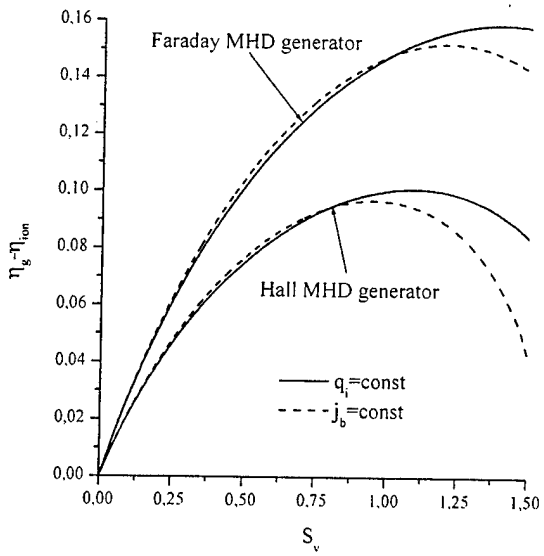

b)

Fig.5 Relative specific impulse (a) and relative power excess (b) vs. MHD interaction parameter for scramjet with Faraday and Hall MHD generators. Solid lines correspond to constant power density spent on ionization; dashed lines correspond to constant density of e-beam current. θ_N=15°, M_d=10, F_{th}=0.12, M_0=6, q_i/q_{cr}=0.01, k_I=0.5

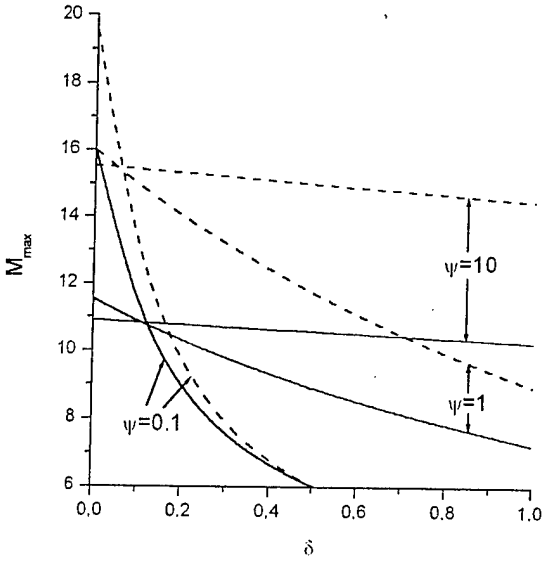

Fig.6 Maximal Mach number for various values of ψ factor, for two inlet with θ_N=15° (solid lines) and θ_N=10° (dashed lines), M_d=10, F_{th}=0.12.

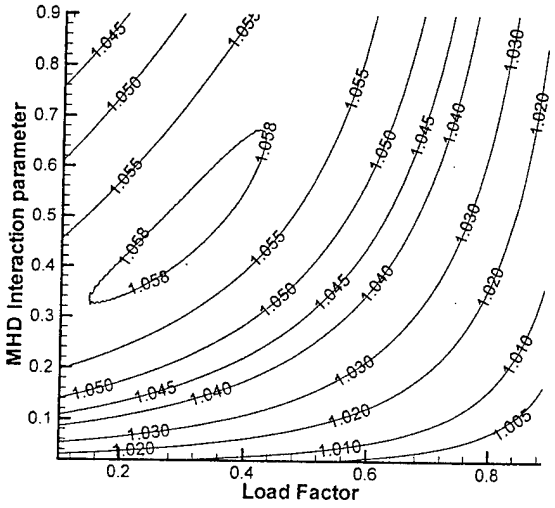

Fig.7 Contours of relative specific impulse for scramjet with MHD control with θ_N=15°, M_d=10, F_{th}=0.12. M_0=6, q_i/q_{cr}=0.01.

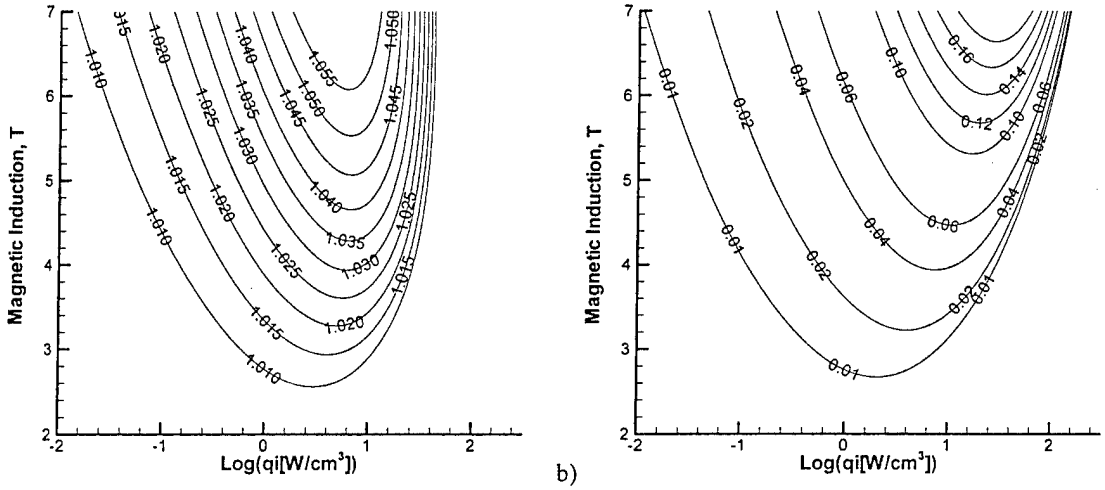

Fig.8 Contours of relative specific impulse (a) and power excess (b) for scramjet with MHD control with θ_N=15°, M_d=10, F_{th}=0.12. M_0=6, L=2m, k_1=0.5, k_3=1.1

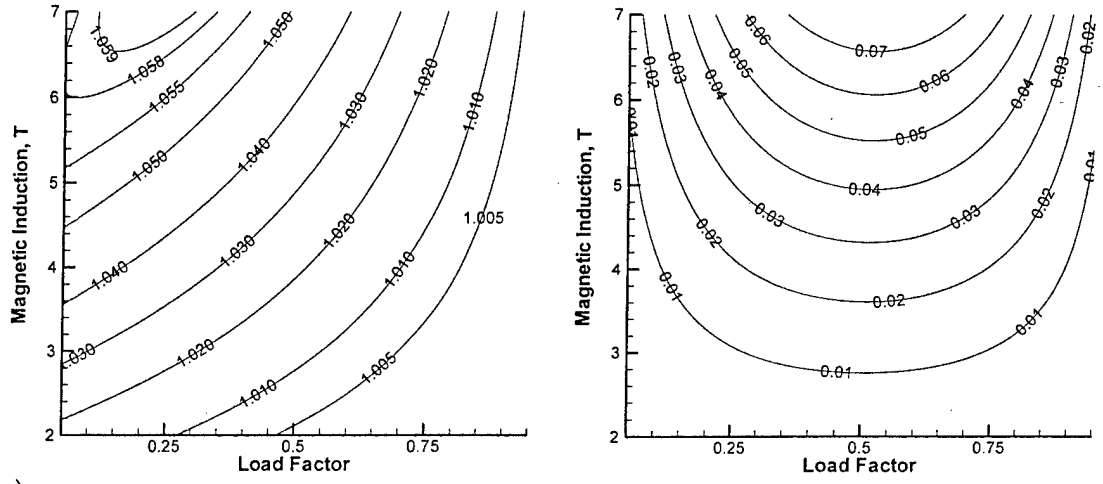

Fig.9 Contours of relative specific impulse (a) and power excess (b) for scramjet with MHD control with θ_N=15°, M_d=10, F_{th}=0.12. M_0=6, L=2m, k_3=1.1, q_i=1W/cm³

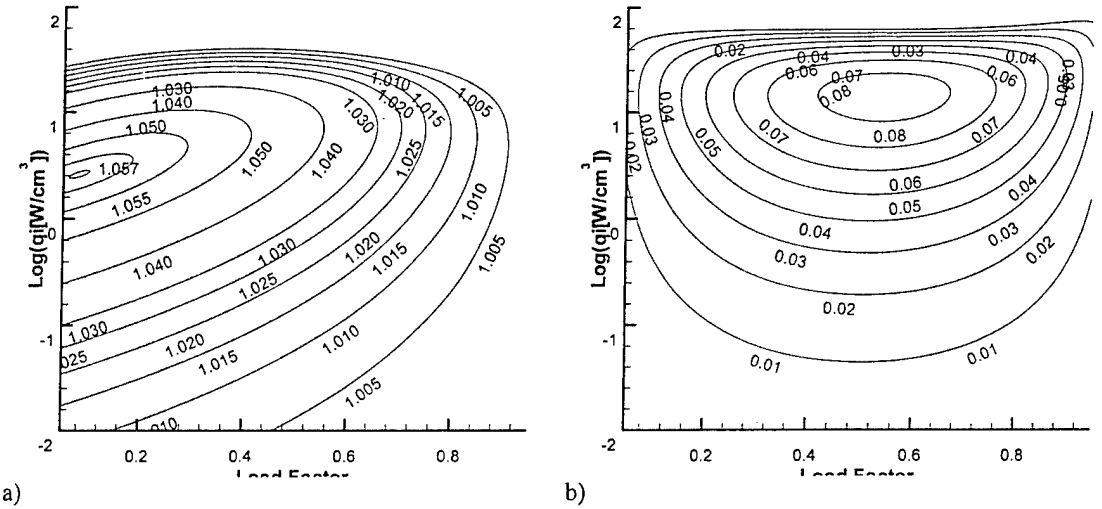

Fig.10 Contours of relative specific impulse (a) and power excess (b) for scramjet with MHD control with θ_N=15°, M_d=10, F_{th}=0.12. M_0=6, L=2m, k_3=1.1, B=5T

Faraday vs Hall MHD generator?

MHD CONTROL BY EXTERNAL FLOW IN SCRAMJET INLET

A.L. Kuranov, E.G. Sheikin

Hypersonic Systems Research Institute, St. Petersburg, Russia

Potentialities of MHD control to modify flow field in scramjet inlet are considered in [1-5]. It is shown in [3,4] that at flight Mach number M_∞ greater than design Mach number M_d MHD control allows us to modify the flow field in inlet in such a way that it becomes like a flow field at design conditions. In situation when $M_\infty < M_d$ MHD control can be used to increase air mass-flow rate in scramjet [1,2,5]. In this paper we consider possibilities of MHD generator with nonequilibrium conductivity to control flow-field and to increase flow compression in scramjet inlet at off-design conditions. Power spent on flow ionization, shape and length of plasma formation, direction and intensity of magnetic field are considered as parameters which can be arbitrarily varied. The aim of the work is to determine how the parameters influence on performance of MHD controlled inlet. It will allow us to understand what configuration of MHD interaction need to be developed in order to obtain desirable effect in MHD controlled inlet.

Flow-field in MHD-controlled inlet of scramjet is calculated in two-dimensional Euler approach in the model described in [5]. Scramjet inlet with design Mach number M_d=10, total turning angle θ_N=15° and relative value of inlet throat F_{th}=0.12 is considered in calculations. Magnetic field is supposed to be homogeneous. It is characterized by two parameters: modulus of magnetic induction $B \equiv |\vec{B}| = \sqrt{B_x^2 + B_y^2}$ and angle of magnetic field orientation α ($B_x = B \cdot \cos(\alpha)$, $B_y = B \cdot \sin(\alpha)$). It is supposed that electrodes of MHD generator are located in the plane of the figure at coordinates z=- and z= . MHD generator is characterized by the load factor k. Flow conductivity depends upon the power density spent on flow ionization q_i and flow parameters [5].

The Fig.1 demonstrates possibilities of MHD interaction, which is located in the range $0 \le x \le 0.5$, to modify flow field in scramjet inlet. Fig.1a shows Mach number contours in inlet at off-design conditions without MHD interaction at flight Mach number M_∞=12. In this case, unlike to design conditions the oblique shocks intersection occurs not in cowl lip. Increase of power density spent on ionization (Fig.1 b-d) causes the oblique shocks angles to be increased. When q_i=0.022 W/cm^3 oblique shocks are intersected in the cowl lip and flow field becomes quite similar to design configuration. When q_i becomes greater than 0.022 W/cm^3 (Fig.1d) the flow field becomes similar to situation with the flight Mach number is less than design one (Fig.3a).

In the Fig.2a MHD interaction is realized in the range 3≤x≤3.5. In this situation oblique shocks intersection occurs not exactly in cowl lip. But the point of shocks intersection is nearer to cowl lip than in the case without MHD interaction (Fig.1a). In the Figs.2b-c MHD interaction is realized in the range with 3≤x≤4 and y≤0.7. When magnetic field is orthogonal to x-axis (α=90°) the shocks intersection occurs not exactly in cowl lip (Fig.2b). But in changing the magnetic field orientation (α=45°) point of oblique shocks intersection moves to cowl lip (Fig.2c). Fig.2d corresponds to ionized range located in $0 \le x \le 5$ and $y \le 0.2 \cdot x$. One can see that in this case the flow field is quite similar to the flow field at design conditions.

Flow field in scramjet inlet in situation when $M_\infty < M_d$ is shown in the Fig.3a. Fig.3b-d demonstrate Mach number contours in MHD controlled inlet for three various configurations of magnetic field with magnetic induction B=1T. Level of MHD interaction corresponding to these figures is not very strong. The angles of

oblique shocks slightly increase for $\alpha \leq 90°$. For $\alpha=135°$ shock wave positions is practically not changed.

Results presented in the Fig.4-5 show that at given region of MHD interaction in inlet the air capture and the flow compression noticeably depend on the orientation of magnetic field and on the value of the load factor. Here φ is air mass flow rate in MHD controlled inlet, φ_0 is air mass flow rate in the inlet without MHD interaction. Similarly π is the pressure increase in MHD controlled inlet and π_0 is the pressure increase in the inlet without MHD interaction.

Fig.6-9 demonstrate that shape and position of ionized region noticeable influence on the air capture and on the flow compression in MHD controlled inlet. One can see that positions of ionized region optimal for increasing the flow compression are slightly differ from positions optimal for increasing the air mass flow rate.

As it follows from Fig.10 there are optimal values of magnetic induction, depending on the power density spent on flow ionization, at which air mass flow rate in MHD controlled inlet achieve maximum. The optimal magnetic induction decreases while increasing the q_i. The Fig.11 demonstrate that the flow compression achieves a maximal value at some optimal magnetic induction and the optimal value of magnetic induction is decreasing function of q_i value similarly to air mass flow rate. The maximal flow compression in the inlet is achieved at maximal power density spent on ionization. Thus both the power density spent on ionization and the value of magnetic induction are important parameters, which determine characteristics of MHD controlled inlet.

Obtained results show that MHD control allows us to modify flow field in inlet of scramjet at off-design conditions. By using MHD influence on flow we can control oblique shocks position, air mass flow and flow compression in inlet. In proper choice of region of MHD interaction, configuration of magnetic field and load factor the MHD control in scramjet inlet allows us essentially improve inlet performance at off-design conditions.

Acknowledgements

This work was supported by EOARD, ISTC grant № 2088p.

References

1. Brichkin D.I., Kuranov A.L., and Sheikin E.G. MHD-technology for scramjet control, AIAA Paper 98-1642
2. Brichkin D.I., Kuranov A.L., and Sheikin E.G. The potentialities of MHD control for improving scramjet performance, AIAA Paper 99-4969.
3. Golovachev Yu.P., Suschikh S.Yu., "Weakly Ionized Flows in Supersonic Inlets Subjected to the External Electromagnetic Fields," in Perspectives of MHD and Plasma Technologies in Aerospace Applications, IVTAN, Moscow, March 24-25, 1999, Proceedings, p.105
4. Macheret S.O., Shneider M.N., and Miles R.B., "External Supersonic Flow and Scramjet Inlet Control by MHD with Electron Beam Ionization," AIAA Paper 2001-0492
5. Kuranov A.L., and Sheikin E.G. MHD control on hypersonic aircraft under "AJAX" concept. Possibilities of MHD generator, AIAA Paper 2002-0490

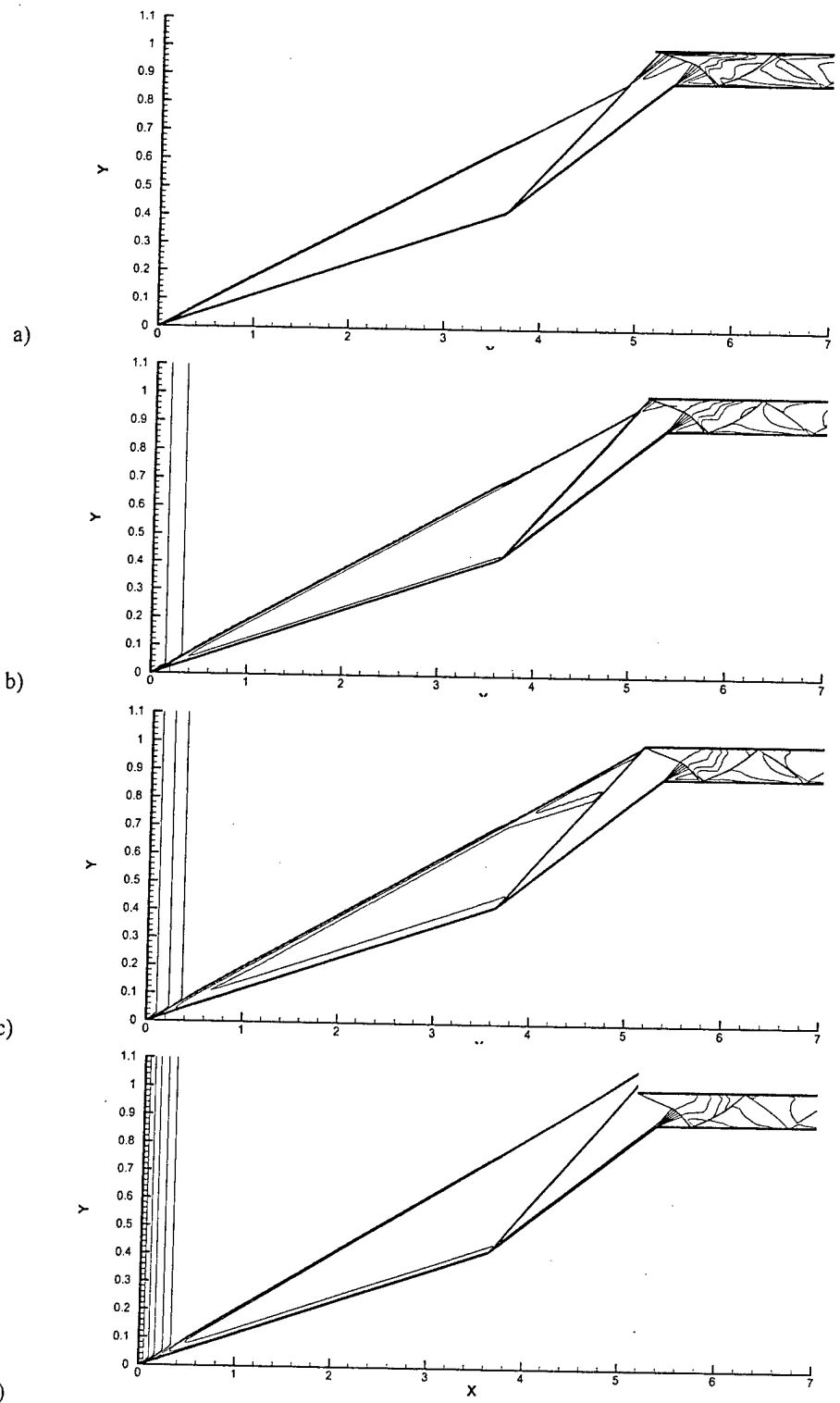

Fig.1. Mach number contours in MHD controlled inlet. M_0=12, M_d=10, B=1T, α=90°, k=0.5. Ionized region located in 0≤x≤0.5, $q_i[W/cm^3]$=a) 0, b)0.01, c) 0.022 d) 0.1

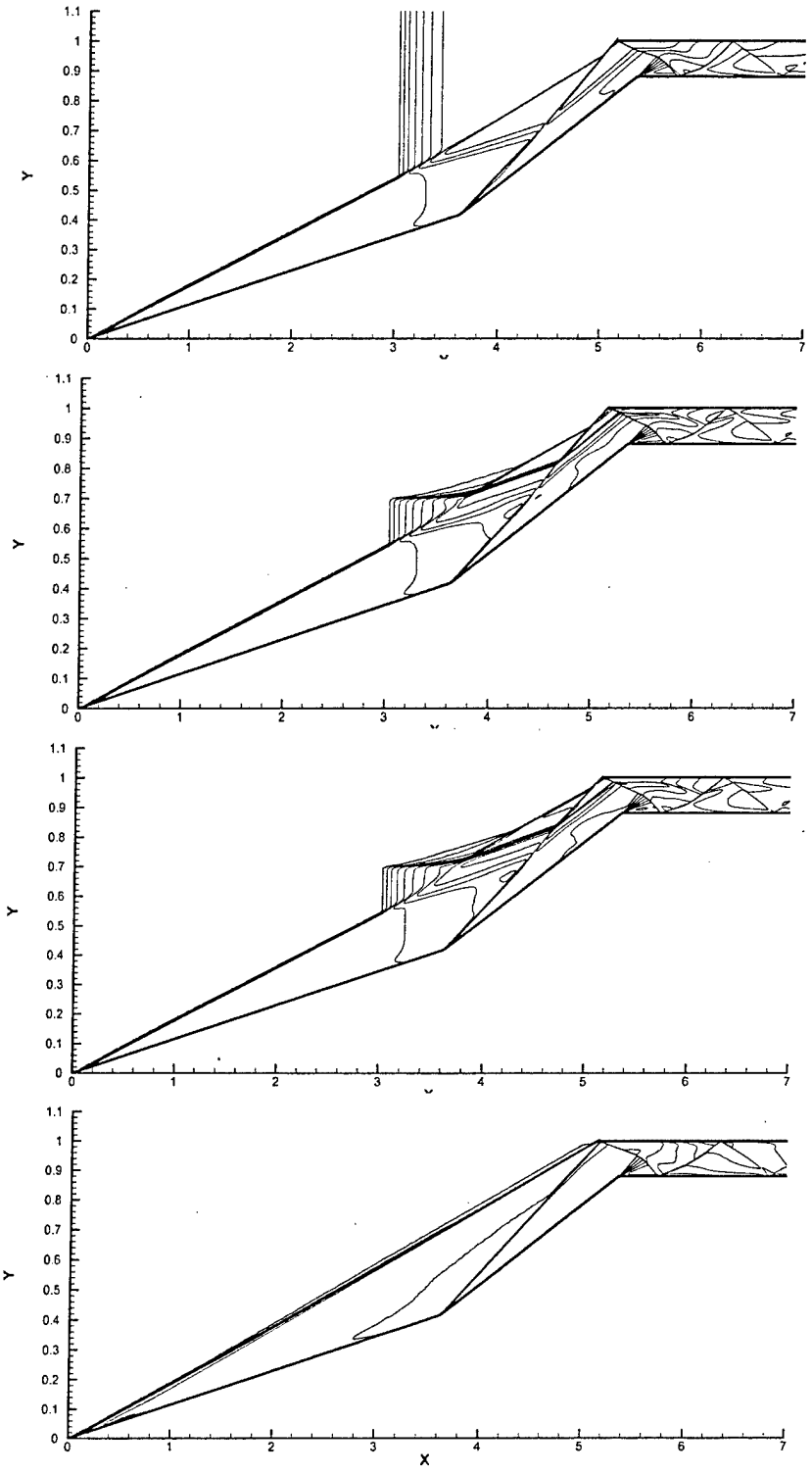

Fig.2. Mach number contours in MHD controlled inlet. M_0=12, M_d=10, B=1T, k=0.5.
Ionized region a) 3≤x≤3.5; b) and c) 3≤x≤4, Y≤0.7; d) 0≤x≤5, Y≤0.2x; α=90° in (a,b), α=45° in (c,d); $q_i[W/cm^3]$=a) 0.2, b) 0.2, c) 4.5, d) 1.2.

a)

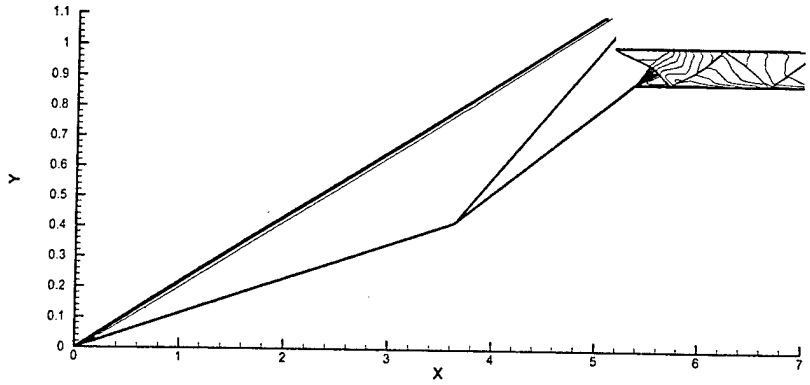

b)

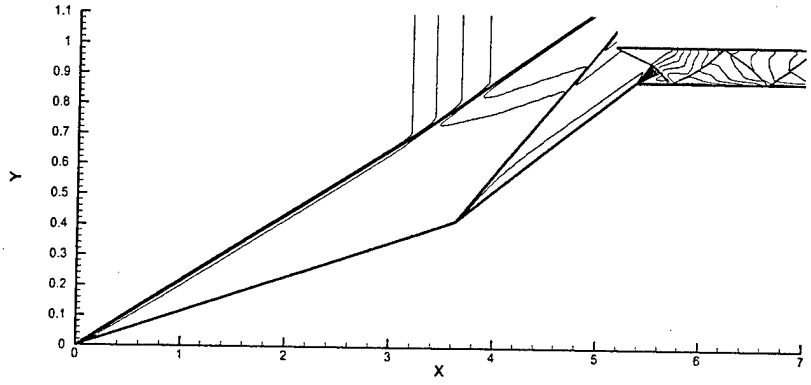

c)

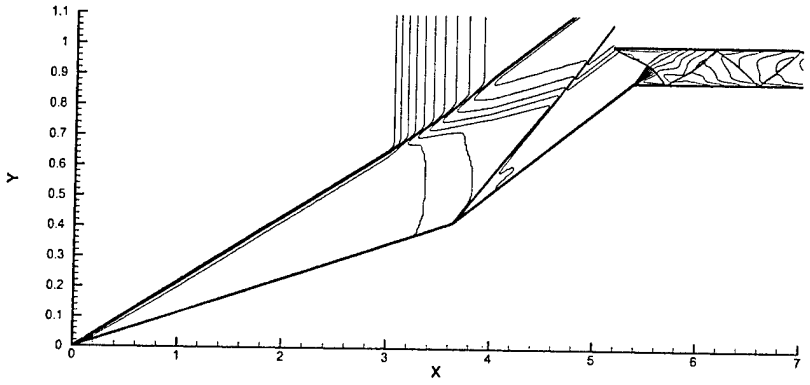

d)

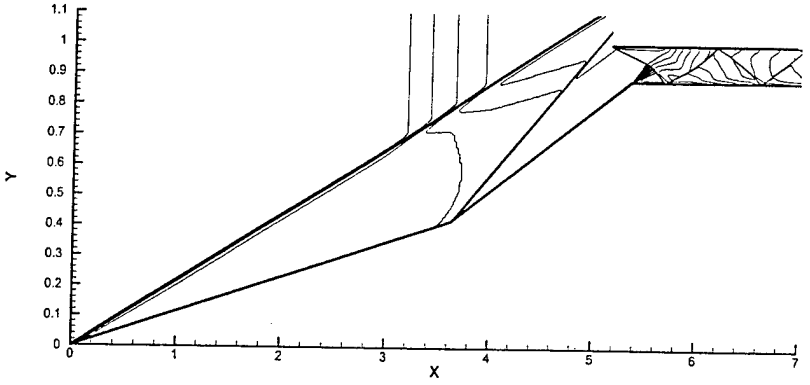

Fig.3. Mach number contours in MHD controlled inlet. M_0=8, M_d=10:
B=0 (a) B=1T, k=0.5, q_i=1W/cm^3 (b-d).
Ionized region is located in $3 \le x \le 4$; b) α=45°, c) α=90°, d) α=135°.

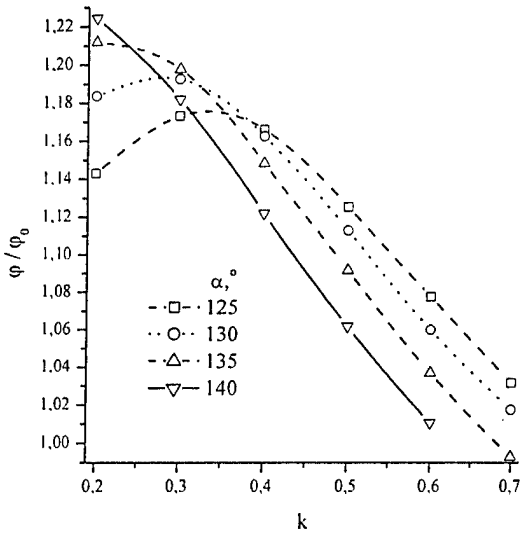

Fig.4. Normalized air mass flow rate in MHD controlled inlet vs load factor for various α. M_0=6, M_d=10B=3T, q_i=1W/cm^3.

Ionized region is located in $3 \le x \le 4$.

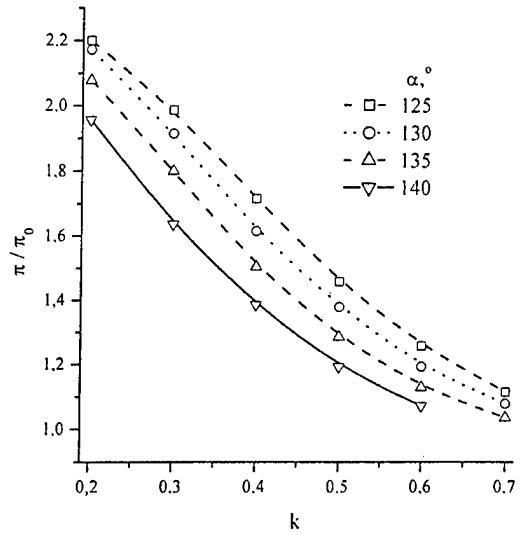

Fig.5. Relative pressure increase in MHD controlled inlet vs load factor for various α. M_0=6, M_d=10, B=3T, q_i=1W/cm^3.

Ionized region is located in $3 \le x \le 4$.

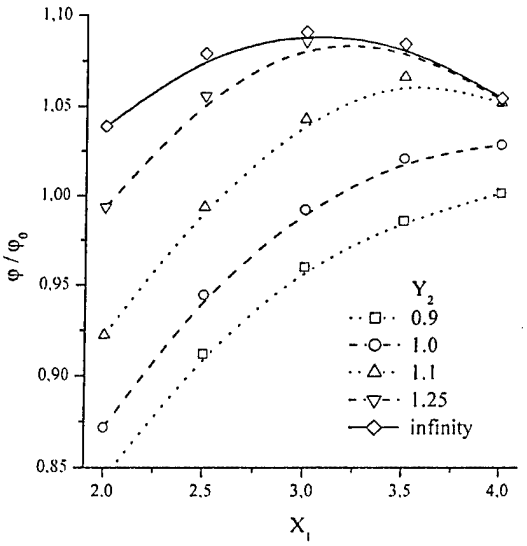

Fig.6 Normalized air mass flow rate in MHD controlled inlet vs X_1 for various height of ionized region Y_2. M_0=8, M_d=10, B=3T, α=135°, q_i=0.1W/cm^3, k=0.5. Ionized region is located in $X_1 \le x \le X_1+1$ and $y \le Y_2$

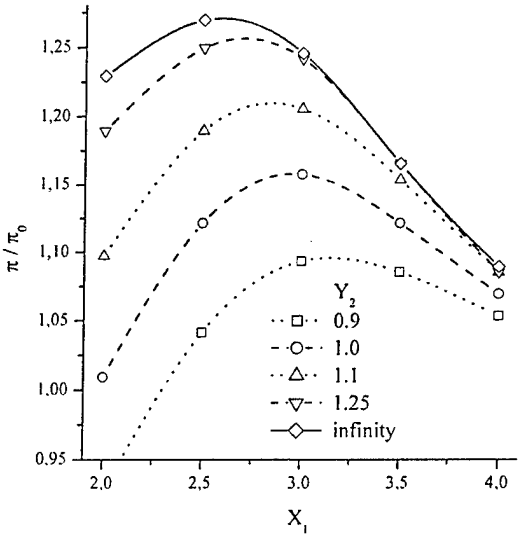

Fig.7. Relative pressure increase in MHD controlled inlet vs X_1 for various height of ionized region Y_2. M_0=8, M_d=10, B=3T, α=135°, q_i=0.1W/cm^3, k=0.5. Ionized region is located in $X_1 \le x \le X_1+1$ and $y \le Y_2$

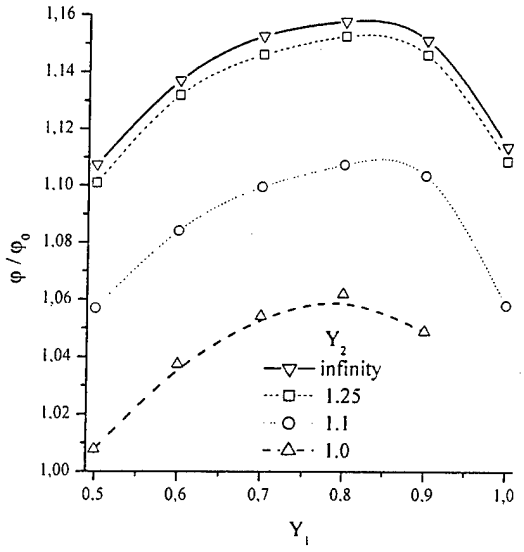

Fig.8 Normalized air mass flow rate in MHD controlled inlet vs Y_1 for various values of Y_2. M_0=8, M_d=10, B=3T, α=135°, q_i=0.1W/cm^3, k=0.5. Ionized region is located in $3 \le x \le 4$ and $Y_1 \le y \le Y_2$

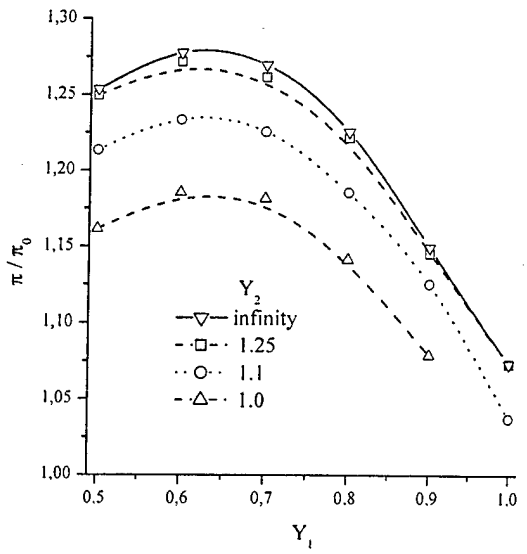

Fig.9. Relative pressure increase in MHD controlled inlet vs Y_1 for various values of Y_2. M_0=8, M_d=10, B=3T, α=135°, q_i=0.1W/cm^3, k=0.5. Ionized region is located in $3 \le x \le 4$ and $Y_1 \le y \le Y_2$

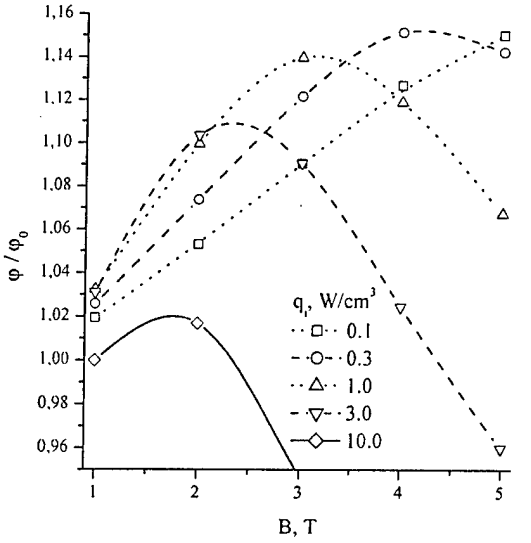

Fig.10. Normalized air mass flow rate in MHD controlled inlet vs magnetic induction B for various values of q_i. M_0=8, M_d=10, α=135°, k=0.5. Ionized region is located in $3 \le x \le 4$.

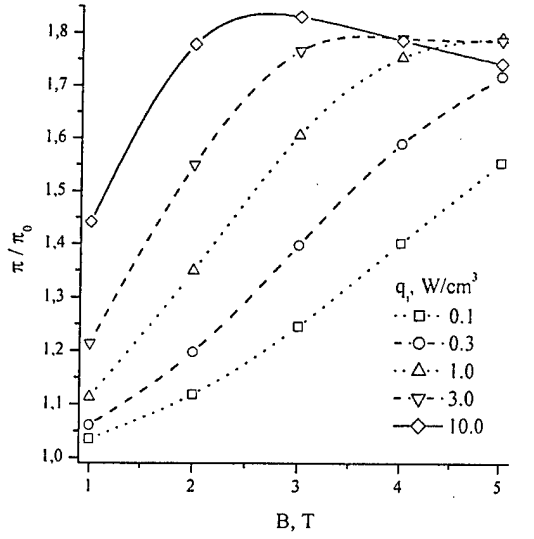

Fig.11 Relative pressure increase in MHD controlled inlet vs magnetic induction B for various values of q_i. M_0=8, M_d=10, α=135°, k=0.5. Ionized region is located in $3 \le x \le 4$.

PHYSICAL PROBLEMS IN DEVELOPMENT OF MHD-CONTROLLED INLET

E.G. Sheikin

Hypersonic Systems Research Institute, St. Petersburg, Russia

In the papers [1-6] it is shown that MHD interaction in scramjet inlet can be used to modify flow field at off-design conditions. At flight Mach number M_0 greater than design Mach number M_d MHD control allows us to modify the flow field in inlet in such a way that it becomes like a flow field at design conditions [3-6]. In situation when $M_0<M_d$ MHD control can be used to increase air mass-flow rate in scramjet [1,2,5,6] and to increase specific impulse and thrust of scramjet [1,2]. Anticipated operating conditions for MHD generator in scramjet inlet dramatically differ from operating conditions for conventional MHD generator. Flow in scramjet inlet is characterized by low gas temperature, low gas density and high velocity of flow. MHD generator can be realized at these conditions only if nonequilibrium conductivity of flow will be created by using external ionizer. In this connection the power spent on flow ionization need to be less than power produced by MHD generator. This limitation determines requirements for ionizer and magnetic system of MHD generator [5]. At high value of magnetic induction B MHD flow will be characterized by high value of Hall parameter for electrons β_e as a consequence of low density of flow. High value of flow velocity will result in high value of induced electric field. Maximal intensity of longitudinal induced electric field E_x which is codirectional with flow velocity (x direction) in Faraday MHD generator with magnetic field directed in y axis ($B=B_y$), is determined by the relation: $E_x=\beta_e B v$, where v is the flow velocity. At high intensity of electric field the electric breakdown of gas can occur. Limitations on electric field intensity lead to limitations on magnetic field intensity. Effect of ion slip, which is characterized by slipping factor $s=\beta_e\beta_i$, can essentially decrease efficiency of MHD interaction at high values of magnetic induction, see e.g. [7].

At conditions typical for scramjet inlet Hall parameter, maximal intensity of induced electric field and slipping factor are calculated. Limiting values for magnetic induction are estimated. In calculating the Hall parameter by the ratio $\beta_e=\mu_e B$, dependency of electron mobility μ_e upon electric field is taken into account, see the Fig.1. Data from [8] on the drift velocity for electrons w_e as a function of E/N, where N – is the gas concentration are used: $\mu_e(E/N,N)=w_e(E/N)/E$. Intensity of induced electric field which is determined as a solution of equation $E=\mu(E/N,N)B^2 v$ and Hall parameter calculated at the determined electric field are shown in the Fig.2. In order to estimate limiting value for magnetic induction at which electric breakdown can occur we use well-known data on the electric breakdown in gases. By using data from [9] on the air breakdown for minimum of Paschen's curve it is easy to obtain limiting relation for intensity of electric field at which breakdown occurs

$$(E/N)=(E/N)^*\approx 10^{-14}\,\mathrm{V\cdot cm^2} \qquad (1)$$

Limitation on the magnetic field intensity which is caused by ion slip can be determined from the relation:

$$s=\beta_e\beta_i=1 \qquad (2)$$

Limiting values for magnetic induction obtained from conditions (1) and (2) are shown in the Fig.3. The Fig.4 demonstrates area of legitimate values for magnetic induction (dashed area) at which self-sustained operational mode for MHD generator with nonequilibrium conductivity is realized ($q_g>q_i$) with MHD interaction parameter $S_v>0.1$ (obtained in [5]) and with ion slip factor $s<1$. (q_g is the power density

produced by MHD generator, q_i is the power density spent on flow ionization). Permissible region of magnetic inductions at which MHD generator allows us to control by the incident flow with the flight Mach number $6 \le M_0 \le 12$ is shown in the Fig.5. The lower curve in the Fig.5 is calculated at optimal value of q_i according to the Fig.4. It follows from the Fig.5 that in the case of magnetic system with a fixed value of magnetic induction the extension of speed range for the flight vehicle causes the permissible range for magnetic inductions to be narrowed.

And now let us consider problems of organization of energy deposition in flow to create nonequilibrium ionization in scramjet inlet. The more preferable method for flow ionization, which is characterized by minimal power spent on flow ionization is the e-beam [4,5]. Electrons in the e-beam at conditions typical for MHD-controlled inlet are characterized by very small value of Larmor radius and thus can penetrate into flow only along the magnetic field lines. So the problem of creation of magnetic field configuration and problem of flow ionization need to be considered together. Electrons from e-beam lose their energy during the motion in the flow it leads to changing the electrons stopping power [10]. The gas dynamic structure of flow in scramjet inlet can be very complicated it can influences on the e-beam penetration and thus on the spatial distribution of conductivity in the flow. MHD interaction modifies gas dynamic structure of flow and thus changes conditions for e-beam penetration into flow and hence the spatial distribution of conductivity in the flow. Thus to calculate characteristics of MHD-controlled inlet with e-beam as an ionizer it is necessary to develop numerical algorithms which allow us to take into account the task self-consistency mentioned above. To estimate significance of effects listed above we have developed the Monte Carlo code for calculation of e-beam penetration in nonhomogeneous medium. The approach developed in [11] is used in the code. The Fig.6 shows that results of calculations in our Monte Carlo code in the case of homogeneous medium are in good accordance with a function proposed in [6] to fitting results of Monte Carlo calculations in CYLTRAN code. To analyze effects of the medium non-homogeneity we consider flow over the wedge in geometry shown in the Fig.7. It follows from the Fig.8-10 that spatial profile of energy deposition by e-beam in the nonuniform flow is essentially differing from one in the case of uniform medium. Modification of the Q spatial distribution is caused by the change of e-beam position, free-stream dynamic pressure and initial energy of electrons E_b in e-beam. MHD flow over the wedge is calculated in 2D Euler approach similarly to [5]. Spatial distribution of the energy deposition is calculated by our Monte Carlo code at flow parameters which are realized without MHD effect. Spatial distributions of flow parameters in MHD flow over the wedge are shown in the Fig.11. Fig.12.a shows that density distribution in flow at x=2m is significantly modified by MHD effect. According to the Fig.12b this modification essentially changes conditions for e-beam penetration and hence will change spatial distribution of the flow conductivity.

References

1. Brichkin D.I., Kuranov A.L., and Sheikin E.G., MHD-technology for scramjet control, AIAA Paper 98-1642
2. Brichkin D.I., Kuranov A.L., and Sheikin E.G. The potentialities of MHD control for improving scramjet performance, AIAA Paper 99-4969.
3. Golovachev Yu.P., Suschikh S.Yu., "Weakly Ionized Flows in Supersonic Inlets Subjected to the External Electromagnetic Fields," in Perspectives of MHD and Plasma Technologies in Aerospace Applications, IVTAN, Moscow, March 24-25, 1999, Proceedings, p.105
4. Macheret S.O., Shneider M.N., and Miles R.B., External Supersonic Flow

and Scramjet Inlet Control by MHD with Electron Beam Ionization, AIAA Paper 2001-0492
5. Kuranov A.L., and Sheikin E.G. MHD control on hypersonic aircraft under "AJAX" concept. Possibilities of MHD generator, AIAA Paper 2002-0490
6. Shneider M.N., Macheret S.O., and Miles R.B., Nonequilibrium Magnetohydrodynamic Control of Scramjet Inlets, AIAA Paper 2002-2251
7. Macheret S.O., Shneider M.N., and Miles R.B., Magnetohydrodynamic and Electrohydrodynamic Control of Hypersonic Flows of Weakly Ionized Plasmas, AIAA Paper 2002-2251
8. Eletsky A.V., "Transfer phenomena in low ionized plasma" in handbook "Physical data", Moscow, Energoatomizdat, 1991 (in Russian).
9. Raizer Y.P., "Physics of gas discharge ", Moscow, Nauka, 1987 (in Russian).
10. Stopping Powers for electrons and Positrons, ICRU report 37, 1984
11. Sheikin E.G., New model interaction potential for the description of charged particle motion in matter, Technical Physics, 1999,v.44, p.481-485.

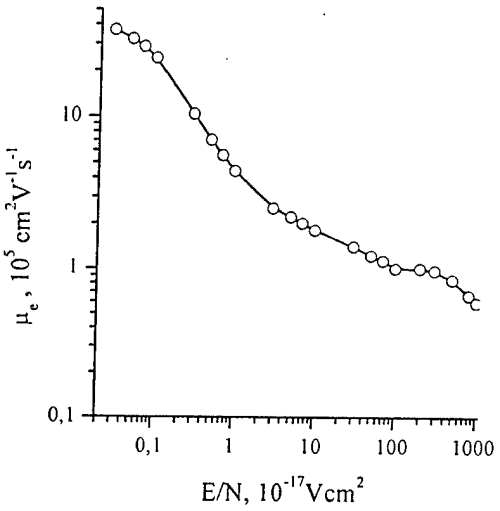

Fig.1 Mobility of electrons in nitrogen at $N=10^{17}$ см$^{-3}$. Obtained from data on electron drift velocity in nitrogen [8].

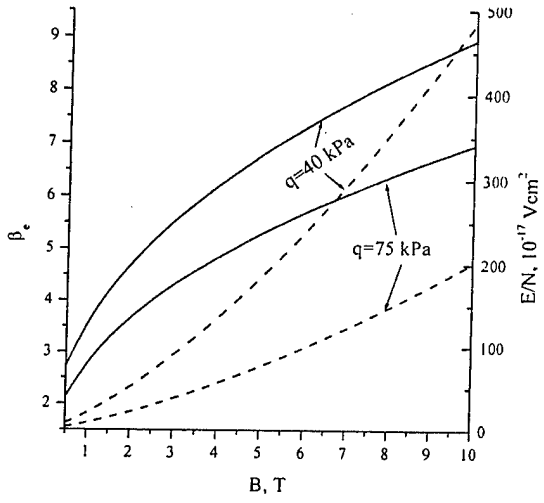

Fig.2 Hall parameter (solid lines) and induced electric field E_x (dashed lines) in external MHD generator at condition of free stream at $M_0=6$.

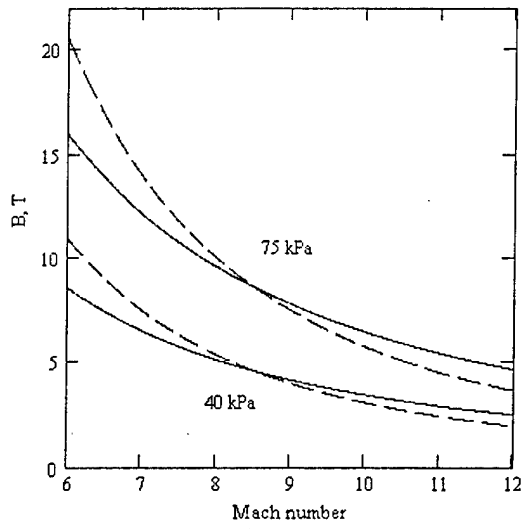

Fig.3 Limiting values for magnetic induction obtained from condition (1) (dashed lines) and condition (2) (solid lines) for MHD generator which interacts with incident flow.

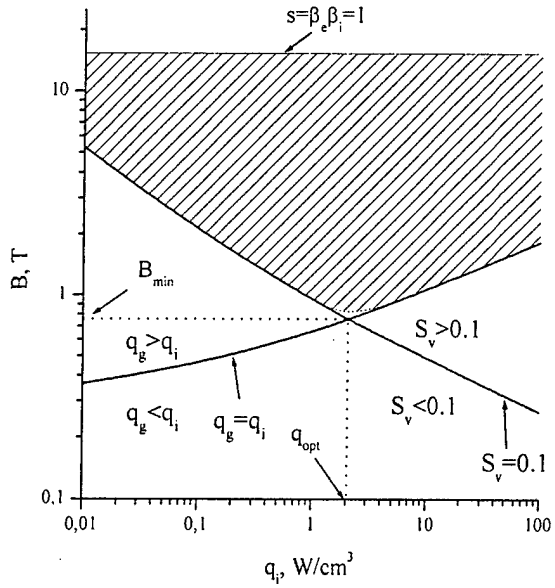

Fig.4 Limitations on ionizer and magnetic system for MHD generator which interacts with flow after the first oblique shock in scramjet inlet with: M_d=10, θ_N=15° , N=2. M_0=6, q=40 kPa.

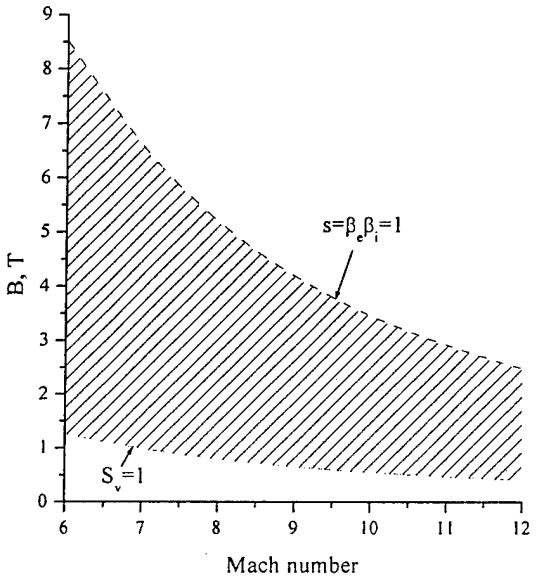

Fig.5 Permissible region of magnetic inductions for MHD generator which interacts with incident flow with free-stream dynamic pressure q=40kPa.

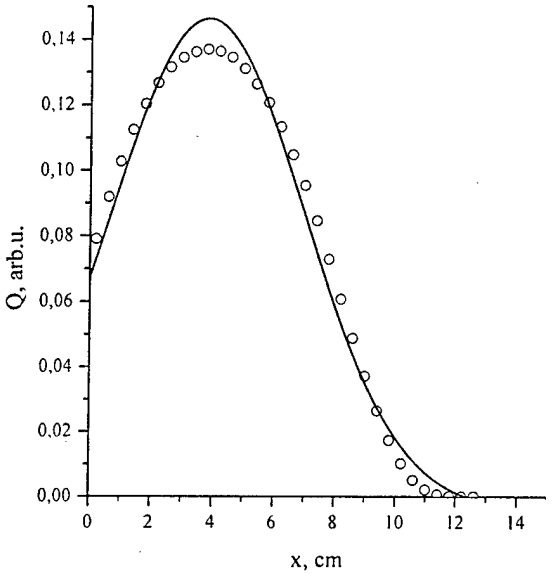

Fig.6 E-beam power deposition profile in homogeneous medium calculated in our Monte Carlo code (points), solid line is calculated in [6]: p=76 Torr, T=293°K, E_b=25 keV

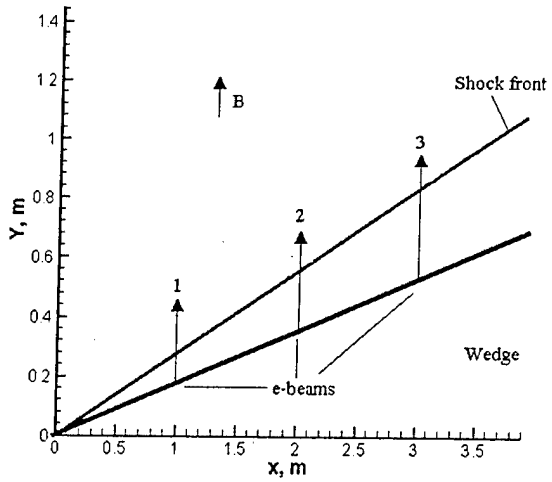

Fig.7 Simplified model used for investigation of the problem of MHD control by external flow. Considered positions of e-beam are shown in the figure.

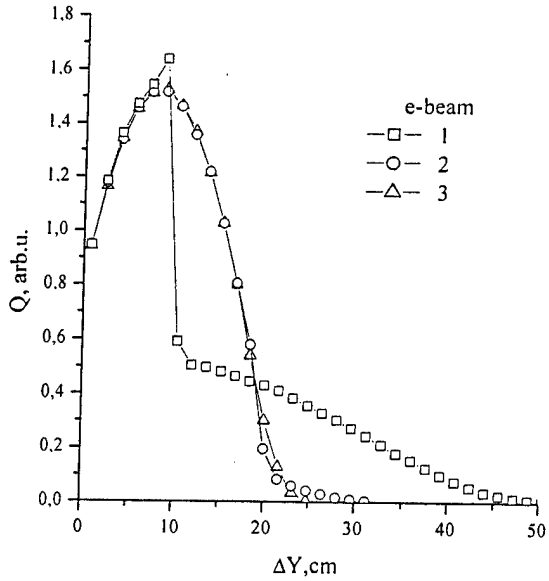

Fig.8 E-beam power deposition profile in flow over the wedge (10°). Positions of e-beam correspond to the Fig.7.
M_0=8, q=75kPa, E_b=25 keV

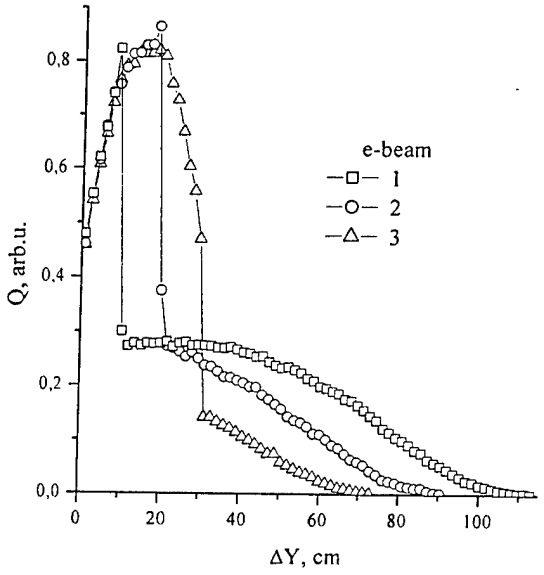

Fig.9 E-beam power deposition profile in flow over the wedge (10°). Positions of e-beam correspond to the Fig.7.
M_0=8, q=40kPa, E_b=25 keV

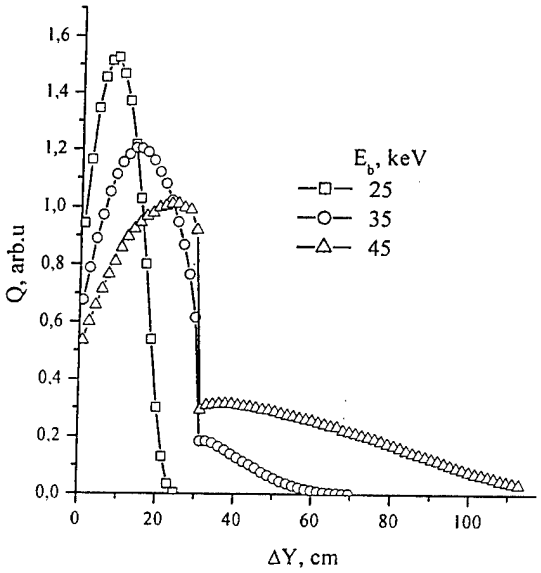

Fig.10 E-beam power deposition profile in flow over the wedge (10°). E-beam is located at x=3m (Fig.7), initial energies in e-beam are shown in the figure.
M_0=8, q=75kPa

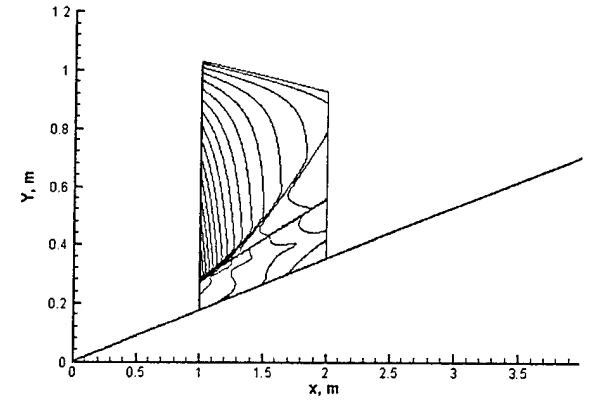

a)

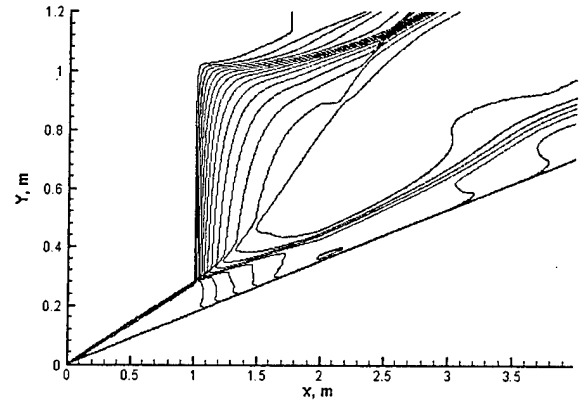

b)

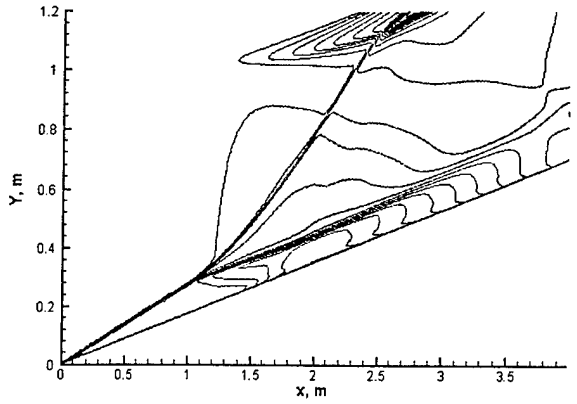

c)

Fig.11 Spatial distributions of parameters in MHD flow over the wedge: a)q_g, b) M, c) ρ.
Area of the flow ionization is restricted by the range $1 \le x \le 2$. E-beam power deposition in the range is calculated for flow without MHD effect. B=3T, E_b=25KeV, j_b=10 mA/cm^2.

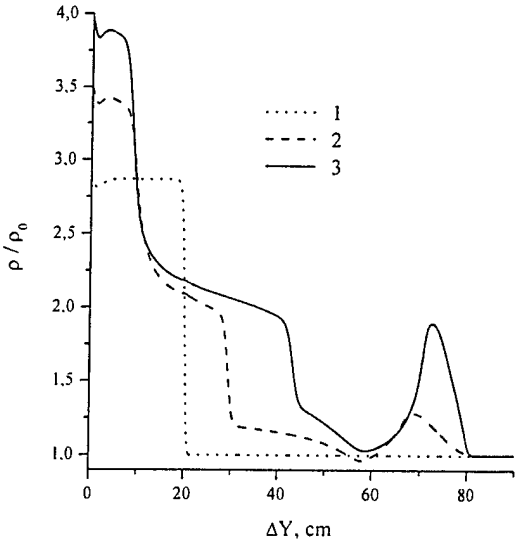

a)

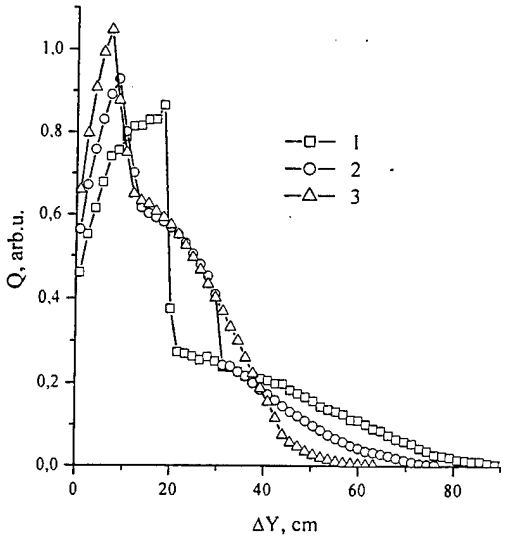

b)

Fig.12 Spatial distributions of flow density at x=2m after MHD interaction (a) and e-beam power deposition profiles corresponding to the density distributions (b). M_0=8, q=40 kPa, E_b=25 keV, B=3T, j_b (mA/cm^2)= 1) 0, 2) 1, 3) 10. Area of flow ionization is restricted by the range $1 \le x \le 2$.

Non-equilibrium Plasma Flow in a Supersonic Intake

Yu.P.Golovachov, Yu.A.Kurakin, A.A.Schmidt, D.M.Van Wie

A.F.Ioffe Institute RAS, yurii.golovachov@mail.ioffe.ru

The MHD flow control supposes preliminary ionization of the incoming stream. To separate the problems of ionization of the incoming stream and the MHD flow control our investigation is conducted with rare gases which are characterised by far greater recombination time as compared with air flows. The report presents the results of numerical investigations of non-equilibrium rare gas plasma flows in the MHD section of the Big Shock Tube of the Ioffe Institute. Present analysis includes the gas viscosity, heat conductivity and diffusion. It is performed assuming plasma quasi-neutrality and two-temperature model. The MHD interaction is taken into account within the framework of MHD approach neglecting the induced magnetic field. Computational procedure is based on high-resolution Godunov-type finite-volume scheme.

1. Basic equations and boundary conditions

In accordance with the conditions of the shock tube experiments, the calculation are carried out for plasma flows which are supposed to consist of atoms (a), positive ions (i), and electrons (e). The analysis is conducted assuming plasma quasi-neutrality and two-temperature model. The magneto-gas dynamic interaction is taken into account within the framework of the MHD approach and neglecting the induced magnetic field. Validity of these assumptions follows from inequalities

$$l_D \ll L, \quad V_\circ \ll c, \quad E_\circ \le V_\circ B_\circ,$$

$$\tau_g = L/V_\circ \gg \omega_p^{-1}, \quad Re_m \ll 1$$

which certainly hold for the flows under study. Here, l_D is the Debye length, L is the flow length scale, c is the light speed, ω_p is the plasma frequency, Re_m is the magnetic Reynolds number. Subscript o denotes the scales for gas velocity, electric field strength and induction of magnetic field.

With above assumptions, non-equilibrium three-component and two-temperature plasma flows subjected to an applied magnetic field are governed by the following equations:

total continuity equation

$$\frac{\partial \varrho}{\partial t} + \nabla \cdot (\varrho \vec{V}) = 0 \qquad (1.1)$$

continuity equation for the electrons

$$\frac{\partial n_e}{\partial t} + \nabla \cdot (n_e \vec{V})$$

$$-\nabla(\mu/Sc\nabla(n_e/\varrho)) = \dot{n}_e \qquad (1.2)$$

total momentum balance equation

$$\frac{\partial \varrho \vec{V}}{\partial t} + \nabla \cdot (\varrho \vec{V}\vec{V} + p - \overleftrightarrow{T}) = \vec{j} \times \vec{B} \quad (1.3)$$

total energy balance equation

$$\frac{\partial}{\partial t}\left(\frac{\varrho V^2}{2} + \frac{3}{2}p\right) + \nabla \cdot \left[\left(\frac{\varrho V^2}{2} + \frac{5}{2}p\right) - \overleftrightarrow{T})\vec{V}\right]$$

$$+\nabla \vec{q}_e + \nabla \vec{q} = \vec{j} \cdot \vec{E} - \dot{n}_e \varepsilon_{ion} \qquad (1.4)$$

energy balance equation for the electrons

$$\frac{\partial}{\partial t}\left(\frac{3}{2}p_e\right) + \nabla \cdot \left(\frac{5}{2}p_e \vec{V}\right) = \vec{V} \cdot \nabla p_e$$

$$+\vec{j}\cdot(\vec{E}+\vec{V}\times\vec{B})-\dot{n}_e\varepsilon_{ion}$$
$$-3\frac{m_e}{m}kn_e(\nu_{ei}+\nu_{ea})(T_e-T)-\nabla\vec{q}_e \quad (1.5)$$

Here, $\vec{V}$ is the mass-averaged flow velocity; $\varrho=\varrho_a+\varrho_i+\varrho_e$ is the plasma density; $p=p_a+p_i+p_e$ is the plasma pressure; p_α is the partial pressure of the α-component ($\alpha=a,i,e$); n_α is the number density of the α-component; k is the Boltzmann constant; $m=m_a\approx m_i$ is the mass of a heavy particle; m_e is the mass of an electron; $\vec{j}$ is the electric current density; $\vec{B}$ is the induction of magnetic field; $\vec{E}$ is the electric field strength; ε_{ion} is the ionization energy per atom; $\dot{n}_e$ is the number rate of electron production per unit volume; ν_{ei},ν_{ea} are the collision frequencies for electrons with ions and atoms; T_e,T are the temperatures of the electrons and the heavy particles, $\overleftrightarrow{T}$ is the viscous stress tensor, $\vec{q}_e$, $\vec{q}$ are the heat fluxes due to the electrons and the heavy particles, μ is the gas viscosity, Sc is the Schmidt number.

The heat flux due to the heavy particles is calculated using the Fourier law

$$\vec{q}=-\lambda\nabla T=-\mu c_p\nabla T/Pr$$

where λ is the heat conductivity, c_p is the heat capacity at constant pressure, Pr is the Prandtl number. The heat flux due to the electrons is evaluated following elementary theory in which

$$\vec{q}_e=-\lambda_{||}\nabla_{||}T_e-\lambda_\perp\nabla_\perp T_e-\lambda_H\vec{b}\times\nabla T_e$$
$$+\psi_{||}\vec{j}_{||}+\psi_\perp\vec{j}_\perp+\psi_H\vec{b}\times\vec{j}$$

where $\vec{b}=\vec{B}/B$ is the unit vector of magnetic induction, indices $||,\perp,H$ correspond to parallel, perpendicular and Hall components. The elementary theory give the following values for the above quantities

$$\lambda_{||}=n_ek^2T_e/m_e\nu_{ea},$$
$$\lambda_\perp=\lambda_{||}/(1+\beta_e^2),$$
$$\lambda_H=\beta_e\lambda_\perp$$
$$\psi_{||}=-7/2kT_e/e,$$
$$\psi_\perp=\psi_{||}/(1+\beta_e^2),$$
$$\psi_H=\beta_e\psi_\perp.$$

where β_e is the Hall parameter for the electrons.

The electric current density is found from the generalized Ohm's law

$$\vec{j}+\beta_e\vec{j}\times\vec{b}=$$
$$\sigma(\vec{E}+\vec{V}\times\vec{B}+\frac{\nabla p_e}{en_e}) \quad (1.6)$$

where σ is the electric conductivity of plasma.

With known induction of magnetic field $\vec{B}$, the electric field strength is evaluated through specification of the external load coefficient k

$$\vec{E}=-k(\vec{V}\times\vec{B}) \quad (1.7)$$

The electron production rate $\dot{n}_e$ is calculated following the theory of non-equilibrium ionization in a low-temperature rare gas plasma developed by Biberman et al. [2]. The main processes which determine the charged particle concentrations within the range of conditions considered are ionization by electron impact and three-particle recombination

$$A+e \iff A^+ +e+e$$

which implies

$$\dot{n}_e=k_in_en_a-k_rn_e^3$$

The recombination rate constant for xenon plasma is calculated following the above theory. The ionization rate constants k_i are found through the equilibrium constants K:

$$k_i = K k_r,$$

$$K = 1.936 \times 10^{22} T_e^{3/2} e^{-140363/T_e} \quad (m^{-3}).$$

The frequency of the charged particle collisions is given by formula [1]:

$$\nu_{ei} = 3.64 \times 10^{-6} n_e \frac{\ln \Lambda}{T_e^{3/2}} \quad (\mathrm{s}^{-1}),$$

$$\Lambda = 1.24 \times 10^7 \sqrt{\frac{T_e^3}{n_e}}.$$

Collision frequency for electron and atom is defined as follows:

$$\nu_{ea} = \frac{4}{3} \sigma_{ea} n_a \sqrt{\frac{8kT_e}{\pi m_e}} \quad (\mathrm{s}^{-1}),$$

where the collision cross-sections are evaluated with the approximations suggested in [3]:

$$\sigma_{ea} = a_\circ^2 \Big(-1.82$$

$$+2.2 \times 10^4 T_e^{-1} + 3.8 \times 10^{-7} T_e^2 \Big)$$

where $a_\circ = 0.529 \times 10^{-10}$m is the radius of the first Bohr orbit.

Stationary solutions of the above equations are found via time-asymptotic technique. In most calculations all plasma parameters are prescribed on the inflow boundary of a computational domain. On the duct walls, the no slip boundary conditions are imposed. The adiabatic wall case was considered. On the outflow boundary of the computational domain the approximate boundary conditios of type $\partial f / \partial x = 0$ were used.

2. Computational technique

The method for solving equations (1.1)-(1.5) is based on the Godunov-type high-resolution fully implicit finite-volume scheme. Stationary solutions are obtained using time-asymptotic technique. The computational procedure is briefly described below.

Equations (1.1)-(1.5) are written for the Cartesian coordinate system (x, y, z) in the form

$$\frac{\partial U}{\partial t} + \frac{\partial F_x}{\partial x} + \frac{\partial F_y}{\partial y} + \frac{\partial F_z}{\partial z}$$

$$- \frac{\partial P_x}{\partial x} - \frac{\partial P_y}{\partial y} - \frac{\partial P_z}{\partial z} = Q + R \qquad (2.1)$$

Assuming gas dynamic variables to be constant within a computational cell and making use of the integral formulae of vectorial analysis, one can write out the finite-volume notation of equation (2.1) for a computational cell i

$$\left(\frac{dU}{dt} \right)_i = -F_i^* + P_i^* + Q + R$$

$$F_i^* = F_i(U_i^*), \quad P_i^* = P_i(U_i^*) \qquad (2.2)$$

where F_i includes convective, viscous, termoconductive and diffusion terms integral via computational cell:

$$F_i = \frac{1}{v} \int_\sigma (F_x n_x + F_y n_y + F_z n_z)\, ds,$$

$$P_i = \frac{1}{v} \int_\sigma (P_x n_x + P_y n_y + P_z n_z)\, ds$$

where v, σ are the volume and the surface of a computational cell; n_x, n_y, n_z are the projections of the unit vector which is normal to surface σ.

Integration over a cell surface is fulfilled with formula

$$\int_{\sigma} (F_x n_x + F_y n_y + F_z n_z)\, ds =$$

$$(F_n)_{i+1/2,j,k} + (F_n)_{i-1/2,j,k}$$

$$+(F_n)_{i,j+1/2,k} + (F_n)_{i,j-1/2,k}$$

$$+(F_n)_{i,j,k+1/2} + (F_n)_{i,j,k-1/2} \qquad (2.3)$$

where subscript n corresponds to the normal to a cell side,

$$F_n = \begin{Bmatrix} \varrho V_n \\ \varrho V_n V_x + p n_x \\ \varrho V_n V_y + p n_y \\ \varrho V_n V_z + p n_z \\ \left(\frac{\varrho V^2}{2} + \frac{5}{2} p\right) V_n \\ n_e V_n \\ \frac{5}{2} p_e V_n \end{Bmatrix}.$$

Calculation of normal projections for 3-D computational mesh can be found in [4].

When evaluating the convective fluxes F_n the values of gas dynamic functions are found from solution of the Riemann problem with the initial data determined with formulae:

$$U^L_{i+1/2,j,k} = U_{i,j,k} + \nabla U_{i,j,k} \cdot \overrightarrow{c}_1,$$

$$U^R_{i+1/2,j,k} = U_{i+1,j,k} + \nabla U_{i+1,j,k} \cdot \overrightarrow{c}_2.$$

where $\overrightarrow{c}_1$ and $\overrightarrow{c}_2$ are the vectors drawn from the centers of the neighbouring computational cells to the middle of their boundary. Similar formulae are used on other sides of a computational cell.

Gradient components in each coordinate are calculated using two one-sided differencies subjected to limitation procedure to ensure monotonicity, for example:

$$\left(\frac{dU}{dx}\right)_{i,j,k} = minmod\left(\frac{U_{i,j,k} - U_{i-1,j,k}}{\Delta x}, \frac{U_{i+1,j,k} - U_{i,j,k}}{\Delta x}\right) \qquad (2.4)$$

The second-order finite differencies were used for the P_x, P_y, P_z approximation.

The implicit scheme for F_i calculation is based on equation:

$$\left(\frac{\partial U}{\partial t}\right)_i = \frac{U_i^* - U_i^n}{\Delta t} =$$

$$-F_i(U_i^*) + P_i(U_i^*) \qquad (2.5)$$

which was solved using Newton method with iterations:

$$\left[\frac{1}{\Delta t} + \left(\frac{\partial F_i}{\partial U}\right)^k_i - \left(\frac{\partial P_i}{\partial U}\right)^k_i\right] \Delta U_i^k =$$

$$-\frac{1}{\Delta t}\left(U_i^k - U_i^n\right) - F_i(U_i^k) + P_i(U_i^k)$$

where Δt is the time step, $\Delta U_i^k = U_i^k - U_i^n$, k is the iteration number, superscript n denotes the previous time level,

$$U_i^* = \lim_{k \to \infty} U_i^k$$

Approximation of Jacobian $\frac{\partial F_i}{\partial U}$ was obtained using the 1-st order upwind characteristics scheme of Steger and Warming [4].

With known F_i and P_i governing equations represent the set of ordinary differential equations which is integrated in time using the simplest two-layer implicit sheme.

The above computational procedure is second-order accurate with respect to the spatial coordinates in the flow regions with smooth function behaviour.

3. Results

The results of calculations pertain to non-equilibrium flows in MHD section of the experimental facility using Big Shock

Tube of the Ioffe Institute. The main objectives of these calculations are evaluation of the implicit computational code and investigation of the effects of variable electrophysical properties on plasma flow deceleration by applied magnetic field.

Plasma parameters in the critical cross-section of the nozzle are the following:

M=1.00, T=T_o=9085 K, T_e=9361 K, $\alpha = 2.5 \cdot 10^{-2}$, $n_a+n_i=n_o=8.957 \cdot 10^{24}$ m^{-3}, where M is the Mach number calculated with the mass-averaged plasma velocity and the heavy particle temperature; $\alpha = n_e/(n_a + n_i)$ is the ionization degree. All distances are referred to the nozzle diameter.

In the figures which follow the density is normalized by ρ_0, the temperature is given in Kelvins. The top figures are computed without the MHD effects, the bottom figures are calculated with account of applied magnetic field equal to 1T. The magnetic field acts along the y-axis. The electrodes represent a pair of metallic stripes of 8 mm width located on the side walls in the vicinity of the angle of the lower wall. Load coefficient was equal to 0.5.

Figs. 1, 2a-b display the nondimensional density and temperature of the heavy particles in the duct. In Fig. 3 the temperature of electrons is presented. It is seen the high increase of the electron temperature in the vicinity of the electrodes which is caused obviously by the energy exchange between electrones and the external electromagnetic field. The next figure represents the isolines of ionisation degree in the vicinity of the duct wall angle. It is seen quite different behaviour of the isolines of the ionisation degree in the cases without and with applied magnetic field.

Fig. 5 presents the velocity contours in the vicinity of the duct wall corner. it is seen that in both cases there are reversal flows which are more intensive for the flow subjected to MHD influence.

CONCLUSION

- The refined mathematical model for non-equilibrium shock-heated three-component viscous plasma flows subjected to applied magnetic field have been formulated.
- Computational procedure has been developed for numerical simulation of laminar MHD flows using the compressible Navier-Stokes equations.
- Computational code has been developed for calculation of viscous MHD flows taking into account non-equilibrium ionization, different electron and heavy particle temperatures, and variable electrophysical properties of plasma.
- The above mathematical model and computational code have been used for numerical simulation of plasma flows in the MHD section of the experimental setup.

REFERENCES

1. M.Mitchner, C.H.Kruger Jr. Partially Ionized Gases. Willey & Sons, 1973.

2. L.M.Biberman, I.T.Yakubov, V.S.Vorob'ev. Kinetics of Low-temperature Nonequilibrium Plasma. M.: Nauka. 1982 (in Russian).

3. Yu.M.Volkov et.al.// Teplofizika Vysokikh Temp. 1966. Vol. 4. P.136 (in Russian).

4. S.R.Chakravarthy, K.Y.Szema.// AIAA Paper 85-1703.

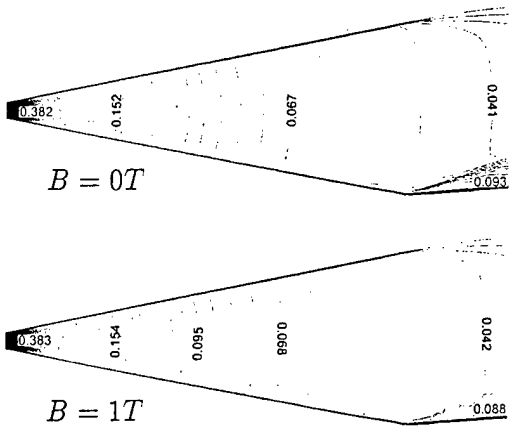

Fig. 1 Nondimensional density field in the experimental setup.

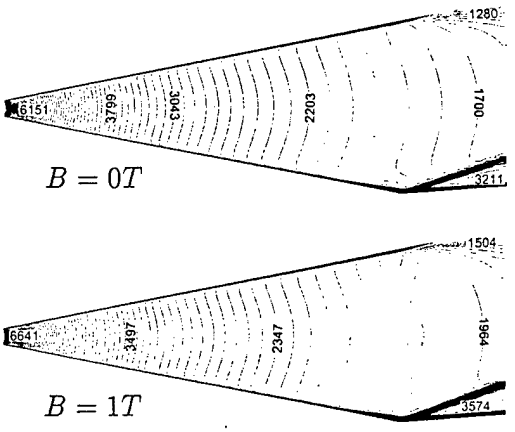

Fig. 2 Heavy particle temperature in the experimental setup.

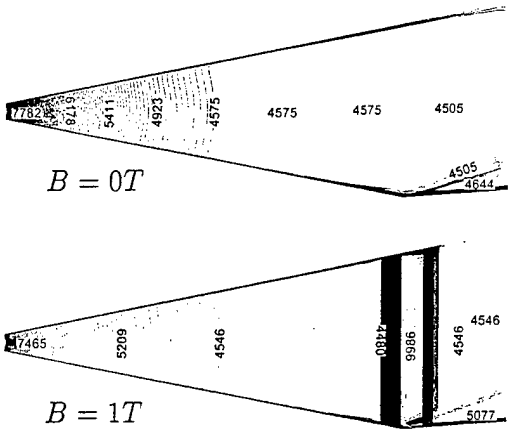

Fig. 3 Electron temperature in the experimental setup.

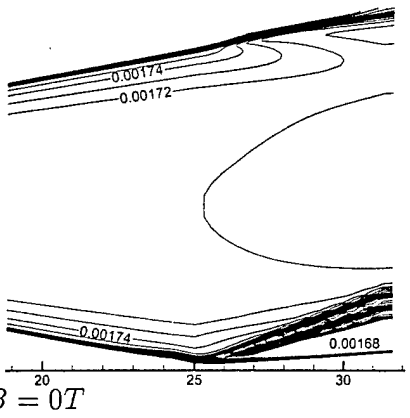

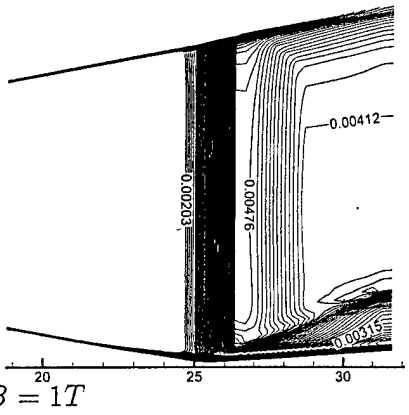

Fig. 4 Ionization degree in the vicinity of the ramp.

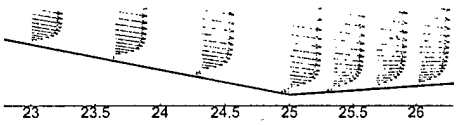

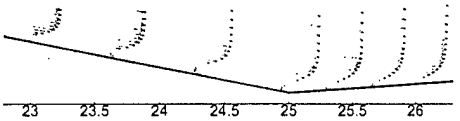

Fig. 5 Velocity maps in the vicinity of the ramp.

ARRANGEMENT OF EXPERIMENTS ON MHD CONTROL OF SHOCK-WAVE CONFIGURATIONS IN SUPERSONIC DIFFUSER

*S.V.Bobashev, R.V.Vasil'eva, A.V.Erofeev, T.A.Lapushkina, S.A.Poniaev,**

*D. M. Van Wi**e*

**Ioffe Physico-Technical Institute Russian Academy of Sciences*
***The Johns Hopkins University, Laurel, MD, USA*
26 Polytekhnicheskaya, St. Petersburg, 194021,RUSSIA
E-mail: alex.erofeev@mail.ioffe.ru

INTRODUCTION

At present time the posibilities of MHD technology for aerospace application are discussed.

The aim of the present work is a creation of the experimental setup with needful technics and an initiative study of the possibility to control the shock-wave configurations arising at the supersonic flow of weakly ionized gas in diffuser by MHD interaction.

EXPERIMENTAL SETUP

The experiment has been performed into a diffuser with a total internal compression of a flow. As a working gas it was taken low-temperature plasma of inert gases. A schematic of the setup is shown in Fig. 1.

Gasdynamic section

A shock tube of 50 mm in diameter incorporates a high-pressure chamber (1) of 1 m in length filled with hydrogen and a low-pressure chamber of 4.5 m in length filled with Kr or Xe. At the diaphragm disrupture separating the above chambers, an incident shock wave arises, then, reaches the shock-tube end, is reflected from it and moves backward. A region of a high-temperature ionised gas has been arisen behind a reflected shock wave. This region exists during a certain period until the reflected shock wave arrives at a contact surface or a head rarefaction wave reflected from the end of the high-pressure chamber. The experiments demonstrated that the largest length of a shock gas region in Xe arises under conditions when the Mach number of the incident shock wave is approximately 8.

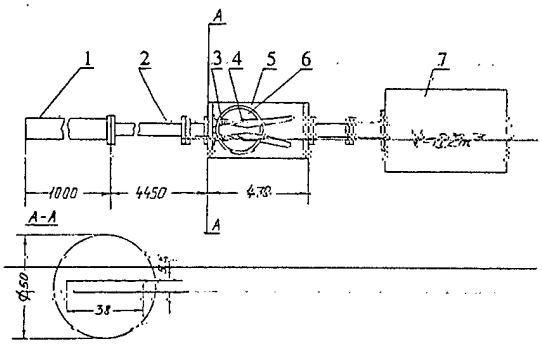

Fig.1 Scheme of setup: 1 is high-pressure chamber, 2 is low-pressure chamber, 3 is acceleration nozzle, 4 is diffuser model, 5 is vacuum chamber, 6 is optical window, 7 is exhaust tank. The size specifies on millimetres.

There is a narrow slit at the end surface of the shock tube separated from the low-pressure chamber with a thin Lavsan diaphragm. When this diaphragm is disrupted by the incident shock wave, ionised gas moving behind it enters a flat divergent nozzle (3) where it is accelerated up to the flow Mach number M = 4.3. The accelerated ionised gas enters the diffuser (4). The nozzle and diffuser are in a vacuum chamber (5), of which lateral walls two optical windows (6) are mounted for a flow visualisation. The gasdynamic tract has its end into a buffer volume (7)

In more details, the nozzle and diffuser are shown in Fig.2. The diffuser operates as Faraday MHD channel with the sectioned electrodes.

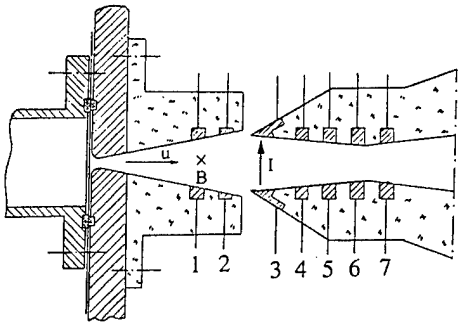

Fig.2. Scheme of MHD channel with electrodes. Figures are numbers of electrodes.

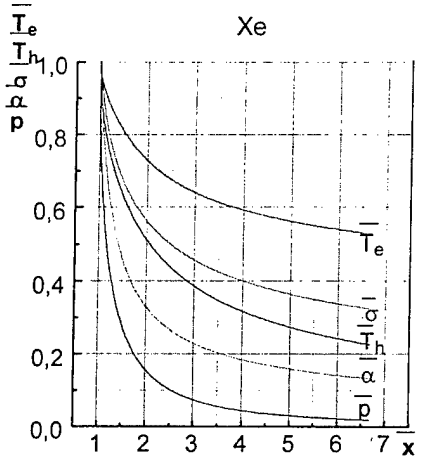

Fig.3. Distributions of the calculated values of electron temperature, heavy component temperature, conductivity, ionization degree, heavy component density, and plasma pressure along an acceleration nozzle. All the parameters reduced to the relevant values at a critical cross section: Xe, $x_{cr}=1.42\cdot10^{-2}$m, $M_{cr}=1.01$, $T_{h\,cr}=7700$K, $T_{e\,cr}=8700$K, $\sigma_{cr}=2500$ S/m, $\alpha_{cr}=1.5\cdot10^{-2}$, $n_{h\,cr}=0.9\cdot10^{25}$ m^{-3}.

Naturally, at the expanse this gas has cooled down but due to a rather slow mechanism of recombination of the charged particles in the inert gas [1] there is a rather high ionisation in plasma to secure the conductivity needed for the MHD experiments. This thesis is confirmed with the calculation of nonequilibrium plasma flow in the nozzle.

Fig.3 shows the distribution of parameters in the nozzle at $M_1=8.3$ and $p_1=30$ Torr. In Xe, at the nozzle outlet: $\sigma_0=975$S/m, $n_{h0}=0.81\cdot10^{24}$m^{-3}, $u_0=1.6\cdot10^3$m/s, $\rho_0=0.176$ kg/m^3. At B=1T and L=1m, $St_0=3.5$m^{-1} and $\beta_0=2.7$.

The calculation showed that the initial Stewart parameter at the entrance of the diffuser $St_0=\sigma_0B^2/\rho_0u_0$ had to exceed the minimum value $St_{0min}=2$ in order to MHD interaction be perceptible. In Fig.4, the initial values of the Stewart parameter for Ar, Kr, and Xe are shown for various Mach numbers of the incident shock wave. A limitation of a range of M_1 is due to the absence of ionization equilibrium in shock heated gas at the low M_1 and a fact that much higher values of M_1 are inasiessible because of the limitation in p_4 in the high pressure chamber. Thus, the initial condition optimization was carried.

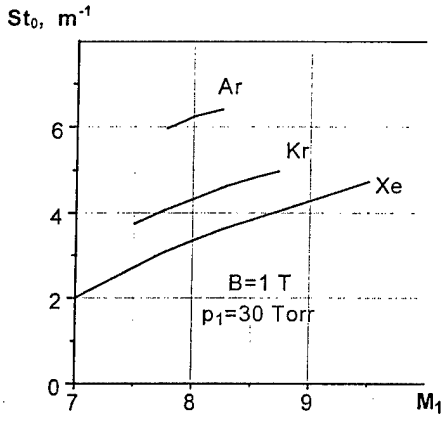

Fig. 4 The values of the initial local Stewart parameter versus the Mach numbers of the incident shock wave for various gases.

Magnetic and electrical fields

The transverse magnetic field of up to 1.5 T induction and a quasi-stationary stage duration of approx. 600 μs was involved with a capacitor bank discharge via the Helmholtz coils of 300 mm in diameter situated axially with the optical windows.

It has been shown in [2], that to compensate a large nearelectrode potential

drop it is need to apply a voltage V from an external source of electrical current to the electrodes. The external electrical field was formed by a long line. The equivalent electrical scheme is shown in Fig.5. In this case the Ohm law is in a form: $I(R_{eff} + R_L) = uBh + V$, where uBh is magneto-induced EMF.

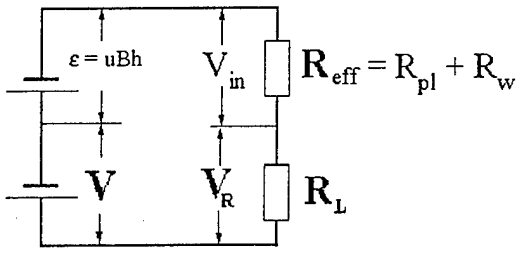

Fig.5. Equivalent electrical scheme

The simple effects on the flows include the force and power ones. General force effect on a flow is due to ponderomotive force F=jB. A power effect includes two aspects. First, there is an energy outflow into external circuit generated under MHD interaction. Second, there is a heat input from the external source of the electric field. The work of the ponderomotive force and heat input decelerate a supersonic flow, heat output results in the flow acceleration.

Visualisation methods

A flow visualisation was carried out with a schlieren system. A laser OGM-20 was used as a illuminator at the single registration, Podmoshenskii's source [3] was used as a powerful illuminator at the frame registration. Figure 5 shows a schematic of the optical registration.

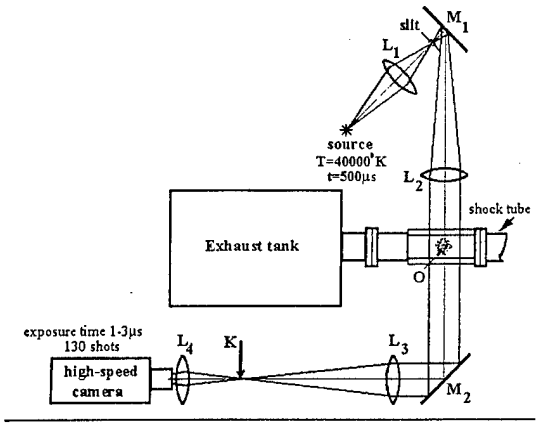

Fig. 6. The schlieren system with high-speed camera and Podmoshenskii's source.

A high-speed camera VSK-5 of up to 130 shoots of the process image with various intervals between the shots from 25 to 4μs is a recording unit of the setup. Besides the high-speed camera was used for a frame shooting of the plasma self illumination in the diffuser bulk. It has been shown that at the experiment conditions a location of the shocks may be determined by the gradients of the self illumination.

As a light source in obtaining a framed shadow picture it was applied a modified source EV-45 primarily advanced by Podmoshenskii [3]. In this source, the discharge of a current of 9kA was initiated through a hole of 0.2 cm in diameter and a length of 1cm in a textolite plate. Within a flat top of the plateau current's impulse of the total duration of about 0.5 ms, the quasi-stationary conditions are accomplished due to a balance between an amount of injected vapors of a wall material into the discharge channel and plasma blown out through the capillary end section.

The temperature T, pressure P_0 and chemical composition of a plasma into the channel are held constant and equal $T=40000^0K$, $P_0=500$ atm. Plasma radiation observed through the open ends of the capillary corresponds to that of the absolutely black body at this plasma temperature.

A source applied here differs from the basic standard source in illumination duration and ignition scheme using the impulse thyratron TGI-1-325/16 with H_2 - filling and ignition time of about 1 μs.

ELECTROPHYSICAL PLASMA PARAMETERS

Technique of measurements

To the main electrophysical characteristics of the MHD channel one should refer its I-V characteristics [2], spatial potential distribution, near-electrode potential drop, effective and bulk resistance (or conductivity) of the interelectrode gap.

Figure 7 shows the sheme of the measurements.

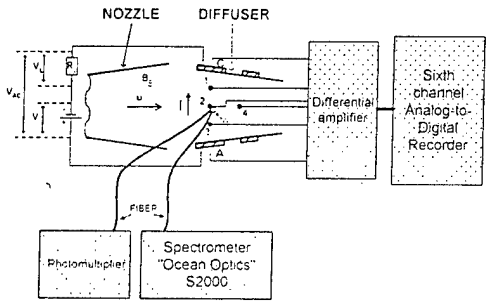

Fig.7. The scheme of electrical and optical measurements.

For the measurement of the potential distribution over the interelectrode gap there are three 'point' probing electrodes of 2 mm in diameter at the lateral diffuser wall in its inlet section; they are protruded inside the channel 2 mm distant from the wall. A potential difference between the electrodes was measured with the use of a six-channel analogue-digital converter.

The measurements of electrophysical plasma parameters and investigations of spectra were carried out in Xe at the conditions, when the Mach number of a shock wave front in the shock tube was 8, and an initial pressure in the low-pressure chamber was 30 Torr. The calculation values at an entrance of the diffuser were following: M = 4.3, u_0 = $1.55 \cdot 10^3$ m/s, ρ_0 = 0.127 kg/m^3, σ_0 = 600 S/m.

Potential distribution

Figure 8 shows potential distributions over the interelectrode gap at different current and magnetic field induction magnitudes. Zero potential corresponds to the cathode. Dashed lines in the figure show uniform potential distributions expected between the cathode and anode.

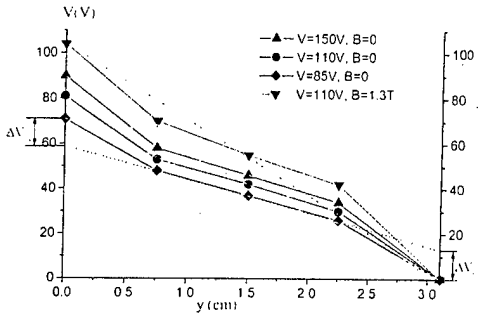

Fig.8. Experimentally determined potential distribution along the path of passing electric current. ΔV_A and ΔV_C are near-anode and near-cathode potential drop, accordingly.

The difference between the results obtained in the experiment and the distributions expected evidences a distinction in the potential behavior in the flow core and near-electrode regions. When setting up an external magnetic field the voltage drop in the flow core increases and the near-electrode voltage drop grows slightly, that is, the near-wall layer resistance grows. Apply owing to it the current drop occurs, one may speak about a decrease of conductivity in magnetic field in flow core.

Figure 9 demonstrates variation of the ratio of the total near-electrode potential drop $\Delta\varphi = \Delta V_A + \Delta V_C$ to the voltage V applied to the electrodes with the current passing through the circuit at $B = 0$ and $B =$

1.3 T. It should be note that this ratio decreases with the current growth.

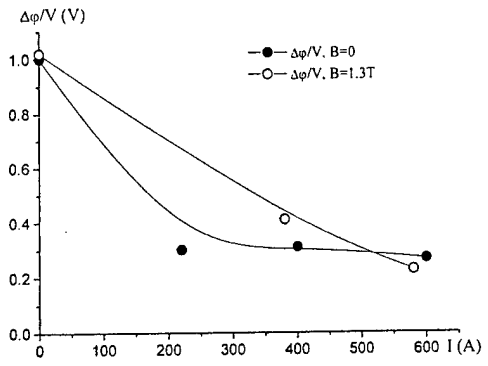

Fig.9. A dependence of the ratio of the total near-electrode potential drop to the external voltage on the current flowing through the circuit.

Plasma conductivity

The effective plasma conductivity is determined as follows $\sigma_{eff} = \frac{Iy_{A-c}}{V_{A-C}S}$, where S is the electrode area, $y_{A\text{-}C}$ is the interelectrode distance. The bulk conductivity or the conductivity in the flow core is determined as $\sigma_{pl} = \frac{Iy_{1-3}}{V_{1-3}S}$, where $y_{1\text{-}3}$ is the distance between the first and third electrodes. Figure 10 demonstrates dependences of σ_{eff} and σ_{pl} on the current through the circuit. It is seen that with no magnetic field σ_{pl} is roughly 1.5 times as large than the effective conductivity. A smooth conductivity growth with increasing the current is observed. Decreasing σ_{eff} and σ_{pl} at the presence of a magnetic field probably conditioned by Hall effect caused by imperfections in the channel sectioning.

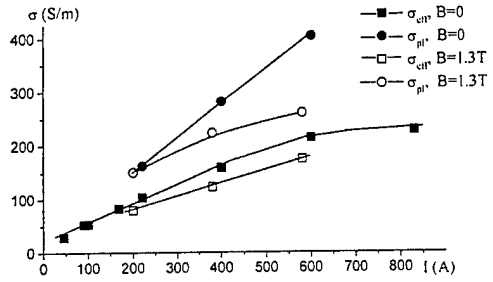

Fig.10. The plasma conductivity in the flow core and the effective conductivity as functions of the passing current.

SPECTRA REGISTRATION AND DETERMINATION OF THE ELECTRON TEMPERATURE AND CONCENTRATION

Characteristics of spectra

In the experiment we recorded plasma radiation spectra using Ocean Optics S2000 spectrometer allowing us during the operational time to obtain the radiation spectrum in a wide band of wavelengths from 200 to 850 nm with a high spectral resolution. Figure 11 shows samples of the radiation spectra obtained with no external voltage ($V = 0$) and at $V = 110$ V. At the background of the continuous xenon spectrum it is well seen some lines and bands of impurities. It is also seen that passing a current through the plasma causes a drastic increase of intensities both the continuous spectrum and the spectral lines. To direct attention to the region $\lambda < 450$ nm, here one can see beautifully the continuous radiation depend on recombination continuum.

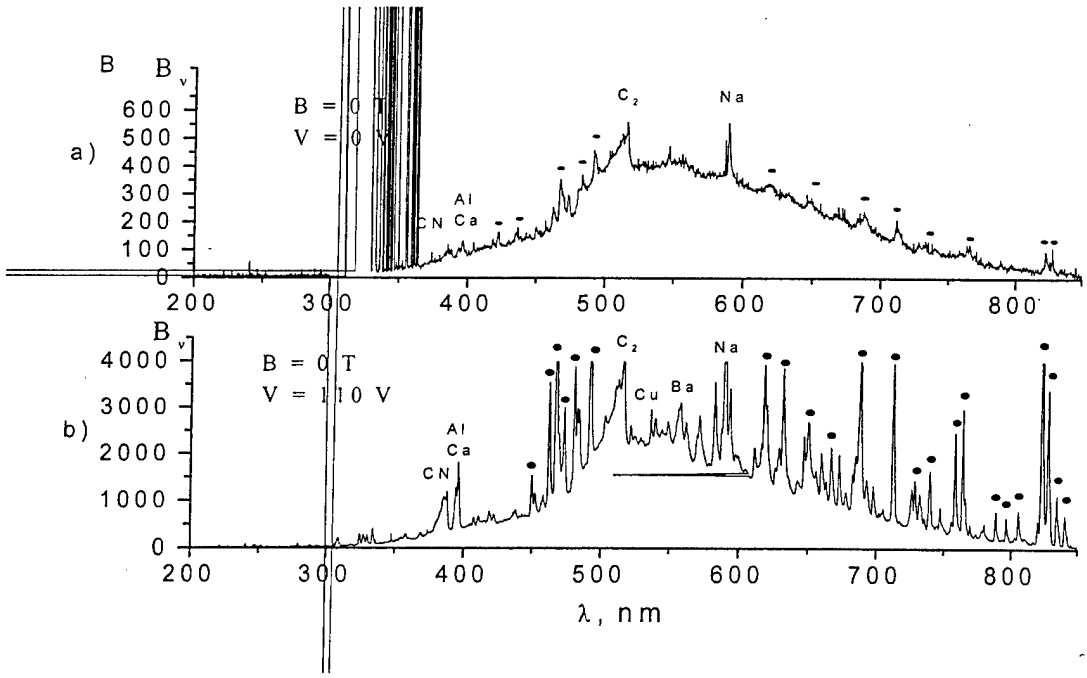

Fig.11. Xe spectra

Measuring methods of the electron temperature and concentration

To measure the electron temperature T_e and concentration n_e we used a technique developed in [4-6]. The technique is based on specific features of the energy levels of inert gases in general and xenon in particular. In the ultraviolet spectrum region ($\lambda < 450$ nm) the radiation intensity of a plasma continuum of inert gases caused by free-free and free-bound transitions can be defined by the formula $I_\nu = C\frac{n_e^2}{\sqrt{T_e}}e^{\frac{h\nu}{kT_e}}$, where n_e and T_e are the electron concentration and temperature, respectively, C is an arbitrary constant, ν is the radiation frequency, h and k are Planck and Boltzmann constants, respectively. From the formula above it is seen that the electron temperature can be determined from the relationship $\ln I_{\nu 1} - \ln I_{\nu 2} \sim 1/T_e$ by measuring the radiation intensity at two frequencies ν_1 and ν_2.

The electron concentration n_e was determined on the basis of plasma radiation measurements at the wavelength λ = 405 nm. The plasma radiation was recorded by a photomultiplier. For the calibration of a spectrometer and the photomultiplier we used as a 'standard source' the radiation of a shock-heated xenon in the shock tube inasmuch as a shock tube is well-studied instrument [7,8].

Results of measurements

Dependencies of the temperature and concentration of electrons on the passing current are shown in Fig. 12. In the same figure, results of the theoretical calculation are given. The measurements of T_e and n_e showed that a selective electron heating occurred at the magneto-induced and external electrical fields. T_e runs into 7500 –8500K, that is enough for a development of nonequilibrium ionization, thus n_e increases about in 2 times, it leads to that a bulk conductivity increases about in 1.5-2 times. The comparison of the experimental and calculated data has shown that the measured and calculated electron concentrations are in good agreement with each other. The temperature measured in the experiment turns out to be slightly low than that calculated. This is explained first by that we used a lavsan diaphragm and there

was an appreciable amount of molecular impurities in the flow, in particular C_2, which was found in spectra. Molecular impurities possess a large factor of nonelastic losses that leads to decreasing the selective plasma heating.

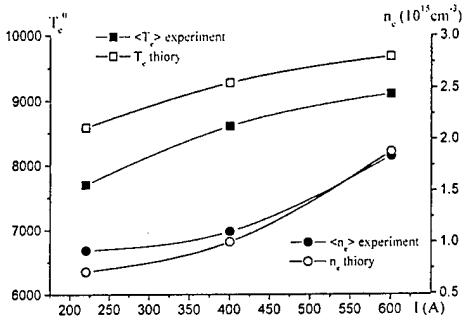

Рис.12. Electron temperature T_e and concentration n_e as functions of the electric current.

THE DIFFERENT TYPES OF MHD INTERACTION

First of all, we show a shock-wave configuration arising into a diffuser with no external fields. Figure 13a gives the results of calculation of the values of the Mach number of a flow into a nozzle and diffuser [9]. Here, dense lines refer to the shocks. Figure 13b gives a schlieren picture of a stable flow to visualise these shocks. Figure 13c gives an interpretation of the general gasdynamic inhomogeneities and denote the most essential parameters representing the flow reaction under the external actions.

In Fig.13, one can note the attached shocks – a; shocks – b arising as a result of deflection of the attached shocks from each other, the Mach lines – c arising at the joints of the electrodes with isolators, and a boundary layer – d. x_c is a distance of intercept of the attached shocks, at B = 0, V = 0, x_c = 42 mm. We consider that this parameter is the main parameter describing a flow reaction on change of the MHD interaction parameter. The experiment was made in Kr at the following parameters in the diffuser inlet: M = 4.2, ρ_0 = 0.0645 kg/m^3, σ_0 = 580 S/m, $u_0 = 2.1 \cdot 10^3$ m/s.

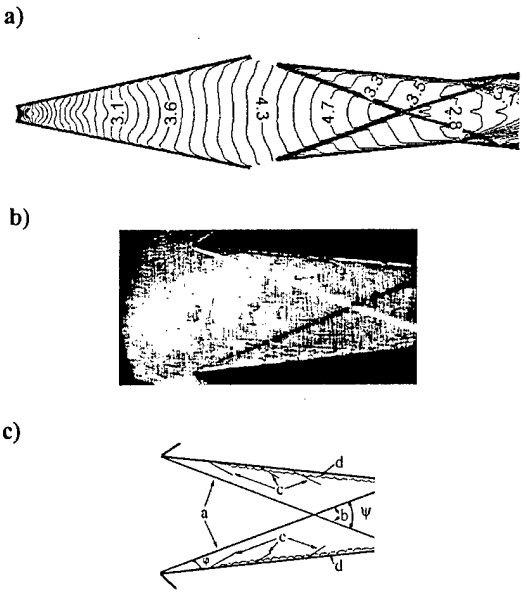

Fig.13. Distribution of Mach numbers, Schlieren picture of a flow and a scheme of MHD irregularities with no external fields.

Fig. 14 contents two schliren pictures (a) showing the shock-wave configurations for two magnetic field afduction applied B=0.8T and B=1.2T. These patterns differ from each other in principle. Case B=0.8T illustrates the conditions when one can see a stationary flow stage, where a structure of the shocks is not changed significantly comparing with case B = 0, but intersection points x_c moved upstream noticeably. Case B=1.2T demonstrates the conditions when the strong rearrangement of shock configurations happens, it leads to formation of subsonic zone with a direct shock. Here there is non-steady-state flow. In experiment as a characteristic parameter x_{sh} is assumed the value reached to the end of MHD interaction.

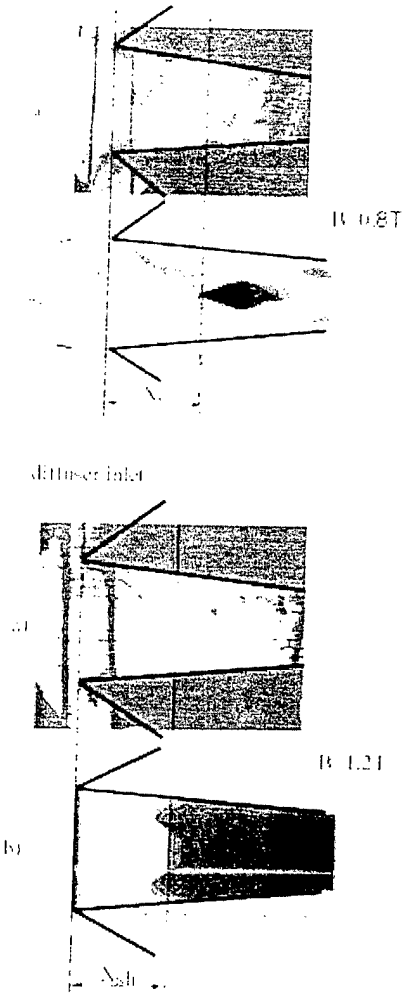

Fig.14. Schliren pictures and calculations at the various magnetic fields. a) Schliren picture; b) calculation.

Total experimental date [10] of changing shock-wave configuration in the diffuser with increasing MHD interaction are shown on Fig.15. In this figure, x_c and x_{sh} distances vs magnetic field are presented. Three domains of the MHD interaction are recognized. A weak interaction with no changes in inlet shock structure and with an increase in shocks' slope angles only due to a MHD deceleration of the flow, the intersection point being shifted toward the channel entrance when rising the magnetic field. The flow throughout the diffuser remains supersonic. Further, a shaded domain, that of an unstable inlet structure due to formation of the local subsonic areas past a region of shocks' intersection. After all, a domain of a strong MHD interaction, namely, formation of a wide subsonic region of a flow at the end of MHD interaction area resulting in formation of a direct deceleration shock.

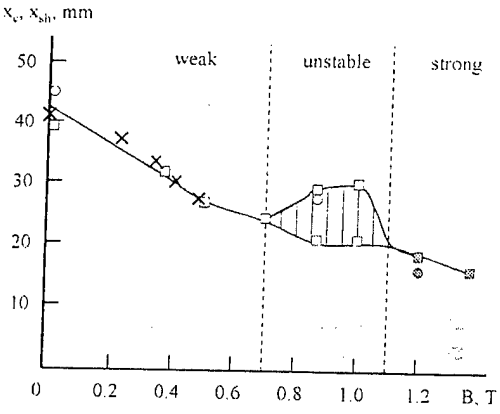

Fig. 12. Position of crossing point of diagonal shocks (x_c) and MHD shock (x_{sh}) versus magnetic induction. Schlieren method and plasma radiation are marked by circles and squares, respectively. Light points respect to x_c, dark points respect to x_{sh}. Crosses are the results of numerical simulation.

CONCLUSION

In result of this study the following electrophysical plasma parameters were determined: the electron concentration and temperature, distribution of potential, near-electrode potential drop, conductivity in flow core and effective conductivity. It has been conducted a comparison of the action of the magnetic and electrical fields on the flow parameters. An essential result of the work is a prove of an opportunity to change the inlet shock-wave structure with the external electromagnetic fields. A difference in the shock-wave structures at the supersonic diffuser's entrance has been investigated, therewith, three types of MHD interaction are revealed: weak, unstable, and strong.

REFERENCES

1. L.M. Biberman, V.S. Vorob'ev and I.T. Yakubov. Kinetics of the Non-Equilibrium Low-Temperature Plasma (in Russian). Nauka, Moscow, 376 p., 1982.
2. S. V. Bobashev, A. V. Erofeev, T. A. Lapushkina, S. A. Poniaev, V. A. Sakharov, R. V. Vasil'eva, and D. M. Van Wie «Effect of the wall layers on the electric current in a model of MHD diffuser», AIAA Paper 2001-2878, 32nd AIAA Plasmadynamics and Lasers Conference and 4th Weakly Ionized Gases Workshop, Anaheim, CA, 2001.
3. N.N. Ogurtsova, I.V. Podmoshenskii, N.I Demidov. OMP, 1, 1, 1960
4. A.P. Dronov, A. G. Sviridov, N.N. Sobolev, Opt. i Spektroskopiya 12(6), 677, 1962.
5. R. V. Vasileva, A. D. Zuev, V. A. Shingarkina. Ionization of xenon by electron impact at moderate temperatures. Soviet Physics - Technical Physics, vol. 28, June 1983, p. 647-652.
6. L. M. Biberman, and G. E. Norman, Opt. i Spektroskopiya 8, 433, 1961.
7. Petschek H.E. and Byron S. Ann.of Phys., 1, №3, p.270, 1957.
8. Aerophysics investigation of subsonic flows (in Russian). Nauka. Moscow-Leningrad. 300 p., 1967.
9. Yu.P. Golovachov, A.A. Schmidt, S.Yu. Suchikh, Numerical investigation of MGD flows in the models of supersonic intakes, The 2nd Workshop On Magneto- Plasma- Aerodynamics In Aerospace Applications, IVTAN, Moscow, April 5-7, pp. 74-77, 2000.
10. S.V. Bobashev, R. V. Vasil'eva, E. A. D'yakonova, A. V. Erofeev, T. A. Lapushkina, V. G. Maslennikov, S. A. Poniaev, V. A. Sakharov and D. Van Wie. The Effect of MHD Interactions on the Input Shock Waves in a Supersonic Diffuser. Technical Physics Letters, Vol. 27, pp. 71-73, 2001.

NONSTATIONARY PROCESSES IN THE DIFFUSER AT SWITCHING ON AND OFF THE ACTION OF MAGNETIC AND ELECTRIC FIELDS

S.V.Bobashev, R.V.Vasil'eva, A.V.Erofeev, T.A.Lapushkina, S.A.Poniaev, D.M. Van Wie***

**Ioffe Physico-Technical Institute Russian Academy of Sciences, 26 Polytekhnicheskaya, St. Petersburg, 194021, RUSSIA*

***The Johns Hopkins University, Laurel, MD, USA*

E-mail: seguei.poniaev@mail.ioffe.ru

ABSTRACT

This report describes results of experimental investigations of non-stationary processes occurring in the case of pulse interaction between an ionized gas flow and magnetic and electric fields in a diffuser with the total internal flux compression. In the experiment, the interaction pulse was determined by the electric current pulse. In the report the processes of formation of the shock-wave structure and its variation after switching-off the pulse are demonstrated. The time of relaxation of the attached shocks' positions to their initial positions in the absence of external fields is found.

INTRODUCTION

This work was aimed at studying the little-known processes of non-stationary gas dynamics, namely, formation of a new shock-wave configuration in a diffuser under the action of external fields and decay of this configuration after switching-off the electric current pulse. In this case the action of external fields results, generally, in a flow deceleration due to the Lorentz force and Joule heating of gas under the external electric field. Duration of the action of these fields is determined by the time of current passage through the plasma bulk in the diffuser along the direction transverse to the applied magnetic field. The current was circuited via the electrodes placed on opposite walls of the diffuser.

The purpose of the experiment was to understand how the flow is formed when current is switched on and to reveal specific features of relaxation of the arising shock-wave configuration to the initial position after switching off the current pulse by using the schlieren pictures obtained.

EXPERIMENTAL

The experimental setup and methodics of measurements is described elsewhere [1]. First of all, we show a shock-wave configuration arising in a diffuser without external fields. Figure 1-a presents calculated values of the Mach number of a flow in the nozzle and diffuse [2]. Here, dense lines refer to the shocks. Figure 1-b gives a schlieren picture of a stable flow visualising these shocks. Figure 1-c gives an interpretation of the general gasdynamic nonhomogeneities and denote the most essential parameters representing the flow reaction to external actions. In Fig. 5, one can see the attached shocks (a); shocks (b) resulting from reflection of the attached shocks from each other, the Mach lines (c) arising at the joints of electrodes with isolators, and a boundary layer (d). The angle between the attached shock and the diffuser wall is denoted by φ, x_c is the distance of interception of the attached shocks; ψ is the angle between the attached shocks. At $B = 0$ and $V = 0$, these parameters are as follows: $\varphi = 15.5$ deg, $\psi = 42$ deg, $x_c = 42$ mm. Parameters at the diffuser inlet are: $M = 4.3$, $\rho = 0.127$ kg/m^3; $u = 1.55 \times 10^3$ m/s: $\sigma = 600$ mho/m

In the first series of experiments, interaction with the external fields occurs in the initial portion of the diffuser when the current is circuited only through the 3rd pair of electrodes. The magnetic field is equal to 1.3 T and is nearly constant during the whole period of flow existence. Figure 2

shows the oscillogram of plasma luminescence recorded with a photoamplifier at the diffuser inlet and the current oscillogram (I = 450 A). They represent the relation between the outflow duration of the ionised gas and the current impulse.

FORMATION OF SHOCK-WAVE CONFIGURATION AS THE FLOW ENTERS THE DIFFUSER

In this series of experiments we paid attention to the flow formation. In Fig. 2 one can see that the onset of current flow coincides in time with the onset of plasma flow.

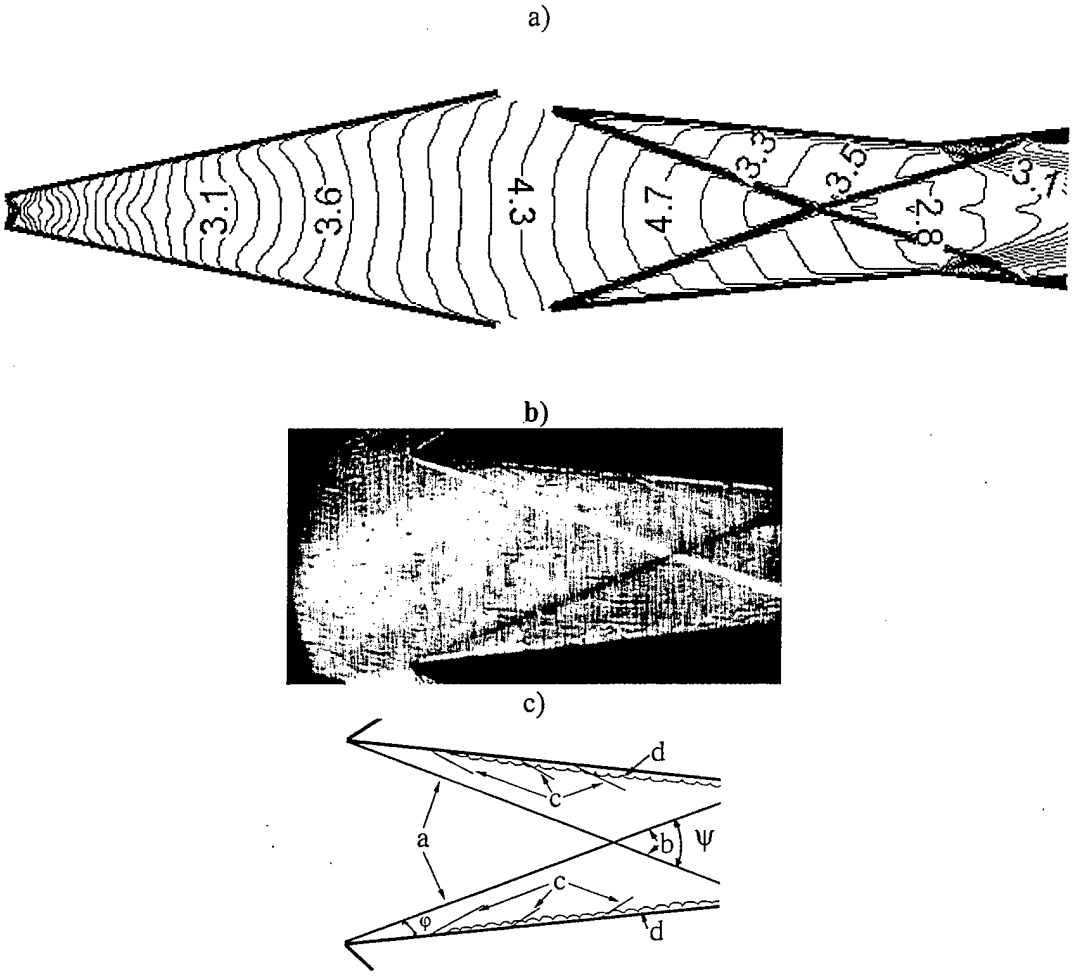

Fig. 1. Distribution of Mach numbers [2], Schlieren picture of the flow and a scheme of gas-dynamic irregularities in the absence of external fields.

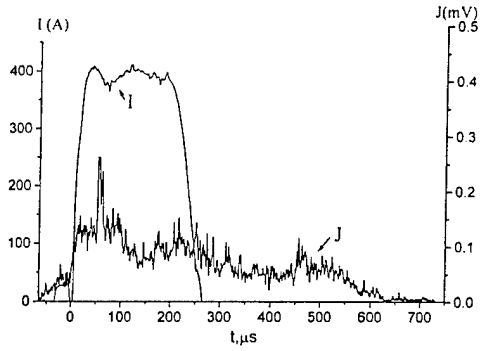

Fig.2. Oscillograms of current (I) and luminescence (J).

Consider the build-up of the stationary picture of the flow in the nozzle and diffuser. There is a great amount of literature data on the nonstationary stage of the flow in the nozzle [3-5]. The characteristic time of the build-up of the stationary flow in a nozzle at a distance x can be approximately determined according to Ref. 4 as $t = \int_0^x \frac{dx}{(u-a)}$, where a is the sound velocity. In our experiment, the stationary flow built up time was estimated to be 80-100 μs.

In the diffuser, the built-up processes of pure gasdynamic flow and flow under the electric and magnetic fields turn out to be simultaneous. Let us demonstrate some details of the flow built-up in the diffuser under above conditions. Figure 3 shows several shots with the schlieren pictures of the flow. It should be noted that due to high sensitivity, the schlieren system revealed all defects of optical windows. These defects can be seen on the schlieren pictures as oblique stripes and spots. The exposure time is 1.9 μs; the time between the shots is 5.7 μs. Shot 6 shows how the ionised gas flow enters the diffuser. One can see a weak direct shock in the flow core. Let us try to understand what is the forward boundary of the flow that manifests itself as a direct shock in the schlieren picture. It is known [6] that the secondary, or divergent, shock wave as well as the discontinuity separating the gases compressed by these shock waves arise when an incident shock wave runs along the nozzle.

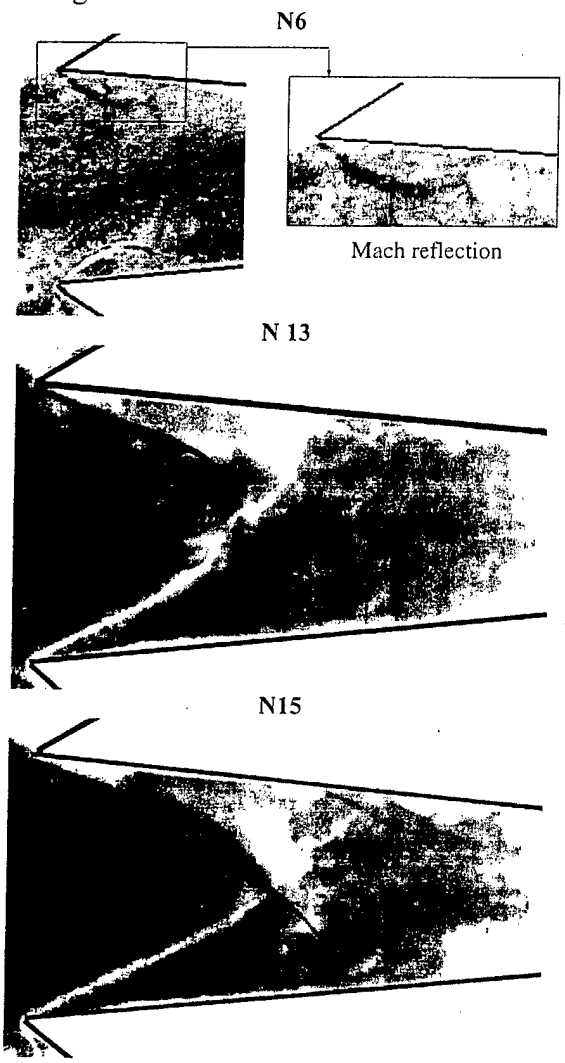

Fig.3. Schlieren pictures of the flow built-up.

But, when the incident shock wave runs in a rarefied gas, the front of this wave and the discontinuity are highly smoothed and are not seen on the schlieren picture due to an infinitesimal density gradient. So, there is reason to believe that the observed forward boundary is a secondary shock wave. The secondary shock wave is supposedly the forward boundary of the ionised gas flow because of a sharp rise in electron density on it. Thus, an ionised flow arrival in the diffuser can be described as follows. The secondary shock wave enters the diffuser, then the Mach reflection from the diffuser walls occurs (see Fig. 3, shot 6). Further, an

attached shock based on the reflected shock wave arises. The 13th shot shows a nonstationary shock-wave configuration at the moment when the secondary wave has already left the zone of observation. This schlieren picture fixes the dramatic events evolving during build-up. One can see that one attached shock is divided, the second experiencing additional disturbances. However, the picture changes with time. Shot 15 shows that the attached shocks take their ordinary form, but a new shock, which is clearly seen near the cathode wall, arises. The point is that, as it was noted earlier [7], the boundary layer grows strongly, essentially near the cathode wall, during the current switch-on so that its effect on the flow core becomes more pronounced. Its sharpest rise takes place at the end of the electrode near the isolator wall, this gives rise here to an additional shock. These are the main features of the flow formation in the diffuser.

RELAXATION OF SHOCK-WAVE CONFIGURATION TO THE INITIAL STATE

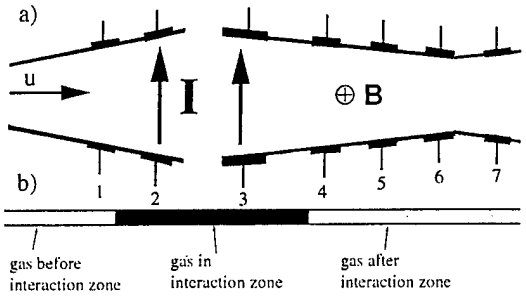

Fig. 4. Current flow (a) and interaction region (b).

In the second series of the experiments, the length of the zone of interaction was enlarged. A schematic of the electrode commutation is shown in Fig. 4.

Figure 4-a shows that, in this case, a magnetically induced current as well as a current supplied by the external source is circuited through the electrodes located at the nozzle end (2nd pair) and the electrodes at the diffuser origin (3rd pair). Below (Fig. 4b) the horizontal band shows the legend of the gas region in the absence of external fields, the gas region subjected to external fields, and a downward region where the gas which was subjected to the interaction earlier enters. Let us consider the relaxation process of the shock-wave configuration toward the initial picture after current switched off. The magnetic field of 1.3 T is quasi-stationary. Figure 5 shows the value of current and pulse shape.

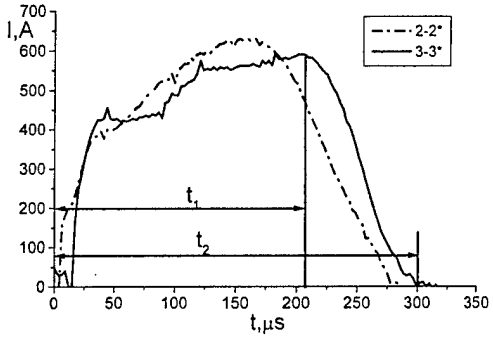

Fig.5. Current pulse shapes for the second series of experiments.

The current is about 500 A, pulse duration t_2 = 300 μs, quasi-stationary state is about t_1 = 220 μs. Following a set of shots shown in Fig. 6, let us demonstrate how the shock configuration formed under the action of external fields changes after switching off electrical current. The time of exposure is 1.9 μs; the time between shots is 5.7 μs. The distances passed by the forward boundary of the gas which was earlier subjected to external fields are shown on the bands on Fig.6. Shot 42 shows the picture for the beginning of the current pulse downfall.

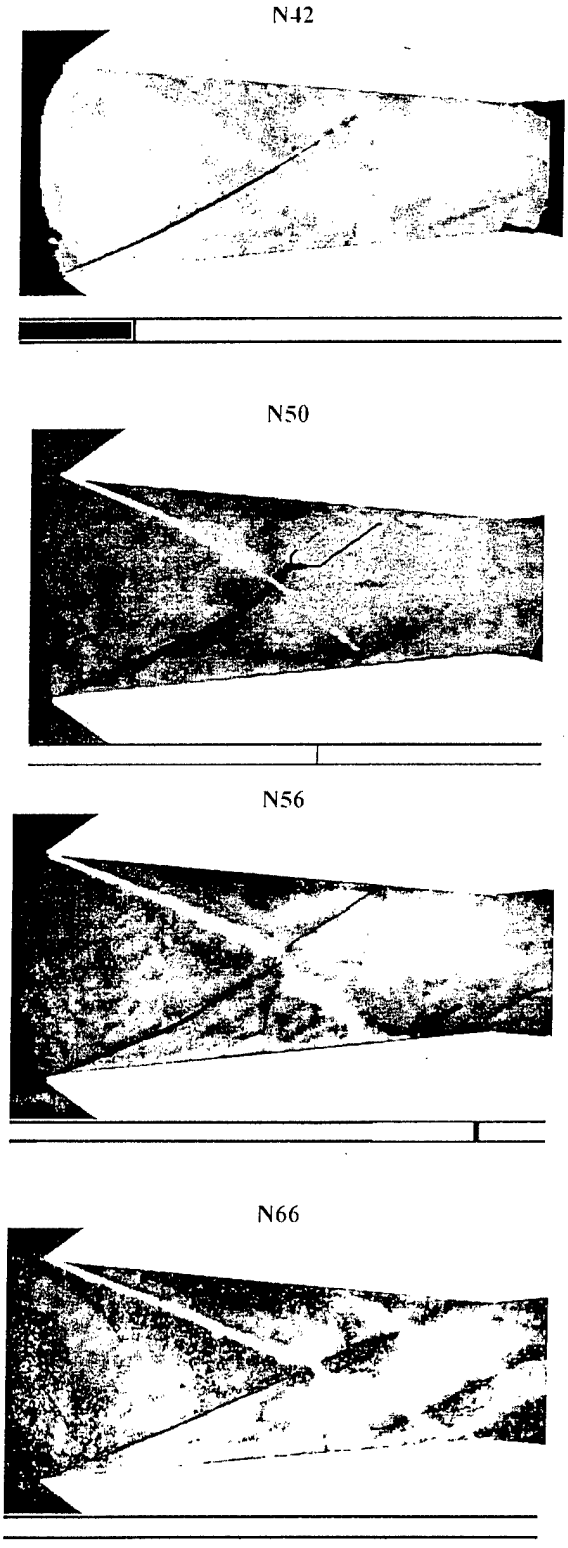

Fig.6. Changing of shock-wave configuration after switching-off electrical current.

Generally, the details are similar to the shock-wave picture at B = 0, V = 0, given in Fig.1, only the main parameters x_c , φ and ψ being changed. Here (Fig. 6) one can see the attached shocks "a" , shocks "b" arising after interaction of the attached shocks with each other, and the shocks reflected from the walls. Shot 50 shows a flow picture after the current is switch off; the forward boundary of gas disturbed by interaction is shifted downward. Shot 56 shows the fate of the shock-wave configuration when there is no current for a long time and when the gas which was earlier in the interaction zone runs downward. By shot 66 the interaction process had exhausted, the time elapsed after that event is approximately equal to the time-of-flight; hence, there is previously undisturbed gas in the diffuser.

To describe the process restoring the initial state of the shock-wave configuration after current's switch-off, Figure 7 shows the time dependence of a slope angle of the attached shock when the current is switched-off. Besides the time scale there are presented the corresponding values of the current at the second scale of the abscissa. Together with the results on an angle φ at the switch-off of current (black circles), Fig. 7 shows the angles φ at the stationary current (hollow squares) of which values correspond to the pulse current at a certain instant of its downfall.

Figure 7 denotes three moments of time: t_1 is the time of a relative plateau to be passed referring to the current oscillogram and its downfall begins, t_2 is the moment of the current's switch-off, t_3 is the time to restore an initial value of φ with no changes in future. The sharpest decrease in φ occurs within a range t_2-t_1 where the current falls from a maximum down to zero. However, a comparison with the stationary values of φ shows that a change in φ is somewhat slower than a change in a current, i.e. the flow picture "remembers" the previous conditions. More clearly it is seen within a range t_3-t_2..

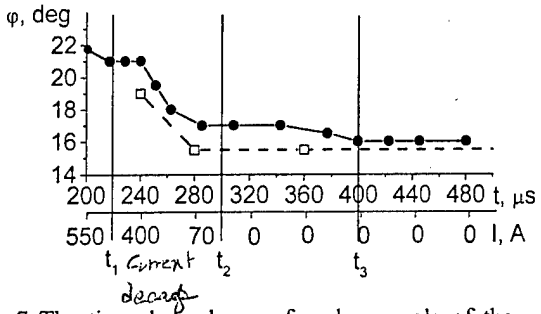

Fig.7 The time dependence of a slope angle of the attached shock (φ). Second abscissa line shows the current at the time on the first abscissa line. t_1 is the time of a relative plateau to be passed referring to the current oscillogram and its downfall begins, t_2 is the moment of the current's switch-off, t_3 is the time to restore an initial value of φ with no changes in future.

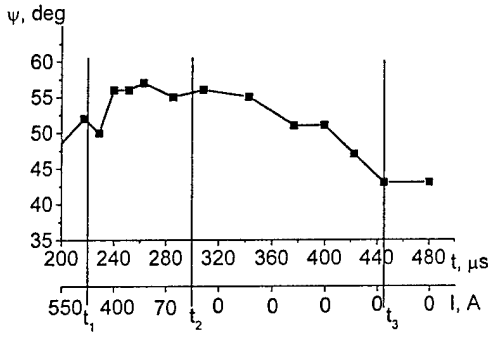

Fig.8. Time changes in an angle ψ between the attached shocks. Second abscissa line shows the current at the time on the first abscissa line. t_1 is the time of a relative plateau to be passed referring to the current oscillogram and its downfall begins, t_2 is the moment of the current's switch-off, t_3 is the time to restore an initial value of φ with no changes in future.

Here, time after the current's switch-off is almost equal to a time-of-flight, a gas filling earlier the interaction region left already the diffuser but a memory about the effect of the external fields is in the φ of which value is still greater than that with no interactions. Figure 8 shows the changes in an angle ψ between the attached shocks reflected from each other obtained when treating the same shots as in Fig. 7. An analysis of the presented dependence may evidence that the value of ψ does not reach its maximum for 200 μs elapsed at the high current, and it is rising after the current's downfall, being unchanged for all time of the current's switch-off (t_2-t_1). After switch-off of the current, when a gas volume experienced the interactions left the observation zone, a value of ψ is conserved for a long time and relaxes toward its initial value slower than φ. Concerning the relaxation process of the shock-wave configuration toward its initial picture after ceasing the effects of the external fields, it can be noted that this process should depend on a spreading velocity of the disturbances relative to a gas (u-a), and, consequently, must proceed in different ways at the different Mach numbers. In our experiment, the values of M at the diffuser's inlet are rather higher compared with those in the second half of the diffuser. Possibly, for this reason, a relaxation time of an angle φ depended mainly on the Mach number at the diffuser's inlet proves to be shorter than a relaxation time of an angle ψ depended on, in its turn, a combination of a number of processes in a mean section of the diffuser where the Mach number is smaller.

CONCLUSIONS

To investigate the effects of the impulse electric and magnetic fields on a shock-wave configuration in a diffuser, it was developed a method with the value and duration of the forces determined by an impulse of a current shaped with a long line. This work presents certain features of a flow origin when switch-on a current. It was determined that, a current being switched-off, a delay arises concerning the main parameters of the shock-wave configuration relative to the changes in the current. It was determined a relaxation time of the shock toward their initial position after switch-off of the current.

This work was supported by ISTC (contract #2009).

REFERENCES

1. S.V. Bobashev, R. V. Vasil'eva, A. V. Erofeev, T. A. Lapushkina, S. A. Poniaev, and D. Van Wie, Arrangment of experiments on MHD control of shock wave configuration in supersonic

diffuser, Termochemical and plasma processes in aerodynamics, St.Petersburg, July 15-18, 2002
2. Yu.P. Golovachov, A.A. Schmidt, S.Yu. Suchikh, Numerical investigation of MGD flows in the models of supersonic intakes, The 2nd Workshop On Magneto- Plasma- Aerodynamics In Aerospace Applications, IVTAN, Moscow, April 5-7, pp. 74-77, 2000.
3. S.F. Chekmarev, Pulse gas flows in supersonic nozzles and jets (in Russian), Institut Teplofiziki, Navosibirsk, 342 p., 1989.
4. V.N. Gusev, To the question about start-up of supersonic nozzles, Ingenernui jurnal, 1961.
5. V.G. Maslennikov, B.M. Dobrynin, Stabilization of the initial region of a two-dimensional supersonic nitrogen jet at various values of the nozzle exit-to-ambient pressure ratio, Zhurnal Tekhnicheskoi Fiziki, vol.51, N6, 1981.
6. T.V. Bazhenova, L.G. Gvozdeva, Non-stationary interaction of shock waves (in Russian), Nauka, Moscow, 274 p., 1977.
7. S. V. Bobashev, A. V. Erofeev, T. A. Lapushkina, S. A. Poniaev, V. A. Sakharov, R. V. Vasil'eva, and D. M. Van Wie "Effect of the wall layers on the electric current in a model of MHD diffuser", AIAA Paper 2001-2878, 32nd AIAA Plasmadynamics and Lasers Conference and 4th Weakly Ionized Gases Workshop, Anaheim, CA, 2001.

EFFECTIVENESS OF PLASMA METHOD OF FLOW/FLIGHT CONTROL.

Sergey B. Leonov, Valentin A. Bityurin, Anatoly I. Klimov

Institute of High Temperatures RAS (IVTAN)

Acronyms:

C_d -drag factor, ΔC_d -change of drag factor, F_x -axial force (drag), h-specific heat of fuel with kinetic energy, M- Mach number, η - efficiency factors, Q - mass expense of gas, ρ -gas density, Tg- gas temperature, V-airflow velocity, W_{pl} -electric power input to plasma generator, W_{kin} -kinetic power of airflow, W_{en} - power of engine.

1. Introduction.

Conventional methods to advance aerodynamic characteristics of aero-vehicles and its parts or to adjust the trajectory are based on application of mechanical elements, which use an energy of approach airflow for re-distribution of pressure on surfaces, and application of jets' power in local areas near the surfaces. There are no doubts now that another methods for flow/flight control have a practical prospective. Among of them the energetic method sounds as the most important [1-3]. An idea of the energetic method can be formulated on the most simple manner as following: modification of flow-field structure and, consequently, changing a pressure and tangential tension near surfaces by means of an energy release into predefined space area with predefined parameters' distribution and at predefined tempering. The diagram below in Fig.1 shows a simple classification of types of the energetic effect on flow-body system.

Several main mechanisms of energy release effect can be described: (1) change of thermodynamic properties of medium, (2) modification of flow-field structure, (3) local artificial separation and (4) boundary layer modification. Technically the effects are become apparent in bow shocks transformation, wave drag reduction (thermodynamic and form-factor effects), base drag reduction, skin friction change, thermal flux reduction (redistribution), adjustment of flow-field structure in inlets/diffusers, etc. Such possibilities can be realized by means of electrical discharge plasma generation; free-localized plasma generation in electromagnetic wave beams; blowing out of high enthalpy plasma jets; and by the other similar phenomena.

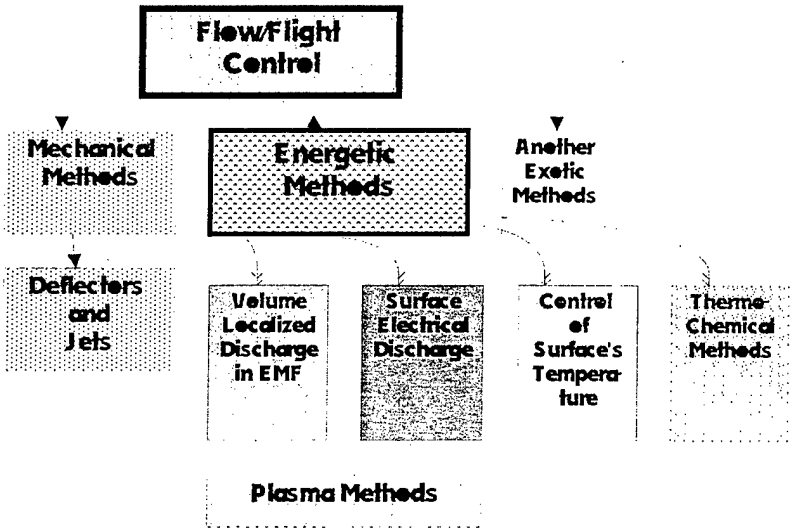

Fig.1. Simplified Scheme of Flow/Flight Control Methods.

The content of this paper is confined by the problem of aerodynamic drag reduction as the most popular in discussions

last 10 years. From the other side such an approach allows one to consider important patterns in field of energetic method's application. The criterion of energy deposition effectiveness is defined more precisely. A short historical survey and the most important results of the last researches in this field are presented. An alternative to electrical discharge plasma method is proposed. Brief discussion on a scaling law is presented. The conclusions on the effectiveness of drag reduction by plasma are done.

The results presented here are a part of extensive work on plasma formation influence on aerodynamic characteristics of models under the conditions of wind tunnels. Last years there were several attempts to organize a flight test. Unfortunately now there no any evidences on plasma behavior and effect in real flying system. So, all our conclusions have a preliminary and prognostic nature.

2. Effectiveness Criteria of Energy Release.

Obviously, that perspective of a new technology's real applications directly depends on effectiveness in comparison with conventional ones. Such competitive methods in this case are geometric factor of aero-vehicle and increase of power and efficiency of craft's engines, which use chemical energy of fuel.

We can describe two criteria of effectiveness of plasma influence on body's drag in airflow: physical and technical [4,5]. A physical one suggests, that change of integral drag factor should be related to specific input power to airflow (electrical, as a rule):

$$\eta_1 = -\frac{\Delta C_d / C_d}{W_{pl}/W_{kin}} = -\frac{\Delta C_d}{C_d}\cdot\frac{C_d \rho V^3}{2W_{pl}} = -\frac{\Delta F_x V}{W_{pl}},$$

where the change of axial force can be obtained from direct measurements at compensation of base effects. Obviously, that such a criterion is correct only for a model situation where the constant velocity of airflow is realized. Under the conditions of flying vehicle, constant power of main engine W_{en}, stationary regime of flight and relatively small energy input to the plasma, the criterion is modified to the following:

$$\eta_1 = -\frac{\Delta C_d / C_d}{W_{pl}/W_{kin}} = \frac{3\Delta V}{V}\times\frac{W_{en}}{W_{pl}}.$$

The technical criterion is more complex. Such a criterion has to take into account the specific scheme of the electric power generation onboard, or electric power transportation from the ground station, or

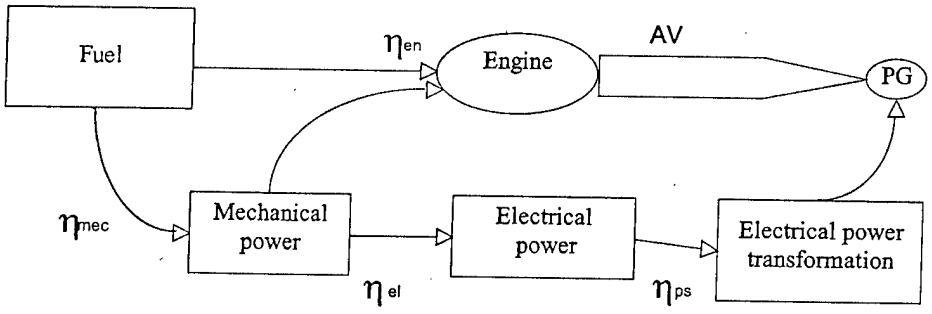

Fig.2. Example of energy transformation scheme.

power needed to accelerate an electricity storage capacity mass. It should include fuel's and electrical efficiency of engine in accordance with specific diagram of energy transformation. If an air-breathing engine is used for transportation, the change of flow structure due to plasma influence can effect

on flow-rate through an inlet, especially at hypersonic conditions.

A sample of energy transformation scheme is shown in Fig.2 for a case of turbojet engine and mechanical driving gear for the electric machine. Here η_{en} is a total efficiency of energy transformation from fuel to an engine mechanical power, excluding secondary internal energy expenses:

$$\eta_{en} = \frac{F_x V}{hQ_{fuel}}$$

η_{mech}—efficiency of energy transformation to a mechanical power, η_{el}—efficiency of electric generator, η_{ps}—efficiency of power supply of PG. So, technical criterion looks as the following:

$$\eta_2 = \eta_1 \times \frac{\eta_{mech} \times \eta_{el} \times \eta_{ps}}{\eta_{en}}.$$

At $\eta_2>1$ the technology promises decrease of fuel expense by vehicle's engine. If we don't take into account exotic schemes of energy transformation, than the criteria are closed each other. A problem of applicability of plasma technology comes to achievement of reasonable physical effectiveness of plasma application, on a careful estimations, $\eta_1>2$. At the same time it is clear that there are no universal technical criterion of efficiency and each scheme should be analyzed individually.

The principal difficulty in realization of such an approach is that an aerodynamically optimized body reveals a low drag already. Probably, its drag can't be reduced effectively in frames of steady-stage interaction.. The chart in Fig.3 shows an experimental dependence of counterblow plasma jet influence effectiveness on the initial drag factor under supersonic airflow conditions [6]. It is clearly seen that an optimal shape of streamlined body doesn't give a chance for the effective enhancement. Another types of plasma formation demonstrate different values of the effect but the similar trend.

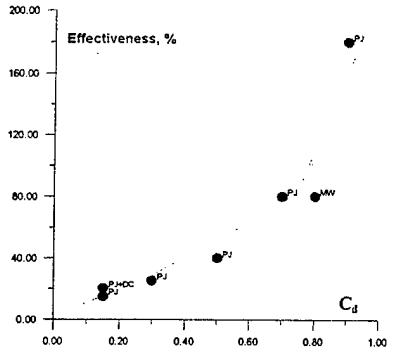

Fig.3. Plasma Jet influence energetic effectiveness vs initial drag factor of body. M=1.7÷2.0.

In general case the drag force of a vehicle at atmospheric flight is represented as the sum of the friction drag and the pressure drag. At the same time the pressure drag includes the wave drag, the base drag, the interference drag etc. The contributions of each component to the total drag at subsonic, transonic and supersonic flight modes are different. Usually the main attention is paid to pressure/wave shares of the total drag. Analysis of aerodynamic situation shows that the friction and interference effects can play an important role as well. Several ways to enhance of physical effectiveness of plasma could be considered as follows:

- Providing of the optimal geometry (spatial) distribution of energy input near the body.
- Decrease of pressure amplitude downstream the bow shock by means of plasma generation with optimal parameters in an area of interaction at supersonic streamlining.
- Using the processes of plasma induced local separation for the form-factor optimization.
- Boundary layer modification for the skin friction reduction.
- Using the time-alternative (variable) operation modes of plasma generation, in particularly, pulse-repetition mode.

The last method assumes some non-linear mechanisms of effect, in respect of amplitude of interaction. Actually, it is well

known, that pulse operation mode of discharge allows to obtain non-equilibrium parameters of plasma (in respect of temperature distribution on degreases of freedom and ionization). Repetition rate can be in accordance of gas-kinetic (L/V) time or less in case of stagnation (circular) area presence, at influence on boundary layer and base area. From the other side, an increase of pulse power, finally, might lead to saturation of effect during a pulse. So, a plasma influence will be less in average at the same mean power of pulse periodic and continuous operation mode.

3. Short Historical Survey and Some Important Results.

Starting from 1970th a serious interest to the problem of plasma generation inflow and the interaction of plasma with flow and flying bodies was appeared. At 1980th the specialized ballistic experiments have been done. Some results have been published later [7]. There was shown that plasma of electrical discharge effects on parameters (stand off) of bow shock and drag of flying bodies. But the regular investigations in wind tunnels have started at 1988.

Practically, simultaneously the experimental works began in TsAGI, MRTI, NIIRP, GosNIIAS, ITAM, MESU and TsNIIMash. The experiments have been simulated and supported by the theoretical investigations in Institute of Mechanics MSU and Keldysh IAM. Probably, the first publications were the [8-15]. Starting from 1995 these works have been supported by BAe/DERA, Rockwell/Boeing Co., APL/JHU and EOARD/AFOSR. At that time the most part of experimental works have been condensed by the Moscow Technical Company (MTC), which has been incorporated to IVTAN in 1998.

Conditionally all efforts can be separated to three cans: background (before 1997), main experiments on drag reduction in 1996-99 and the last years' works in frames of Advance Flow/Flight Concept (AFFC).

The most results from the first group are presented in the proceedings of WIG workshops [16] and Russian publications. That time very popular notion was the "plasma magic" approach. Different plasma generators were used by authors to explore the plasma effect on drag and lift [17] of bodies, namely: plasma jets, laser sparks, longitudinal AC/DC electric discharge, HF corona, discharge on body's surface. There were found the following results:

- Plasma of electrical discharges and laser beam decreases the drag of axe-symmetrical bodies in supersonic and subsonic flow in value up to 50% of initial level.
- The effectiveness of plasma influence can be more than 1 for blunt model.
- Stand off of the BSW is increased and stagnation pressure in top point is decreased due to plasma generation.
- Lift/drag ratio of a simple airfoil can be enhanced.

As a sample of early work the results of counterblow plasma jet effect can be described [13,17]. Some results of this work have been repeated and improved later [4,18-20].

A high enthalpy erosive plasma jet has features, which are important for application it as a factor of drag reduction: large specific length of initial laminar part of jet and high level of specific pressure counteraction. Using a hydro-carbon working medium gives possibility to obtain less value of mass density in comparison with air at same temperature (due to large share of H2 in a thermo-destructive mixture). Besides of this, hydro-carbonic plasma has got high level of chemical activity: there is a lot of energy release at mixing with air. Aerodynamic models were a combination of cylinder (40, 60 and 70mm of diameter) and the cone with 30° of half angle or hemisphere. Base area was plain. Preliminary runs had shown that drag factor of such models was about 0.8-1.0 at Mach number 1.7-2.0. Sample of Schlieren photo

of the plasma jet blowing out is shown in Fig.4. In the Schlieren photos a change of

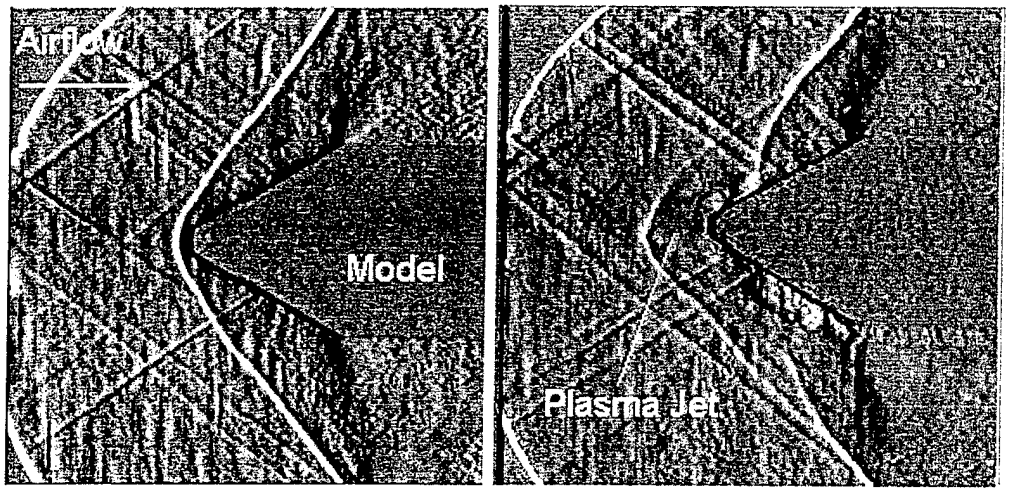

Fig.4. Schlieren photo of plasma jet interaction with supersonic airflow.

stand off of BSW is seen as well as generation of week turbulent heat layer around the model. Week parasitic shocks in a field of observation were due to mechanical junctures on a wall of WT.

A sample of balance measured parameters and primary calculations for one of runs at M=1.6 is presented in Fig.5. It is seen, that pressure in airflow is changes during a time of experiment. It happens due to blow in WT pumped contour and some increase of temperature of air during the run. Resulting values of Cd are well compensated by taking into account all data at procedure.

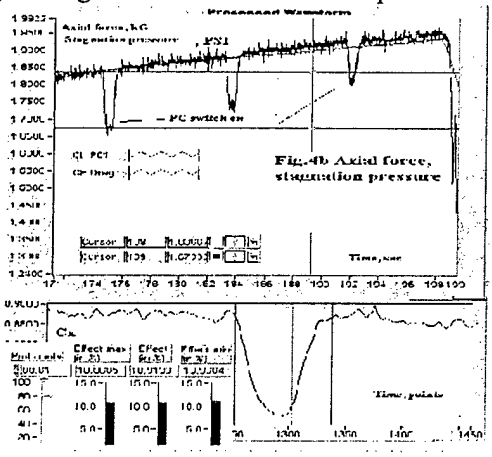

Fig.5. Sample of the drag measurements at plasma jet generation.

In Fig.6 the data on physical efficiency η_1 of Plasma Jet influence on drag of model are presented in depending on Mach number. Well seen that the efficiency of interaction is maximal at transonic mode. In this case the stand-off of BSW was maximal too. The value of efficiency in this work is large and, important, more than 1.

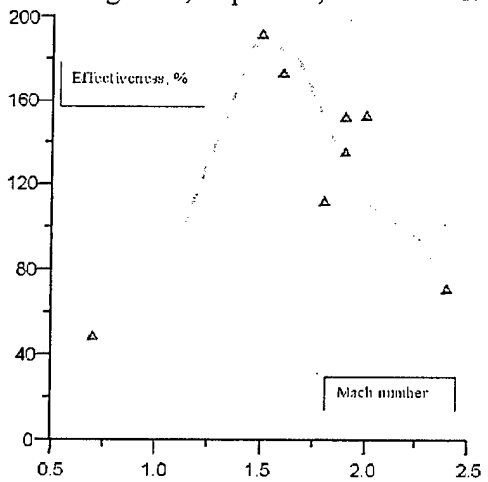

Fig.6. Effectiveness of plasma jet influence vs Mach number.

The increase of efficiency of plasma influence more than 1 is the key moment of this work. Well known that calculations show such exceeding in many times [21]. But at experimental conditions and for "non-blunted" bodies it is not so simple problem. In that work statistically reliable results on

drag reduction in dependence on input power, Mach number and model parameters were obtained as well as the first summarizing of experimental results on plasma jets influence on airflow-body system was made.

Several important experimental works are related to the second group. The first of those was the work, which has been supported by BAe and DERA in 1996-97 [22]. The combination of plasma jet generator with the surface discharge was utilized. The feature of the experiment was the low initial drag factor of the model C_d=0.09-0.14. The main result was that at low drag the plasma effect is small and non-effective. Later, the analysis of the data shows that a skin friction reduction can explain such an effect.

In 1997-98 the experiment on AC/DC plasma influence on drag of the axial-symmetric model was made at EOARD/AFOSR support [23]. The wind tunnel of TsAGI is used. The measurements of plasma parameters were done by MSU team. Different modes of the discharge were described (see Fig.7). The resulting drag reduction was $\Delta C_d/C_d$ =10-15% at physical efficiency 30-100%.

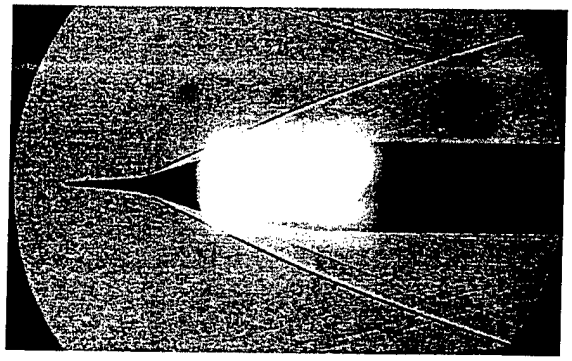

Fig.7. Longitudinal surface discharge at supersonic airflow.

A sufficiently different type of the interaction has been observed at short pulse plasma excitation with a sequential influence of heated ("processed") area of flow-field on the shock structure and the body. In such a case the essentially unsteady and non-linear processes play the role. The work on short-pulse MW free-localized discharge effect on flow and drag was performed in 1997-98 at Boeing Co. support [24-25]. The gasdynamic installation of IMM St-Petersburg University and MW installation of RDI of Radioapparature were utilized.

A sample of Schlieren photo of shock wave structure is presented in Fig.8. The photo has been obtained under the following conditions: microwave pulse duration 1.5us, pulse period 1.1ms, MW pulse power about 200kW, localization 5cm and 3cm upstream the model, exposure 1us, time delay between MW pulse and photo 30us, Mach number of airflow M=1.5.

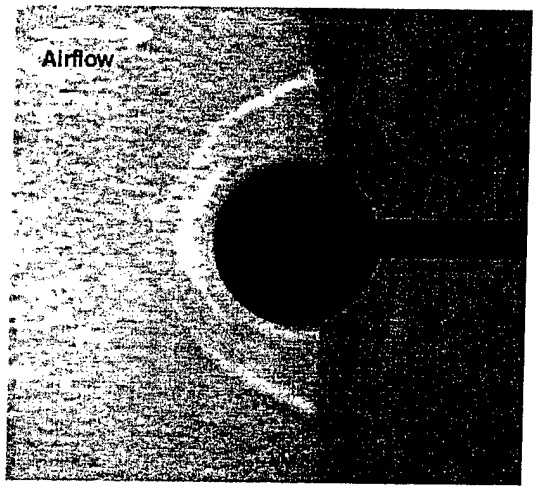

Fig.8. Unsteady shock wave structure at free-localized MW discharge excitation in upstream airflow.

It is clear that such a SW structure like a "splitting" can be observed only at unsteady conditions. The mechanism of interaction includes three main stages: momentary (during the MW pulse) plasma generation (1) in volume about 20cm^3, streamlining of the model by relaxating plasma (2) at unsteady SW structure realization and reconstruction of the initial SW structure (3). Whole process spends up to 120÷160us and repeated again in about 1ms. The measured mean drag reduction has been in a range 5÷9% on a spherical model. The sample of the balance's record is shown in Fig.9. At the same time the measurements of the stagnation pressure on the top of the

model show a large level of fluctuations. A formal recalculation of instant effect gives 30÷40% of drag reduction at efficiency η_I=50÷100%.

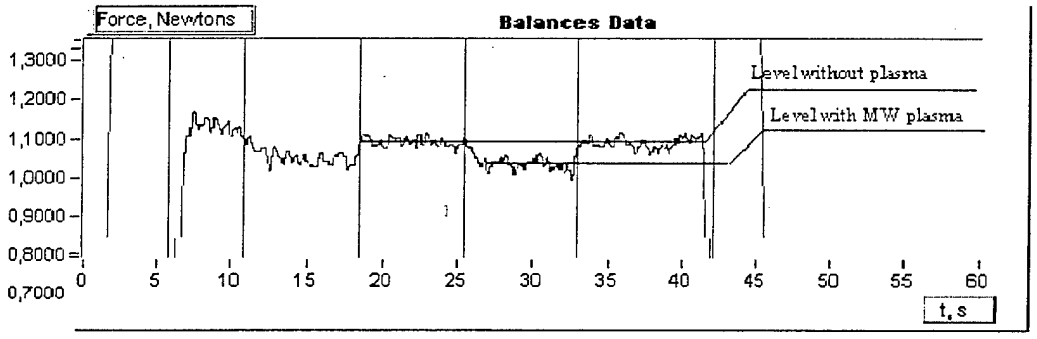

Fig.9. Sample of balance's record at MW plasma effect. M=1.5.

Analyzing this specific situation the conclusion might be considered that the unsteady type of interaction at the volume type of the energy release can provide a sufficient positive effect in drag reduction of bodies in supersonic airflow.

An effort of drag reduction with single-electrode high frequency (HF) filamentary discharge has been done in 1998-99 at BAe support [26,27] in experimental facilities of GosNIIAS, TsAGI and IVTAN. In frames of this work at the first time there was demonstrated specific behavior of plasma filaments in high-speed flow and effect of plasma filament penetration through the BSW with sequential modification of BSW (see Schlieren photo in Fig.10). Several different mechanisms of interaction were found. Among of them the mechanism of drag reduction of well shaped bodies with drag factor $C_d \approx 0.1$ gave the effect $\Delta C_d/C_d$ =5÷6% at physical efficiency 30-180%.

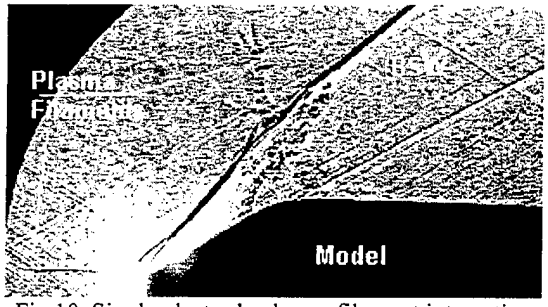

Fig.10. Single-electrode plasma filament interaction with BSW at M=2.

A comparison of data on HF discharge with another results allows suggesting, that a main mechanism of drag reduction at HF discharge could differ specifically from plasma jets and AC/DC discharges as well as at MW free localized discharge.

In 1997-99 the WT experiments with large models were fulfilled at Boeing Co. support on test facilities of TsNIIMash and, later, TsAGI. The first model was 1/3 scale nose part of F-15 vehicle (320mm of diameter), the diameter of the second model was two times less. Unfortunately, the work with large model has not been completed due to technical faults. A preliminary result was $\Delta C_d/C_d$ =4±3% at physical efficiency 20÷100%. The 1/6 scale model test was conducted with specific plasma generators arrangement. Formally, the highest efficiency has been demonstrated in case of AC discharge on forehead spike, namely

$\Delta C_d/C_d$ =6% at up to 360% of physical efficiency [24,28,29].

These efforts show that plasma method of flow/flight control makes a sense. The problem is in understanding of specific mechanisms of the plasma effects in details and sequential optimization. In general case the drag force of a vehicle at atmospheric flight and/or in inlets and ducts is represented as the sum of the friction drag and the pressure drag. At the same time the pressure drag includes the wave drag, the base/obstacle drag, the interference drag etc. The contribution of each component to the total impulse loses at subsonic, transonic and supersonic flight modes are different. Usually the main attention was paid to pressure/wave shares of the total drag. Analysis of aerodynamic situation shows that the friction and interference effects can play an important role as well.

The third group of works in the field of AFFC is devoted to the problems of boundary layer and separation control. These efforts have own extensive background, for example [30]. The experimental works have started in 1999 at support by EOARD/AFOSR [31-34]. The preliminary results of these researches can be formulated as follows:

- can be The strong effect of surface discharge on the flow-field structure has been demonstrated experimentally.
- Global separation in duct-driven flow due to the surface plasma generation has been found.
- The generation of plasma overlayer is the method to control the shocks position near the surface as well as the flow parameters in whole duct.
- Structural (non-homogeneous and unsteady controlled modes) plasma generation allow one to decrease required power for the realization of flow control effect.
- The transversal surface discharge is much more effective than longitudinal discharge in terms of energy input density and flow structure control. The transversal discharge reveals the instability of relaxation type.
- The value of power input effects directly on amplitude of the plasma influence. The energetic threshold for global boundary layer separation is defined in level about 5÷8W/cm.Torr under the conditions of described tests.
- In some important cases the structure of duct-driven flow (configuration of oblique shocks) can be modified by means of surface plasma generation gently (without dramatic changes of Mach number).

At the same time the anticipated positive effect in FFC (drag reduction) due to inflow energy release are associated with some penalties to be paid for. This statement illustrated by several examples.

Reducing the wave drag of the vehicle forehead leads to pressure redistribution in the base area. Simple analysis shows that such a pressure change can has the same sign, i.e. the resulting net effect for whole body is much less, than for individually considered forepart.

If the air-breathing engine is utilized in the vehicle a drag reduction can lead to decrease of air mass flow-rate through the inlet. Thus, any specific AD situation requires the analysis of all aspects and possible negative sequences.

4. Thermo-Chemical Method of Drag Reduction.

Obviously, that perspective of a new technology's real applications directly depends on effectiveness in comparison with conventional ones. Such competitive methods in this case are geometric form-factor of vehicle enhancement using mechanical energy and chemical energy of fuel. A new method of flight control is proposed and analyzed.

The base of the method is in turning from electric process of the energy deposition to chemical and mechanical one as the more effective from the viewpoint of energy transformation. The mini-bodies are shooting upstream the vehicle with needed

frequency and velocity. They have the defined mass to provide the optimal distance of moving off. The mini-bodies should be made from energy extracting substance. One of the variants is the solid hydrogen pellet. The pellets are evaporated under the thermal load of approaching airflow and vapor (gas) sequentially is burning in own base trace. The process can be quasi-continuous in dependence on the parameters. Such a way the area of significant energy release is generated upstream the main vehicle.

The results of simulations in frames of this idea are optimistic. Four main interrelated problems are considered: the mini-body motion in hypersonic approaching airflow at mass loosing (1); heat-mass transfer between flow and mini-body (2); fuel combustion in separated trace of the pellet (3) and influence of such a trace on the main body (4). The preliminary conclusion is done that the method of pellet shooting can be prospective after the parametrical optimization.

5. Scaling Laws.

Using the non-homogeneous discharges, like filamentary HF discharge or MW discharges, can give a possibility a significant decrease of needed power of plasma generator in case of middle and large vehicle. Well known that generally a needed power for AV moving in atmosphere is proportional of square degree of AV dimension at the same other parameters. If we need to use volume type of discharge than a power for discharge excitation rises in accordance with cubic degree of dimension. At surface type of discharge we need a square degree of power rise. In the case of filamentary one we have a prospect that needed power rises in accordance with degree between 1 and 2. In this case there should be growth of plasma effectiveness with increase of scale of aircraft.

Typically, in-flow generated plasma appears as a non-uniform and unsteady formation. Utilization of a fully controllable electrical discharge could significantly decrease the required energy input to airflow. A special interest in electrodeless and single-electrode plasma generation has arisen due to its possibility to provide the energy deposition and gas property modifications at a pre-defined zone of the flowfield, prospectively, under the effective electronic control of plasma location.

6. Conclusions.

The vehicle designed for one of specific modes of flight conditions can spend a large part of the flight time at non-optimal aerodynamic situation. Probably, the most critical fractions of the trajectory lies under transonic mode of airflow-body interaction, especially at a complex shape of the vehicle. The plasma technology can provide an effective influence on position and amplitude of local shocks and parameters of separation zones as well as to change the temporal pressure redistribution on the surface of aircraft.

Mentioned above the objectives of AFFC concept could be now formulated as follows:

- Plasma technology can be applied effectively for a drag reduction of bodies under non-optimal conditions of atmospheric flight.
- Discharge plasma technology promises the advantages in a field of the boundary layer control, including stabilization of line of laminar-turbulent transition, guiding of separation processes, and control of the local shocks position.
- MPA technique can give a possibility of fast, inertia-less, effective control of flight trajectory and thermal loads, as well as for objectives of internal flows and combustion, prospectively.
- Structural (non-homogeneous and unsteady controlled modes) plasma generation allow to decrease required consuming power for the effect realization.
- MPA technique can be a key component for an objective of 2-D and 3-D separation processes stabilization.

References

1. G. G. Chernyi, The impact of electromagnetic energy addition to air near the flying body on its aerodynamic characteristics. 2-nd WIG Workshop, proceeding, Norfolk, VA, April 24-25, 1998.
2. G. Chernyi "Energy release effect in areas of electric discharge near bodies in airflow." Eight All-Russian Congress on Theoretical and Applied Mechanics, August 23-29, 2001 / Perm, Russia, p.594.
3. V. Bityurin, A. Klimov, S. Leonov "Assessment of a Concept of Advanced Flow/Flight Control for Hypersonic Flights in Atmosphere." 3rd Workshop on WIG. November 1-5, 1999 / Norfolk, Virginia, AIAA 99-4820.
4. S. Leonov, V. Nebolsin, V. Shilov "Effectiveness of plasma jet Effect on Bodies in an Airflow", Proceedings of Workshop "Perspectives of MHD and Plasma Technologies in Aerospace Applications", Moscow, IVTAN, 1999, pp. 58-65.
5. T. Cain, D. Boyd "Electrodynamics and the effect of an electric discharge on cone/cylinder drag at Mach 5"; 37th AIAA Aerospace Sciences Meeting and Exhibit, January 11-14, 1999/Reno, NV, AIAA 99-0602.
6. S. Leonov, V. Bityurin, A. Klimov, Yu. Kolesnichenko, A. Yuriev "Influence of Structural Electric Discharges on Parameters of Streamlined Bodies in Airflow." 32th AIAA Plasmadynamics and Lasers Conference and 4th Weakly Ionized Gases Workshop 11-14 June 2001 / Anaheim, CA, AIAA-2001-3057.
7. G. Mishin, Yu. Serov, I. Yavor "Streamlining of the sphere in plasma of gas discharge at supersonic speed", J. of Technical Physics, Letters (Rus), 1991, v.17, No.11, p.65.
8. P. Georgievsky, V. Levin "Supersonic flow over space-distributed energy sources", Mechanics, modern problems. Moscow, MSU Pub. 1987, pp. 93-99.
9. A. Yuriev, V. Borzov, N. Savischenko et all. "Method of Flight Control", Patent RU-2173657, May 1990.
10. V. Vstovsky, L. Grachev, Yu. Kuznetsov et all. "Study of unsteady supersonic flow over the body in longitudinal electrical discharge", TVT (rus.), 1990, v.28, No 6, p.1156.
11. V. Borzov, I. Rybka, A. Yuriev "The influence of local energy supply at hypersonic flow on wave drag of bodies of different blunting", IFJ (rus), 1994, v. 67, No 5-6, pp.355-361.
12. V. Alatortsev, Yu. Kuznetsov, V. Skvortsov, L. Grachev, K, Khodataev et all. "Experimental study of drag force control on the model at the flow excitation by the longitudinal electrical discharge", TsAGI Proceedings, No 2552, 1994.
13. Leonov S.B., Pankova M.B., Shipilin A.V. "Modeling of ball lightning interaction with bodies in atmosphere" "Ball Lightning in Laboratory." ed. Avramenko R.F., Klimov A.I. and oth. Moscow: Chemistry, 1994.
14. A. Gridin, A. Zabrodin, A. Klimov, Yu. Kuznetsov, A. Lutsky, V. Skvortsov, K. Hodataev et all "Numerical and experimental research of supersonic flow over bluntnose body in presence of electric discharge", KIAM RAS Preprint No 19, 1995, Moscow.
15. Burdakov V.P., Baranovsky S.I., Klimov A.I., Lebedev P.D., Leonov S.B., Pankova M.B., Puhov A.P. "Improvement of aerodynamic and thrust-energetic parameters of hypersonic aircrafts and engines using algorithmic discharges and plasmoid formations". Proceeding of the International Conference of Advance Technology, Moscow, MSU, 1995.
16. Workshop on Weakly Ionized Gases. Proceedings. USAF Academy, Colorado, 9-13 June 1997; Second Workshop on Weakly Ionized Gases. Proceedings. Norfolk, 24-25 April 1998.
17. Workshop on Weakly Ionized Gases, USAF Academy, Colorado, 9-12 June

1997. Proceedings , Vol.1, section J.; Leonov S.B. "Plasma Jet Generation for influence on drag of bodies in a supersonic airflow". \\Contributed Papers of HAKONE VI, Cork, Ireland, 1998, p.318-323.

18. Gordeev V.P., Krasilnikov A.V., Lagutin V.I. "Experimental study of possibility of drag reduction by means of plasma", MLG (rus.), N2, p.177-182, 1996.
19. J. Chang, J. Hayes, J. Menart, "Hypersonic flow over a Blunt Body with Plasma Injection", AIAA 2001-0344.
20. Fomin V.P., Maslov A.A., Fomichev V.P. Review of IPTM works on plasma aerodynamics. Proceedings of Meeting "Perspectives of MPA Technology in Aerospace Applications", March, 24-25, IVTAN, Moscow, 1999.
21. Levin V.A., Afonina,N.E., Georgievsky P.Y., Gromov V.G., Larin O.B., Terenteva L.V. "Study of possibility of control of supersonic airflow...", Preprint IM MSU, N24-97, Moscow, 1997.
22. MCEwen R & Gilmor M. Plasma Aerodynamics Meeting Report SRC BAe, II Nov1996; R. MCEwen, Workshop on Weakly Ionized Gases, USAF Academy, Colorado, 9-12 June 1997. Proceedings , Vol.1.
23. Chuvashev S.N., Ershov A.P., Klimov A.I., Leonov S.B., Shibkov V.M., Timofeev I.B. "Flow around body and characteristics of AC/DC discharges in plasma aerodynamic experiment." In Proceedings of 2nd Weakly Ionized Gases Workshop, AIAA, Norfolk, VA, April 24-25, 1998. P.59-61.
24. W. Beaulieu, A. Klimov, S Leonov, Yu. Kolesnichenko, V. Brovkin, "Development of Cold Plasma Technology Joint BNA and Russian Program", Second Weakly Ionized Gases Workshop, Proceedings supplement, April 24-25, 1998, Norfolk, p.207.
25. V.G. Brovkin, Yu.F. Kolesnichenko, S.B. Leonov, A.I. Klimov , A.A. Krylov, V.A. Lashkov, I.C. Mashek, M.I. Ryvkin, "Study of Microwave Plasma-Body Interaction in Supersonic Airflow", AIAA 99-3740, 30th AIAA Plasmadynamics and Lasers Conference, June 28-July 1, 1999 / Norfolk, Virginia.
26. S. Leonov, T. Cain, A. Klimov, A. Pashina, V. Skvortsov, B. Timofeev "Influence of a HF Corona Plasma Structure on Drag of an Axial-Symmetric Body in a Supersonic Airflow." 3rd Workshop on WIG, November 1-5, 1999 / Norfolk, Virginia, AIAA 99-4856.
27. S. Leonov, V. Bityurin, Yu. Kolesnichenko "Dynamic of a Single-electrode HF Plasma Filament in Supersonic Airflow." 39th AIAA Aerospace Sciences Meeting & Exhibit, 8-11 January 2001 / Reno, NV AIAA-2001-0493.
28. Beaulieu W., Bityurin V., Klimov A., Leonov S. et al., Plasma Aerodynamic WT Tests with 1/6 Scale Model of Nose Part of F-15, AIAA 99-4825 Paper, 3rd WIG Workshop, Norfolk,1999.
29. W. Beauliew, V. Bityurin, A. Klimov, S. Leonov, A. Pashina, B. Timofeev, Study of characteristics of 1/6 scale model...-Proceedings of Meeting "Perspectives...", March, 24-25, IVTRAS, Moscow, 1999.
30. Kazakov A., Kogan M., Kuriachi A., Influence on the friction of local heat addition to the turbulent boundary layer. Mech. Of Fluids and Gases, N1, 1997. // Kurjachi A. P., Boundary layer transition by means of electrodynamics method. Prikl. Math. I Mech., vol.49, issue 1,1985. // A.V. Kazakov, A.P. Kuryachii, Electrogasdynamic influence on the development of the small disturbances in a boundary layer in the thin profile Izv. AN USSR, Mekhanika zhidkosti i gaza, 1, 1986
31. S. Leonov, V. Bityurin, N. Savischenko, A. Yuriev, "Study of Surface Electrical Discharge Influence on Friction of Plate in Transonic Airflow". AIAA-2001-

0640, 39th AIAA Aerospace Meeting and Exhibit, 8-11 January, Reno, NV, 2001.
32. S. Leonov, V. Bityurin, A. Bocharov, E. Gubanov, Yu. Kolesnichenko, K. Savelkin, A. Yuriev, N. Savischenko "Discharge plasma influence on flow characteristics near wall step in a high-speed duct." The 3-rd Workshop on Magneto-Plasma Aerodynamics in Aerospace Applications, Proceedings, Moscow, IVTAN, 24-26 April, 2001.
33. S. Leonov, V. Bityurin, A. Klimov, Yu. Kolesnichenko, A. Yuriev "Influence of Structural Electric Discharges on Parameters of Streamlined Bodies in Airflow", AIAA-2001-3057, AIAA 32nd Plasmadynamic and Laser Conference, June, 2001, Anaheim, CA.
34. S. Leonov, V. Bityurin, K. Savelkin, D. Yarantsev "Effect of Electrical Discharge on Separation Processes and Shocks Position at Supersonic Airflow" AIAA-2002-0355, 40th AIAA Aerospace Meeting and Exhibit, 14-17 January, 2002, Reno, NV.
35. S. Leonov, V. Bityurin, K. Savelkin, D. Yarantsev "The Features of Electro-Discharge Plasma Control of High-Speed Gas Flows." AIAA-2002-2180, 33-th Plasmadynamic and Laser Conference, 20-24 May, 2002, Maui, HI.

MW TECHNIQUE FOR SUPERSONICS

Yuri F. Kolesnichenko, Vadim G. Brovkin and Dmitry V. Khmara, Valery A. Lashkov, Igor Ch. Mashek and Mark I. Ryvkin***

**Institute of High Temperatures RAS, Moscow, Russia, **St.-Petersburg State University, St.-Petersburg, Russia*

Basic research efforts for high power microwaves emphasize the fundamental understanding of the limitations of microwave technology and its application, and investigation of promising new approaches and concepts. The attractive options of microwave technique are:

- Distant action and speed of light energy delivery at defined point
- Electronic control of microwave beam focus shape and position, tracking
- High efficiency of generation
- Suitable properties of microwave discharge

Application of directed MW energy for different concepts is well known. Among them the problem of flow/flight control via non-inertial technique provided by energy injection in front of super- and hypersonic bodies is still urgent [1,2]. The basic idea is to change flow parameters in front of a body by creation of discharge and, as a result, get the defined modification in aerodynamic coefficients. Different tools were proposed for such concept realization. Among them the use of electromagnetic (MW) beams for energy delivery and deposition at a distant spatial domain seems to be problem-inherent.

Finding out of conditions for efficient influence on AD characteristics can be divided in two general trends. The first is aimed at specifying of desirable parameters of disturbance in airflow, which effects in a defined manner on AD-body characteristic. The second one defines how to create this disturbance in a flow by means of electric discharge. The first trend is mostly gas dynamic one, the second – electrodynamic and kinetic. The results of our investigation are presented in accordance with such approach. Firstly modeling and experimental data of energy deposition in supersonic flow for drag reduction of a blunt body is given. Modeling is aimed at getting answer at the following questions: what are the optimal geometry (shape) of disturbance and parameters inside it; what type of energy deposition rate - quasi-static or explosive – is more efficient; what are scaling laws for the incoming parameters. Both modeling and experiment deals with non-stationary interaction of gas dynamic discontinuity with AD body in supersonic flow. Then MW discharge structure evolution is considered. The efficiency of EM energy concentration, it's coupling with gas and plasma and air heating is also analyzed.

I. Energy injection in SS flow - modeling

As an introduction to the problem let us consider the most evident situation, specifying simultaneously an inherent important parameters. An aerodynamic body with cross-section S is streamlined by supersonic flow, and quasi-static isobaric heating of a flow in front of the BSW provides drag reduction. If cross-section of the heated region S_h is about S and, therefore c_x is weakly dependent on M-number, one can easily obtain the efficiency η of such method,

$$\eta = c_x \cdot \rho_0 v^2 S / 2 c_p p_0 S_h .$$

Efficiency means the ratio of saved power over deposited in the form of heat in a discontinuity, ρ_0 and p_0 – density and static pressure in the undisturbed part of the flow, c_p – specific heat at constant pressure per unit molecule, and v – flow velocity. For $S \sim S_h$ and $\gamma = 1.4$ this formula can be rewritten in another form, using Mach number M_0 of the flow

$$\eta = 0.2 \cdot c_x \cdot M_0^2.$$

This simple formula shows the most important influential parameters and dependency between them. Two main parameters quantify efficiency in this case – the quality of aerodynamic shape (c_x) and the Mach number. The better shape the body has, the more difficult is to enhance it. Situation dramatically depends on the Mach number, so for every AD body shape there exist a critical M-number, over which the efficiency becomes greater unity. But if take into account that the efficiency of direct gas heating generally is not high, in practice this way, demanding very high level of total power, is not perspective. Therefore external action should be more localized in order to launch both more delicate mechanism of gas dynamic interaction and deliberate those kinetic processes, which lead to more efficient gas heating.

General relations

To formulate the aim of modeling more definitely, we write in a dimensionless form the expression for the energy E_s saved (or spent) due to modification of the flow. If u is the flow velocity at infinity, p and p_0 – pressure over the front (plane) surface of the body for the disturbed and non-disturbed flow, correspondingly

$$E_s = u \cdot \int dt \iint (p - p_0) dS.$$

Introducing the longitudinal dimension of disturbance (along the flow) L, characteristic time $\tau_* = L/u$, cross-section square of the body S and stagnation pressure p_0^{stg}, which is proportional to M_0^2 for Mach numbers not very close to the unity, one obtain

$$E_s = L \cdot S \cdot p_0^{stg} \cdot \int d\tau \iint (p - p_0) ds.$$

Thus, the aim of numeric modeling is to obtain the dependencies of ΔI

$$\Delta I = \int d\tau \iint (p - p_0) ds$$

on the main incoming parameters of the problem. For 2D plane geometry E_s has dimension of energy per unit length, and S means the transverse dimension D of a body.

Two limiting regimes of energy deposition are quasi-static isobaric heating and very fast (explosive-like) isohoric heating. In the first case as a result of energy deposition a density well appears. In the second case shock (or sound) wave is formed along with density decrease in a heated region. In neglecting of dissipative processes, the result of interaction of density well with the shock layer is independent of its initial position upstream the body. On the contrary, disposition of the energy injection domain in respect of the body is essential parameter for the explosive heating.

Efficiency of interaction is defined as the ratio of saved energy over deposited into a discontinuity. For the case of density well the energy for its production E_h is

$$E_h = L \cdot d \cdot p_{static} \cdot (1 - \alpha) \cdot c_p / R,$$

where d is transverse dimension of discontinuity, p_{static} – static pressure of the flow, gas density ρ in discontinuity $\rho = \alpha \cdot \rho_0$ ($\alpha < 1$). Therefore, expression for efficiency is given by

$$\eta = M_0^2 \cdot (D/d) \cdot R / c_p \cdot |\Delta I| / (1 - \alpha).$$

The aim of investigation is to eliminate and systemize the fundamental regularities of non-stationary interaction of gas dynamic discontinuity with AD body in supersonic flow under different energy injection regimes, dimensions of energy dissipation domain and their position, Mach number, etc. Two-dimensional plane geometry was chosen both for its simplicity and all characteristic features being seen especially distinct. Therefore, the present investigation should be treated as more qualitative one, reflecting general peculiarities of actual situation under consideration.

Description of interaction mechanism

In almost all cases the *vortex* is being generated inside the perturbed area between the bow shock wave and the body. This phenomenon is accompanied by the temporary increase of the bow shock wave standoff. It can be seen that this increase is greater for the case of the longitudinal energy area shape and the maximum increase corresponds to the greatest length

of the energy deposition area. The vortex flow moves to the right boundary and leaves the area of calculation. At the same time the second, weaker shock wave is shown to arise between the body and the bow shock wave, later on it is catching up with the first one. At this time the bow shock wave returns to its previous position and the second shock wave has practically no effect upon the position.

In the case of energy injection area across the flow the standoff increase is considerably less but the shock front deformation takes place on the greater part of the front.

These pictures are in qualitative agreement with Schlieren images, obtained in experiment.

Principle features of interaction

The following distinctive features can characterize non-stationary interaction of thermal discontinuity with a blunt body (blunt-nosed "cylinder") in SS airflow.

Pressure evolution at stagnation point can be conditionally divided in four stages:

- arrival of shock and/or rarefaction wave
- phase of relatively constant pressure (vortex formation in front of body surface)
- interaction with vortex
- post -vortex relaxation (temperature rise at stagnation point).

Pressure evolution at the *first* stage depends upon the regime of energy input in discontinuity and includes the pressure splash-downfall in the case of adiabatic regime and pressure downfall in the case of quasi-static regime. The *second* stage is characterized by approximately constant reduction of stagnation pressure this reduction being the more pronounced, the wider discontinuity is. This time interval corresponds to vortex formation in a shock layer and is directly proportional to the length of discontinuity. The *third* stage is interaction with a vortex drifting towards the model. If the length of discontinuity is not too large (about model "diameter" or less), the splash of pressure may precede the vortex - body interaction phase oncoming. This effect takes place due to the return back of the wave that falls at the body surface (stage 1), reflects from it and then reflects from the boundary of cold gas – back front of discontinuity, which comes by that time to the BSW position. In the case of long discontinuity this peak is not distinguished, as a reflection from the hot region is not effective. The *last* stage, which is characterized by increasing of stagnation pressure over its unperturbed value, corresponds to relaxation of gas dynamic parameters to normal values. This is the only stage where gas temperature is higher, than stagnation temperature for unperturbed flow. *The most effective is the phase of vortex interaction with the front surface of a model.*

The vortex is forming during thermal discontinuity absorption by the shock layer and starts its movement towards the model after the back fronts of discontinuity and vortex coincidence. Vortex appearance demands satisfying some conditions for the length and width of discontinuity and density inside it.

Diminishing of transverse dimension of discontinuity leads to noticeable increase of interaction efficiency even under the same gas temperature of discontinuity (i.e. under the total energy input decrease). *The value of the effect remains practically the same.* Increase of longitudinal dimension (length) of discontinuity does not affect efficiency (it remains constant in the area of parameters considered), but leads to the more pronounced decrease of mean pressure reduction. On the contrary, diminishing of longitudinal length and increasing of the transverse one leads to the sufficient fall down of the value of the effect. From the viewpoint of efficiency, quasi-static energy deposition (i.e. under a constant pressure in discontinuity, which is equal to that in a medium) is more efficient than explosive one. For the adiabatic regime of energy input the distance of the domain from the body also becomes an influential parameter. Efficiency dramatically increases with Mach-number increase.

Symmetric off-line shift of each half of discontinuity at a distance equal its width leads to a qualitative change in stagnation pressure evolution. The pressure difference at third stage

changes the sign and the overall effect, as well as interaction efficiency becomes equal to zero.

It should be noted that temperature evolution curve for stagnation point repeats in general that for pressure or density, therefore, its mean value during interaction is *less* in comparison with steady one.

Scaling

Most of the cited above conclusions are the consequence of ΔI–function behavior. This function turned out to be independent or weakly dependent of 3 from 4 of the incoming parameters – L, d and M_0. For $\alpha=0.5$ variation of these parameters in a wide range led to $|\Delta I|$ change in an interval 0.43 – 0.50. The unique parameter of influence is α - the relative density in the well. Thus, the efficiency of density well effect for drag reduction in the area of parameters considered is

$$\eta \approx M_0^2 \cdot (D/d) \cdot R/c_p \cdot |\Delta I(\alpha)|/(1-\alpha).$$

High efficiency of interaction can be explained by the fact that vortex formation consumes energy of a flow and less of this energy is dissipated as a heat. In another words, streamlining by a structured flow is more regular motion than non-structured one. Cooling of the region around stagnation point during interaction phase confirms this.

II. Dynamics of MW channel formation and local parameters

The physical mechanisms for discharge propagation in super- and sub-breakdown fields may be quite different. The behavior of MW discharge in super-breakdown field is very sensitive to EM field and initial electrons distributions and its mechanism is the wave of breakdown. In principle, such a discharge may propagate at any defined velocity and it depends mainly on EM field distribution. The SMD is much less sensitive to this factor and is much more affected by its own self-organization processes. This MW discharge phenomenon will be presented here in a more detailed way as it becomes more and more evident that structural factor plays the most important role in MW field – gas interaction.

What are the possible mechanisms of MW field-plasma interaction? As it is well known, the most effective is the resonant interaction. At low pressures, when the angular MW frequency ω sufficiently exceeds the frequency of electron elastic collisions ν_m EM field interacts resonantly with plasma in a spatial region where the Langmuire frequency is equal to ω (or, in the presence of magnetic field, to electron cyclotron frequency). At high pressures, when $\omega<<\nu_m$ the resonance is suppressed by dissipation and there can not be local plasma resonance's. But there may be resonance in interaction with plasma structure as a whole, if it forms, for instance, the appropriate slowing structure. Such structures are well known from theory of antennas.

Coupling of the EM field of breakdown intensity with gas and plasma goes through several stages. The first is the beginning of the breakdown process and electron avalanche development. On the scale of light emission signal from the discharge it corresponds to the delay time. During this stage MW energy absorption is close to zero and electron "gas" fills the entire focal region. After electron concentration grew up to the value equal ne0, the process of polarization takes start and redistribution of EM field begins. The field falls down inside the focal region and then saturates at some value. Simultaneously, the field in the polar regions increases. As the entire region becomes more elongated, concentration inside it continues to grow up. At some moment a thin channel inside it appears and the structure becomes highly reflective. The reflected wave summarizing with the incident one, forms new intensive field maximum and the zone of discharge formation jumps to a new spatial point towards energy source.

Thus, discharge movement towards the radiation source limits the effective interaction time with EM wave as well as energy deposition in a specific volume. Of

course, this is rather simplified picture of discharge evolution in super-breakdown field, but it shows both general regularities and limitations in energy deposition. The most effective way for overcoming some of them is formation of another shape of MW pulse – with high peak at the beginning and the value about breakdown one after it. This allow diminishing of the delay time in discharge formation and elongation of effective time coupling phase, thus raising the efficiency of this phase up to the unity. Moreover, the absolute value of energy deposition can be also increased. Another way is combination of low mean-power laser and microwaves.

Discharge channel evolution scenario – theory

Electric field maps deliver information of field distribution in the area of focus. The shape of high field region can be estimated via inspection of the surface of constant field intensity. One can see that it looks like a prolate ellipsoid of revolution - "lens". As the characteristic dimension in the direction of the wave vector of EM wave is determined by its length, in the transverse directions such dimension is dictated by characteristics of the focusing system. Usually, focal radius exceeds the spatial period of longitudinal field distribution (not the depth of the focal region!). In our case this excess constitutes about 6 times.

To understand the features of discharge structure evolution, it is useful to investigate the early phase of discharge development, from the moment of applying the intense electric field and start of avalanche process to the moment when complex part of dielectric permittivity of MW plasma reaches unity. This moment manifests the onset of reverse action of plasma on the MW field distribution.

Assuming the distribution of initial electron concentration as constant over space and distribution of electric field intensity along k-direction as $E = E_0 \cos kx$, one obtain the electron concentration and its distribution in avalanche for a moment t

$n_e(x,t) = n_e(0,t) \cdot \exp[\tau \cdot \exp((1-1/\cos kx) \cdot BN/E_0) - \tau]$,

where $\tau = \nu_i t$ and ionization frequency $\nu_i = A \cdot \exp(-BN/E_0)$, $n_e(0,t)$ – electron concentration in the central point of avalanche, the point of the maximal concentration in it.

Due to high sensitivity of ionization coefficient to electric field intensity ($BN/E_0 \sim 10$) initially uniform spatial distribution of electrons very soon becomes extremely non-uniform. Its form is gaussian with equivalent "radius" $R_x = k^{-1} \cdot (2E_0/\tau BN)^{1/2}$. For values of $\tau \sim 15\text{-}20$ the longitudinal dimension of structure is about $\lambda/(57\text{-}60)$. It saturates at this value at least until new ionization processes begin to contribute in the total ionization flux.

Analogous consideration can be applied for the transverse distribution with obtaining of the same result, except the characteristic dimension is 6 times larger, according to the initial field distribution parameters.

The next (second) stage in plasma creation development is connected with the process of EM field polarization inside the structure. As plasma becomes conductive, it strives to "push out" the electric field from inside. Simultaneously, the amplification of electric field at the poles of ellipsoid begins, which lead to fast elongation of conductive polar domains in the direction of electric field vector. This is well known mechanism of streamer propagation. Thus, the wave of breakdown spreads in the area of less intensive field until the amplified field on the poles will drop to that in the center of structure. Elongation in E-direction prevents external field screening and provides conditions for better penetration of it inside structure. Depolarization coefficient of plasma structure becomes smaller and smaller. Another consequence is that the shape of plasma volume changes – it exerts transition from prolated to elongated one. This stage of development is rather complicated for analytic calculations. According to experiment, the process of

elongation increases the dimension in E-direction in 3 - 4 times. It means that depolarization coefficient drops to the value about 1/20.

The third stage manifests the onset of some kind of ionization instability in already conductive media, which is also highly non-equilibrium. The most fundamental is ionization-thermal instability, which possesses the amplification of ionization due to rarefaction of gas along the center axis of the channel. Non-linear phase has an explosive, i.e. finite-time solution. The sense of this process is in further diminishing of the transverse spatial scale, which allows further growth of electron concentration, conductivity and energy concentration. For free MW beam and sufficient MW pulse duration limitation comes from arising of intense scattering of the incident flux, which occur when active (dissipative) resistance of plasma structure drops below the radiative one. A bunch of other processes accompany this stage. Two of them are of principle importance. The first is the onset of breakdown conditions in maximums of interference structure of the incident and scattered waves. This fact leads to plasma structure creating in domains, which are disposed more closely to MW radiation source and, thus, to interrupting of energy supply to the initial plasma object. The second is the intensive ultra-violet radiation from the channel, which ionizes the surrounding gas. As the free path of this radiation is anomalously large, the conditions for breakdown in mentioned above domains become more favourable.

Thus, two principle conclusions can be made from this brief description. Scenario of plasma structure evolution in breakdown field is a consecutive diminishing of transverse dimension, which results in some collapse-like creation of very thin channel(s) with high electron and energy concentration. But even under the lack of limitation on MW pulse duration, compensative processes result in saturation of energy deposition in a separate plasmoid and termination of its active phase. The time interval of this active phase depends upon the over-breakdown parameter, but can be estimated in other way - as limitation to number of electron generation born. This number seems to be limited by about 30 generations.

III. Efficiency of MW discharge utilization

As creation of density well or explosive-type energy deposition seems to be the basic way for altering the aerodynamic characteristics of a body, and in general such discontinuities are to be created at some distance upstream of it, efficiency of MW energy utilization is critically important.

Efficiency of the number of subsystems defines the overall efficiency of the MW discharge utilization. According to MW energy flow, let us start with the radiating-focusing system, then coupling with gas and plasma and, finally, transfer of the deposited energy in a form of gas heating. The efficiency of the typical focusing system is about 50%, i.e. only half of the radiated power is collected in the main maximum of the focal region, and the rest 50% are distributed among the lateral lobes of the radiation pattern. This is the consequence of the wave character of electromagnetic radiation. Convergence angle is also very important parameter, as well as radiation wavelength. They determine both focal region dimension and electric field distribution in it. The last defines greatly MW discharge dynamics and, consequently, efficiency of coupling with plasma.

The last stage in the chain of energy transformation is relaxation of the dissipated energy into air heating. It is well known that under breakdown conditions less than 1% of the energy deposited in discharge goes directly in translational and rotational degrees of freedom. The rest, i.e. practically entire energy input, is shared between electronic and vibrational degrees in equal portions. Approximately 20% of energy stored in electronic degree of freedom are

transferred quickly to translational degree that is about 10% of the entire deposited amount. The destiny of the 70% - those in vibrational degrees of freedom - is strongly dependent of the gas temperature. The process of gas heating gives start for ionization-thermal instability, which in turn leads to thin channel – filament – formation via collapse-type scenario. This very important element of discharge structure has therefore high value of energy concentration and electron density. The physics of this strongly non-linear plasma object is not well understood till now. But it seems to be an adequate candidate for use in plasma-BSW interference. Thus, kinetic stage has also some reserve for the efficiency raise.

Summing up one can see that efficiency of energy deposition in discharge can be increased from 4 to 8 times and reach the value of about 25 or even 30% in comparison with several percent in our experiments now.

Conclusions

Investigation was focused on putting the valid and realistic physical basis in exploration of the challenging phenomenon in plasma aerodynamics – interference of electric discharge in supersonic flow with bow shock wave of aerodynamic body. According to our present understanding the key of the problem lies in the area of fine discharge structure in supersonic flow. Gas dynamic phenomena only make this issue explicit. That is why so much attention is paid for obtaining of reliable data in discharge structure area.

Results of numeric simulation and experimental investigation reflect the most important inherent features of gas dynamic processes in non-stationary interaction of gas dynamic discontinuity created in front of a blunt body in SS flow. The most important among them is that the integral action of thermal well is independent of its transverse dimension. It means that if there is very thin (probably, invisible) filament in discharge domain, the resultant effect may be determined mostly by this structure element, but not by the bulk luminescent volume. Moreover, the density drop down inside the well should not be necessarily large. Even 3-4 times reduce of density (i.e. gas temperature of about 1000K) in elongated structure might cause noticeable effect on AD characteristics of blunt body in super- and hypersonic flow. It is important to note that attaining of the discharge phase when thin channel is formed is beneficial both for deliberating of energy stored in vibrational degrees of freedom and for launching of effective mechanism of flow structuring in shock layer for drag reduction. Processing of discharge spectra obtained in nitrogen flow gives a thread for further deeper understanding of discharge fine structure formation paradigm. In our opinion, exactly discharge fine structure is responsible for phenomena, which seems as anomalous. This refers to unusually fast velocities of BSW detachment and comparatively large stand-off, which were registered in experiment.

Simultaneously, interaction of very thin and extended discharge channel with BSW brings an example of bifurcation in a complex system. Small disturbance in initial conditions leads to dramatic changes in resultant flow-field. The processes of self-organization make the effective shape of the streamlined region as better adopted to the conditions of supersonic flow, dramatically reducing the drag. The transition from initially blunt region to final streamlined one occurs.

Thus, the importance of discharge structure for organization of the critical influence on the flow structure is obvious. Thermal mechanism for drag reduction may be rather delicate and efficient under the condition that discharge structure will provide intensification of the air heating process. As it is shown, the efficiency of energy deposition method rises with both Mach number of the flow and model dimension increase, therefore, we are intended to demonstrate the possibility of its efficient application on the modernized stands.

Acknowledgments

We are sincerely grateful to Dr. Joseph Shang (WPAFB) and Dr. Charbel Raffoul (WPAFB-EOARD) for their support of this work. Our deep gratitude is also addressed to the European Office of Aerospace Research and Development (EOARD). Dr. Olga Azarova, Dr. Victor Grudnitzkiy, Dr. Yury Anisimov, engineers Sergey Afanas'ev, Anatoly Gorynya and Evgeny Osetrov are greatly acknowledged for their credit in investigations.

Literature

1. 4th Weakly Ionized Gases Workshop. 11-14 June 2001, Anaheim, CA. Proceedings.
2. 3rd Workshop on Magneto-Plasma-Aerodynamics in Aerospace Applications. 24-26 April 2001, Moscow. Proceedings.

INFLUENCE OF INITIATED MICROWAVE DISCHARGE ON SUPERSONIC FLOW AROUND MODELS

L.P.Grachev, I.I.Esakov, K.V.Khodataev

Varshavskoe shosse, 132, Moscow, 117519, Russia,
Tel. 315-24-97, Fax. 312-10-53, E-mail:esakov@dataforce.net

Introduction

At the same time it was elucidated that air heating in a high speed flow by means of electric discharges is not an easy problem. It is connected with the fact that electric discharges in high density air represent a complex organized system of relatively thin, strongly heated channels practically in all ranges of electromagnetic fields from those of constant current to microwave discharges. Evidently because of this circumstance in some experimental realizations there was not detected any effect on a flow near models in spite of considerable mean level of electric power

Goals of presented work are: experimental investigation of deeply under critical microwave discharge created in a supersonic (SS) air flow; investigation of effect possibility on SS flow around a model characteristics by means of this discharge type and determination of electric efficiency of this effect. In the present communication we give an account of a first stage of investigations.

Tests were carried out in three formulations: with creation of a microwave discharge before a bow shock wave (SW), behind a bow SW and in a base part of a model.

Experimental set up

A scheme of experimental set up is presented in Fig.1.

It includes: a gasdynamic system for forming of a submerged SS jet in a working chamber; a microwave generator with an electrodynamic system and measuring equipment.

A submerged jet is formed in a working chamber with a volume about of 0,5 m^3 in a space between a Laval's nozzle and a confuser, connecting the working chamber with a receiver with a volume about of 4 m^3. The nozzle inlet opens to an atmosphere by an electrically controlled valve. The system ensures a SS jet of 30 mm diameter at Mach number M=2, static pressure about of 100 Torr and a flow velocity about of 500 m/s in a working region of a chamber. Jet characteristics stay stationary for several seconds.

A microwave system is constructed on a base of a generator of a magnetron type with continuous power $P = 2,6$ kW at a wavelength $\lambda = 12,5$ cm. A microwave energy is leaded to a prescribed place of SS jet with a help of electrodynamic system insuring a strength of electromagnetic (EM) field electric component up to $\mathbf{E} \cong 160$ V/cm. A discharge is created along an SS jet axis with application of a special initiator.

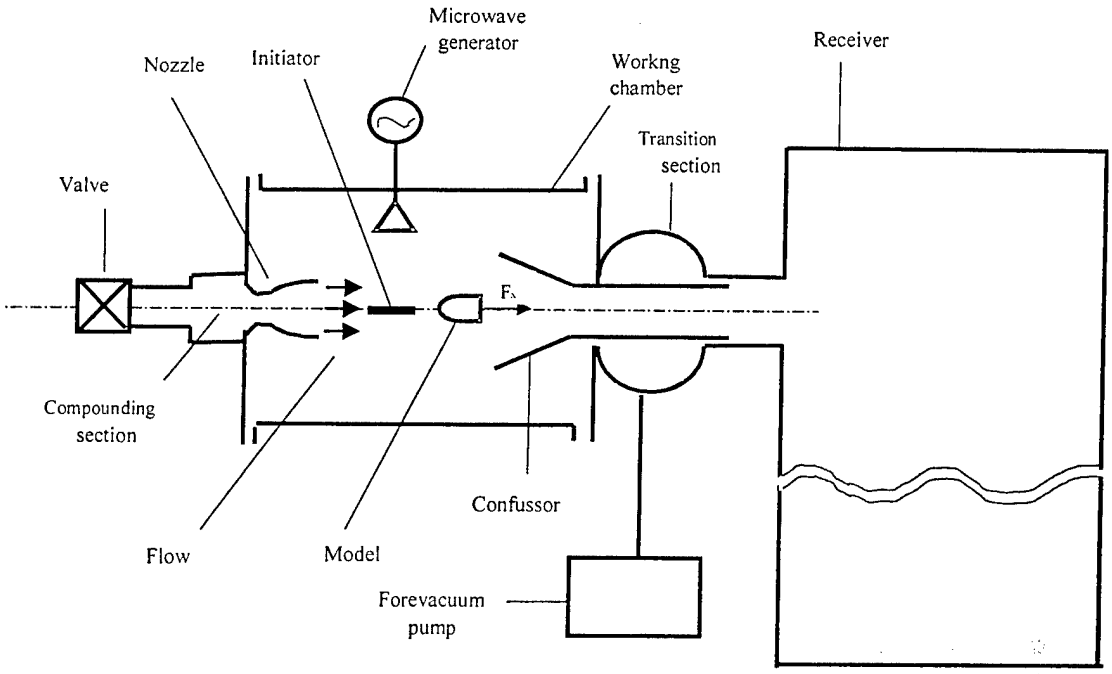

Fig.1. A scheme of experimental set up.

The following characteristics were measured during experiments:

The following characteristics were measured during experiments: static pressure in a working chamber and in a jet at an outlet of a nozzle with application of an inductive pressure sensor; stagnation pressure in different points of jet axis with application of a Pitot pipe in a combination with an inductive pressure sensor; stagnation temperature in different points of jet axis was measured by a thermal couple; and an aerodynamic force of models was measured one component aerodynamic balances.

A microwave discharge in a steady air is studied comparatively well [7-10]. It is well known that it exists in different forms with respect with conditions. Values of a gas density and electromagnetic field strength that a realized in the present experiment correspond to an existence region of so called deeply undercritical microwave discharge [11]. For its creation is necessary to create a local area in which EM field strength exceeds critical breakdown value. Most often an initiator is applied for its creation. In a course of its development such a discharge does not detach from the initiator's surface. It high efficiently absorbs a microwave energy, insuring a temperature of several thousand degrees in a region of a discharge plasma.

This discharge has not been well studied [12] yet in a supersonic flow.

An initiator was inserted into SS flow in order to create deeply undercritical microwave discharge. It represented a rather thing metallic cylinder with sharpened tip. Its length was approximately equal to a half of a microwave radiation wave $\lambda/2 \cong 6{,}2$ cm. An initiator's design in each definite experimental scheme was specially elaborated with accounting of definite experimental problem conditions.

Experimental results

Deeply undercritical microwave discharge in SS flow was realized and investigation of its effect on jet parameters was carried out.

A typical external view of such a discharge is presented in Fig.2.

It was created during a stationary phase of a stream. An initiator in this experiment represented a metallic cylinder,

located on a flown around pylon at the axis of a jet. Its diameter 2a = 0,3 cm can be used as an image scale in photos.

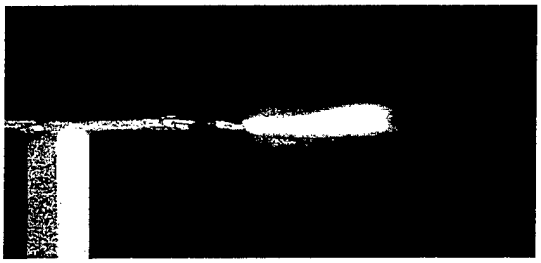

Fig.2 Deeply undercritical microwave discharge in SS flow , M = 2, P = 2,1 kW

In Fig.3. typical temporary dependencies of stagnation pressure variation are presented, and at Fig.4. stagnation temperatures in the nearest wake behind a discharge at P = 2,1 kW are presented.

One can see that stagnation pressure drops practically to zero. It means that as if an "air hole" is created in a nearest wake behind a discharge. Change of a stagnation

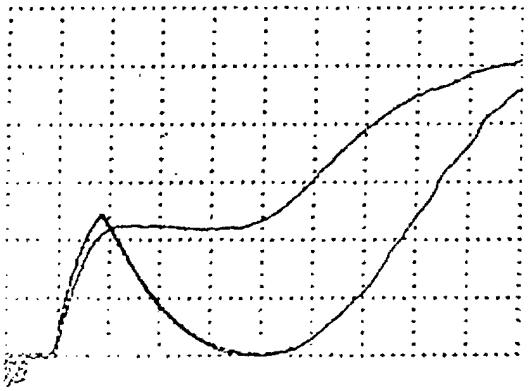

Fig.3 Stagnation pressure of a flow without of a discharge (upper curve) and with a discharge. (horizontal scale – 0,2 s/point, vertical scale – 150 Torr/point)

temperature reaches about of 1000°C that is more than by 7 times greater than its undisturbed value. In the same proportion air density drops in a wake in isobaric conditions. That, as a matter of fact, obviously, is illustrated by a temporary dependence of a stagnation pressure dependence in Fig.3.

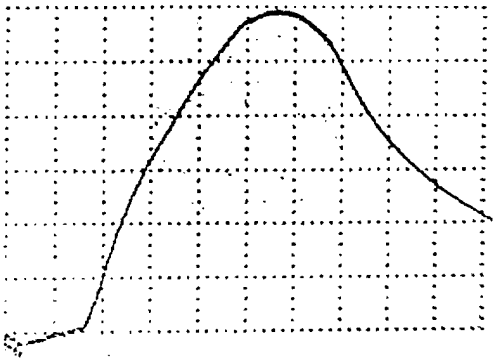

Fig.4 Stagnation temperature of a flow with a discharge (horizontal scale – 0,2 s/point, vertical scale – 180 degrees/point)

Decrease of aerodynamic force was detected during all these three experimental formulations at different localization of a microwave discharge with respect to a model.

Typical temporary dependence of an axial force component is presented in Fig. 5 acting a model in a flow in case of creating of a discharge before a bow SW.

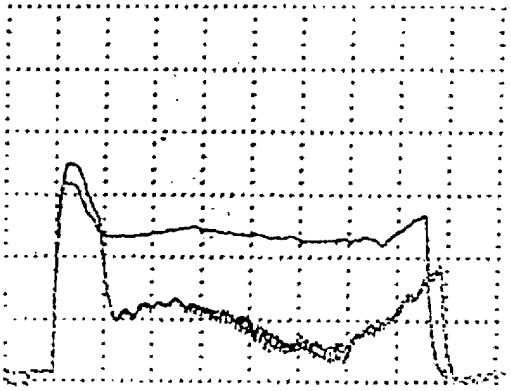

Fig.5 Aerodynamic force temporal dependence acting a model without of a discharge (upper curve) and with a discharge horizontal scale – 0,2 s/point, vertical scale – 46 g/point).

A model in this case represented a dielectric cylinder of 7 mm diameter directed along a flow. A discharge was created at application of a initiator configuration close to those shown in Fig.2 at a distance about 2 cm from a model upstream a flow. One can see that maximal force decrease reaches 4.6 times.

A compound model of complex design was used in experiments on discharge creation behind bow SW. It represented a dielectric cylinder with low

value of dielectric permeability and low losses at high frequencies. An initiator was located in the cylinder. Its sharpened tip was leaded to the head part of the cylindrical model. Insurance of discharge burning behind the bow SW met considerable difficulties in the experiment. They were connected with high pressure value in model's head part. In Fig.6 a typical temporary dependence of an aerodynamic

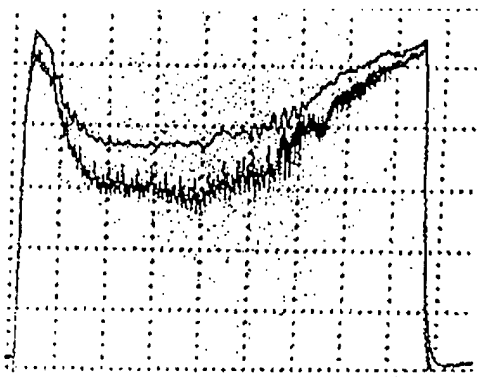

Fig.6 Temporary dependence of a drag force acting a model without a discharge (upper curve) and with a discharge (lower curve) (horizontal scale – 0,2 s/point, vertical scale – 23 degrees/point)

drag acting a model in this case is presented. Decrease of the drag due to the discharge was relatively small in all the experiments undertaken by this scheme. One can see that the maximum value of drag force decrease was about 20%.

In the third experimental scheme a discharge was created in a model's base. The model represented wedge-shaped form with a base sloped at 45° made of fluoro-plastic directed along a flow. A metallic initiator was located inside a wedge. Its sharpened tip was for 0,1 cm out of base plane cut.

In Fig.7 a typical temporary dependence of aerodynamic drag is presented. Maximum decrease of aerodynamic drag decrease in this experiment was about 15%.

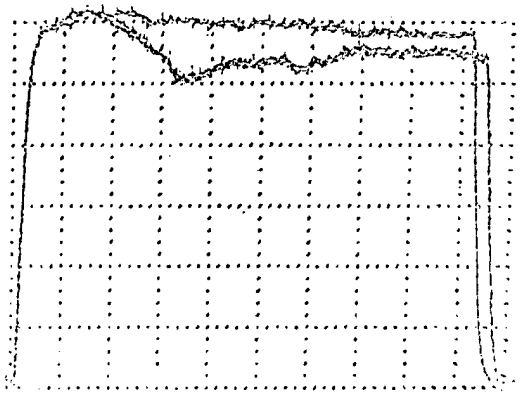

Fig.7 Temporary dependence of a drag force acting a model without a discharge (upper curve) and with a discharge (lower curve) (horizontal scale – 0,2 s/point, vertical scale – 23 degrees/point)

Conclusions

1. Deeply undercritical microwave discharge in a supersonic flow has been realized. In so doing the electric field level was 60 times less than the critical one.
2. Model aerodynamic experiments were executed on putting of microwave energy into a region before a bow shock wave, behind a bow shock wave and into a base model part.
3. Bow drag decrease was detected at microwave discharge creation before a bow shock wave up to 80 %; behind a bow shock wave up to 24 %; and decrease of longitudinal component of aerodynamic force at discharge burning in model's base part up to 17 % .

So during experiments it was shown the principle application possibility of initiated undercritical microwave discharge created in a supersonic flow to change aerodynamic forces acting bodies placed into this flow.

References

1. Bychkov V.L., Grachev L.P., Esakov I.I., Deriugin A.A. et al. Numerical and experimental investigation of supersonic flow around blunt body at the existence of the Zhurnal Tekhnicheskoi Fiziki. longitudinal discharge. Preprint of Keldysh Institute of Applied Mathematics, RAS, 1997, № 27, Moscow.

2. Grachev L.P., Esakov I.I., Khodataev K.V. "Plasmogasdynamic experiments in Russia and prospects of plasma technology applications in aerodynamics" VIII Ukrainian Conference and School on Plasma Physics and Controlled Fusion, Alushta (Criema), September-16, 2000, Book of Abstracts, Kharkov, 2000, p.5-6
3. Vitkovskii V.V., Grachev L.P., Gritsov N.N., Egorova Z.M. et.al. Experimental investigations of constant current electric discharges in supersonic and subsonic air flows. Works of TsAGI. №.2505, 1991.
4. Grachev L.P., Esakov I.I., Mishin G.I., et al. Interaction of a shock wave with decaying plasma of electrodeless microwave discharge. Zhurnal Tekhnicheskoi Fiziki. 1985. V.55. N.5. P.972-975
5. Vitkovskii V.V., Grachev L.P., Gritsov N.N., et. al. Investigations of non-stationary flow around bodies by a supersonic air flow heated by a gas discharge. Teplofiza Vysokikh Temperatur. 1990. V.28. №.6. P.1156-1163.
6. Grachev L.P., Gritsov N.N., Esakov I.I., et al. Heating of bodies in a supersonic plasma flow. Zhurnal Tekhnicheskoi Fiziki. 1995. V.65, N.1. P.167-171.
7. Grachev L.P., Esakov I.I., Л Mishin G.I., et al. Electrodeless discharge in air at average pressure. Zhurnal Tekhnicheskoi Fiziki. 1985. V.55. N.2. P.389-391.
8. Collection of scientific papers "High frequency discharges in wave fields" Gorkii, IAP AS USSR 1988.
9. Zarin A.S., Kuzovnikov A.A., Shibkov V.M. Freely localized microwave discharge in air. Moscow. Neft i gas. 1996.
10.
11. Borisov N.D., Gurevich A.V., Milikh G.M. "Artificial ionized region in atmosphere." Moscow :1986. IZMIR AS USSR.
12. Grachev L.P., Esakov I.I., Khodataev K.V. Range of existence of self developing undercritical streamer microwave discharge. Zhurnal Tekhnicheskoi Fiziki. 1999. V.69. N.11. P.1924.
13. Grachev L.P., Esakov I.I., Khodataev K.V. Streamer microwave discharge in a supersonic air flow. Zhurnal Tekhnicheskoi Fiziki. 1999. V.69. N.11. P.14-18.

MICROWAVE TORCH. PLASMA PARAMETERS AND GAS TEMPERATURE

S.I. Gritsinin, V.A.Kop'ev, I.A. Kossyi and M.A. Misakyan

General Physics Institute, Russian Academy of Sciences, 38 Vavilov str., Moscow, 119991 Russia

1. Introduction

Microwave torches are widely applied as plasma sources in various plasma technologies, as well as useful instruments in physical laboratories.

Until now, the torches of TIA-design were commonly used. The classical scheme of such microwave torches is discussed for example in [1]. The energy from a microwave generator is transmitted through a waveguide (usually, rectangular and tunable) line into a coaxial section (which also may be regulated). The inner electrode of this section also serves to supply the torch with the working gas and has a refractory nozzle. The sizes of the inner and outer electrodes of the coaxial line are nearly equal. In this case, there is the open coaxial output at the end of the line. In the presence of the torch, a considerable portion of the input microwave energy is absorbed in the formed gas-discharge plasma, whereas the remainder energy is emitted into space. When the torch quenches (occasionally, because of a certain failure), the microwave energy is almost completely emitted into space. For this reason, this design of torches does not guarantee the radiation safety. There is also another disadvantage in this design. Notwithstanding the presence of a sharp edge of the nozzle, for lower generator microwave powers (usually, on the order of 1 kW), it is difficult to ensure the enhancement of the electric field to levels required for gas breakdown at atmospheric pressure. Under these conditions, the initial ignition of the torch cannot occur spontaneously. In addition, in the torches of this design, the field is enhanced near the nozzle, but drops sharply with distance away from it because of the geometry of the device. For this reason, such torches are usually small in size, 1-2 cm.

Earlier [2 - 4] we had proposed another design of the microwave coaxial plasma torch. From physical standpoint, a this torch can be classed among plasma waveguide discharges [5]. Characteristic of these discharges is that a gas-discharge plasma produced in the wave field is one of main components of the guiding waveguide structure for wave propagation. In this paper, we consider a special case of this class of discharges – a plasma coaxial line, when the plasma plays role of one of the electrodes of the coaxial line. The version in which the plasma acts as the outer electrodes was considered in [6, 7, 2 - 4]. Here, we consider another version, specifically, when the plasma forms the inner electrode of the coaxial line.

2. Experimental setup

The design of the microwave coaxial plasma torch proposed in this paper differs from the commonly used design in that the outer electrode is longer than the inner one. Such an insignificant (at the first glance) modification of the design radically changes the principle of operation of the torch. The device is shown schematically in Fig. 1. A rectangular resonator is fed with microwave energy from a rod antenna coupled with a production 2.45 GHz magnetron with a mean power of ~ 1 kW at half-wave

rectification. From the rectangular resonator, the microwave energy is transmitted into the coaxial section of the device with the help of a current loop; continuation of this loop inside the coaxial line is the inner electrode. This loop is made of a pipe and serves for working gas supply. There is a refractory metal nozzle at the end of the inner electrode, it has the sharp edge to facilitate the gas breakdown. The outer coaxial electrode is longer than the inner one; consequently, for the electromagnetic wave propagating through the system, the coaxial transmission line terminates with a circular wavequide section. This section which has a diameter of 2–3 cm is a below-cutoff waveguide for the pumping microwaves with a wavelength of ~ 12 cm. In the absence of a torch (plasma), the microwave approaches the end of the inner electrode and reflects from the circular waveguide inlet. For this reason, the high-power microwave in the absence of a torch cannot be emitted into space and remains inside the system. A similar picture is also observed in the presence of the torch if its size is shorter than the sizes of the outer electrode: unabsorbed radiation reflects backward and again passes through the torch plasma. Therefore, the proposed design ensure the radiation safety. For convenient observation and diagnostic purposes, a certain part of the outer electrode can be made in the form of a "basket" – a bunch of thin rods (wires) 2–3 mm in diameter positioned at a distance of 0.5–1 cm from each other. Since the currents in the coaxial line flow in the longitudinal direction, such a basket successively plays the role of the solid electrode.

The microwave energy reflected from the circular waveguide is accumulated in the system of resonators, namely, the rectangular, coaxial, and magnetron resonators. The length of the inner electrode from the inlet into the coaxial section is chosen such that the nozzle exit falls to a maximum of the electric field of the standing wave which is formed due to the reflection of the running wave from the circular waveguide. As a consequence, as the energy is accumulated in the standing wave, the field at the nozzle end grows with time and ultimately reaches the threshold level. This is the reason why operating with a relatively low microwave power, we have managed to achieve the breakdown (and then the plasma formation) in the pulsed mode (half-wave operation regime) in various gases (argon, nitrogen, air, carbon dioxide, hydrogen, methane, propane) over a wide range of pressures including atmospheric pressure.

After breakdown, the formed plasma, if it is sufficiently dense, becomes the part of the waveguide structure, as it were the extension of the inner electrode, so that the wave can propagate further and then reflect from the circular waveguide at the other point at which the breakdown conditions will be also fulfilled. Thus, as the breakdown advances inside the coaxial, the inner electrode "grows" in length. In this case, the torch length can reach 10—20 cm which substantially exceeds the torch length attainable with usual design.

In our study, main attention was give to the time evolution (propagation) of the torch in the pulsed mode of operation with half-wave rectification. The discharge glow was measured with collimated photomultipliers and a photodiode, and a streak camera. Microwave radiation was probed with a half-wave antenna located at a certain distance from the torch. The plasma density was estimated from the passage of diagnostic microwaves (2.3 mm and 337 μm) through the torch.

Gas temperature in the region occupied by plasma stream has been determined by measurements of radiation spectrum of a torch as well as microparticles or metallic samples introduced into it. Holographic

measurements of a neutrals concentration have been applied also for gas temperature estimation.

3. Time evolution of the discharge glow. Parameters of plasma and gas.

In this section, we present results from studies the time evolution and spatial structure of the plasma torch glow. In our case, the device operates in the pulsed mode (50 Hz). The pulse duration was about 8 ms and pause was 12 ms. This implies that the torch is initiated in every successive pulse; then it grows propagating along the guiding structure until reaches a certain size. It was reasonable to expect that, behind the front of the propagating torch, both the glow and the gas and plasma parameters should rapidly come to a steady state. However, the experimental results demonstrate a complicated temporal and spatial evolution of the glow and medium parameters.

Visually, the torch under study differs substantially from the torches of traditional TIA design. For argon and other noble gases, a bright core 1–2 mm in diameter and 1–2 cm in length is observed near the nozzle as in the case of usual TIA. This region corresponds to maximum values of the energy deposition and plasma density. However, in the usual torches, the core is followed by the recombination region in which the plasma density (together with the energy deposition) drops sharply because of less intense ionization processes. The reason is that the pumping wave energy is partially absorbed in the core, and then the wave field weakens because of the geometrical factor – the wave that was not completely absorbed in the core is emitted by the core, as by a rod antenna, into space. In our case, the core is followed by a region that is substantially larger in size, but less bright, with curved boundaries. The volume of this region is 2—3 orders of magnitude greater than the core volume. This region spans over the most part of the inner plasma electrode of the coaxial line. The unabsorbed wave energy can propagate along the formed plasma electrode (i.e., through the coaxial line), thus significantly increasing the size of the glow region and maintaining the plasma density at a rather high level. The mere fact that there exist the region in which the wave can propagate through a distance on the order of the wavelength indicates that the plasma density in this region is on the order of the cutoff value for the pumping wave frequency with allowance for the high value of the frequency of electron collisions with heavy particles.

When the molecular gas (nitrogen, air) is used as the working gas, the bright core with well-defined boundaries is absent.

Figure 2 shows how the torch size varies with time; this dependence was obtained with the help of the collimated photodiode. It is seen that the glow front propagates at a nearly constant velocity V = 20 m/s through a maximum (under these conditions) distance of l = 10 cm. This effect is similar to the plasma (and glow) propagation along the guiding structure of the launcher in the surfatrons based on surface electromagnetic waves. It may be assumed that, in our case too, we have surface waves which make their contribution to the torch propagation mechanisms.

The process of glow propagation was studied also with the streak camera. Its slit was oriented along the axis of the coaxial system. Figure 3 illustrates the photochronograms of the torch propagation for different working gases – argon and nitrogen. The initial phase is globally traced with a time resolution of 2.5 ms/div. It is seen that, in the case of argon, the processes begins with the appearance of a core glow 1–2 mm in diameter and 1–2 cm in length. The core glow continues throughout the microwave pulse. In Fig. 3, one can notice the modulation in the core

glow with a frequency of nearly 10 kHz, that is, regular bursts in the core glow and variations in its size with a characteristic time about 100 μs. After a certain time (0.5–1 ms) after the appearance of the core glow, a less intensive glow wave arises near the core and begins to propagate along the axis of the system. The velocity of the glow front corresponds to that given in Fig. 2. After the primary glow front goes away from the core, secondary glow waves arise near the core, which are associated with its periodic bursts. The secondary waves overtake the primary front which is therefore an envelope of a great number of the secondary front. One can notice that the intensity of secondary fronts is also modulated with a characteristic time about 1 ms.

With high time resolution, we detected the higher modulation frequencies in the torch-core glow at times preceding to the formation of the propagating glow. It is seen that a rather uniform burst arises along the entire core length and then the core is completely quenched with characteristic times of 5–10 μs. Simultaneously, microwaves are generated in short high-power pulses. It is seen that the magnetron initially begins to generate short radiation pulses with frequencies about 100—200 kHz. After a period of several hundreds of microseconds, over which the pulse generation frequency gradually increases, the first burst occurs in the core and then such bursts occur synchronously with the magnetron pulses. The pulse generation frequency gradually increases, and the generation becomes continuous. The glow intensity at the continuos-generation stage is several times lower than that for the pulsed generation stage. It is reasonable to assume that the microwave power in pulses is significantly higher than a mean magnetron power of 1 kW. Obviously, this circumstance makes the gas breakdown near the nozzle much easier. The duration of the pulse generation stage and the pulse duration depend on the magnetron load which is a complex unsteady electrodynamic load depending on the torch parameters. In the case of free generation (full matching)the generation becomes continuos after 5—10 pulses. With the closed end of the coaxial line, the generation ultimately becomes suppressed completely.

Totality of measurements, based on exposure of torch by microwave and submicron radiation, permits us hold that investigated microwave torch excited in the flowing argon contains a "kernel" with electron density as high as $n_e \cong 10^{16}$ cm^{-3} and relatively large volume of torch "body" with $n_e \cong 10^{14} - 10^{15}$ cm^{-3}.

Spectral and holographic measurements allow to make following conclusions concerning to the gas temperature in the volume of microwave torch:

- Gas temperature is maximal in the volume, occupied by "kernel" and slowly falls down with distance from it;
- Gas temperature in the "kernel" achieves 4000 – 5000 K.

This work was supported in part by the ISTC (project N 908) and NWO (Netherlands) (project no. 047.011.000.01).

References

1. Moisan M., Sauve G., Zakrzewski Z., and Hubert J. An atmospheric pressure waveguide-fed microwave plasma torch: the TIA design. // PSST 1994, v 3, pp 584-592.
2. Gritsinin S.I., Kossyi I.A. at all, 14th Intern. Symp. on Plasma Chemistry, Prague, **2**, 675, (1999).
3. S.I.Gritsinin, I.A.Kossyi, M.A.Misakyan., Proc. of ESCAMPIG XI, Miskolc-Lillafured, Hungary, August 2000, v. 24F, pp 216-217.

4. Gritsinin S.I., Kossyi I.A., Malykh N.I., Misakyan M.A., Temchin C.M. and Bark Y.B., Plasma Coaxial Discharge as a New Type of the Microwave Surface Wave Discharge. // Preprint GPI RAS N 1, Moscow, 1999, 24 p.
5. Yu M Aliev, I Ghanashev, H Schluter, A Shivarova and M Zethoff. Analytical estimations on the axial structure of plasma-waveguide discharges // Plasma Sources Sci. Technol. 3 No 2 (May 1994) 216-225.
6. Rauchle E. Duo-plasmaline, a surface wave sustained linearly extended discharge // 3 IWMDFA, 1997. - J. Phys. IV France, 1998, v 8, N 7, pp 99-108.
7. Walker M., Baumgartner K.-M., Schulz A., Rauchle E. Silicon nitride films from the PLASMODUL-a new microwave plasma device // Proc. of ISPC 14, Prague, 1999, v 3, pp 1427-1432.

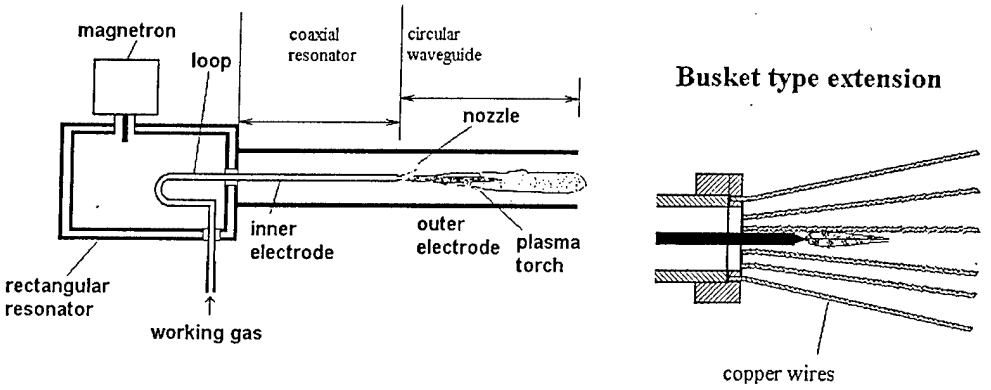

Fig.1. Microwave coaxial plasma torch design.

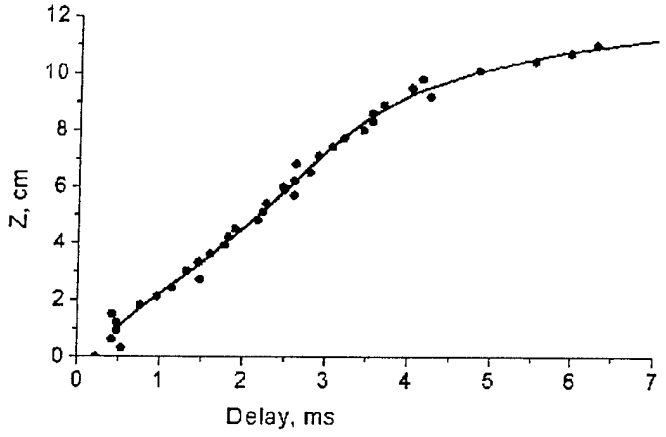

Fig.2. Delay time of the light appearance vs distance from the nozzle.

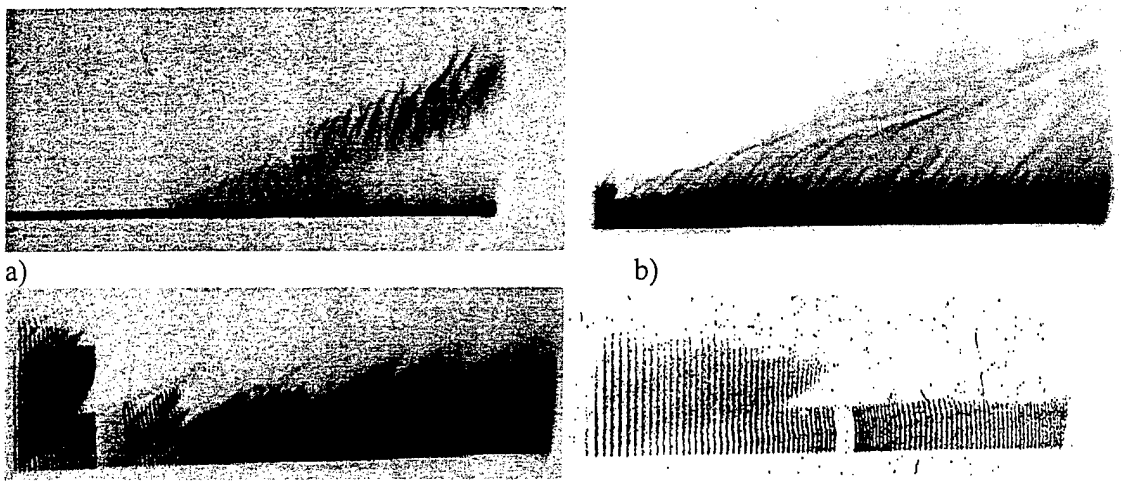

a) b)

c) d)

Fig.3. Streak camera photo of microwave torch for N2 (a) and Ar (b-d) as a working gas. Time scanning is 3 ms (a,b), 750 μs (c) and 250 μs (d) for full scale.

NON-SELF-SUSTAINED MICROWAVE DISCHARGE AND CONCEPT OF A MICROWAVE AIR JET ENGINE

G.M.Batanov, S.I.Gritsinin and I.A.Kossyi

General Physics Institute of Russian Academy of Sciences, Vavilova 38, 117942, Moscow, Russia

The possible utilization of an energy source situated outside the propelled craft in order to produce propulsion has fairly long been discussed in the literature [1-3]. As initially proposed as long ago as 1917 by K. E. Tsiolkovskii [4], energy transfer is produced by electromagnetic waves. A high-power laser is considered as a candidate for generation - the laser air jet engine (LAJE) concept.

The employment of a microwave beam for energy transfer (the microwave rocket concept) was proposed for the first time in [5] and was further developed in [6, 7]. The versions considered in [5—7] differ in the method of exciting a microwave discharge. Thus, the microwave rocket is based on self-sustained discharge in [5] and microwave corona in [6]. In [7], it is proposed to use non-self-sustained microwave discharge maintained by an external source of UV radiation ionizing the gas

A system that employs outside generation of a high-power microwave beam, the transfer of the beam to the propelled craft, and the use of microwave energy in a jet engine has some advantages over a laser system. The most obvious are: the high efficiency of microwave devices, the possibility of using RF-transparent components in the construction of the propelled craft, all-weather operations in the microwave range, the possibility of using phased arrays for controlling the microwave beam, etc.

Possibility of propulsion production with help of energy source disposed outside of an accelerated craft are discussing. Powerful microwave generators are considered as an energy source, whereas microwave beams focused on the surface of craft are treated as an energy carrier. Non-self-sustained microwave discharge, excited near the face of rocket transforms microwave energy received by craft into its kinetic energy.

Original scheme of such a discharge formation, which doesn't include source of near the rocket gas ionization independently of the microwave radiation is described. The main part of scheme is specially designed metal-dielectric target having low threshold of microwave slipping surface discharge excitation. UV radiation of this discharge plays role of an external source of ionization creating photoionized gas layer in which with the high efficiency microwave energy releases.

Estimations of specific trust and the cost of trust values characterizing efficiency of microwave energy utilization are presented.

An experimental setup to study the non-self-sustained surface discharges is shown in Fig. 1. Pulsed microwave radiation was launched into a cylindrical metal chamber with the help of a horn-lens antenna forming a convergent microwave beam. The lens was made of quartz. The diameter of the chamber and the lens was $\approx$ 350 mm. A dielectric (organic glass) target with metal inclusions was positioned in the focal plane of the beam. Metal

(stainless-steel, titanium, or other) grains were introduced into the target surface irradiated with the beam and are chaotically distributed over the surface. The cross size of the target is larger than the beam diameter.

The parameters of the microwave generator were the following: wavelength $\lambda_f \cong 0.8$ cm, pulse duration $\tau_f \leq 10$ μs, peak power $P_i \leq 40$ kW, repetition frequency $f \leq 10$ Hz.

The beam radius in the focal plane was $r_f \approx \lambda_f$; consequently, the cross size of the beam was much less than the chamber size.

A profiled load to absorb microwave radiation was placed on the end flange of the chamber.

The chamber was evacuated to high ($p \leq 10^{-5}$ torr) vacuum and was filled with the working gas at pressures $10^{-3} \leq p \leq 760$ torr.

As the measurements at a low ($P_i < P_{thr}$) power level showed, the metal—dielectric target was transparent to microwaves. However, above from a certain threshold level $P_i = P_{thr}$, slipping surface discharge was excited on the target surface, resulting in perturbations (absorption and reflection) of the microwave beam. The threshold power density for slipping discharge depends weakly on the gas pressure and fairly satisfies the equality

$$\Pi_{thr}\,\tau_f \approx 0{,}1\ (\mathrm{J/cm^2}), \qquad (1)$$

where Π_{thr} is the threshold power density on the target near the beam focus (in $\mathrm{W/cm^2}$).

Slipping microwave discharge on the target was accompanied by generation of a plasma in the gas medium near the irradiated surface. The parameters and sizes of the plasma depend substantially on the chamber pressure. At $p \leq 10^{-3}$ torr the plasma is diffusive; it is produced on the target surface and then expands into the surrounding space and fills the chamber volume. At $10^{-3} < p < 10^{2}$ torr, the plasma formation occurs as a self-sustained discharge arising near the target surface and expanding in the counter direction to the radiation beam. Finally, at $p \geq 10^{2}$ torr the plasma formation occurs as a surface non-self-sustained microwave discharge occupying a narrow ($d \leq 1$ cm) region near the metal—dielectric surface of the target.

Measurements of the recoil momentum acquired by the target under the action of the microwave beam were performed over a wide range of working gas pressures. A target made of a thin organic-glass plate (thickness 0.27 mm, diameter 30 mm, weight 0.29 g) with metal surface inclusions (stainless steel) was placed at the end of the arm of a torsion balance, as shown in Fig. 1. A mirror was mounted at the other end of the balance. A laser beam reflected from the mirror was sent onto a screen placed at a distance of L = 1550 mm from the chamber axis. The moment of inertia of the system was $I_b \cong 35.4$ g $\mathrm{cm^2}$, and the frequency of free oscillations was $\omega_o = 2\pi/T_o = 0.33\ \mathrm{s^{-1}}$.

The balance deflection by an angle ϕ from the initial position corresponds to the recoil momentum

$$J_t = I_b(\omega_o/\ell_m)\phi\ (\mathrm{g\ cm/s}), \qquad (2)$$

where ℓ_m is the distance from the target center to the hanging point ($\ell_m \cong 9$ cm). Under our experimental conditions, we have

$$J_t \cong 4.10^{-4}\ (\Delta x),\ (\mathrm{g\ cm/s}) \qquad (3)$$

where Δx is the displacement of the laser beam on the screen (in mm). The actual sensitivity of this method is about 4.10^{-4} g cm/s.

Figure 2 shows how the recoil momentum depends on the background air pressure in the chamber. The curve was constructed over a wide range of pressures from 10^{-4} to 700 torr. The

microwave pulse duration was τ_f = 1 μs. When the experiment was conducted in high vacuum, the absolute value of J_t was on the order of 8.10^{-4} g cm/s; the specific momentum defined as $j \equiv J_t/W_\tau$ was on the order of 10^{-9} s/cm. Here, W_τ is the total energy of the microwave beam in (J): $W_\tau = \Pi S \tau_f$ (where S is the cross area of the microwave beam on the target surface).

As the background pressure increased up to 10^{-2} torr, the momentum varied only slightly and began to fall at $p > 10^{-2}$ torr down to its minimum value $J_{tmin} \cong 10^{-4}$ g cm/s ($j_{min} \cong 10^{-10}$ s/cm) at $p \cong 10^{-1}$ torr. As the pressure further increased, the mechanical momentum increased up to the level substantially exceeding that observed in the vacuum experiment. The maximum value of the mechanical momentum obtained at p = 250 torr amounts to $J_{tmax} \cong 3.10^{-2}$ g cm/s ($j_{max} \cong 3.10^{-6}$ s/cm).

Therefore, in the presence of non-self-sustained discharge the microwave beam energy converts most efficiently into gas heating near the target surface which in turn is accompanied by an excessive pressure exerted on the target.

Figure 3 demonstrates a typical dependence (in relative units) of the mechanical momentum on the microwave pulse duration for $p \cong 700$ torr. It is seen that in the presence of the surface non-self-sustained discharge the mechanical momentum increases approximately as a quadratic function of the microwave pulse duration: $J_t \sim \tau_f^2$.

References

1. Pirri A.N., Monsler M.J., and Nebolsine P.E., Propulsion by absorption of laser radiation. – AIAA Journal, 1974, vol. 12, No 9, pp. 1254-1256
2. Barchukov A.I., Bunkin F.V., Prokhorov A.M., and Konov V.I. Laser Air Jet Engine, Pis'ma Zh. Eksp. Teor. Fiz., 1976, vol.35, no. 5, pp. 273-274 (in Russian).
3. Ageev V.P., Barchukov A.I., Bunkin F.V. et al. Experimental Modeling of a Laser Air Jet Engine, Pis'ma Zh. Tekh. Fiz., 1976, vol.2, no. 22, pp. 1032-1035 (in Russian).
4. Tsiolkovskii K.E., Rocket Engineering, M: Oborongiz, 1947, 189 p. (in Russian).
5. Shad J.L. and Moriarty J.J. Microwave rocket concept. – XVI Intern. Astronaut. Congr., Athens, 1965, v. 5, Propulsion and reentry, pp. 175-186
6. Batanov G.M., Kossyi I.A., and Rabinovich M.S., Propulsion by Microwave Discharge in Inhomogeneous Gas Flow, Pis'ma Zh. Tekh. Fiz., 1979, vol.5, no. 7, pp. 432-435 (in Russian).
7. Batanov G.M., Gritsinin S.I., Kossyi I.A. et al., High-Pressure Microwave Discharges. – In "Plasma Physics and Plasma Electronics", Ed. by L.M.Kovrizhnykh, Nova Science Publishers, 1989, pp. 241-282

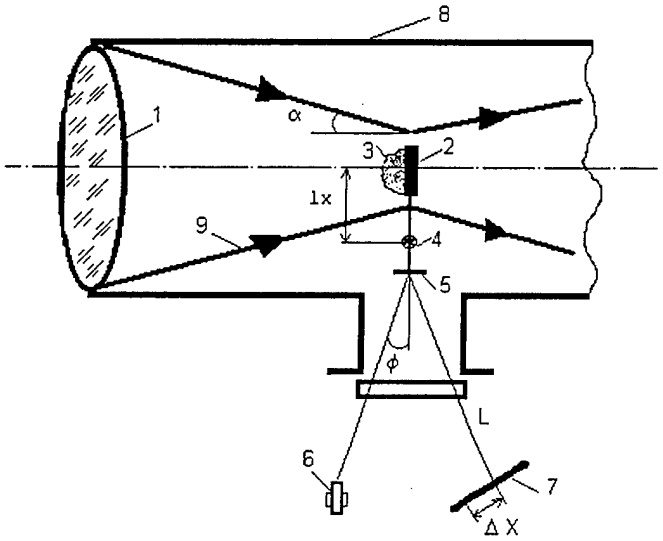

Fig.1. Scheme of modeling experiment

1 – lens forming of convergent microwave beam; 2 – metal-dielectric target; 3 – plasma of non-self-sustained microwave discharge; 4 – pendulum; 5 – mirror; 6 – laser; 7 – screen; 8 – vacuum chamber; 9 – convergent microwave beam

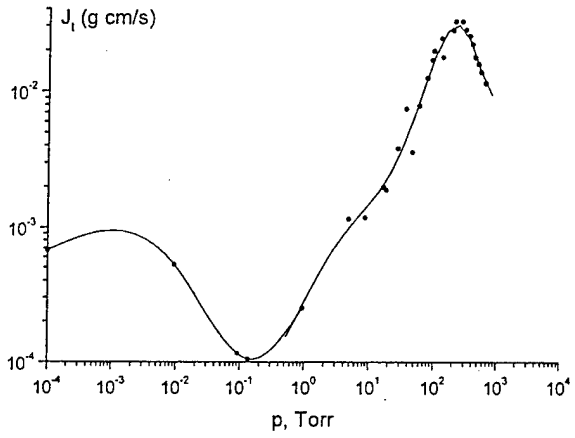

Fig. 2. Recoil momentum dependence on the background pressure.

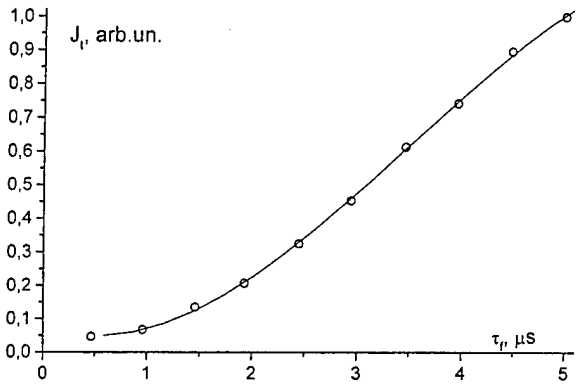

Fig. 3. Recoil momentum dependence on the MW pulse duration.

ACTION OF MAGNETIC AND ELECTRICAL FIELDS ON FLOW PATTERN IN DIFFERENT PARTS OF DIFFUSER.

S.V.Bobashev, R.V.Vasil'eva, A.V.Erofeev, T.A.Lapushkina, S.A.Poniaev, D.M. Van Wie***

**Ioffe Physico-Technical Institute Russian Academy of Sciences26, Polytekhnicheskaya, St. Petersburg, 194021,RUSSIA, E-mail: tanyusha@mail.ioffe.ru*

***The Johns Hopkins University, Laurel, MD, USA*

Abstract

This work continues a series of [1,2] initiated under AJAX program [3] with a purpose to study the external effects on the shock-wave structures arising in a diffuser with a total inner flow compression. The main part of the diffuser is a linearly convergent channel. The shock-wave structure incorporates two attached shocks affected by each other in the diffuser. A study of current-voltage (C-V) characteristics carried out in [1] brought out a large potential drop near the electrodes which impeded passage of the electrical current induced by an external magnetic field. To compensate this potential drop it was necessary to use external electric field arranged in such a manner that it enhanced a magneto-induced current. A flow is a result of the MHD interaction itself as well as a gas heating under the external electric field.

Statement of the problem

A general aim of the work is a treatment of a shock-wave structure's dynamics under the external fields and of what processes and of what part of the diffuser are more important in flow shape changes. For this aim, a comparison is carried out between the flow pictures under effects in a diffuser's bulk and its separate parts when an external influence was localised due to the passage of transverse or longitudinal electrical current through a limited part of the diffuser.

MHD interaction itself consists of two elementary effects: a) the work of a ponderomotive force with the power density juB causing either deceleration or acceleration of a flow according to orientation of the current direction and b) removal or release of an energy produced by the electromotive force induced by an external magnetic field with the power per a unit volume defined as $kjuB$. The action of an external electric field results in a Joule heating of a plasma with the power density defined as $Q = (1 - k)jV/h$. The heating of plasma leads to deceleration of supersonic flow always.

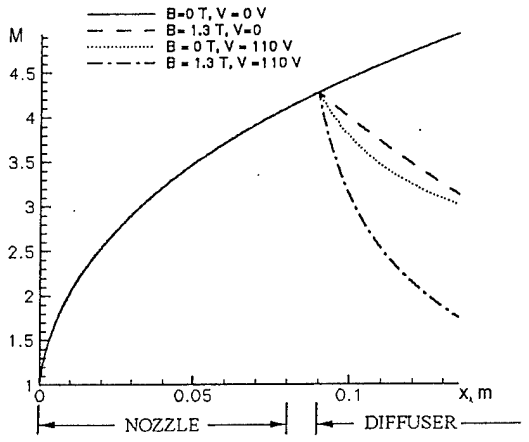

Fig. 1. Changes in the Mach number of the flow along the axis of the gasdynamic tract under influence of the magnetic and electric fields.

Figure 1 gives a calculated Mach number of the flow along the axis of the gasdynamic tract under influence of the magnetic and electric fields. Calculation data have been obtained solving a system of the equation giving the changes in a flow velocity, state parameters, Mach numbers, and Ohm law under conditions nearest to those of the present experiments [4]. Calculation has been carried out when X=0 - a critical cross section, T_{cr} =7700K, ρ_{ocr}=2,2kg/m^3, a_{cr}=940 m/s. As a value of conductivity in the interaction region it have been used that of effective conductivity

obtained experimentally, σ_{eff}=150 S/m. A load coefficient k=0,3.

One can see in Fig. 1 that the separated effects of the electric and magnetic fields are strong decreasing Mach number about 25%. A mutual action of the external fields illustrated by the data of calculation results in a sharp drop of the Mach number of the flow over an interaction length.

For later comparison, Fig. 2 gives a schlieren picture of the flow in a diffuser obtained in the one-fold regime with no external fields as well as a scheme of arising discontinuities. Here, the inlet shocks are well seen with a point of their interaction distanced by X_c=(44±1.5) mm from the diffuser's inlet.

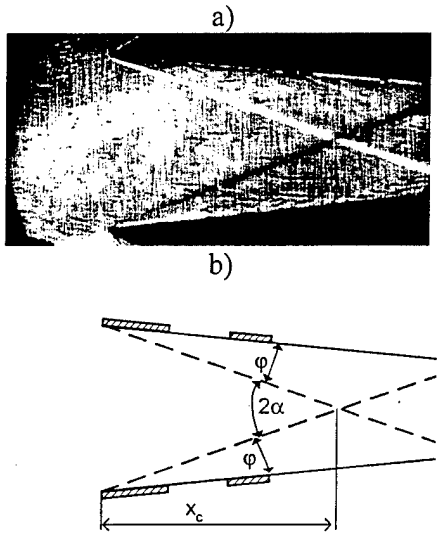

Fig. 2. Schlieren picture of a flow and a scheme of HD irregularities with no external fields.

To clarify what parameters of a shock-wave configuration can characterise the flow response to an external influence we present a schematic diagram of shocks in a diffuser in Fig.2-b. The diffuser is formed by two 5.5° wedges. An attached shock forms an angle φ with the diffuser wall. The attached shocks intersects at an angle 2α at a distance x_c from the inlet diffuser cross section. All of three parameters (φ, 2α, and x_c) can serve as a measure of an external impact. For example, a flow deceleration accompanied by the corresponding decrease of the flow Mach number causes increasing the slope angles of the shocks, their intersection point nears to the diffuser inlet, and the angle between them increases. A flow acceleration causes the inverse changes in these three parameters.

The experiments were carried out at the shock wave Mach number 8 in xenon at an initial xenon pressure of 30 Torr. The designed gas and flow parameters at the diffuser inlet were: the flow Mach number 4.3, xenon plasma density 0.127 kg/m^3, flow velocity 1550 m/s, plasma conductivity 600 S/m. The efflux duration was roughly 0.5 ms.

Faraday connection of the current

A schematics of the connection of transverse electrical current through the plasma are shown in Fig.3. Arrangement of current through one pare of electrodes are shown on it. Needful number of electrodes in investigated bounded region are connected reciprocally.

In this case, the diffuser operates similar to Faraday's MHD channel, where an electromotive force is induced due to the interaction between the plasma flow and the external magnetic field. This electromotive force is $\varepsilon = uBh$, where u is the flow velocity, B is the magnetic induction, and h is the interelectrode distance. The voltage V applied to the electrodes may be of different polarity. If the electromotive force and the external electric field between the electrodes are codirectional as shown in Fig.3-a, we deal with deceleration regime. When the directions of the electromotive force and the external electric field are opposite, such a regime is conventionally named as acceleration that (Fig.3-b). In last case acceleration of flow due to action of ponderomotive force competes against deceleration due to a Joule heating of a plasma.

a)

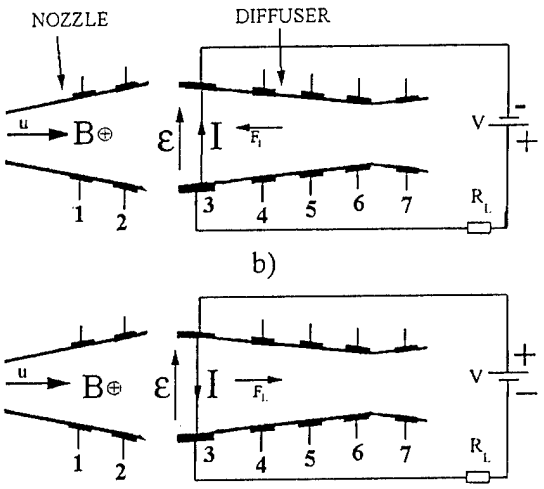

Fig.3. Scheme of transverse current localization. Figures are numbers of electrodes. a) deceleration regime, b) acceleration regime.

In this case, Ohm's law has the form

$$IR_{eff} = (1-k)(uBh \pm V), \quad (1)$$

where k is the load factor and R_{eff} is the resistance of the interelectrode gap;

$$k = \frac{R_L}{R_L + R_{eff}}. \quad (2)$$

The positive sign in (1) corresponds to the deceleration regime and the negative sign - to deceleration one.

Interaction with the external fields in a bulk of the diffuser

In Fig. 4 are shown the flow pictures in the diffuser obtained with the schlieren technique when transversal current in deceleration regime was applied on all electrodes in diffuser.

Figure 4-a shows a flow structure arising under the electric field effect only. The wall layer is well seen on a schlierengramm. One can see that its thickness is increased along the diffuser and the wall layer are greater with a current than that with no current (Fig. 2). Compared with flow picture with no fields (Fig. 2), in this case, a slope angle of the attached shocks grows, an intercept point of the shocks X_c shifts toward the diffuser inlet, X_c=(36±1,5)mm, and the points of the shocks' reflection from the walls, also, are closer to the inlet. Qualitatively, a flow picture formed under effect of the electric field on the flow is similar to that arisen under a weak MHD interaction.

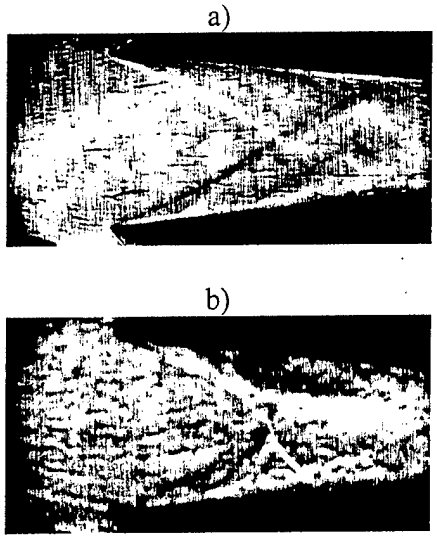

Рис.4. Shlieren pictures of flow at the interaction in a bulk of the diffuser
a) V=110V, B=0, b) V=110V,B=1.3T.

Figure 4-b demonstrates a schlieren picture of the main observed gasdynamic irregularities arisen in the diffuser as a result both of the electric and magnetic fields. One can see that the flow picture is essentially changed. Attention is to a strong development of the wall layer, especially, near the top wall. It is of importance the principal change in the inlet shocks' structure. Instead of the intercepting oblique shocks we can see a triple structure including a direct shock in the flow core and two oblique shocks. Picturing the flow as a whole, we can confirm that it is a pattern of a strong interaction when there is a direct shock of MHD deceleration in the flow core due to action of ponderomotive force and a Joule heating of a plasma. The shock of MHD deceleration changes over the supersonic flow to the subsonic. However, the flow picture is very complicated due to an effect of a highly developed wall layer.

Interaction on the various sections of diffuser

To found the most effective conditions for influence on the shock-wave structures let us consider changes of it when the current exists on the various sections of diffuser.

Fig.5 shows the structure of flow when transversal current in deceleration regime was applied to all electrodes in diffuser except third pare.

a)

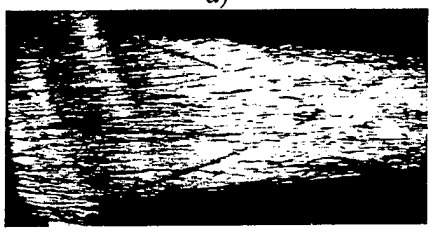

b)

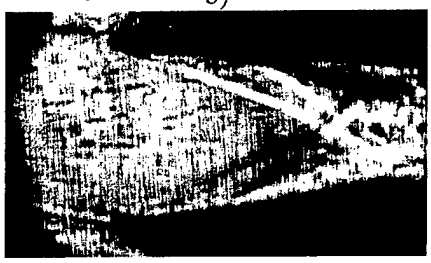

Рис.5. Shlieren pictures of flow at the interaction in a bulk of the diffuser except inlet part of diffuser.
a) V=110V, B=0, б) V=110V, B=1.3T

The schlieren picture under the electric field only is presented in Fig. 5-a. One can see that the slope angles of the attached shocks φ are slightly changed compared with Fig. 2, a distance X_c is not changed in practice. However a current does effect a growth of the wall layer, its growth being originated near the first electrode under this connection.

Involving additional magnetic field (Fig 5-b) does not give a noticeable shift of the attached shocks, one can see only a weak distortion and more increased wall layer.

In a case when the external electric field involves only the first pair of electrodes situated on the diffuser's noses a shock-wave structure arises given in Fig. 6.

a)

b)

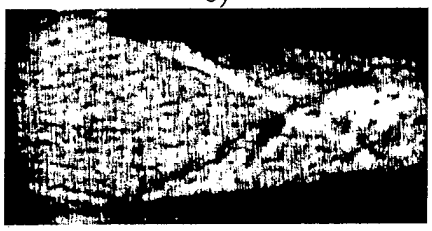

Рис.6. Shlieren pictures of flow at the interaction in the inlet part of diffuser.
a) V=110V, B=0, б) V=110V, B=1.3T

Already with closing a circuit of a current with no magnetic field (Fig.6-a) a pronounced change in the slope angles of the shocks is observed, a point of their intercept shifts toward the diffuser's inlet, X_c=(37±1.5)mm, also, is noticeable a growth of the wall layer beginning the very inlet of the diffuser. Under MHD interaction (Fig.6- b) there is no additional change in X_c but the attached shocks become more concave and the wide wall layers are well seen, a top layer being gather wider that the low one.

This experiment demonstrates that connection from 4^{th} to 7^{th} pare electrodes is of more weak influence on a shock-wave structure than connection in inlet part despite a more stretched interaction region. Region 4-7 is closely packed with the dissipative structures. While in region 3 the main volume is filled by a continuous flow. Naturally, the observed inertia of the shocks in region 4-7 can be related to energy consumed by their formation under interaction between the flow and the diffuser's walls. In the case when there are several shocks, partially or completely, in the interaction region, energy dissipated in the shocks is probably added. A ratio of this

energy to interaction energy could be a measure of inertia of the shocks when tending to change their location under the external factors.

Then to act effectively on attached shocks the external effects should be applied to the inlet part of the diffuser. Therefore naturally to continue investigation of interaction with magnetic and electric fields when it is localised in the shot inlet part of diffuser. We have tried not only to decelerate flow, but to accelerate it, that is to reduce angels φ and α and to show possibilities are studied of control of a shock-wave configuration.

Shown in Fig.7 are Schlieren patterns of steady-state flows for two different situations. Fig.7-a there is a Schlieren pattern of the flow affected by electric and magnetic fields simultaneously in an MHD deceleration regime ($V = 125$ V, $B = 1.3$ T). In the figure it is seen that a joint action of electric and magnetic fields leads to more intensive flow deceleration, that is, causes increasing the angle α and decreasing the distance x_c in comparison with Fig.2.

Fig.7-b demonstrates a Schlieren pattern corresponding to an acceleration regime under the conditions $V = -150$ V and $B = 1{,}3$ T. It is seen that additional shocks have formed that, in essence, join together with the attached shocks. This has probably occurred due to a strong heating of the near wall layers by the passing current.

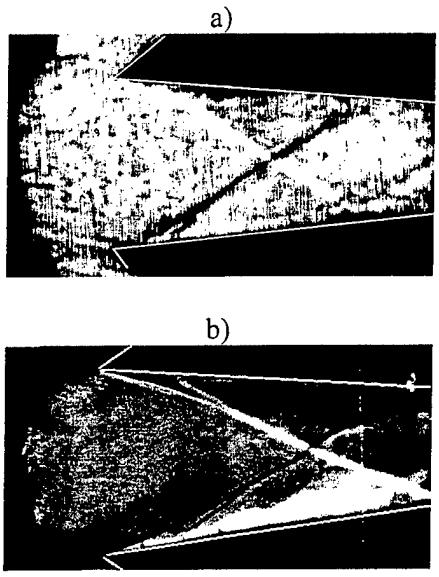

Fig.7. Examples of changes in shock-wave configurations.
a) V =125 V, B=1.3 T - deceleration regimes.
b) V =-150 V, B=1.3T - acceleration regime.

As a whole, the flow pattern shows that the angle α has increased and the distance x_c has decreased as compared with the flow pattern at $V = 0$ and $B = 0$, that is, no flow acceleration is observed. Probably, this has resulted from that the deceleration due to the Joule heating turned out to be stronger than the acceleration caused by the action of the ponderomotive force. However, connection of accelerate action of the ponderomotive force decreased effect of deceleration under Joule heating of the gas.

An analysis of the experimental data allows us to show up effects of acceleration and deceleration of the flow conditioned by the action of the ponderomotive force on the background of the flow deceleration due to Joule's heating caused by the external electric field. Let us show how one can do this. Select from the set of data presented three regimes at the same current I=(500±50)A, and with different directions of the ponderomotive force including a case with no ponderomotive force (B=0). We assume that a ponderomotive force causing deceleration of the flow corresponds to a negative magnitude of the magnetic

induction (B=-1.3T) and an accelerating ponderomotive force corresponds to a positive magnetic induction (B=1.3T).

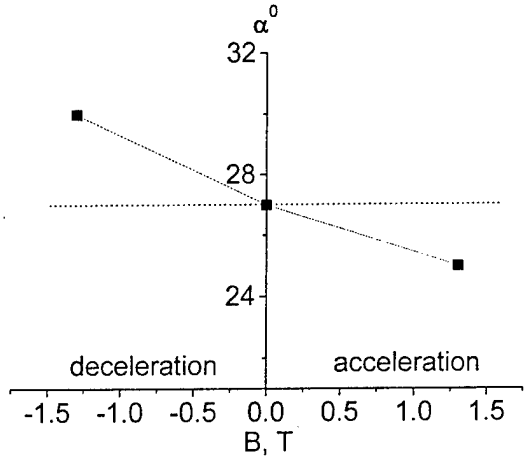

Fig.8.Variation angle α with magnetic field.

Fig.8 shows variations the angle α with magnetic induction obtained on the basis of such an approach to the data processing. The horizontal line corresponds to $\alpha = 27^{\circ}$ at $B = 0$. As it seen in Fig.8 the angle α, as it was expected, increases in the deceleration regime and decreases in the acceleration one.

Connection of the longitudinal current

A schematic of the experiment is shown in Fig.9. The current passes through a local region beyond the attached shocks near the walls between the electrodes 3 and 4. In Fig.9 directions of the current and Lorentz force are shown by arrows. The strength of the current passing through the electrodes is 400 A. The magnetic induction B is 1.3 T.

Fig.10 shows a sequence of steady-state flow patterns. An asymmetric location of the attached shocks is observed. In this figure there is a location of the attached shocks at no external influences (dashed lines) and their positions extracted from experiment with the second way of the current localization (solid lines) too.

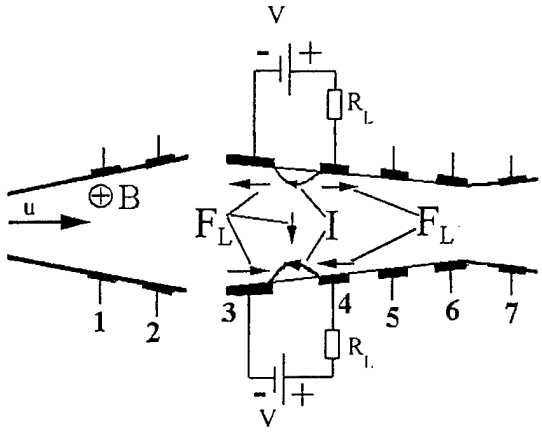

Fig.9. A schematic of the current localization.

At $B = 0$ and $V = 0$ the shocks are symmetrically positioned relative to the flow axis and make an angle with the diffuser walls of 15°.

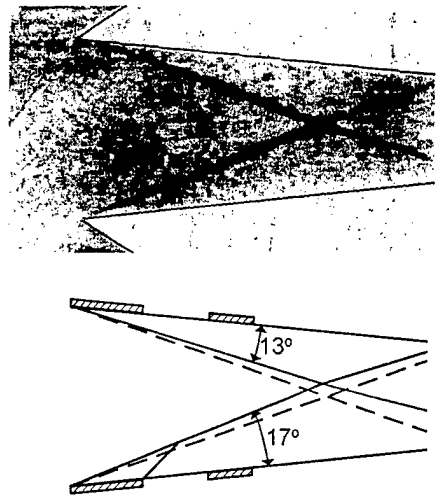

Fig.10. A sequence of the a steady-state flow pattern and comparison between positions of the attached shocks.

After establishing the magnetic field and passing the longitudinal current from the external source through the local region 3-4, the slope angle of the shock attached to the upper wall has decreased and became equal to 13°, that is, the shock displaced downstream. Near the upper diffuser wall the slope angle of the attached shock has increased up to 17° and the shock displaced upstream. Such a behaviour of the attached shocks is conditioned by that as a result of

action of the Lorentz force the gas pressure against the upper diffuser wall has decreased and the shock neared the wall. Against the lower diffuser wall the Lorentz force has caused an increase of the pressure and the shock shifted from the wall.

We can see the stronger action of ponderomotive force in a series of experiments to be discussed there existed an appreciable component of an electrical current directed along the flow axis. For this purpose, an electrode-to-electrode voltage of V=150V from an external source was applied to the second and fifth electrodes at the upper and lower diffuser walls in such a way that the second ones serve as cathodes and the fifth as anodes.

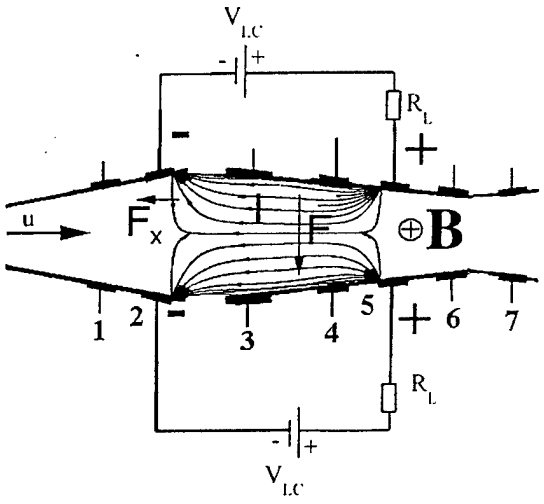

Fig.11. A schematic of the longitudinal current localization.

Fig.11 shows an electric diagram of the connection of the electrodes and lines of the electrical field calculated under the of infinitely small electrode areas. The Lorenz force directions are shown by arrows. A mean strengths of the current through the circuits including the upper and lower pairs of electrodes amount to 600 A.

In Fig.12 there are flow patterns observed with the presence of only electric field (Fig.12-a) and under the joint action of electric and magnetic fields (Fig.12-b). When a magnetic field is absent the flow pattern is symmetric. After establishing an external magnetic field the flow pattern becomes asymmetric as it seen in Fig.12-b. The asymmetry origin can be explained by that the Lorentz force causes a growth of the gas pressure against the lower wall resulting in increasing the slope angle of the lower attached shock, while near the upper wall the Lorentz force action leads to a decrease of the gas pressure followed by approaching the wall by the shock.

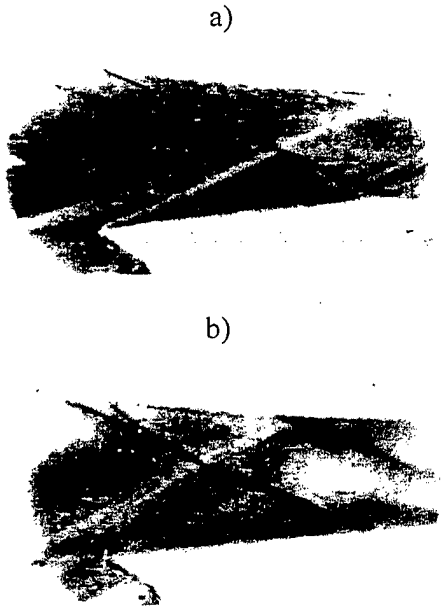

Fig.12 Shlieren pictures
а) V = 150 V, B = 0 T;
б) V =150 V, B =1.3T

Most probably there is a deflection of velocity vector of flow toward lower wall under action of ponderomotive force. It brings into the reducing of angle of attack near upper wedge and the increasing one near lower wedge.

The experiment carried out shows that to control the shocks the presence of a longitudinal electric current near the wall and a transversal magnetic field is enough. An attached shock can change its slope angle toward one or the other side depending on the current direction.

Conclusions

The main results of this work are presented as follows.

An effect of the wall layer on a flow picture in the diffuser is revealed.

It is maintained that the external effects should be applied to the inlet part of the diffuser with a purpose to control the attached shocks.

It is demonstrated that a flow with shocks has a certain inertia relative to the external effects, being connected with energy dissipated in the shocks during their formation as a result of an interaction of the flow with diffuser's walls.

It has been shown a possibility of increasing or decreasing the slope angle of an attached shock by the action of the ponderomotive force when:

a) passing a transverse electric current in inlet part of diffuser;

b) passing a longitudinal electric current in a limiting region near the diffuser wall with a transversal magnetic field.

References

1. S.V. Bobashev, R. V. Vasil'eva, E. A. D'yakonova, A. V. Erofeev, T. A. Lapushkina, V. G. Maslennikov, S. A. Poniaev, V. A. Sakharov and D. Van Wie. The Effect of MHD Interactions on the Input Shock Waves in a Supersonic Diffuser. Technical Physics Letters, Vol. 27, pp. 71-73, 2001
2. S.V. Bobashev, E.A. D'yakonova, A.V.Erofeev, T.A.Lapushkina, V.G. Maslennikov, S.A.Poniaev, V.A.Sakharov, R.V.Vasil'eva and D. M. Van Wie. Shock-tube facility for MGD supersonic flow control. AIAA Paper No 2000-2647, 2000
3. Gurijanov E.P. and Harsha P.T. "AJAX: New Direction in Hipersonic Technoloigy." AIAA Paper 96-4609. 7th Aerospase Planes and Hipersonic Technology Conference. Norfolk, VA, 1996.
4. L.A.Vulis, A.L.Genkin, B.A.Fomenko. Theory and Calculation of Magnetogasdynamic Flows in the Channels (in Russian). Atomizdat, Moscow, 384 p., 1971

PECULIARITIES OF TRANSVERSAL DISCHARGE IN A FLOW AS NON SELF MAINTAINED IN AIR.

I. TRANSVERSAL ELECTRIC DISCHARGES IN SUPERSONIC FLOWS

Bychkov V.L., Ershov A.P., Chernikov V.A., Shibkov V.M, Surcont O.S., Timofeev B.I. and Timofeev I.B.

Moscow State University, Physics Department, E-mail: igortim@orc.ru

Introduction

Effective solution of such aerodynamic problems as decrease of bow drag of flying vehicles or fuel ignition in ramjets at supersonic velocities is evidently impossible without an application of plasma technologies.

Most attention at investigation of electric discharges in supersonic flows was paid to forming of a discharge in a flow and to plasma influence on aerodynamic body characteristics [1-5]. Experiments in wind-tunnels usually were carried out with constant current discharges. However up till now a discharge picture in supersonic flows stays weakly investigated. This is conditioned by high cost and laboriousness of experiments in wind-tunnels and strong non stationarity of discharges in supersonic flows.

From this point of view investigations of pulsed or pulse-periodic discharges in supersonic flows seem to be more appropriate. Their application allows to considerably widen a range of discharge external parameters, and it is fundamentally important for clarification of discharge in flow physical picture. In presented work we expose results of transversal discharge investigations in the following range of characteristics: reduced pressure p ~ 0,1 – 1 atm, discharge current I ~ 0,1 – 40 A, inter electrode gap d = 6 – 20 mm, flow Mach number M= 2 and 6.

Typical picture of a discharge development in a supersonic flow

Integral topology of luminescence of transversal discharges (during exposure time of hundredth part of a second) is well known: thing extensive channels stretch out along a flow behind discharge electrodes, their brightness is substantially greater than that of a bridging area between them and a discharge channel seems to be unclosed. Such a picture is typical both for small and hypersonic Mach numbers (see Fig.1).

A discharge channel, transversal to a flow, after inter electrode breakdown begins to be drifted out by a flow. This leads to formation of discharge channels behind each of electrodes, they are directed along a flow. However, whereas luminescence of a channel along a flow is integrated over time the luminescence of a channel transverse a flow is "spread" over space. Hence the bridging region has a considerably weaker brightness in integral in time discharge photos.

Changing for pulsed discharge with varied pulse duration τ does not lead to changing of integral luminescence topology (during a pulse now), but it changes a discharge extension along a flow $L=v\tau$. Limiting value L corresponds to a case of a constant current [6]. Pulsed mode of the discharge work allows to apply a method of supersonic photo detection (SPD) and thoroughly investigate a discharge dynamics.

A typical picture of transversal pulsed discharge development in a supersonic stream is represented in Fig.2. A flow is directed top-down. One can see that a discharge is stretched down along a flow with a velocity of a flow. A discharge size in a last frame in SPD –form exceeds a size of chamber side port-hole and goes out from field of vision. In Fig.2 this moment corresponds to t ≈ 256 μs. A maximum observed size is limited by a length L ≈13 cm.

Results of SPD from the point of view of discharge propagation in space show that effects of transport processes (ambipolar diffusion, thermal conductivity and drift) are negligible outside near electrode regions at given conditions, so a velocity of a discharge propagation and a discharge configuration is wholly set by corresponding flow characteristics. Thereby a discharge in a flow with transversally applied electric field can not be stationary in principle, since a part of a positive column is always perpendicular to a flow and continuously drifted by it.

Burning instability mechanism of a transversal discharge in a gas flow

A process of a discharge propagation along a flow can not be infinite and it breaks at a definite moment. In Fig.3. this corresponds to a time moment between 416 and 448 μs – the discharge extension sharply decreases. Newly formed current channel begins to be drifted out by a flow. A secondary breakdown between an anode and a cathode plasma streams usually takes place near a Mach disk.

The process of a discharge development in time is most simply quantitatively illustrated by typical voltage at discharge electrodes waveforms. Such waveforms and waveforms of a current are represented in Fig.4. Increasing of the discharge extension along a flow is accompanied by close to linear increasing of a voltage between electrodes. After a definite time this increasing is interrupted by a sharp drop of a voltage, corresponding to a breakdown between the anode and the cathode streams. Later the process repeats the discharge passes to a vibrational mode.

Discharge electric field

Continuous increasing of discharge channel length indicates that a discharge in a flow is non stationary even in an idealized case of discharge feeding from a generator of a current $I = I_0$. Therefore in classic AVC of a discharge dependence $U(I)$ – a set of values of potential difference between electrodes (at definite time moments) corresponds to a current value.

So from a physical point of view makes sense a dependence of electric field with respect to a current $E(I)$, but not the dependence $U(I)$. Results of floating potential measurements and direct measuring of E by floating probes (signals from which were given to an inlet of differential amplifier) showed that the field value change with time rather weakly both in the anode and the cathode parts of the discharge. A mean field value $\langle E \rangle$ (over whole discharge length) can be determined from the voltage on the discharge waveforms (see Fig.4) , since $\partial U/\partial t = \langle E \rangle v$. It is important that a sum of near electrode potential drops is automatically extracted.

Data for a transversal discharge obtained in such a way with respect to a discharge current in the range of three orders of its magnitude are represented in Fig.5. They are constructed at fixed values of the full pressure P_0.

One can see that obtained dependencies of $E(I)$ are falling. An electric field reaches values close to 1 kV/cm in a region of respectively small currents then it quickly, practically for an order of magnitude drops with increase of a current, and later it changes weakly. Transition region from one mode to another corresponds to the current I ~ 1 A and it shifts in direction of lager currents with pressure.

A discharge current through a gas in absence of a flow is accompanied by a constriction in investigated range of parameters. Usually a connection between a current and a voltage is close to a power dependence $I \sim E^{-m}$, and the case $m = 1$, or $I \sim E^{-1}$ corresponds to the region of weak currents i.e. to weakly constricted glow discharge. Value m increases with increase of a current, at high currents it reaches $m = 3$, or $I \sim E^{-3}$ i.e. the arc mode. Representation of data in double logarithmic scale shows that the power dependence with $m = 2 \pm 0{,}2$ corresponds to weak currents – region of quick field drop in the range of investigated pressures. At the same time $m \approx 3$

corresponds to large currents. So a discharge in typical for plasma aerodynamic conditions can be classified as intermediate between strongly constricted and free burning arc. Type of *E(I)* dependence does not connected only with temperature and correspondingly with conductivity changes but with changes in sizes of current conducting region [8]. Results of luminescent discharge channel diameter and its hot region is represented in Fig.6. One can easy see that diameter size increases with the current rise as $d \sim E^{-0.5}$, and the hot region diameter is by ≈1,5-2 times smaller than those of the luminescent region.

Conclusions

Undertook investigations of transversal discharges in supersonic flows have shown that secondary breakdowns between the anode and the cathode plasma streams lead to origin of periodic voltage and discharge current pulsations.

A visible size of the discharge channel is considerably different from the size of the hot region – the region of high conductivity (especially at high discharge currents) This circumstance has to be accounted during plasma temperature determination by spectroscopic methods.

References

1. Alfyorov V.I., Bushmin A.S., Kalachev B.V. Experimental Study of Properties of an Electric Discharge in an Airflow.ZhETF, 1966, v.51. N.5(11). pp.1281-1287.
2. Alfeyorov V.I. Peculiarities of electric discharge in high-velosity air flow with great density gradients. The 3rd Workshop on magneto-plasma-aerodynamics in aerospace applications. Moscow, 24 April – 26 April 2001, p.121 – 128.
3. Vitkovskii V.V., Grachev L.P., Gritsov N.N., Egorova Z.M. et.al. Experimental investigations of constant current electric discharges in supersonic and subsonic air flows. Works of TsAGI. №.2505, 1991.
4. Bychkov V.L., Grachev L.P., Esakov I.I., Deriugin A.A. and others. Numerical and experimental investigation of supersonic flow around blunt body at the existence of the longitudinal discharge. Preprint of Keldysh Institute of Applied Mathematics, RAS, 1997, № 27.
5. Chernyi G.G. Some recent results in aerodynamic applications of flows with localized energy addition., 9 International Space Planes and Hypersonic Systems and Technologies Conference and 3 Weakly Ionized Gases Workshop, 1-5 November 1999, Norfolk, VA, USA, AIAA-99-4819.
6. Chernikov V.A., Dvinin S.A., Ershov A.P., Shibkov V.M., Timofeev I.B., Van Wie D.M. Experimental and theoretical research of DC transversal gas discharge in a supersonic gas flow. The 3rd Workshop on magneto-plasma-aerodynamics in aerospace applications. Moscow, 24 April – 26 April 2001, p.129 – 134.
7. W.Finkelnburg und H.Maecker. Electrische Bögen und thermisches Plasma. Handbuch der Physik, Bd.XXII, S. 254-444, 1956.
8. Sinkevich O.A., Stakhanov I.P. Plasma physics. Stationary process in partly ionized gas. M. Vysshaya shkola. 1991, 191 P.
9. Ershov A., Ardelyan N., Chuvashev S., Shibkov V., Timofeev I. Probe diagnostics of gas discharge in supersonic airflow. AIAA Journal, vol.39, No.11, November 2001, pp.2180-2187.

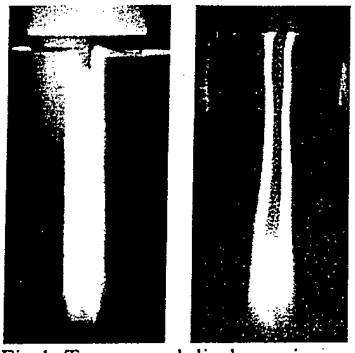

Fig.1. Transversal discharge in a supersonic flow:
a - M = 2, b - M = 6

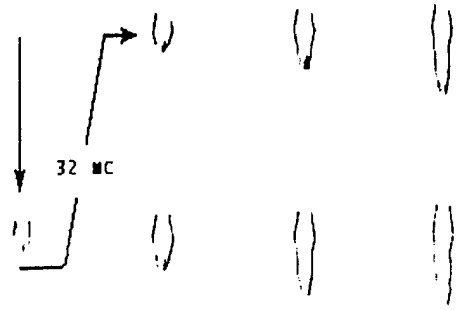

Fig.2. Typical SPD –forms of a transversal discharge in a supersonic flow .

a b

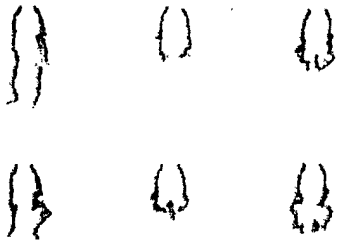

Fig.3. Secondary breakdown between the cathode and the anode streams. M = 2, I = 20 A, P_o = 2 atm, p = 100 Torr, τ = 200 μs

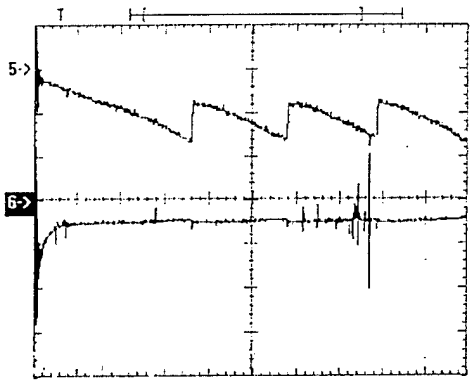

Fig.4. Transversal discharge waveforms of voltage (upper beam) and current in a supersonic flow: P_o = 1 atm, p = 45 Torr, τ = 200 μs.

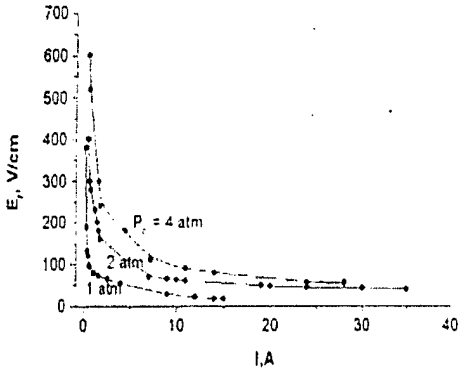

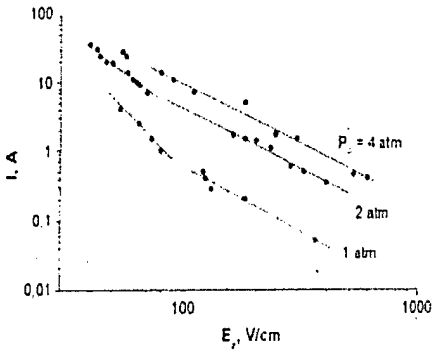

Fig. 5. Electric field in transversal discharge plasma in a supersonic flow. τ =200 μs , M = 2.

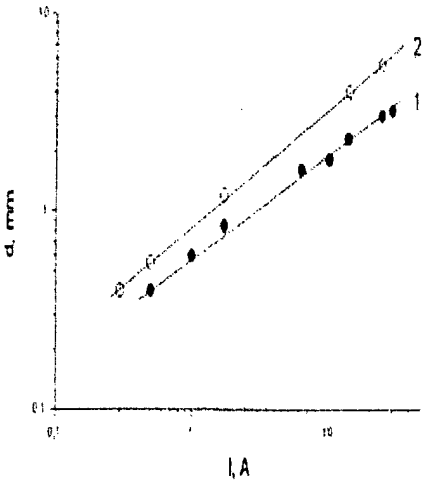

Fig.6. Discharge channel diameter.
1. blew filter, 2 – no filter

PECULIARITIES OF TRANSVERSAL DISCHARGE IN A FLOW AS NON SELF MAINTAINED IN AIR.
II. THEORETICAL MODEL OF ELECTRIC DISCHARGE IN A SUPERSONIC FLOW.

Ardelyan N.V., Bychkov V.L., Gordeev O.A., Ershov A.P., Timofeev I.B.

Moscow State University, Physics Department, E-mail: bychvl@orc.ru

Introduction

Development of plasma technology for aerodynamics requires detailed investigation of different discharge types with selfmaintained and non selfmainetained gas ionization [1-5]. Sometimes it is difficult to unanimously determine the discharge type due to complexity of plasma chemical process display in flow conditions. In works [1-3] applications of longitudinal and transversal discharges were considered for model bow drag decrease in a discharge wake. A transversal air discharge in a flow was studied [4] for its application in ignition of a flammable mixture, in [5] plasma jets and electron-beam plasma were studied for creation of excited plasma regions with properties required for aviation application.

In [1-4] plasma at gas discharge investigations was created at static pressure 30-100 Torr, initial gas temperature 130-170 K and Mach number of oncoming flow M=2-2.5.

Electric breakdown in [1-3] initially took place between two nearly located electrodes (transverse to a flow), see Fig.1. In so doing a breakdown field reached several kilovolts at the distance of several mm between electrodes. After this the created plasma was drifted to another electrode at a distance of several cm, and a current of about 1 A was realized between far located electrodes (~10 cm). Pulsation of some tens of μs were observed in a discharge. Measurements of gas temperature were in the range T=1700-2900 K. Estimates of electron density gave a value $N_e \sim 10^{13}$ cm^{-3} at visible diameter of the channel r_0 ~ 0.2 cm. At the same time value of a parameter E/N (E is an electric field strength, and N neutral gas particle density) was $5 \cdot 10^{-17} \div 1.2 \cdot 10^{-16}$ $V \cdot cm^2$ in a discharge, and it is less of necessary value for air breakdown $E/N > 1.05 \cdot 10^{-15}$ $V \cdot cm^2$. Analysis of this situation was made in [3], where it was shown that a model of stationary discharge in heated channel could not explain obtained results.

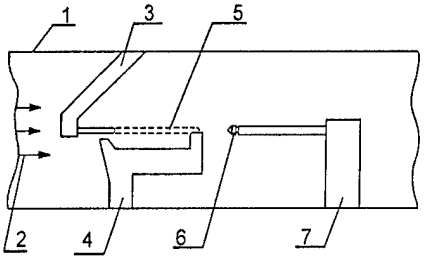

Fig.1. A scheme of a discharge in a flow. 1- wind tunnel, 2-air flow, 3-anode, 4-cathode, 5-discharge, 6- modelь, 7-balances.

In works [4] (see part I) experiments with a discharge in a flow was ignited in a flow at a voltage of several kV at static pressure of P=10-500 Torr and at distance between electrodes L=0.5-2 cm, then it was maintained by a generator of a current. The discharge current was in the 50 mA - 30 A, and a discharge

voltage was about of several hundreds of volts. So by estimates a parameter E/N was in the range $2\text{-}5\cdot10^{-17}$ V·cm^2, and it considerably less than necessary for air breakdown. Visible discharge channel diameter was in the range 0.3-6 mm with respect to experimental conditions. Pulsed-periodic mode with typical period 80-100 μs was established in this discharge. Mechanism of discharge burning was not studied in [4].

The goal of this part of the work is analysis of discharge burning mechanism on the basis of rather simple model.

Simplified discharge model

A consequent discharge model has to include a large number of components and plasma chemical reactions in plasma which have to be considered mutually with electric circuit. This approach requires solution of a system of stiff differential equations of particle balance, electron energy and gas temperature, see for example as it is done in [5]. However in such a complex formulation many important details can be missed, so a simplified approach is necessary as a first step to outline main important features of discharge processes.

In simplified formulation we consider definite air plasma conditions: static pressure P=100 Torr (N=$6.4\cdot10^{18}$ am^{-3}) and a gas temperature T=167 K. It is initially formed under action of fast electrons in Earth atmosphere ground layer. Then air ionization in a strong external electric field posed over a discharge gap takes place during 1 μs, in so doing a value of a discharge parameter is E/N =$1.05 - 2.\cdot10^{-15}$ V·cm^2. After this the external electric field drops to a value of E/N = $3\cdot10^{-16}$ V·cm^2. During this decrease of external electric field a Joule heating in a channel takes place, so there is a possibility of increase of E/N and ionization in a channel by plasma electrons and additional heating of a gas.

In such an approach we suppose that ion and electron concentrations and their velocities change weakly along a channel in main region between electrodes and $div(N_i \cdot v_i) \approx 0$, so main decrease of charged particles is caused by plasma chemical processes inside a channel and their diffusion from it. Besides according to experimental data we suppose that a voltage U in a discharge in a flow increases proportionally to a discharge length L (which is drifted by a flow), or $E \approx U / L \approx const$.

For description of this situation let us consider air plasma model consisting of ions O_2^+, N_2^+, O_2^-, O^- and electrons. The following processes take place in this plasma. Direct ionization of molecules O_2 and N_2 is realized by background fast electrons $\hat{e}$ and plasma electrons e:

$$\hat{e} + O_2 \rightarrow O_2^+ + \hat{e} + e, \quad (1)$$

$$\hat{e} + N_2 \rightarrow N_2^+ + \hat{e} + e, \quad (2)$$

$$e + O_2 \rightarrow O_2^+ + 2e, \quad (3)$$

$$e + N_2 \rightarrow N_2^+ + 2e. \quad (4)$$

An effective charge exchange of positive ions takes place in this plasma

$$N_2^+ + O_2 \rightarrow O_2^+ + N_2, \quad (5)$$

dissociative recombination of electrons and ions occurs also

$$e + O_2^+ \rightarrow O + O, \quad (6)$$

electrons attach to oxygen molecules in three-body process

$$e + O_2 + O_2 \rightarrow O_2^- + O_2. \quad (7)$$

Dissociative attachment acts at imposing of strong external electric field

$$e + O_2 \rightarrow O^- + O, \quad (8)$$

positive and negative ions recombine

$$O_2^- + O_2^+ + M \rightarrow O_2 + O_2 + M \ . \qquad (9)$$

Information on rate constants is given in [3,6-10].

For a sake of a simplicity let us suppose that excitation and quenching of electronically and vibrationally excited states takes place quickly, so that inputted to molecules energy is quickly transferred to heating. It is possible at E/N $=0.8 - 2\cdot10^{-15}$ V·cm^2 and at gas temperatures T >500 K [3,6-10] when the fast quenching of excited molecules occurs.

Starting from such problem formulation let us divide a temporal picture of a discharge development into following stages of selfmaintained and non selfmaintained burning.

a. In initial stage main processes are (1),(2), (7) and (9) as estimates show. The corresponding equations for positive, negative ions and electrons are:

$$N_0^+ \approx N_0^- \approx \sqrt{Q/\alpha_{ii}}\ ,\ N_{e0} < \frac{Q}{k_{tr\,att}\cdot(\eta\cdot N)^2},$$

here Q is rate of appearance of electron-ion pairs in air at a given pressure (at P=100 Torr Q = 0.5 - 0.8 см$^{-3}$·с$^{-1}$), α_{ii}- is a coefficient of ion-ion recombination (9), $k_{tr\ att}$- is a coefficient of three body attachment (7), η-portion of oxygen molecules in air, N is concentration of neutrals. Inserting definite values one can obtain that concentrations of ions in considered conditions are in the range $N_0^+ \approx N_0^- \approx (1.5 \pm 0.2)\cdot10^3$ см$^{-3}$, and of electrons N_{e0} <6.0·10^{-8} см$^{-3}$. In spite of a small value of initial electron concentration it is important factor of electron production at imposing of strong external electric field, since at E/N > 1.05·10^{-15} V·cm^2 sharp increasing of electron concentration takes place

$$N_e \approx N_{eo}\cdot exp(k_i\cdot N\cdot t),$$

where k_i is ionization rate constant in processes (3,4), and t is period of electric breakdown field action.

b. Stage of strong external electric field. At fulfillment of a condition

$$N_e > \frac{k_{disatt}\cdot\eta\cdot N}{\alpha_{disrec}},$$

where k_{disatt}, α_{disrec} are coefficients of attachment (8) and recombination (6), (N_e>4·10^{14} cm^{-3} at P=100 Torr), which is realized in strong electric field, one can determine an electron concentration by an equation:

$$N_{ein} \approx \frac{k_i N - k_{disatt}\cdot\eta\cdot N}{\alpha_{disrec}},$$

(which gives N_{ein}≈7·10^{14} cm^{-3} at E/N ≈1.1·10^{-15} V·cm^2 and N_{ein}≈5·10^{15} cm^{-3} at E/N ≈1.2·10^{-15} V·cm^2 , at P=100 Torr).

c. Stage of weak external electric field. System of equations for electron concentration and gas temperature at decreasing of external electric field to E/N≈3.·10^{-16} V·cm^2 can be reduced to quasi two-dimensional form:

$$\frac{\partial N_e}{\partial t} = k_i N\cdot N_e - \alpha_{disrec}\cdot N_e^2 - \frac{6D_a}{R^2}\cdot N_e, \quad (10)$$

$$c\frac{\partial T}{\partial t} = \zeta\cdot e\cdot N_e\cdot w_{dr}\cdot E - \frac{6\chi}{R^2}\cdot T, \quad (11)$$

where $D_a = D_i\cdot\left(1+\frac{T_e}{T_i}\right)\cdot\frac{T}{T_0}$ is ambipolar diffusion coefficient, T_0 is initial temperature, $\chi = \chi_0\cdot\left(\frac{T}{T_0}\right)^\beta$ is a gas thermal conductivity coefficient, $\chi_0 = \chi_{T=T_0}$, R is discharge channel radius, c heat capacity of a gas, e is electron charge, E – electric field strength, w_{dr} – drift velocity, ζ - energy portion coming from excited molecules to a gas (ζ≈0.8).

In equation (10) we account direct ionization in external electric field, elimination of electrons in dissociative recombination and in ambipolar diffusion from the channel. We neglect dissociative attachment what

is valid at E/N ~ 1-3.·10^{-16} V·cm^2 at the condition

$$N_e / N > \frac{k_{dis\,att} \cdot \eta}{\alpha_{disrec}}, \text{ or } N_e / N > 5 \cdot 10^{-11}.$$

In equation (11) we account a Joule heating of a gas and its thermal conductive cooling. Let us suppose that (10)-(11) satisfy isobaric conditions, they are realized in a channel after $t \sim R / c_s$ (in our case t ~1-2 μs) and heat capacity is $c = 7/2 \cdot N \cdot k_B$. This allows to analyze the stage of decrease of external electric field (c_s, k_B-sound velocity and Boltzmann constant).

At solution (10)-(11) equations we also account that a condition of constant current $I(t) \approx const$ is fulfilled. It allows to include channel radius changing and to test it's influence:

$$R^2 \approx R_0^2 \cdot \frac{N_e}{N_{ein}},$$

R_0 is initial channel radius and N_{ein} is electron concentration created during a breakdown.

In Fig. 2-3. temporary dependencies of electron density and air temperature in a channel are represented at accounting of E/N dependencies of electron- molecule reactions and drift velocity, initial electron density $N_{ein} \approx 5 \cdot 10^{15}$ at channel diameter 1 mm. This diameter corresponds to photos without a filter. A question about effective channel diameter is very important since the electron distribution in a channel is strongly non uniform with respect to radius. And it is not evident which effective radius size has to be chosen in calculations. Our calculations have shown that at increase of this diameter value leads to practically no changes in results on the moment of sharp jump of temperature and electron concentrations.

In Fig. 4-5 temporary dependencies of electron density and air temperature in a channel are represented at channel diameter of 0.3 mm. One can see that plasma characteristics are strongly dependent on the diameter.

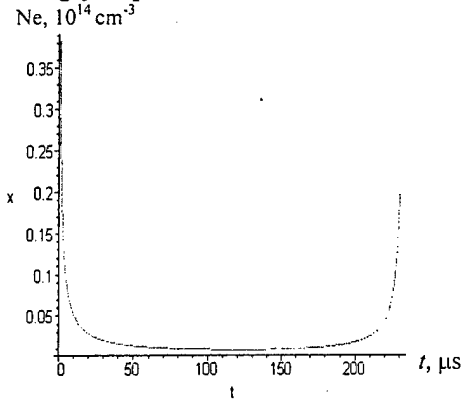

Fig.2. Temporary dependence of electron concentration in a channel in weak electric field stage at initial channel diameter 1 mm.

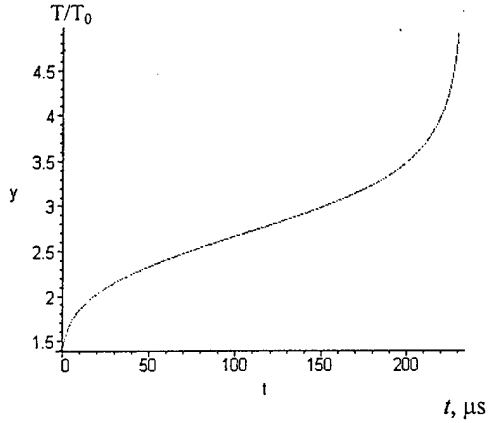

Fig.3. Temporary dependence of a gas temperature in a channel in weak electric field stage at initial channel diameter 1 mm.

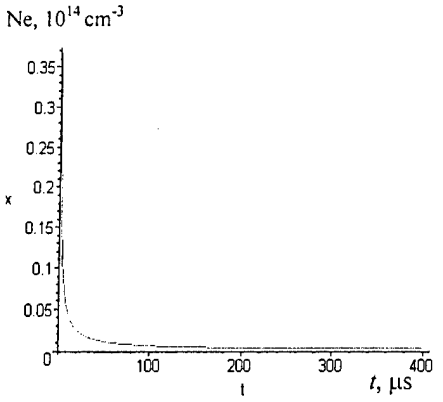

Fig.4. Temporary dependence of electron concentration in a channel in weak electric field stage at initial channel diameter 0.3 mm.

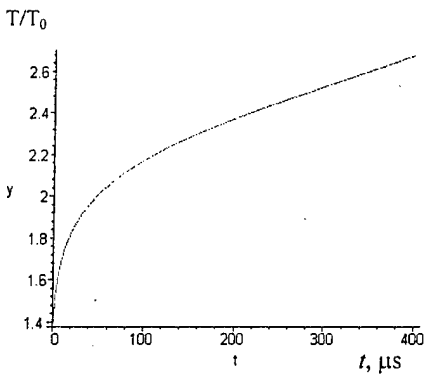

Рис.5. Temporary dependence of tempera-ture in a channel in weak electric field stage at initial channel diameter 0.3 mm.

Strong temperature increase comparable with experimental one takes place only at large channel values.

Calculations of the same characteristics at model initial electron concentration $N_{ein}\approx 1\cdot 10^{18}$ cm^{-3} in a weak E/N=1.5·10^{-16} V·cm^2, at initial channel diameter 1 mm have shown that the channel heating does not take place in this case and electron concentration decreases with time.

Decrease of a channel size does not lead to strong gas heating, it leads only to decrease of electron concentration and discharge decay. Evidently this mode can be realized in [1-4] at increase of flow velocity.

Comparison of results obtained by simplified model with experimental ones on increase of a temperature shows that the volume mode is realized in experiments when neither diffusion no thermal conductivity play significant role in discharge picture. A current in this case is constant for some time then discharge transits into unstable explosive state. Local decrease of discharge diameter due to gasdynamic disturbance leads to discharge decay.

Decrease of weak field below E/N =2.0·10^{-16} V·cm^2 in all calculations lead to weak heating and electron concentration decay as in Fig.4-5.

Detailed model

Starting from simplified model computations of plasma parameters in air at breakdown in electric field E=11.28 kV/cm (E/N≈1.75·10^{-15} V·cm^2) at gas pressure P =100 Torr and temperature K=167 K were made. Following particles were included into the model: fast (background) and plasma electrons $\hat{e}$, e, positive ions O_2^+, N_2^+, O^+, NO^+, N^+, negative ions O_2^-, O^-, O_3^-, neutrals O, N, O_3, NO, vibrationally $N_2(v)$, $O_2(v)$ (v=1), and electronically excited states состояния молекул $O_2(a^1\Delta)$, $N_2(A^3\Sigma_u^+)$, $N_2(B^3\Pi_g)$ of molecules. Diffusion and thermal conductive process were included, basing on results of the simplified model(R=∞). Electron temperature T_e was calculated on basis of rate constants (direct and reverse) of electron-molecule processes obtained by application of package [11]. Gas temperature was calculated with using of energy defects of plasma chemical reactions. Rate

constants of plasma chemical reactions were chosen from [3,6-10,12].

Stable results were obtained at initial electron concentration at E =11.28 kV/cm. A rise of charged particles was not obtained at smaller values of electric field, but already at E =11.3 kV/cm sharp unlimited rise of electron concentration and temperature during microseconds took place.

In Fig.6-7. temporary dependence of charged particles is represented. In Fig. 8-9. electron and gas temperatures are represented. In Fig.10-11. temporary dependencies of vibrationally and electronically excited states of molecules are represented.

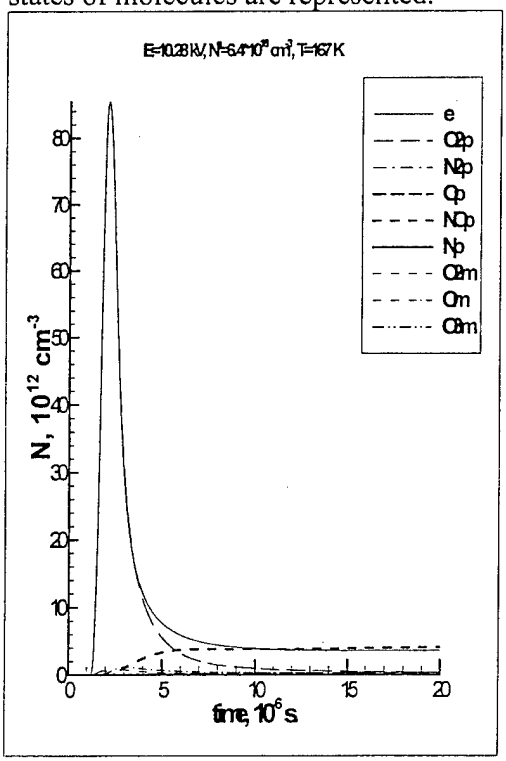

Fig.6.

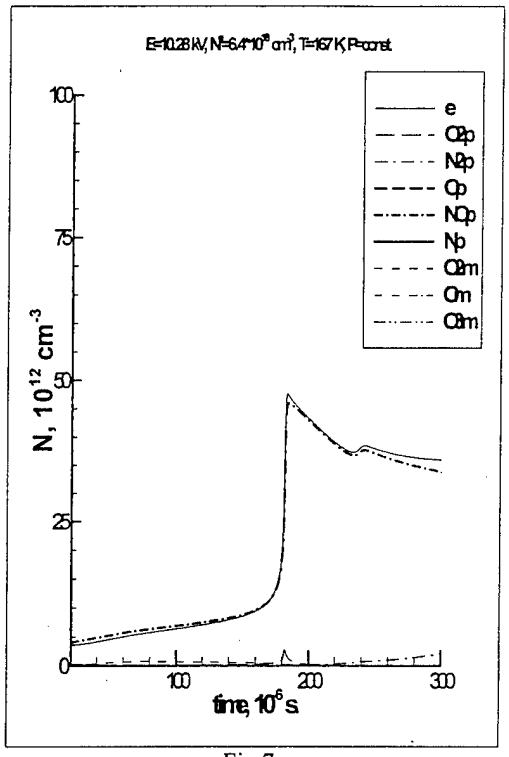

Fig.7.

Calculations have shown that simplified approach adjust results of detailed model at temperatures $T/T_0<10$. In calculations is also necessary to account high temperature kinetics at $T=10^3$- 10^4 K. Complex kinetics of heat exchange with accounting of vibrationally and electronically excited states of molecules decreases period of plasma state before thermal explosion, to which correspond second maximums of electron concentration and gas temperature (t~180 μs).

Then a stable state with characteristics of arc is established.

Mean electron concentration at t<180 μs stable state, $N_e \approx 5 \cdot 10^{12}$ см$^{-3}$, is in reasonable agreement with experiments.

Discussion

Presented results show that in conditions of experiments [1-3] the electron concentration in a channel at

first rises due to ionization of background and plasma electrons, and then it drops in result of dissociation recombination of electrons and molecular ions. In so doing a gas temperature in a channel rises due to a Joule heating in nonselfmaintain stage. This leads to increase of a gas temperature in a channel, increase of E/N and of ionization in a channel. A non selfmaintained quasistationary discharge is realized in a channel.

Electron concentration does not change for a definite time, but simultaneously the gas temperature in a channel increases. This in its turn leads to thermal explosion and possible channel break. It can lead to pulse periodic type of this discharge in a flow. After this stage a discharge transits to an arc.

At strong channel size decrease the sharp drop of electron concentration can occur and the corresponding discharge decay.

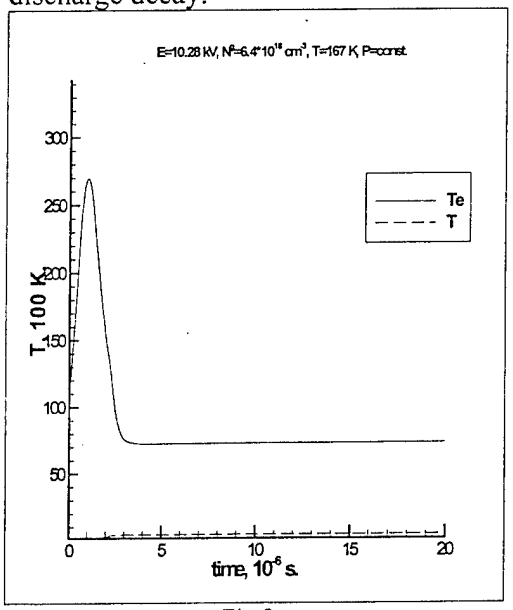

Fig.8.

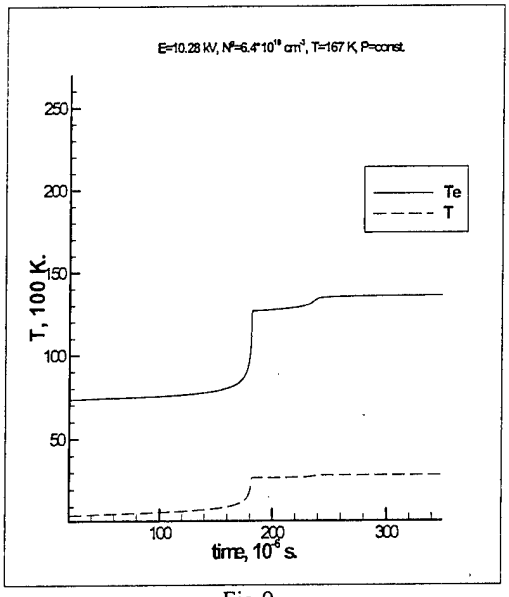

Fig.9.

Development of a discharge in experiments [4] takes place near electrodes but not in plasma gap drifted by a flow, where a state with E/N < $2.0 \cdot 10^{-16}$ V·cm^2 is established. It is possible at $\frac{N_e w_{dr}}{L} > \alpha_{disrec} N_e^2$. Taking L~20 cm we obtain $N_e \leq 10^{12}$ cm^{-3}.

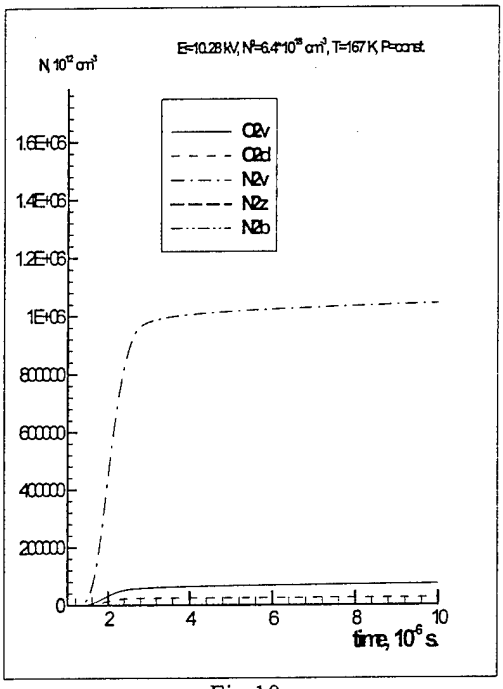

Fig.10.

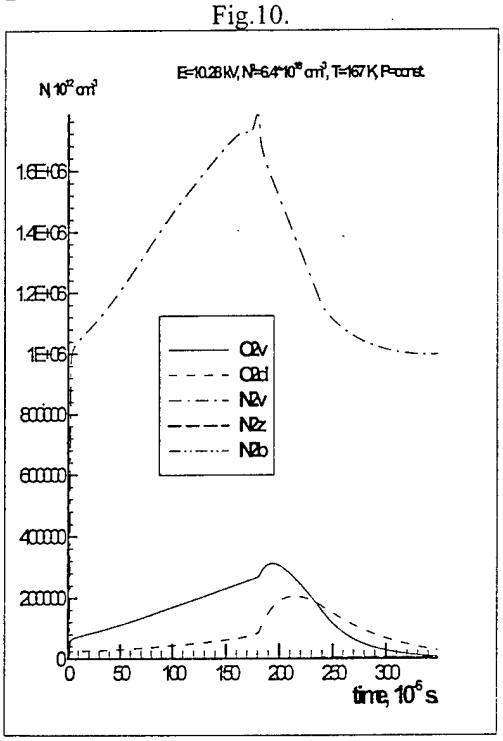

Fig.10.

Electrons drift out of plasma gap without recombination. So at consideration of this discharge is necessary to consider near electrode processes.

Conclusions

A model of pulse-periodic discharges in a flow [1-3] has been developed it allows to explain some of their properties. Non self maintained ionization by background electrons in strong electric field takes place. At decrease of a field to a weak one the maintenance of this discharge at ionization-recombination processes takes place at Joule heating of a channel. Unstable conditions realize in a channel that can lead to discharge decay at its gasdynamic narrowing, thermal explosion or transition to arc.

Investigations of transversal discharges in a flow [4] require analysis of near electrode processes.

Opportunity of quick channel heating makes it attractive for its application in plasma aerodynamics.

References

1. Vitkovskii V.V., Grachev L.P., Gritsov N.N., et. al. Investigations of non-stationary flow around bodies by a supersonic air flow heated by a gas discharge. Teplofiza Vysokikh Temperatur. 1990. V.28. №.6. P.1156-1163.
2. Vitkovskii V.V., Grachev L.P., Gritsov N.N., Egorova Z.M. et.al. Experimental investigations of constant current electric discharges in supersonic and subsonic air flows. Works of TsAGI. №.2505, 1991.
3. Bychkov V.L., Grachev L.P., Esakov I.I., Deriugin A.A. and others. Numerical and experimental investigation of supersonic flow around blunt body at the existence of the longitudinal discharge. Preprint of Keldysh Institute of Applied

Mathematics, RAS, 1997, № 27, Moscow.

4. a) Chernikov V., Dvinin S., Ershov A., Shibkov V., Surkont O., Timofeev I., Van Wie D. Parameters and peculiarities of the transversal gas discharges in supersonic flows. AIAA-2001-3085. 32nd AIAA Plasmadynamics and Lasers Conference and 4th Weakly Ionized Gases Workshop 11-14 June 2001. Anaheim, CA. b) Previous paper of this issue.
5. Ardelyan N., Bychkov V., Chuvashev S., Kosmachevskii K., Malmuth N. Modeling of plasmas in electron beams and plasma jets for aerodynamic applications. AIAA-2001-3101. 32nd AIAA Plasmadynamics and Lasers Conference and 4th Weakly Ionized Gases Workshop 11-14 June 2001. Anaheim, CA.
6. Zarin A.S., Kuzovnikov A.A., Shibkov V.M. Freely localized microwave discharge in air. Moscow. Neft i gas. 1996.
7. Akishev.Yu.S., Deriugin A.A., Karalnik V.B., Kochetov I.V., Napartovich A.P., Trushkin N.I. Experimental Studies and Numerical Simulation of Glow Constant Current Discharge of Atmospheric Pressure. Fizika Plasmy. 1994. V. 20. N. 6. P. 571-584.
8. Eliasson B., Kogelschatz U., J. de Chimie Physique. 1986. V.83. P.279.
9. Maetzing H. Chemical Kinetics of Flue Gas Cleaning by Irradiation with Electrons. Adv. in Chemical Physics. V. LXXX/Ed. by I. Prigogine and S.A. Rice. ISBN 0-471-53281-9 © John Wiley & Sons, Inc. (1991).
10. Kostinsky A.Y., Matveev A.A., Silakov V.P., Plasma Sources. Sci. Tech. 1992. V.1. N.3. P.207.
11. Gordeev O.A., Khmara D.V. Package of programs of kinetic properties of gas discharge plasma. Matematicheskoe modelirovanie. 2001. V.13.N.9. P.3-22.
12. Konovalov V.P., Son Degradation spectra of electrons in gases. In Collection of works Khimia Plazmy. Ed. Prof. B.M.Smirnov, V. 14, Moscow, Energoatomizdat, 1987, C. 194-227.

ESTIMATE OF PLASMA PARAMETERS OF GLOW DISCHARGE BY DATA OF SHOCK WAVE

Kuchinsky V.V., Golyatin V.Yu,

"HSRI", HC "Leninetz", Saint-Petersburg, Russia

The articles [1,2] devoted to diagnostic of plasma using the shock or acoustic waves are among the first ones in this sphere. The research was made using probes (of Lengmur probe) in the argon plasma at the pressure from 2 to 30 Torr. Sharp change of potential registered by means of oscillator (fig.1) allowed one to evaluate a summary speed:

$$c_s = a_0\sqrt{\frac{T}{T_0}} + u = a_0\sqrt{\frac{T}{T_0}} + u_0\frac{T}{T_0}, \qquad (1)$$

where a_0 - sound velocity without plasma, T - temperature of plasma, T_0 - temperature of the gas out of plasma volume (i.e. $a_0\sqrt{\frac{T}{T_0}}$ – local sound velocity in plasma), $u_0 = \frac{Qp_0}{\sigma p}$, - gas consumption, p – pressure in the camber, p_0 - external pressure, σ - section. Solving the equation relatively $\sqrt{T/T_0}$, we shall have [1]:

$$\sqrt{\frac{T}{T_0}} = \frac{a_0}{2u_0}\left[\sqrt{\left(1+2\frac{u_0}{a_0}\right)^2 + \frac{4u_0(c_s - a_0 - u_0)}{a_0^2}} - 1\right]. \qquad (2)$$

This equation has allowed to calculate dependence of the discharge temperature from gas consumption Q (fig.2).

The following development of experimental engineering has allowed to diversify the methods of shock and acoustic waves velocity registration. The present report is based on the experimental results published by Dr. D.Van Wie with colleagues in works [3,4]. In these works the time of a shock wave passing between two registration points has been registered by means of two lasers. The measurements have been done in air under the pressure values of 1.6 and 10 Torr. The shock wave passed through the plasma of a gas discharge while the direction of an electrical field has been applied was perpendicularly to a shock wave propagation. The discharge could be located in various parts of operating chamber (fig.3). Specification of parameters accepted to describe a space discharge is presented in fig.4.

Generally the time of a shock wave passing between two registration points is calculated as following:

$$t_p(j) = \int_{x_0}^{x_e} \frac{dx}{V(j,x)}, \qquad (3)$$

where time t_p may depends on many parameters, for example, on the current density j, which determines a temperature of the areas occupied by plasma, $V(x)$ - velocity of a shock wave in the point x. Example of results obtained in works [3,4] is given in fig.5.

The detailed study of change of a shock wave structure during passing through the space thermal heterogeneity is performed in the works [5,6]. The procedure presented in this work allows one to derive a simple approximate formula to calculate a shock wave velocity:

$$V(x) \approx \begin{cases} u(x, M_0, a_0, x_d) & \text{if} \quad x \le x_p, x \ge x_f \\ a(x) + \dfrac{M_x - 1}{\dfrac{1}{a_0} + \dfrac{x/x_p - 1}{a\left(\dfrac{x_p + x_f}{2}\right)}} & \text{if } x_p < x < x_f,, \end{cases} \qquad (4)$$

where $a(x) = \sqrt{\gamma R T(x)}$ - sound velocity in the point x, R - gas constant, $a_0 = a(T_0)$, T_0 - constant temperature out of area of a space heterogeneity, $T(x)$ - temperature distribution, x_p, x_f - coordinates of the beginning and the end of the space heterogeneity area temperature (fig. 6), M_0 - Mach number of an undisturbed shock wave, $M(x) = V(x)/a(x)$ - local Mach number, x_d - coordinate started movements of a shock wave (diaphragm coordinate)

$$u(x, M, a, x_d) = a \cdot \left[1 - \frac{1}{\sqrt{1 + \dfrac{x}{x_d} \dfrac{2M-1}{(M-1)^2}}} \right]^{-1}, \quad M_x = u(x_p, M, a_0, x_d)/a_0 \qquad (5)$$

Comparison with numerical solving of accurate one-dimensional equations presented in work [5], allows one to evaluate correctness of this formula at various configuration of a temperature distribution and Mach number (рис.7,8). For the case of quadrate distribution $T(x)$ (fig.6a) more exact formula may be used

$$V_s(x) \approx \begin{cases} u(x, M_0, a_0, x_d) & npu \quad x \le x_p, x \ge x_f, \\ u\left(x, \dfrac{M_x + \omega}{\omega + 1}, (\omega + 1)a_0, x_p\right) & npu\ x_p < x < x_f, \end{cases}$$

$$\omega = \frac{\sqrt{\gamma R T_p}}{a_0} - 1 = \sqrt{\frac{T_p}{T_0}} - 1 \,. \qquad (6)$$

The time of a shock wave passing between two registration points for a case of quadrate distribution $T(x)$ will be (as per formulas (3),(6)):

$$t_s = \begin{cases} t_0\left(\dfrac{M_x + \omega}{\omega + 1}, (\omega + 1)a_0, x_0, x_f, x_p\right) + t_0(M_0, a_0, x_f, x_e, x_d), & npu\ x_0 > x_p \wedge x_f < x_e \\ t_0\left(\dfrac{M_x + \omega}{\omega + 1}, (\omega + 1)a_0, x_p, x_e, x_p\right) + t_0(M_0, a_0, x_0, x_p, x_d), & npu\ x_0 < x_p \wedge x_f > x_e \\ t_0\left(\dfrac{M_x + \omega}{\omega + 1}, (\omega + 1)a_0, x_0, x_e, x_p\right), & npu\ x_0 > x_p \wedge x_f > x_e \\ t_0\left(\dfrac{M_x + \omega}{\omega + 1}, (\omega + 1)a_0, x_p, x_f, x_p\right) + t_0(M_0, a_0, x_0, x_p, x_d) + & \\ \quad + t_0(M_0, a_0, x_f, x_e, x_d), & npu\ x_0 < x_p \wedge x_f < x_e \\ t_0(M_0, a_0, x_0, x_e, x_d), & npu\ x_0 > x_p \wedge x_f < x_0 \end{cases}, \qquad (7)$$

where

$$t_0(M, a, x_0, x_e, x_d) = \frac{1}{a_0}\left[x_e - x_0 - 2\frac{x_d}{c}\left(\sqrt{1 + c\frac{x_e}{x_d}} - \sqrt{1 + c\frac{x_0}{x_d}} \right) \right], \quad c = \frac{2M-1}{(M-1)^2}.. \qquad (8)$$

So, if solve a transcendental equation (8) relatively value ω, it is possible to determine T_p (fig.9).

$$T_p = \frac{a_0^2(\omega+1)^2}{\gamma R} = T_0(\omega+1)^2. \qquad (9)$$

Thus the temperature (or density) in the field of spatial heterogeneity is defined at the moment of passage through it of a shock wave,

To show how to use the obtained formulas we shall calculate the time of a shock wave passing between two registration points which has been measured in works [3,4]. To evaluate the temperature of a gas discharge it is possible to use a semiempirical formula proposed by V.S. Sukhomlinov [7]:

$$T_p(j,p) = \frac{T_w}{\sqrt{3}}\left[1+\left(\frac{1-q}{1+q}\right)^{0.4}\right]\left(\frac{1+q}{1-q}\right)^{0.2}, \quad q = q(j,p) = \sqrt{1-\left(\frac{2}{3\sqrt{3}A_0\left(\frac{E}{p}\right)pj}\right)^2} \qquad (10)$$

where T_w - temperature of the wall surrounding discharge, field intensity E has a dimension V/sm, constant $A_0 = 0{,}018$, current density – in mA/sm^2, pressure in Torrs. In our case a discharge has not wall, so the value T_w should be derived approximately to half of sum of plasma temperatures and outside of it (is more exact $T_w \approx 0.475 \cdot (T_p + T_0)$).

The results of preliminary calculation are presented in fig.10. Unfortunately, in order to check out and base the method a lot of data is required. Having sufficient amount of experimental material it is possible to obtain information on the gas and plasma pressure.

Thus, the simple approximate formulas to determine of a space heterogeneity parameters (temperature or density) based on the data of a passing shock wave are given in the present work.

References

1. Gentle K.W., Ingard U. Determination of Neutral Gas Temperature in a Plasma Column from Soun Velocity/ Appl.Phys.Lett. v.5, №5, 1964, p.105-106
2. Gentle K.W., Ingard U., Bekefi G. Effect of Gas Flow on the Properties of Plasma Column. Nature, v.23, № 4952, 1964, p. 1369-1370
3. Van Wie D.M., Wesner A.L., Gauthier L.R. Shock Wave Characteristics Measured in Gas Discharges. Proceedings of the 3 Workshop on Weakly Ionized gases, AIAA-99-4824, Norfolk 1999
4. Van Wie D.M., Gauthier L.R. Shock Propagation in a Weakly Ionized Gas With Transverse Electric Field. Works of II symposium 'Thermochemical processes in plasma aerodynamics; SPB 2001
5. Sukhomlinov V.S., Kolosov V.Y., Sheverev V.A., Otugen M.V. Formation and Propagation of a Weak Shock Wave in a Gas Temperature Gradient. AIAA 99-4943, 9th International Space Plane and Hypersonic Systems and Technologies Con. Norfolk 1999
6. A. Kuranov, V. Kuchinskiy, and V. Sukhomlinov. The Main Features of Distribution of Shock Waves in Nonuniform Mediums Created with the Help of Discharge Plasma. In V. Bityurin, editor, The Second Workshop on Magneto-Plasma-Aerodynamics in Aerospace Applications, pages 25-28, Moscow, April 2000. Institute for High Temperatures, Russian Academy of Sciences
7. Sukhomlinov V.S. The private message

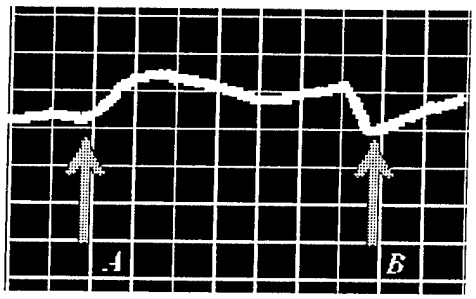

Fig.1. Oscilloscope data which registers passing of density sudden change bypass the probes (points *A* and *B*) [1].

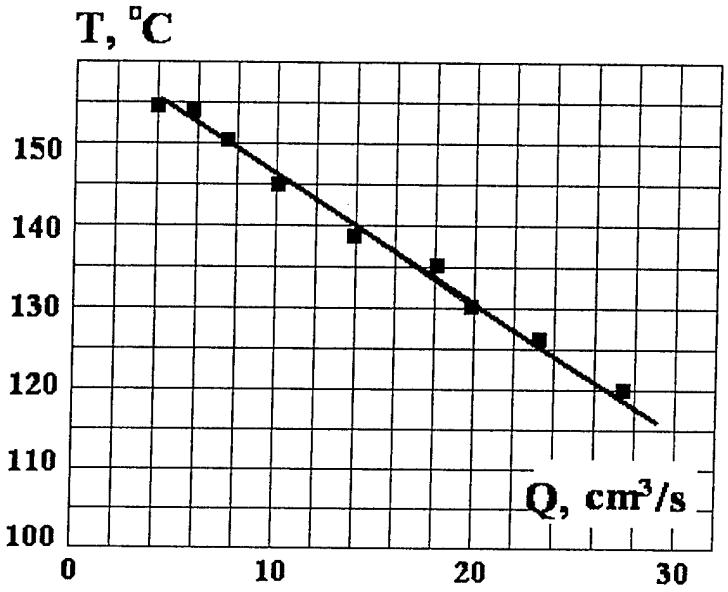

Fig.2. Dependence of a discharge temperature T from gas expense Q at pressure of 5 Torr and current of 100 mA, obtained in work [1].

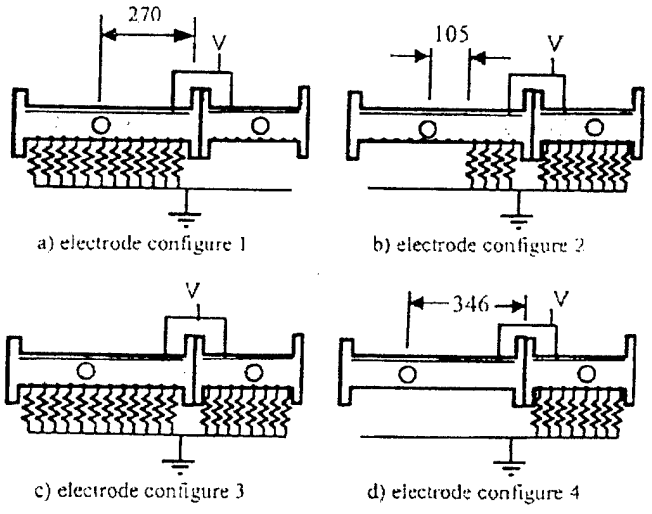

Fig.3. Distribution of heating areas (by means of various electrodes combinations) in work [4]. *A* – window to fix beginning of a shock wave passing, *B* – window for registration of passing time.

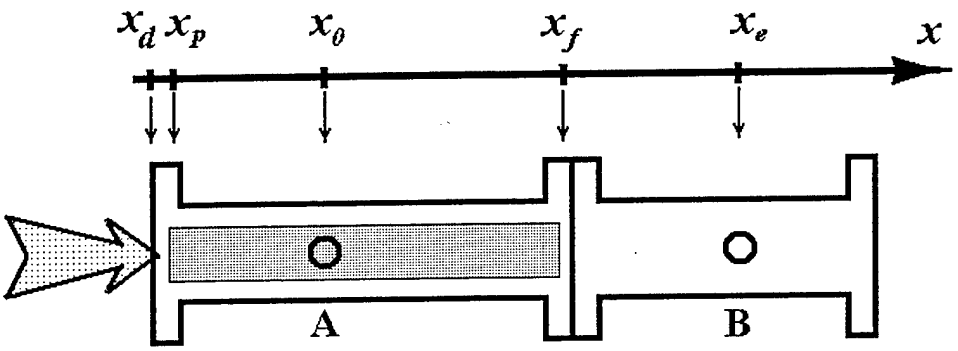

Fig. 4. Definition of reference system and indication.
x_p - beginning of the area of a temperature space heterogeneity (beginning of a gas discharge),
x_0 - location of a little window fixing the time initial reading,
x_f - termination of the area of a temperature space heterogeneity ,
x_e - location of a window registering the time of passing (example of information coming on the oscilloscope display is presented in fig.5),
x_d - diaphragm coordinate.

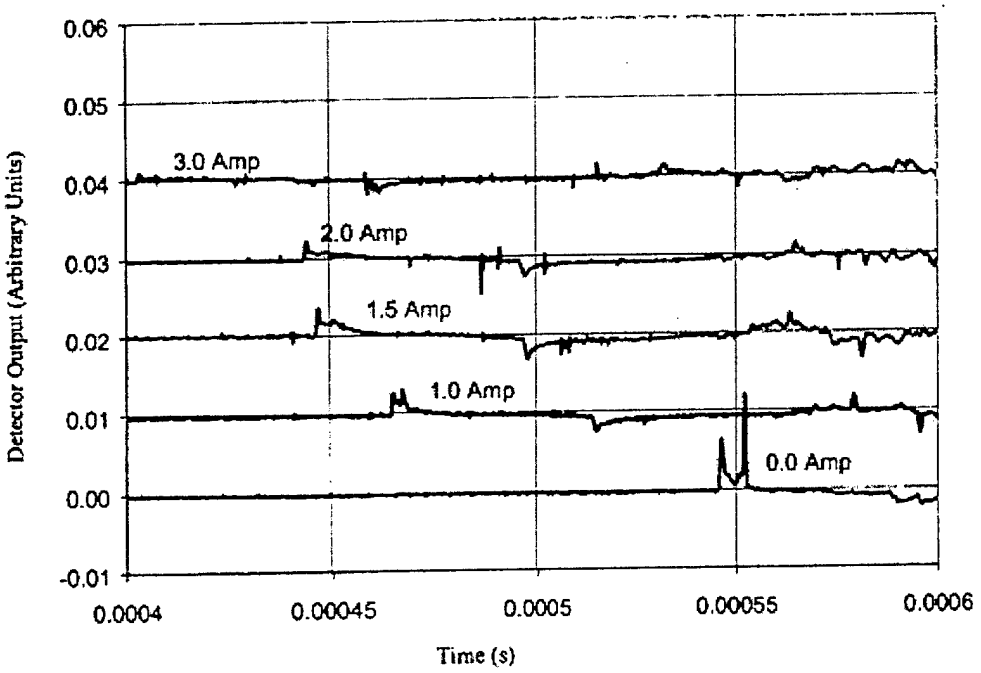

Fig. 5. Effect of discharge on shock propagation for electrode configuration 3 with initial pressure of 1.6 Torr [4].

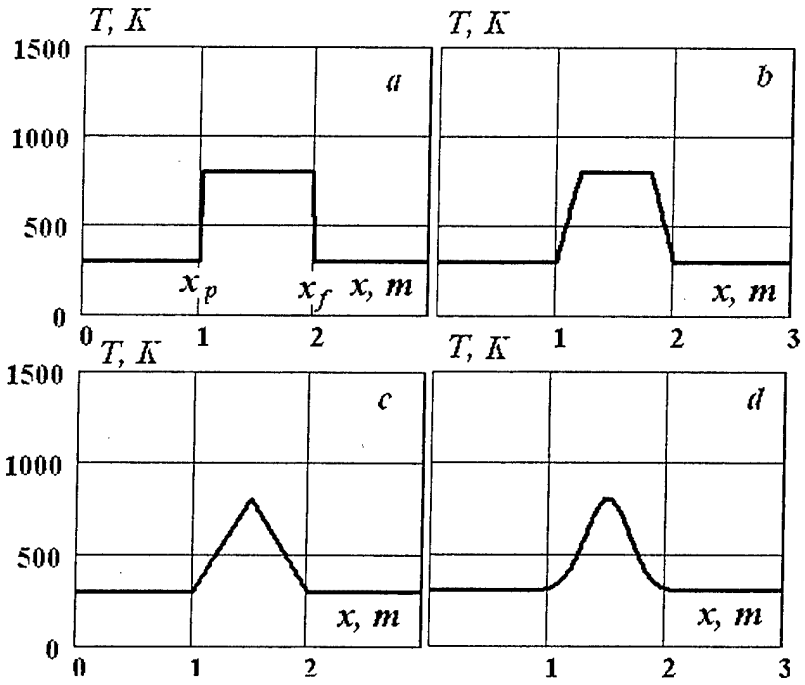

Fig.6. Temperature distribution for which the fig.8 is calculated.

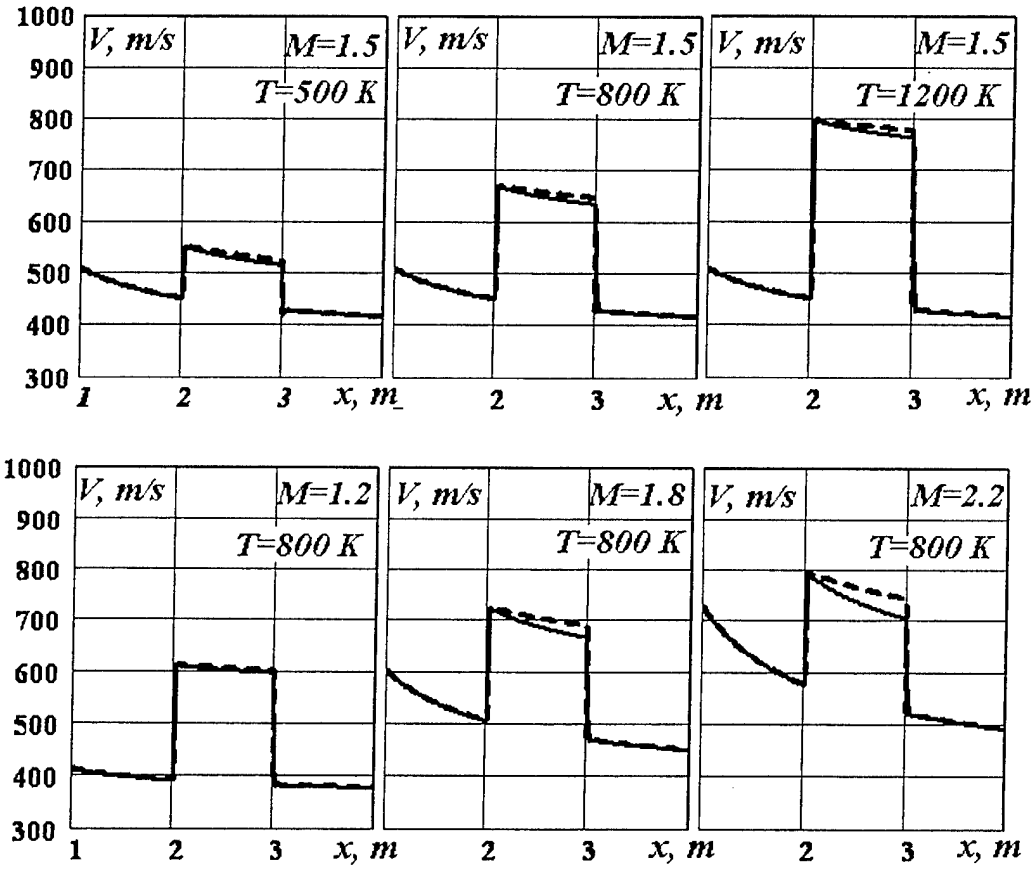

Fig.7. Comparison of numerical solving of accurate one-dimensional equations (continuous curve) with calculation using an approximate formula (4) (broken line) ($T_0 = 300$ K, quadrate temperature distribution, fig. 6a)

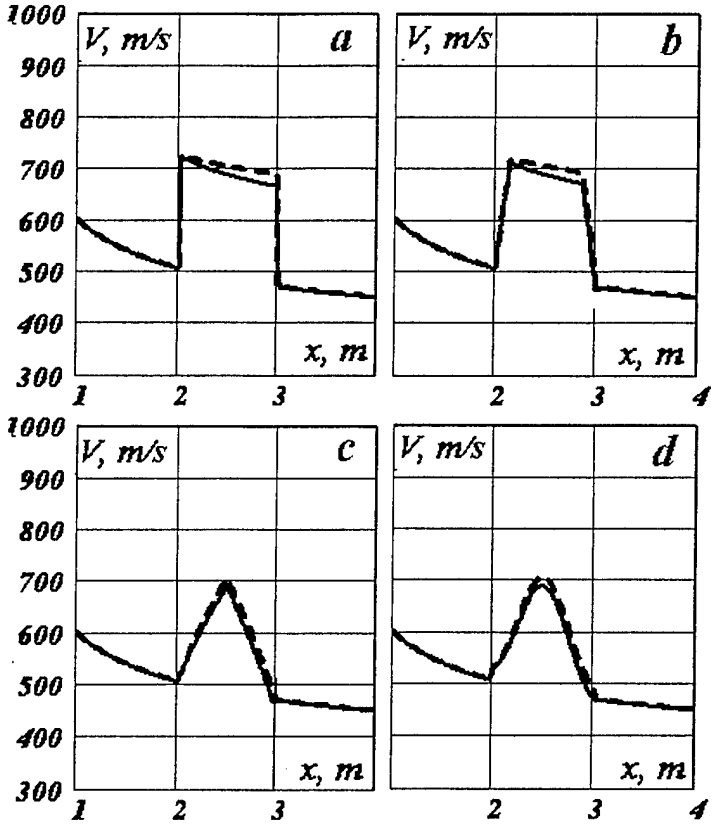

Fig.8. Comparison of numerical solving of accurate one-dimensional equations (continuous curve) with calculations using an approximate formula (4) (broken line) ($T_0 = 300$ K, $M_0 = 1.8$, $T = 800$ K) for temperature distribution indicated with corresponding letters (a – quadrate distribution, b- trapezoidal, c- triangular, d- Gaussian).

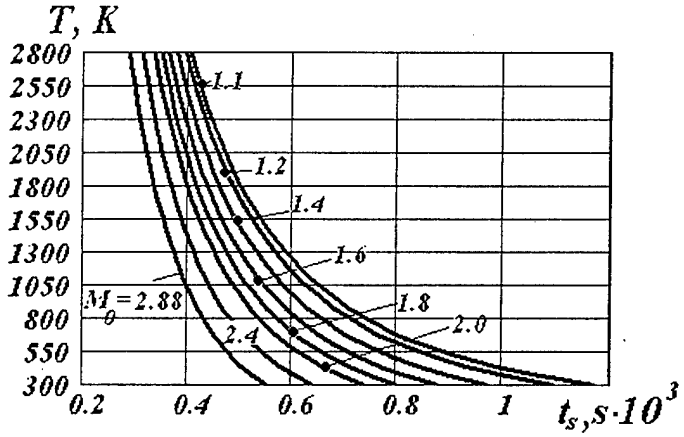

Рис. 9. Example of calculation of temperature dependence from time of passage between registration points t_s (for the conditions appropriate to a configuration 3 in work [4], (see fig. 3c), at different Mach number (figure about curves)

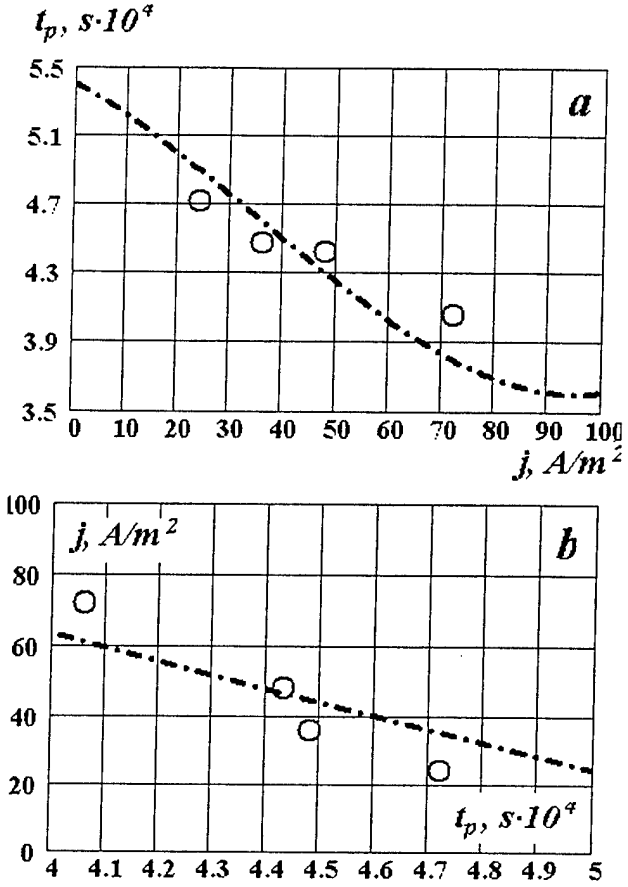

Fig.10. Time of a shock wave passing between two registration points (a) and inverse relationship of current density j from time t_p (b). Curve – calculation by formulas (7-10), points – data obtained from the work [4]. (The electrode configuration is considered 3, fig.3c and fig.5)

A NUMERICAL METHOD TO INVESTIGATE 3-D NON-IDEAL MAGNETOGASDYNAICS

Datta V. Gaitonde

Air Force Research Laboratory, Wright-Peterson AFB, Ohio

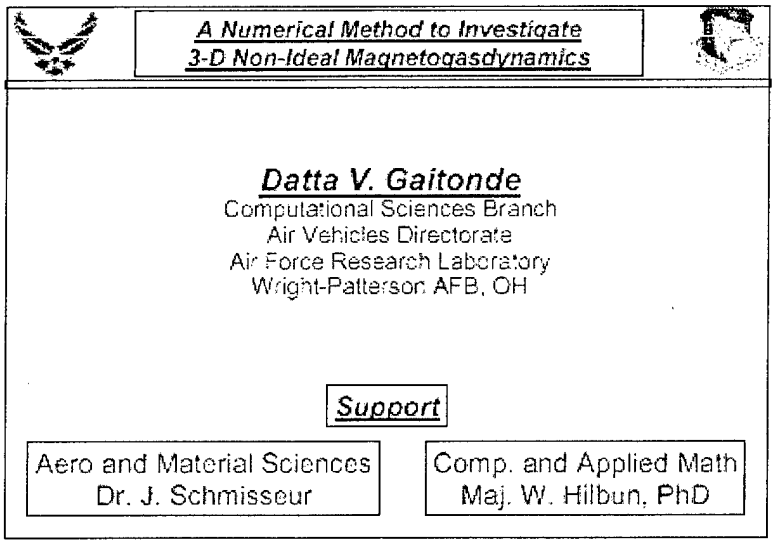

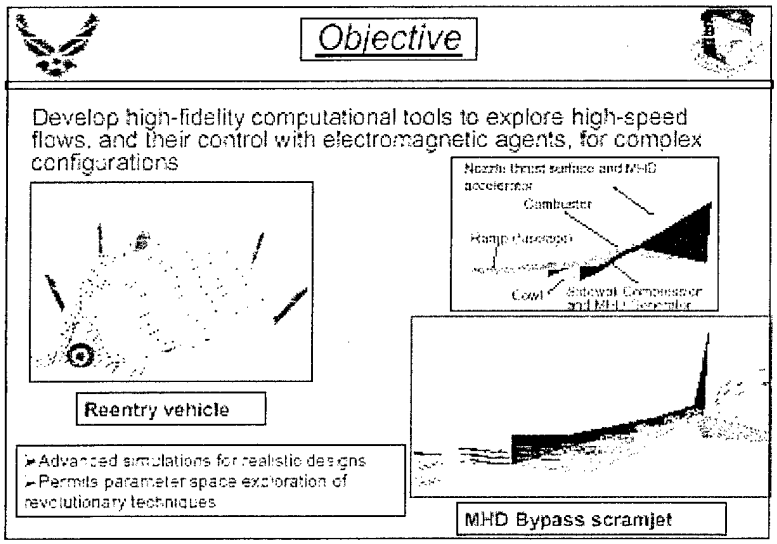

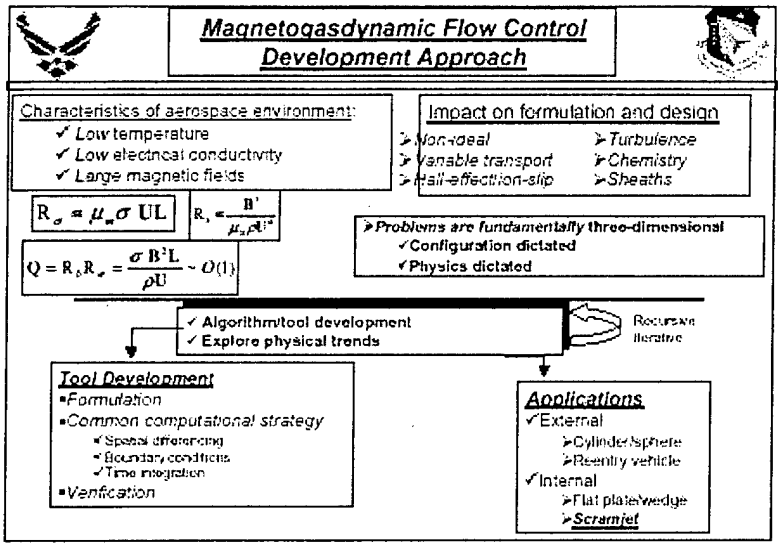
Magnetogasdynamic Flow Control Development Approach
Characteristics of aerospace environment:
✓ Low temperature
✓ Low electrical conductivity
✓ Large magnetic fields
Impact on formulation and design
➢ Non-ideal
➢ Variable transport
➢ Hall-effection-slip
➢ Turbulence
➢ Chemistry
➢ Sheaths
$R_\sigma \approx \mu_m \sigma UL$
$R_h \approx \frac{B^2}{\mu_m \rho U^2}$
$Q = R_h R_\sigma = \frac{\sigma B^2 L}{\rho U} \sim O(1)$
➢ Problems are fundamentally three-dimensional
✓ Configuration dictated
✓ Physics dictated
✓ Algorithm/tool development
✓ Explore physical trends
Recursive/iterative
Tool Development
▪ Formulation
▪ Common computational strategy
✓ Spatial differencing
✓ Boundary conditions
✓ Time integration
▪ Verification
Applications
✓ External
➢ Cylinder/sphere
➢ Reentry vehicle
✓ Internal
➢ Flat plate/wedge
➢ Scramjet

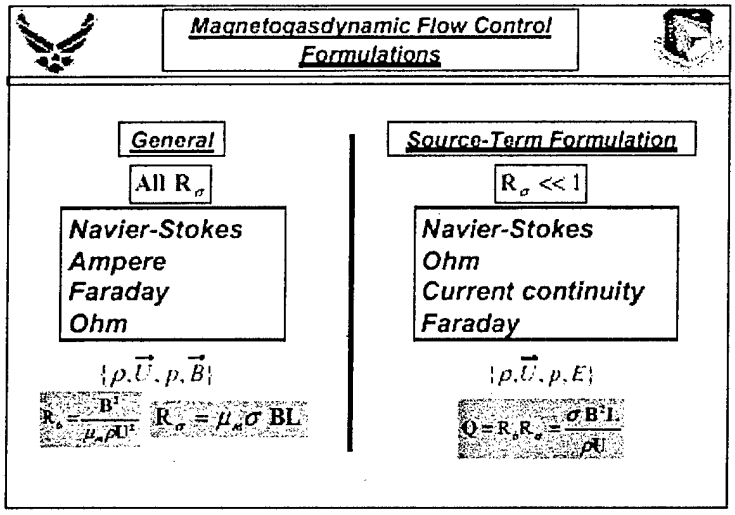
Magnetogasdynamic Flow Control Formulations
General
All R_σ
Navier-Stokes
Ampere
Faraday
Ohm
$\{\rho, \vec{U}, p, \vec{B}\}$
$R_h = \frac{B^2}{\mu_m \rho U^2}$
$R_\sigma = \mu_m \sigma BL$
Source-Term Formulation
$R_\sigma << 1$
Navier-Stokes
Ohm
Current continuity
Faraday
$\{\rho, \vec{U}, p, E\}$
$Q = R_h R_\sigma = \frac{\sigma B^2 L}{\rho U}$

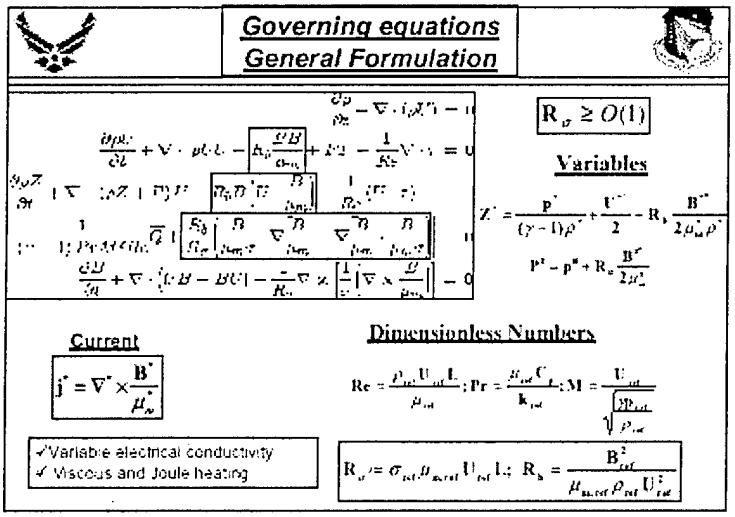
Governing equations
General Formulation
$R_\sigma \geq O(1)$
Variables
Current
$\vec{j}^* = \nabla^* \times \frac{\vec{B}^*}{\mu_m^*}$
Dimensionless Numbers
$Re = \frac{\rho_{ref} U_{ref} L}{\mu_{ref}}$; $Pr = \frac{\mu_{ref} C_p}{k_{ref}}$; $M = \frac{U_{ref}}{\sqrt{\frac{\gamma p_{ref}}{\rho_{ref}}}}$
✓ Variable electrical conductivity
✓ Viscous and Joule heating
$R_\sigma = \sigma_{ref} \mu_{m,ref} U_{ref} L$; $R_h = \frac{B_{ref}^2}{\mu_{m,ref} \rho_{ref} U_{ref}^2}$

Governing Equations
Source Term Formulation

Continuity

$$\frac{\partial \rho}{\partial t} + \nabla \cdot [\rho \mathbf{U}] = 0$$

Momentum

$$\frac{\partial \rho \mathbf{U}}{\partial t} + \nabla \cdot \left[\rho \mathbf{U} \otimes \mathbf{U} + p\bar{\bar{\mathbf{I}}}\right] - \frac{1}{Re} \nabla \cdot \bar{\bar{\tau}} = Q(\mathbf{j} \times \mathbf{B})$$

Energy

$$\frac{\partial \rho e}{\partial t} + \nabla \cdot \left[(\rho e + p)\mathbf{U} - \frac{1}{Re}(\mathbf{U} \cdot \bar{\bar{\tau}}) - \frac{1}{(\gamma-1)PrM^2Re} \bar{q}\right] = Q\,\mathbf{E} \bullet \mathbf{j}$$

$R_\sigma << 1$

Navier-Stokes
Ohm
Current continuity
Faraday
~~*Ampere*~~

$\{\rho, U, p, E, j\}$

$Q = R_e R_\sigma \frac{\sigma B^2 L}{\rho U}$

✓Variable electrical conductivity
✓ Viscous and Joule heating

Magnetogasdynamic Flow Control
3-D Curvilinear Equations

Strong Conservation Form

$$x = x(\xi, \eta, \zeta) \quad y = y(\xi, \eta, \zeta); \quad z = z(\xi, \eta, \zeta)$$

$$\frac{\partial}{\partial t}\left(\frac{X}{J}\right) + \frac{\partial F'}{\partial \xi} + \frac{\partial G'}{\partial \eta} + \frac{\partial H'}{\partial \zeta} - \frac{\partial F'_v}{\partial \xi} + \frac{\partial G'_v}{\partial \eta} + \frac{\partial H'_v}{\partial \zeta} + \frac{S}{J}$$

Spatial scheme

- Standard upwind methods
- Reconstruction (MUSCL)
- Limiting options
- Compact Differencing
- Filtering

Time integration

- Approximately Factored Implicit
- Sub-iteration strategy
- Runge-Kutta

Numerical Solution Procedure
High-order options

Compact differences

$$\Gamma\phi'_{i-2} + \alpha\phi'_{i-1} + \Gamma\phi'_{i+1} + \alpha\phi'_{i+2} =$$

$$\frac{a_1\Delta x_{i+1/2} + a_2\Delta x_{i+3/2}}{1} + \frac{a_1\Delta x_{i-1/2} + a_2\Delta x_{i-3/2}}{2}$$

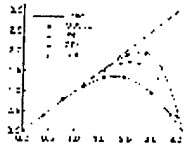

	OA	Stencil	Description
0.00	4	5	Explicit (E4)
0.25	4	3	Compact (C4)
0.33	6	5	Compact (C6)
0.0	2	3	Explicit (E2)

Low-pass Filtering

$$\alpha_0\bar{\phi}_{i-1} + \bar{\phi}_i + \alpha_0\bar{\phi}_{i+1} = \sum_{n=0}^{N} \frac{a_n}{2}(\phi_{i-n} + \phi_{i+n})$$

a_n = coefficient obtained with Fourier Transform analysis

Properties
- Non-dispersive
- Odd-even mode annihilated

Magnetogasdynamic Flow Control
Computational Efficiency: Time integration

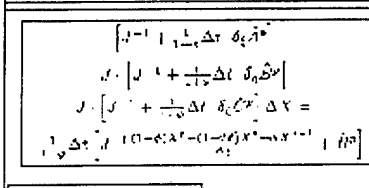

Features
- Loosely coupled
- Sub-iterations
- 2nd-order accurate

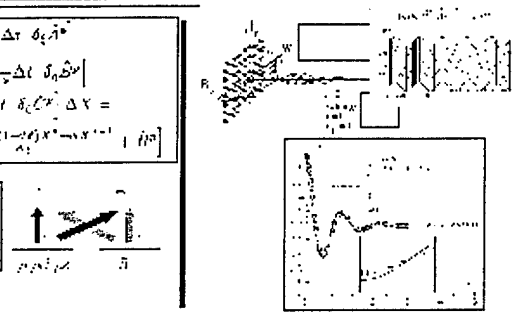

- Method is
  - ✓highly stable (~10^5 increase in Δt)
  - ✓highly efficient (~10^4 reduction in CPU)
- Subiterations recover accuracy at high step-sizes

MGD Control
Verification and Exploration

- Self-similar solution of Bush
- Problem setup issues

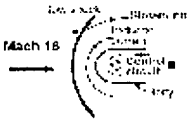

- M=16.34, Re=295,176, T_∞=530R
- R_g ~ 12.5 (nominal)

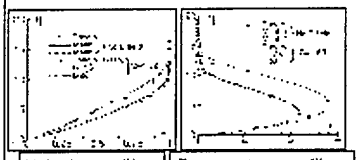

Velocity profile | Temperature profile

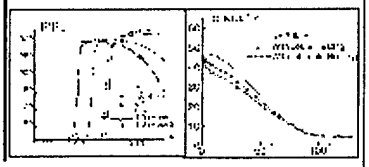

Generalized Ohm's Law
Phenomenological Implementation

$$\vec{j} = \hat{\vec{\sigma}} \cdot \left[\vec{E} + \vec{U} \times \vec{B} \right]$$

$$\hat{\vec{\sigma}} = \frac{\sigma}{D} \begin{bmatrix} \sigma_{11} & \sigma_{12} & \sigma_{13} \\ \sigma_{21} & \sigma_{22} & \sigma_{23} \\ \sigma_{31} & \sigma_{32} & \sigma_{33} \end{bmatrix}$$

$$D = \left(1 + I_x \omega \vec{B}^2\right)^2 + \left(R_H \vec{B} \sigma \vec{B}\right)^2$$

$$\sigma_{12} = \sigma \left[I_x \alpha B_z B_y \left(+ I_x \omega \vec{B}^2 \right) - R_H \omega (B_z - R_H \sigma B_x B_y) \right]$$

$$j = \sigma_{eff} U_{eff} B_{eff}$$

$$E_y = U_{eff} B_{eff}$$

$$R_H = \sigma_{eff} \beta_{eff} B_{eff}$$

$$I_x = \sigma_{eff} \alpha_{eff} B_{eff}^2$$

Hartmann Flow

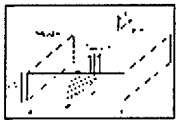

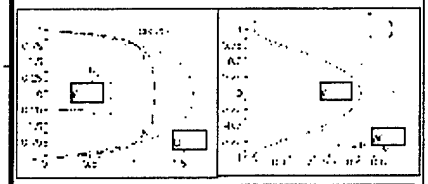

- Velocity profile develops inflection points
- Significant spanwise velocity

Electric Field Computation
Low R_m formulation

$$\nabla \cdot \vec{j} = 0$$

$$\vec{E} = -\nabla \phi$$

$$\nabla \cdot \left[\bar{\bar{\sigma}} \cdot \left[-\nabla \phi + \vec{U} \times \vec{B} \right] \right] = 0$$

$$\frac{\partial \hat{F}}{\partial \xi} - \frac{\partial \hat{G}}{\partial \eta} + \frac{\partial \hat{H}}{\partial \zeta} = 0$$

- ✓Scalar equation
- ✓Fully three-dimensional
- ✓Filtering
  - ✓Interior (shocks)
  - ✓Boundary
- ✓Implicit "time" integration

Boundary Conditions

Electrode

Potential specified

Insulator

$$\hat{n} \cdot \vec{j} = 0$$

$$\hat{n} \cdot \left[\bar{\bar{\sigma}} \cdot \nabla \phi \right] = \hat{n} \cdot \left[\bar{\bar{\sigma}} \cdot \left(\vec{U} \times \vec{B} \right) \right]$$

Electric Field Computation
Verification and Exploration

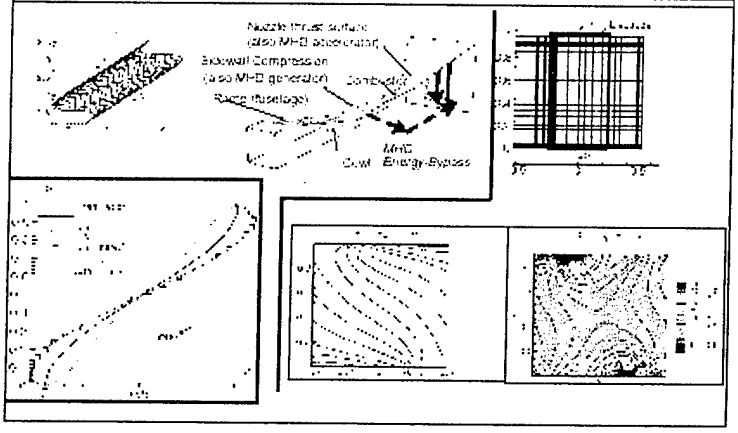

MHD Turbulence
3-D Implementation of k-ε model

Magnetic fields
- lead to enhanced anisotropy
- impact transition and turbulence

2-equation k-ε model
- Mean flow
- Fine-scale effects

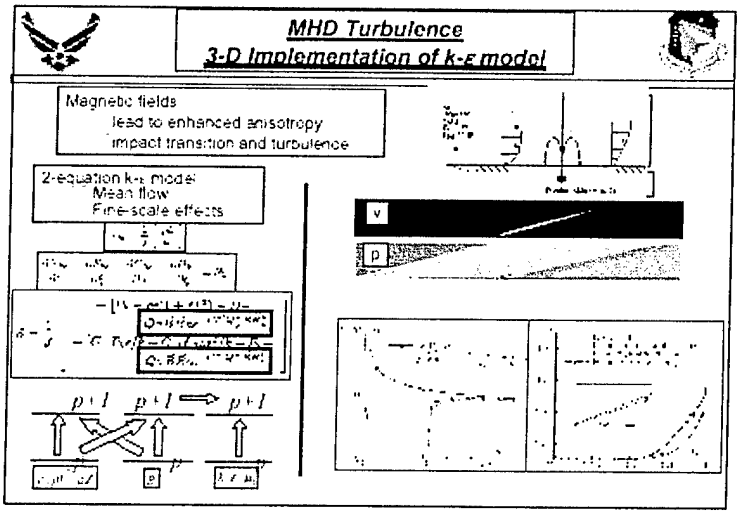

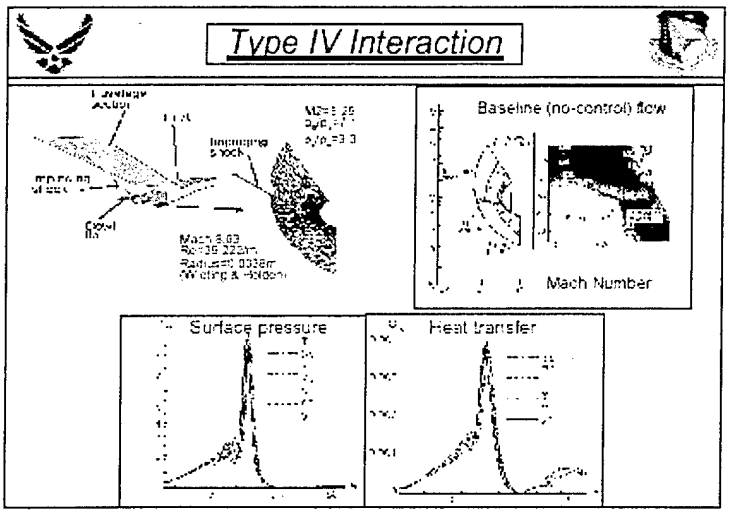
Type IV Interaction
Baseline (no-control) flow
Mach Number
Surface pressure
Heat transfer

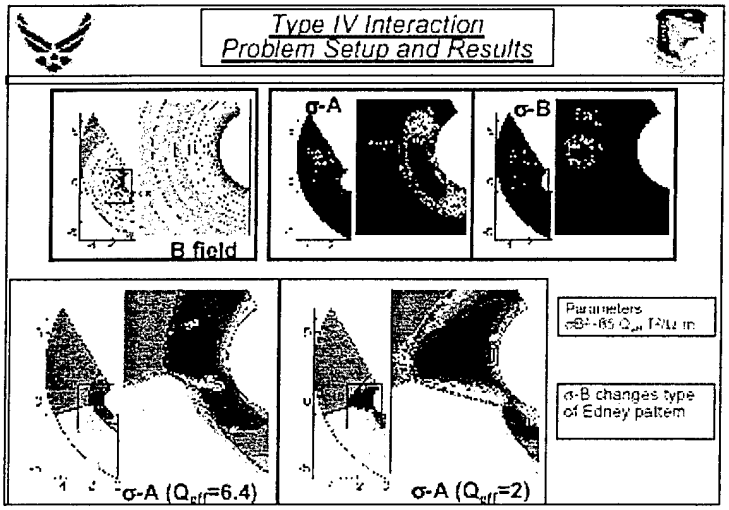
Type IV Interaction
Problem Setup and Results
B field
σ-A
σ-B
σ-A (Qeff=6.4)
σ-A (Qeff=2)
σ-B changes type of Edney pattern

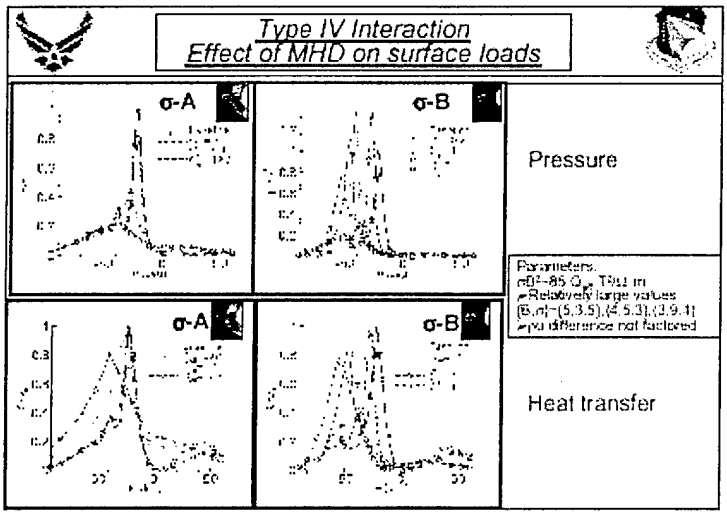
Type IV Interaction
Effect of MHD on surface loads
σ-A
σ-B
Pressure
Heat transfer

MGD Flow Control Application
Exploratory simulation: X24C

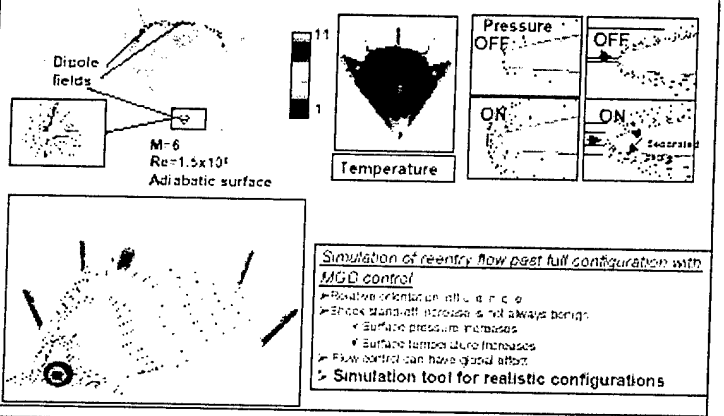

Simulation of reentry flow past full configuration with MGD control

- Shock stand-off increases & not always benign
  - Surface pressure increases
  - Surface temperature increases
- Flow control can have global affect

➢ Simulation tool for realistic configurations

Scramjet Flowpath
Configuration Details

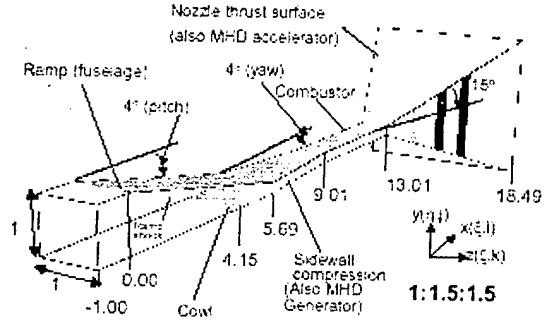

- ✓Dual-plane compression
- ✓Artificial aspect ratio

- ✓No combustor heat
- ✓Overexpanded nozzle
- ✓***Will evolve***

Scramjet Flowpath
Flow structure without MGD

- ✓ 3-D separation in diffuser
- ✓ Separated region grows
- ✓ No significant reversed flow
- ✓ Mesh resolution

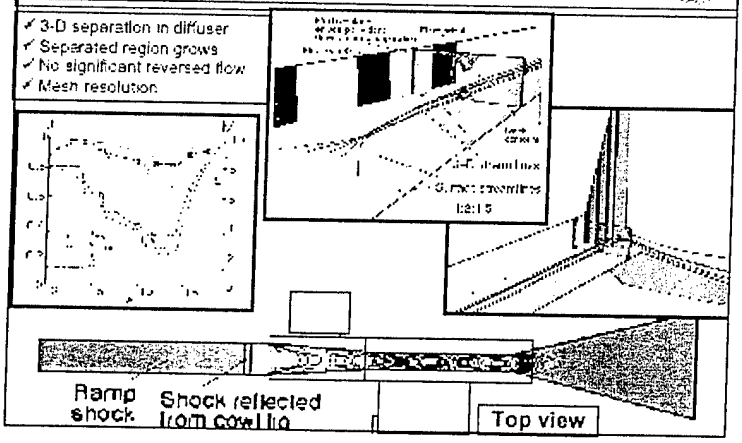

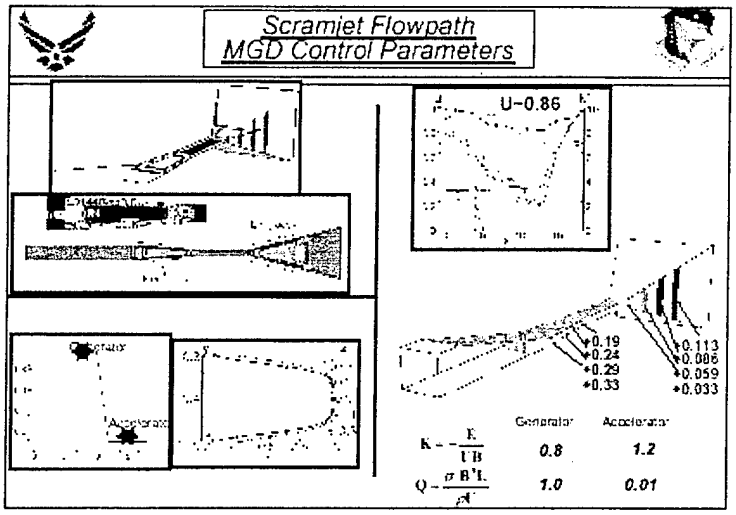
Scramjet Flowpath
MGD Control Parameters
U=0.86
0.19
0.24
0.29
0.33
0.113
0.086
0.059
0.033
Generator
Accelerator
$K = \frac{E}{UB}$
0.8
1.2
$Q = \frac{\sigma B^2 L}{\rho U}$
1.0
0.01

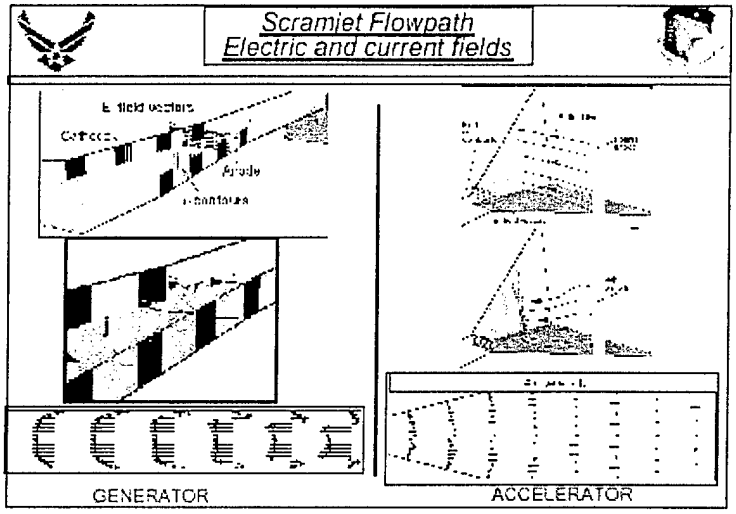
Scramjet Flowpath
Electric and current fields
GENERATOR
ACCELERATOR

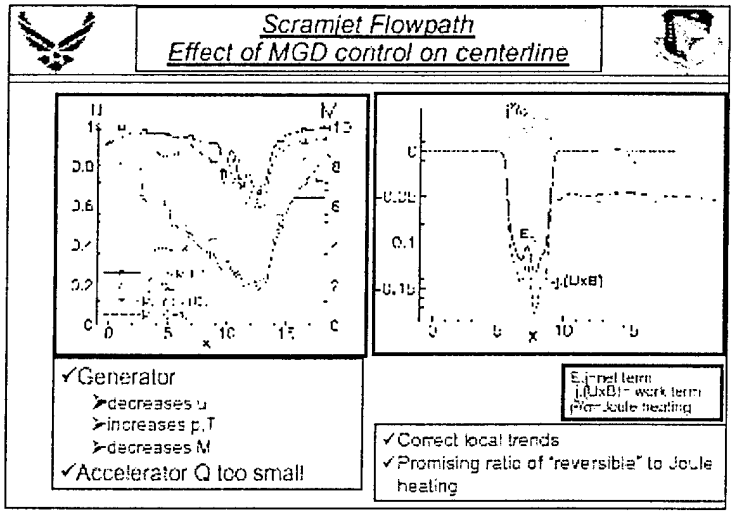
Scramjet Flowpath
Effect of MGD control on centerline
✓Generator
➢decreases u
➢increases p,T
➢decreases M
✓Accelerator Q too small
✓Correct local trends
✓Promising ratio of "reversible" to Joule heating

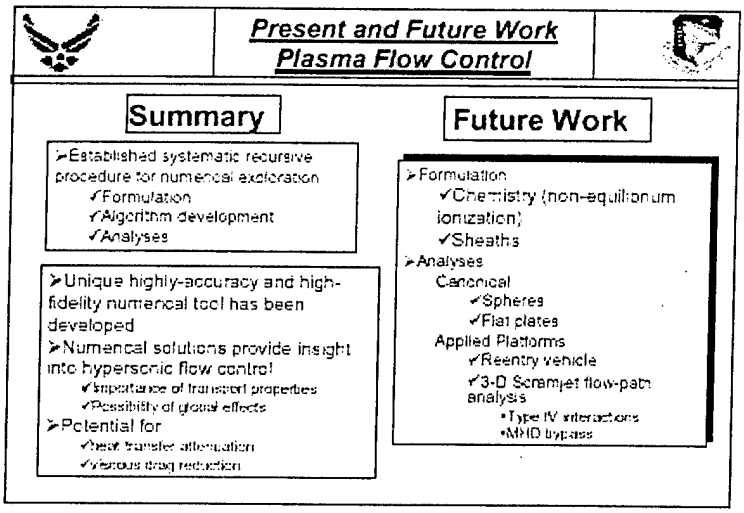
Present and Future Work
Plasma Flow Control
Summary
➢Established systematic recursive procedure for numerical exploration
✓Formulation
✓Algorithm development
✓Analyses
➢Unique highly-accuracy and high-fidelity numerical tool has been developed
➢Numerical solutions provide insight into hypersonic flow control
✓Importance of transient properties
✓Possibility of global effects
➢Potential for
✓Heat transfer attenuation
✓Viscous drag reduction
Future Work
➢Formulation
✓Chemistry (non-equilibrium ionization)
✓Sheaths
➢Analyses
Canonical
✓Spheres
✓Flat plates
Applied Platforms
✓Reentry vehicle
✓3-D Scramjet flow-path analysis
•Type IV interactions
•MHD bypass

NUMERICAL SIMULATION OF PLASMA SHEATHS IN AERODYNAMIC APPLICATION

Jonathan Poggie

Air Force Research Laboratory

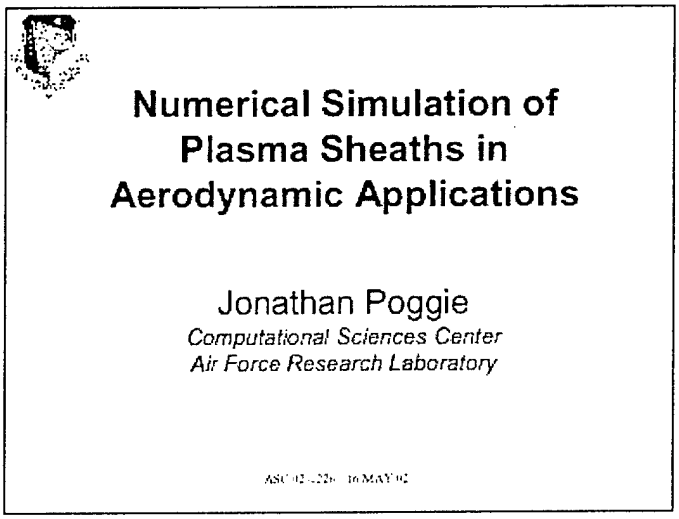

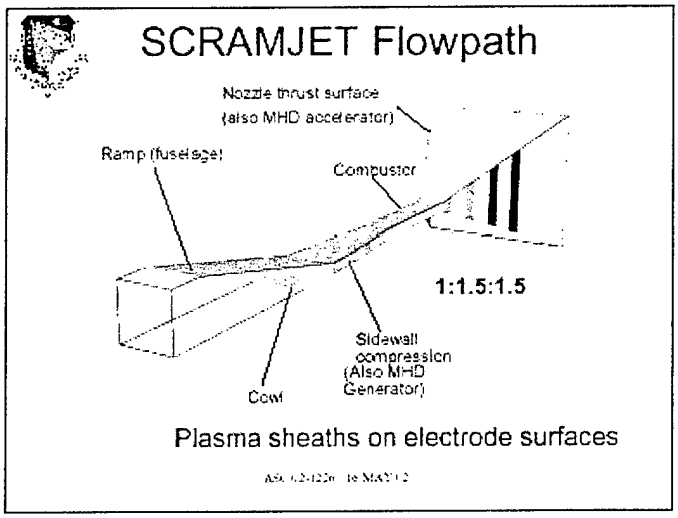

Present Effort

- Prototype code for flow with charge separation
- Solve fluid equations and Poisson equation simultaneously – fully coupled
- One-dimensional
  - Validation problems: steady sheath, transient sheath
  - Low-density regime
- Two-dimensional
  - Flow over cylindrical cathode
  - High density regime

Low-Density Regime

$$\frac{\partial}{\partial t}(m_i n_i) + \nabla \cdot (m_i n_i u_i) = m_i \omega_i$$

$$\frac{\partial}{\partial t}(m_i n_i u_i) + \nabla \cdot (m_i n_i u_i u_i + n_i k_B T_i) = -e n_i \nabla \varphi - \frac{\pi |u_i|}{2\lambda_i} m_i n_i u_i$$

$$T_e = \text{const}$$

$$\nabla^2 \phi = -e(n_i - n_e)/\varepsilon_0$$

$$n_e = n_i \exp(e\varphi / k_B T_e)$$

Numerical Methods

- Conservation equations
  - Implicit Steger-Warming method
  - MUSCL scheme for flux derivatives
  - Extrapolation to nodal interfaces (2rd order, upwind)
  - Block tridiagonal solution
- Poisson equation
  - 2rd order differences
  - Thomas algorithm
  - Linearization of implicit source term

Transient Plasma Sheath

- High negative potential suddenly applied to electrode in uniform, low-density plasma
- Low-density model
- No chemical source term
- Xenon, Φ_w = -50 V, T_e = 1 eV, p = 0.5 mtorr, $n_{e0} = 10^{14}$ m^{-3}

Transient Sheath

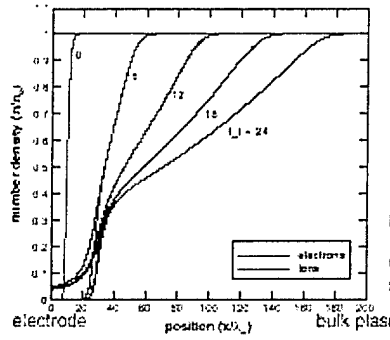

Good agreement with computations and experiments of Widner et al (1970)
Electrons initially repelled
Ions respond: current to electrode
Space charge diminishes
Wave expands into bulk plasma
Quasi-steady sheath: ions uncovered by expanding wave supply ion current to sheath

Effect of Collisions

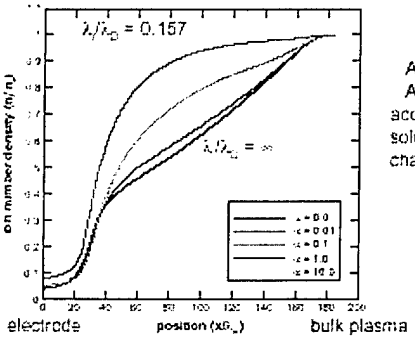

All curves t_{pi} = 24
As collisions increase, ion-acoustic wave disappears, solution takes on diffusive character

Steady Sheath

- Plasma contained between pair of electrodes
- Current to electrodes balanced by 'direct' ionization
- Low-density model
- Baseline conditions: Xenon, Φ_w = -50 V, T_e = 1 eV, T_i = 0.026 eV, $n_0 = 10^{14}$ m^{-3}

Steady Sheath

- 'Direct' Ionization
- Ionization rate: $\omega_i = z\, n_e$
- Find eigenvalue z corresponding to steady-state
- Iterative numerical procedure

Steady Sheath

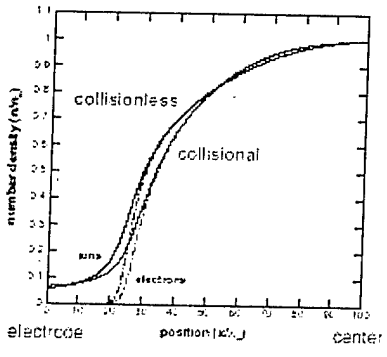

Non-neutral sheath
Quasi-neutral presheath
Direct ionization balances ion current to electrode
Collisional case: finite ion mean free path $\lambda_i/2_{cl}$ = 15.7

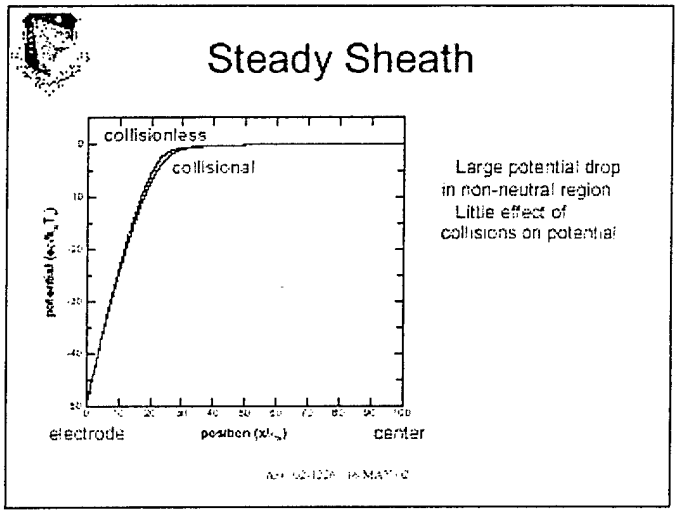
Steady Sheath
collisionless
collisional
potential
electrode
position
center
Large potential drop in non-neutral region
Little effect of collisions on potential

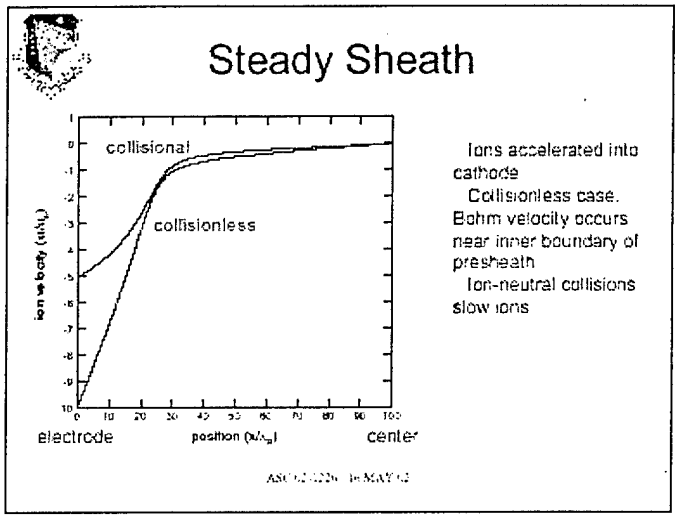
Steady Sheath
collisional
collisionless
ion velocity
electrode
position
center
Ions accelerated into cathode
Collisionless case. Bohm velocity occurs near inner boundary of presheath
Ion-neutral collisions slow ions

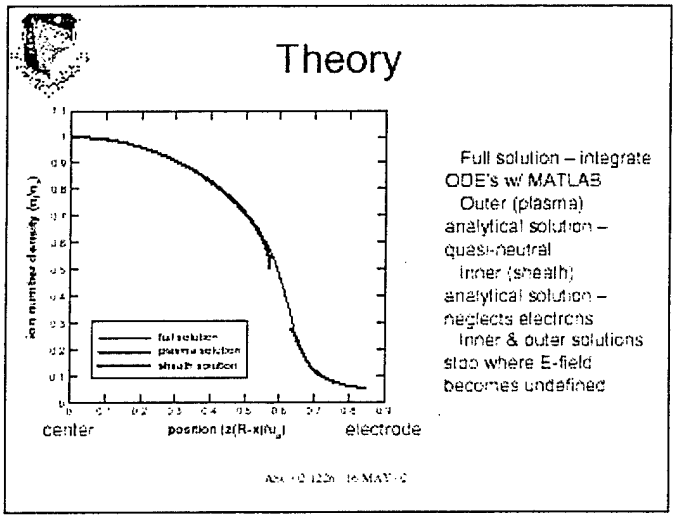
Theory
ion number density
full solution
plasma solution
sheath solution
center
position
electrode
Full solution – integrate ODE's w/ MATLAB
Outer (plasma) analytical solution – quasi-neutral
Inner (sheath) analytical solution – neglects electrons
Inner & outer solutions stop where E-field becomes undefined

Comparison with Theory

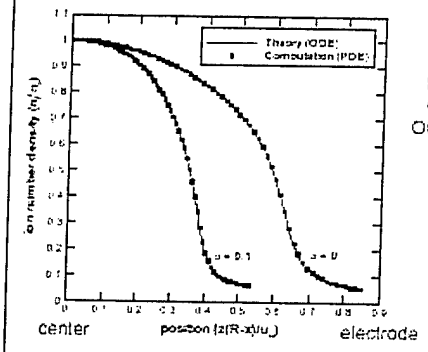

PDE: every 8th point shown
Good agreement between ODE and PDE solutions

Comparison with Experiment

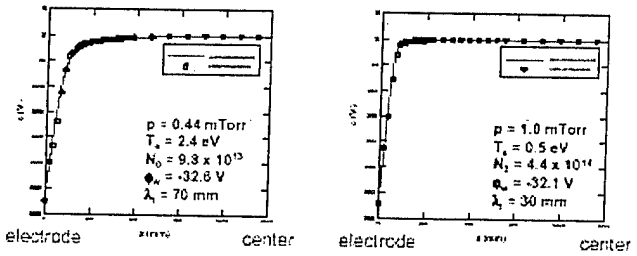

Experimental data of Oksuz & Hershkowitz
Multi-dipole argon plasma
Good fit of model to data

High Density Regime

$$\frac{\partial \rho}{\partial t} - \nabla \cdot (\rho \vec{u}) = 0$$

$$\frac{\partial}{\partial t}(\rho \vec{u}) - \nabla \cdot (\rho \vec{u}\vec{u} - \Sigma) \quad \zeta \vec{E}$$

$$\frac{\partial \mathcal{E}}{\partial t} + \nabla \cdot (\vec{u}\mathcal{E} - \Sigma \cdot \vec{u} - \vec{Q}) - \vec{E} \cdot \vec{j}$$

$$\frac{\partial n_p}{\partial t} - \nabla \cdot (n_p \vec{u} + \vec{\Gamma}_p) \quad 0$$

$$\nabla^2 \Phi - \zeta/\varepsilon_0$$

$$\mathcal{E} - \rho/\epsilon + v^2/2)$$

$$\zeta \quad e(n_{p_0} \quad n_e)$$

$$\vec{j} \quad \zeta \vec{u} + \vec{u}_p$$

$$\vec{\Gamma}_p \quad n_p u_p \vec{e} \quad D_p \nabla n_p$$

$$n_e \quad n_{e_0} \exp(e\Phi/k_B T_e)$$

$$\Sigma_{ij} = -p\delta_{ij} + \mu_0 \left[\frac{\partial u_i}{\partial u_j} + \frac{\partial u_j}{\partial u_i}\right] - \lambda_v \frac{\partial u_k}{\partial x_k} \delta_{ij}$$

$$Q_i = -k_t \frac{\partial T}{\partial x_i}$$

Numerical Methods

- Conservation equations
  - Two-dimensional
  - Curvilinear coordinates
  - Explicit, 2nd order MacCormack method, 4th order damping
- Poisson equation
  - 2nd order central differences
  - SOR/ADI with Thomas algorithm
  - Linearization of implicit source term

Supersonic Cylinder Flow

- Argon gas flow, 0.03 m diameter cylinder
- Mach 3, Re_D = 1140, adiabatic wall
- Laminar flow, Φ_w = -50 V
- Freestream: p = 22 Pa, T = 247 K, T_e = 1 eV, $\alpha \sim 10^{-8}$
- Computational exercise to examine wind tunnel class of flows

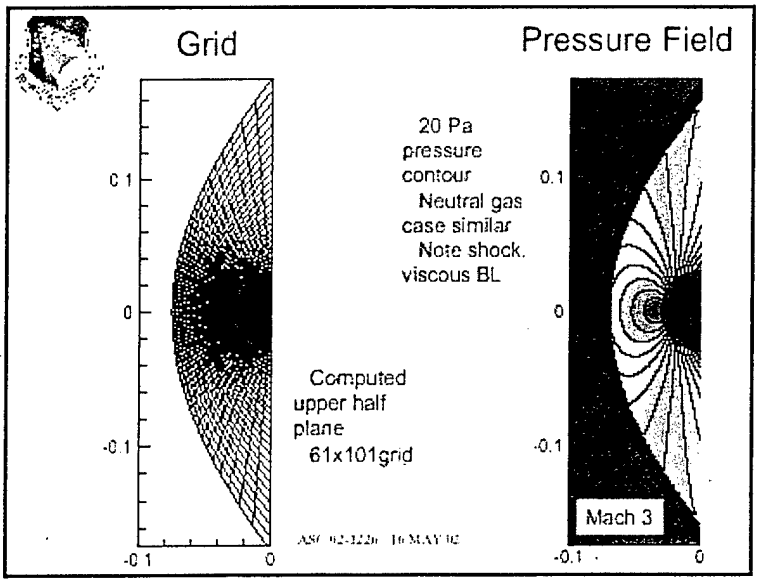

Electric Potential

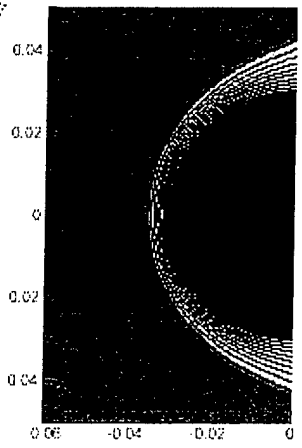

5 V contour
Note close-up view
Potential only varies close to electrode surface
Sheath thickness grows w/ viscous BL

Supersonic Cylinder Flow

Stagnation Streamline

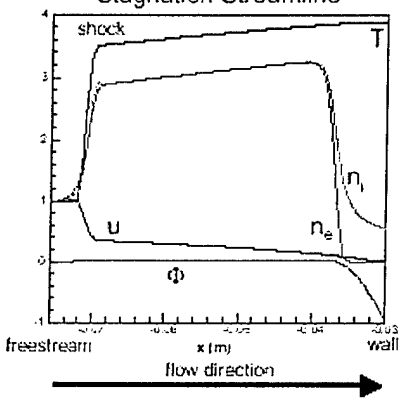

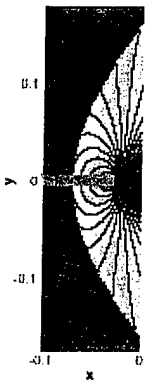

Supersonic Cylinder Flow

Outlet Profile

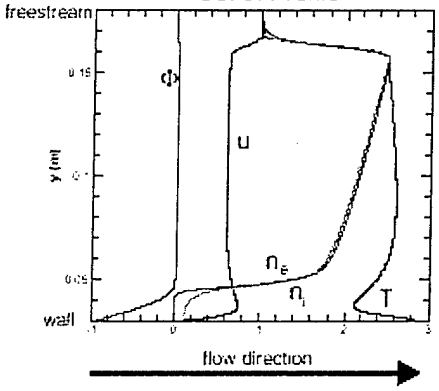

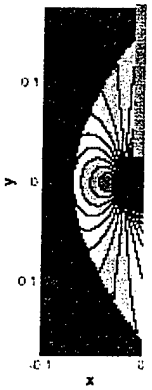

Concluding Remarks

- Implemented implicit scheme
  - Eventually drop Boltzmann equilibrium for electrons
- Validated & verified code
  - Steady sheath theory
  - Oksuz & Hershkowitz experiments
  - Widner & al. computations and experiments
- Demonstrated calculation of wind-tunnel type flow
- Calculate electrode potential drop
- Finite space charge in sheath
  - Opportunity for flow control?
  - Manipulate bulk flow via sheath?

ASC 02-1226 16 MAY 02

Please deliver using DHL.

EXTERNAL PLASMA ASSISTED COMBUSTION IN SUBSONIC AND SUPERSONIC AIRFLOW

Klimov A., Bityurin V., Kuznetsov A., Vystavkin N., Tolkunov B., Sukovatkin N., Serov Yu., Yuriev A.

Institute for High Temperature RAS, Izhorskaya 13/19, Moscow, Russia, aklim@orc.ru

Introduction

Plasma- assisted combustion (PAC) of the hydrocarbon fuel in subsonic airflow and supersonic one was studied in our previous works [1-4].

Present work is continuation of the previous ones [1-4].

Main goals of this work are the followings:

1. Study of the stable external plasma-assisted ignition and combustion in supersonic airflow
2. Control of the aerodynamic model characteristic change by the local plasma-assisted combustion zones (such as drag, surface pressure distribution, base pressure).

The following tasks are studied in this work namely:

1. Design and tuning of the different plasma generators for the PAC experiment.
2. Measurements of plasma and gas flow parameters in the PAC experiment.
3. Study of the stable external plasma-assisted ignition and combustion in subsonic and supersonic airflow
4. Measurements of the aerodynamic model characteristics in PAC experiment (such as surface pressure distribution, base pressure and others).

New plasma generator (PG) designs used in the plasma-assisted experiments and its tuning are considered in this work.

New experimental results obtained in PAC experiment are described in this work also, namely

- Supersonic airflow around model F1 at external PAC.
- Surface pressure on the model F1 with external PAC and without it.
- Study of the stable external PAC near model F in wind tunnel experiment.

There were realized about 20 runs in wind tunnel during experimental Program fulfilment. Experiment scheme is shown in fig.1. Modified model F1 was used in this experiment, fig.1-3. Propane was injected through model's needle (4). 8 orifices (5) were located on the model surface for the pressure measurement. Axial position of the external electrode was in front of the model F1. Propane injection through the model needle could be towards incoming airflow and in the transverse direction to incoming airflow. Electrical current I_d was changed in the range I_d= 2,5- 25 Amp. Pressure sensor was located in the positions #1.

Diagnostic instrumentation used in these experiments:

- Pressure sensor IKD-6.0 (maximal measured pressure - P_0< 6Bar) used for model surface pressure measurements
- PMA- photo multi-amplifier with optical filter (optical green and violet bands).
- Shadow picture and video.
- Resister divider and shunt for measure of the volt – ampere characteristics.

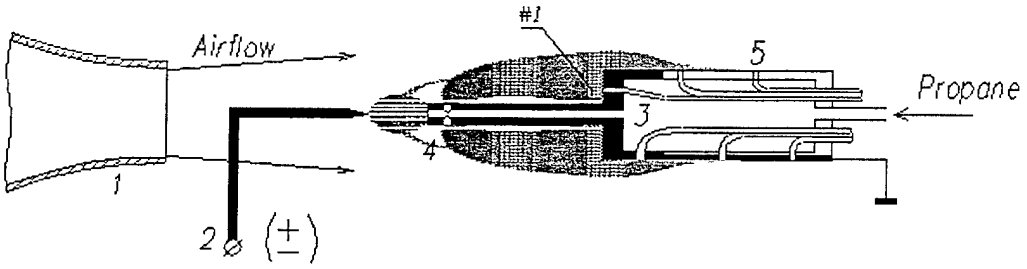

Fig.1 . Scheme of experimental setup (variant−2):

1. *Nozzle;*
2. *External hot needle electrode;*
3. *Aerodynamic model;*
4. *Fuel injection tube−grounded electrode;*
5. *Surface pressure measurment tubes.*

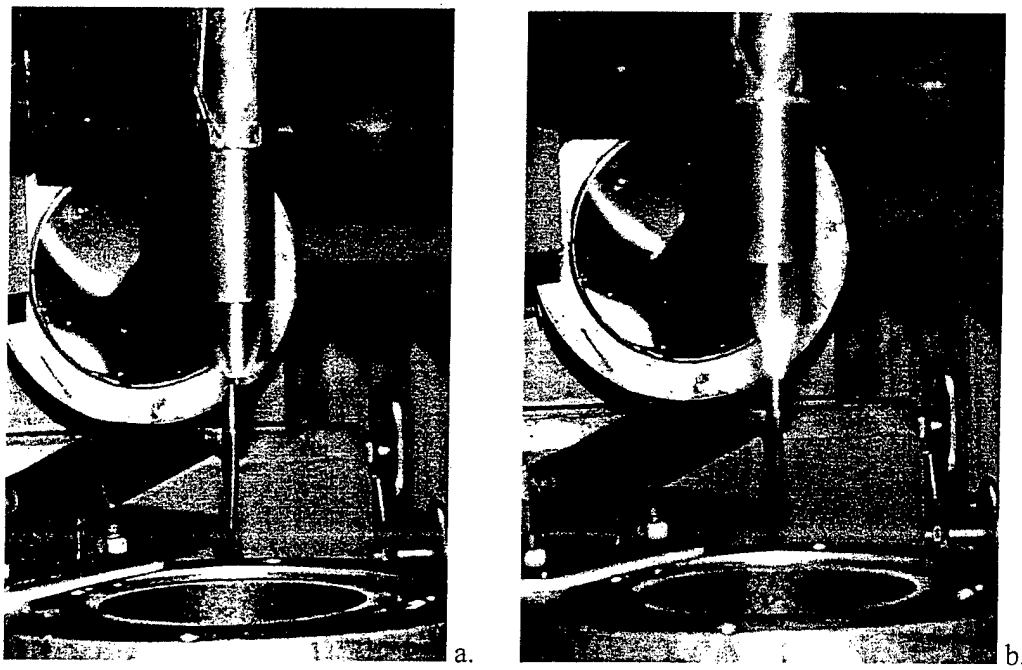

Fig. 2. Model F1 with propane injection (without combustion) in supersonic airflow (M~2) – a., model F1 with external PAC in supersonic airflow (M~2, discharge current- I_d~5 Amp) b., photos

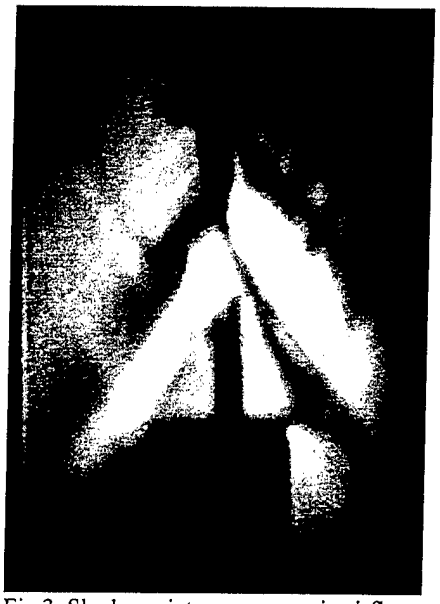

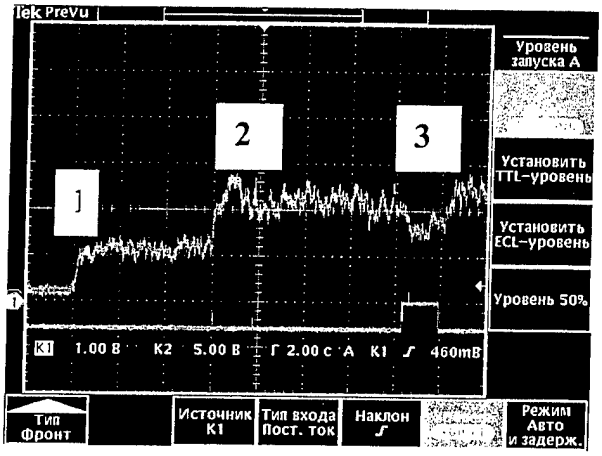

Fig.3. Shadow picture supersonic airflow around model F1 with external PAC (M~2, P_{st}~1Bar, right photo), surface pressure signal: 1 – wind tunnel start, 2 – supersonic regime begin, 3 – plasma switch on

Main experimental results

Stable PAC was realized in this experiment, fig. 2. However the local PAC was created near discharge region only. Large part of the injected propane was non-ignited one near model F1 (non full combustion regime).

Shadow pictures and video frames proved this conclusion. Temperature measurements (registered in the additional experiment in small wind tunnel) proved this conclusion also.

It was revealed the bow shock (SW) modification (dissipation) near model F1 and external electrode took place in this experiment. In turn this SW modification changed surface pressure distribution. Pressure sensor #1 recorded the pressure increase up to 23%.

Significant voltage modulation ($\delta V/V$= 50-100%, T_i~10-50 μs, F_i~10-30 kHz) in DC electric discharge was recorded in supersonic flow at propane combustion. Electric current modulation was not large: - about $\delta I/I$< 10%.

Non-stationary PAC was created at small electric current (I_d< 2 Amp) in this experiment only. Pressure signal and PAC luminescence signal prove this conclusion. It is very important to note that stationary stabile PAC was created near model F1 at large electric current (I_d> 5 Amp).

It was revealed that non-equilibrium plasma of the electric discharge near model F1 in supersonic flow has very week luminescence in the optical green band (λ~5600-5700A). On the other hand the PAC has very intensive optical radiation in this optical region. So registration of optical radiation in the optical green band is very important for the PAC registration and its identification.

Experimental results obtained with model F2.

Model F2 (model with onboard erosive plasma generator (PG-jet) and propane injection) was described in our previous work [1] in detail. Improved ***Model F2*** consists of (fig.4):

Cylindrical dielectric body with diameter about 30 mm (5, Nylon 6),
Metal nozzle (1, copper),
Stagnation pressure sensor (7),
Propane injection tube (6),
Pulse repetitive plasma jet generator (PG-jet),
Anode of the PG-jet (1),
Graphite cathode electrode of the PG-jet (3),
Ceramic discharge channel (boron nitride), (2)

Air injection tube.

Parameters of PG-jet in model F1:

Mean (or pulse) power	< 20 kW
Operation mode	Pulse repetitive one with repetitive frequency <30 Hz, continuous one
Air mass injection flux	< 1 g/s
Propane injection mass flux	< 3 g/s

Stable external PAC near a model F2 in subsonic flow (M~0,9; P_{st} ~ 1 Bar) and without it (in air) were obtained in the experiment, fig.5. Note that PAC near model F2 in an external airflow was a non- stationary one. But average position of PAC front near this model was very stable. It was revealed that a quasi-continual PAC was created near a model F2 at f~ 30 Hz. This regime was possible due to PAC "memory" revealed in our experiment [4]. Results of the stagnation pressure measurements on head part of model F2 at subsonic flow (M<0,9) are presented in [1].

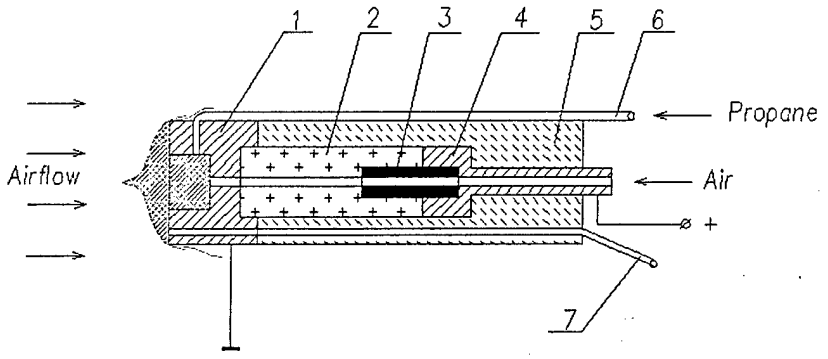

Fig.4 Scheme of modified model F with erosive plasma generator:

1–grounded anode (cuprum);
2–boron nitride;
3–carbon cathode;
4–metal holder;
5–model F (Nilon 6);
6–tube for propane injection;
7–pressure sensor tube.

Parameters and conditions of this PAC experiment were the followings:

Propane mass flux	<0,4 g/s
Airflow mass injection	<1 g/s
Repetitive frequency of PG-jet	F= 20 Hz
Static pressure of external airflow	~ 1 Bar
Mach number	~ 0,1- 0.9

Plasma parameters of plasma erosive jet created by PG-jet were the followings [1, 5]:

Electron concentration	N_e~ 10^{14}- 10^{15} cm^3
Mean gas temperature	T_g~ 2000K,
Vibration temperature	T_v~ 6000K

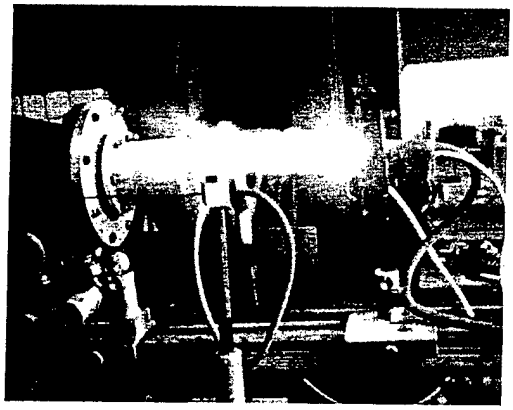

Fig.5. Erosive plasma generator operation mode on the model F2 without external airflow.

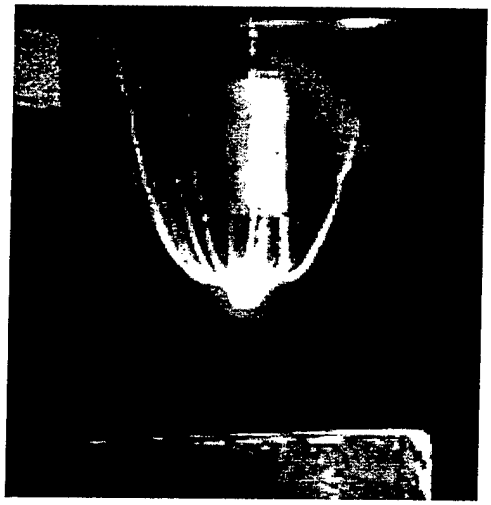

Fig.6. Erosive plasma generator operation mode of the on the model F2 in supersonic airflow, M~2, P_{st}~1Bar, I_d~50 Amp

From the analysis of the experimental results it was obtained that stagnation pressure decrease was about 30% at small airflow injection through PG-jet (without plasma). This value depended on airflow injection flux. It is well known gas dynamic result connected with vortex separation zone generation near head part of the model F2. Propane injection (without combustion) decreases stagnation pressure P_o up to 10% also. Total stagnation pressure decrease on head part of model F2 was about 60-80 % at the PAC generation.

Stable external PAC near improved model F2 (fig.4) in supersonic airflow (M~2, P_{st} ~ 1 Bar) was generated in our preliminary experiment, fig.6. These results were obtained at the following conditions

Mach number	M~2
Static pressure	P_{st}~1Bar
Stagnation pressure of the injected airflow	P_o<10 Bar
Stagnation pressure of the injected propane	P_o<10 Bar
Mass propane flux	m < 3 g/s
Discharge current	I_d<50 Amp

Measurements of the pressure distribution on the model F2 surface at external PAC in supersonic airflow will be obtained in future experiments.

Conclusion

1. Two aerodynamic models F were designed, manufactured and tested. External PAC was used in these models.
2. Stable external PAC was created in subsonic and supersonic airflow near model F.
3. Preliminary experimental results on surface pressure decrease of the model F1 by external PAC were obtained.

Acknowledgments

This work was sponsored by the Air Force Office of Scientific Researches. The author would like to acknowledge helpful discussion of present work with Dr. Brovkin V., Dr. Nedospasov A., Dr. Leonov S. and technical help by Sakharov A.

References

1. Klimov A., Bityurin V., Brovkin V., Vystavkin N., Kuznetsov A., Van Wie D., Optimization of Plasma Generators for Plasma Assisted Combustion, Paper AIAA 2001-2874, 32nd AIAA Plasmadynamics and Lasers Conference and 4th WIG Workshop, 11-14 June 2001/ Anaheim, CA, P.10,
2. Klimov A., Bityurin V., Brovkin V., Vinogradov V., Van Wie D., Plasma Assisted Combustion, Paper AIAA 2001-0491, 39th AIAA Aerospace Sciences Meeting & Exhibit, 8-11 January 2001/ Reno, NV, P.9,
3. Klimov A., Bityurin V., Brovkin V., Leonov S., Plasma Generators for Combustion, Workshop on Thermochemical Processes in Plasma Aerodynamics, Saint Petersburg, May 30- June3, 2000, P.74,
4. Klimov A., Bityurin V., Van Wie D., at. el, Plasma Assisted Combustion, Paper AIAA 2002-0493, 40th AIAA Aerospace Sciences Meeting & Exhibit, 14-17 January 2002, Reno, NV, P.9,
5. Ball Lightning in Laboratory, Editors: Avramentko R., Bychkov V., Klimov A., Sinkevich O., Moscow, Chimiya publishes, (in Russian), 1994, P.291.

GASEOUS MIXTURES COMBUSTION INITIATED BY HIGH-CURRENT GLIDING SURFACE DISCHARGE (NEW EXPERIMENTAL RESULTS)

I.A.Kossyi, V.P.Silakov and N.M.Tarasova

General Physics Institute of Russian Academy of Sciences, 119991, Vavilov Street, Moscow, Russia. E-mail: kossyi@fpl.gpi.ru

The basic physical problem investigated in this work is combustion of gaseous mixtures initiated by high-current highly radiating pulse discharges. The characteristic scheme of experiment is shown on Fig.1.

The chamber of the reactor (1) represents a cylindrical quartz pipe of a diameter $\Phi_c \approx 50$ mm and a length $L_c \approx 100 - 200$ mm. The chamber is evacuated up to a pressure of $p_o < 10^{-2}$ Torr and filled with a working gas ($CH_4 + O_2$; CH_4 + air; $CH_4 + O_2 + CF_2Cl_2$) at pressures in the interval $100 \le p \le 500$ Torr. It is in this gas mixture that combustion is initiated with the help of a discharger (2).

The discharger represents a multielectrode system fixed in a particular way [1-4] on a dielectric (crystal, teflon, ceramics) tube of a diameter $\Phi_d \approx 6$mm. The length of the metal-dielectric cylindrical discharge system is: $L_d \approx 40$ mm. The discharger is located close to one of the end flanges of the reactor chamber. When a high-voltage pulse is applied to the discharger, it gives rise to the formation of a high-current ($I \le$ 1-10 kA) low-threshold «slipping» discharge along the discharger and an extended plasma layer at its surface. Such discharge systems have been widely applied at the General Physics Institute of the Russian Academy of Sciences for generating the dense hot collisionless plasma [1] , as sources of the metal plasma [2] , for excitation of converging toroidal shock waves in gas medium [3,4] , etc.

Electrical discharge is one of the most widely used techniques for initiating combustion in gaseous combustible mixtures. It has been comprehensively discussed in a series of monographs [5,6]. As a rule electric discharges represent a relatively low-power spark excited between two electrodes immersed in combustible gas medium (analogous to a spark in internal combustion engines). In the present work a high-current pulse slipping surface discharge was used instead of a spark.

A comparison with the already published data allows to point out in the performed research, based on using a new high-power electro-discharge device, results which are of obvious interest as for physics (physicochemistry) so for some actual applications.

The present work is the first attempt to use dischargers on a slipping surface discharge for initiating combustion in a gas mixture. In the present work two generators of high-voltage pulses were used as power supplies of dischargers (2), with the following parameters:

1. Generator G_1 with low pulse energy: pulse amplitude: $U \cong 40$ kV; pulse duration: $\tau \cong 40$ nsec and energy in a pulse: $E \le 0{,}1$J.

2. Generator G_2 with high pulse energy: $U \cong 20$ kV, $\tau \cong 20$ μsec; $E \le 30$ J.

Investigations have been performed in [7-10] have shown that in spite of extremely small volume occupied by discharge and extraordinary low duration of discharge (from several tens of nanoseconds up to several microseconds) after a delay time much higher than discharge duration practically in all reactor volume "flash" of explosive combustion (based on a branched-chain reactions) has been observed. One from the most interesting phenomena that were seen by authors of [7-10] is for the first time observed wave of a non-complete combustion preceding the volume explosive "flash". This wave conceptually differs essentially from ordinary "slow" combustion wave with mechanism of propagation based on the thermal conductivity as well as from the "fast" detonation wave.

The characteristic time relations of the mixture combustion are exhibited in a signal from the photomultiplier. It records the glow from the end face of the chamber integrated over the spectrum and the volume. At the origin of the beam sweep a short splash of the glow is observed, the source of which is a breakdown of the metal-dielectric discharger. Then after some delay (~ 2-3 msec), which is much longer than the life-time of a plasma formation (~ 1-5 μsec), a «long-lived» (10-100 msec) glow from the reacting volume of the gas mixture appears. This glow builds up rather slowly, reaches its peak and then slowly decreases. Apparently, it is precisely this glow, which is characterized by the life-time $\Delta\tau$ determined by a half-height of a «long-lived» part of a pulse, which accounts for the process of the gas mixture combustion. The characteristic life-time of the post-discharge glow, $\Delta\tau$, depend on the properties of the discharge initiating the combustion, decreasing with the increase of the energy in the pulse igniting the slipping surface discharge.

The dynamics of the glow from the working gas mixture exposed to an electrical discharge, which was localized at the end flange, was investigated with the help of the photo-electric recorder (streak camera) PHER-7. The slot of the recorder was placed along the axis of the chamber, creating a field of view area of length Z 90 mm and width Y 5 - 6 mm.

The starting time of the streak camera is selected to catch the time of excitation and existence of the electrical discharge initiating the combustion in the reactor

As it is shown in this work "induction" time (τ_i) (time of a non-complete combustion wave propagation along the reactor chamber with repeated reflection from chamber ends) – essentially depends on energy (W) released in gliding surface discharge: τ_i falls down with rise of W.

Measurements of temperature (T_g) attainable in a gaseous mixtures (CH_4+O_2; $CH_4+O_2+CF_2Cl_2$) burning initiated by gliding surface discharge have been performed. Spectral and thermocouple methods have been applied for T_g determination. Thermocouple method gives only relative values of temperature.

One from spectral methods is based on a registration of continuous radiation spectrum of burning double or triple mixtures. Spectrum has been determined with help of spectrometer Avantis S-2000 (Ocean Optics Co.). For spectrometer calibration lamp СИ8-200 has been applied. Characteristic spectrogram is presented in Fig. 2a. In the interval of wavelength $4500 \leq \lambda \leq 6500$ A spectral distribution of radiation intensity (I) is very close to the spectrum of planckian source [5]:

$I_\lambda \cong 2\pi c/\lambda^4 \; 1/\exp(hc/\lambda kT)-1$ (1)

that after proper manipulation comes to the equation:

$1{,}4388\ 10^8/\lambda = \text{const}-T \ln(I_\lambda \lambda^4)$, (2)

where λ in A.

Characteristic dependence of quantity $1{,}4388\ 10^8/\lambda$ on a logarithm $\ln(I_\lambda \lambda^4)$, slope of which in accordance with (2) gives gas temperature $Tg \cong T$, is shown on the Fig. 2b.

The second spectral method is based on a registration of Na duplet lines with determination of their self-absorption.

The main experimental results are as following:

- Combustion temperature does not depend on energy released in the ignitor;
- Characteristic magnitude of temperature T_g for binary mixtures is close to the "adiabatic" temperature. As an example for mixture $CH_4:O_2=45:180$ Torr temperature attaining in the course of combustion is $T_g \cong 3100$ K;
- On addition of CFC temperature of burning mixture increases. As an example in a triple mixture $CH_4:O_2:CF_2Cl_2=45:180:45$ Torr temperature $T_g \cong$ 3800-4300 K.

The degree of CFC decomposition in the triple mixture does not depend practically on energy W.

This work was supported partially by Russian Foundation for Fundamental Investigations (Project No 02-02-16066).

References

Barkhudarov, E.M., Berezhetskaya, N.K., Bolshakov, E.Ph., Eletskiy, A.V., Kossyi, I.A., and Taktakishvili, M.I., "Ring source of a dense collisionless plasma and ionizing radiation", *Letters to Journal of Technical Physics*, Vol. 54, No 6, 1984, pp. 1219-1222.

Anpilov, A.M., .Barkhudarov, E.M., Berezhetskaya, N.K., Kop'ev, V.A., Kossyi, I.A., Malykh, N.I., Matossian, J., Taktakishvili, M.I., and Terekhin, V.E., "Source of a Dense Metal Plasma", *Plasma Sources Sci. Technol*, Vol.7, 1998, pp. 141-148.

Berezhetskaya, N.K., Bolshakov, E.Ph., Golubev, S.K., Kossyi, I.A., Semienov, V.E., and Terekhin, V.E., "Gas-dynamic phenomena accompanying a ring surface discharge", *Zhurnal Eksperimental'noi i Teoreticheskoi Fiziki*, (in Russian), Vol. 87, iss. 6, 1984, pp. 1926-1931.

Kossyi, I.A., Krasnobaev, K.V., Sokolov, I.V. and Terekhin, V.E., "Cumulation of shock waves raised by an axially symmetrical slipping discharge", *Brief Messages on Physics*, (in Russian), No 11, 1987, pp. 3-5.

Lews, B. and Elbe, G, *Combustion, flame and explosions in gases*, State Publishing House of Foreign Literature, Moscow, 1948, 446 p.

Semienov, N.N., *Chain reactions*, (in Russian), Nauka, Moscow, 1986, 534 p.

I.A.Kossyi, V.P.Silakov and N.M.Tarasova. Combustion of Methane-Oxygen and Methane-Oxygen-CFC Mixtures Initiated by a High-Current Slipping Surface Discharge. – Plasma Physics Reports, v. 27, No 8, (2001), pp. 715-725.

I.A.Kossyi, V.P.Silakov and N.M.Tarasova. Methane-Oxygen and Methane-Oxygen-CFCs Gaseous Mixtures Combustion Initiated by High-Current Slipping Surface Dischargde. – 15th Intern. Symposium on Plasma Chemistry, Symposium Proceedings, v. II, Oral Contributions, (2001), Orleans, France, Ed. by

A.Bouchoule, J.M.Povesle et al., pp. 721-726.

S.I.Gritsinin, E.G.Korchagina, I.A.Kossyi, M.A.Misakyan, V.P.Silakov N.M.Tarasova and S.M.Temchin. Decomposition of Chlorine and (or) Fluorine-Bearing Substances in a Gas Mixture Ignited by a Slipping Surface Discharge. – Plasma Sources Sci. Technol., V. 10, No 2, (2001), pp. 125-133.

S.I.Gritsinin, I.A.Kossyi, Yu.F.Kolesnichenko, M.A.Misakyan, V.P.Silakov, N.M.Tarasova and S.M.Temchin. The Features of Gaseous Mixtures Combustion Initiated by High-Current Slipping Surface Discharge. – 32nd AIAA Plasmadynamics and Laser Conference, (2001), Anaheim, USA, Report AIAA 2001-2947.

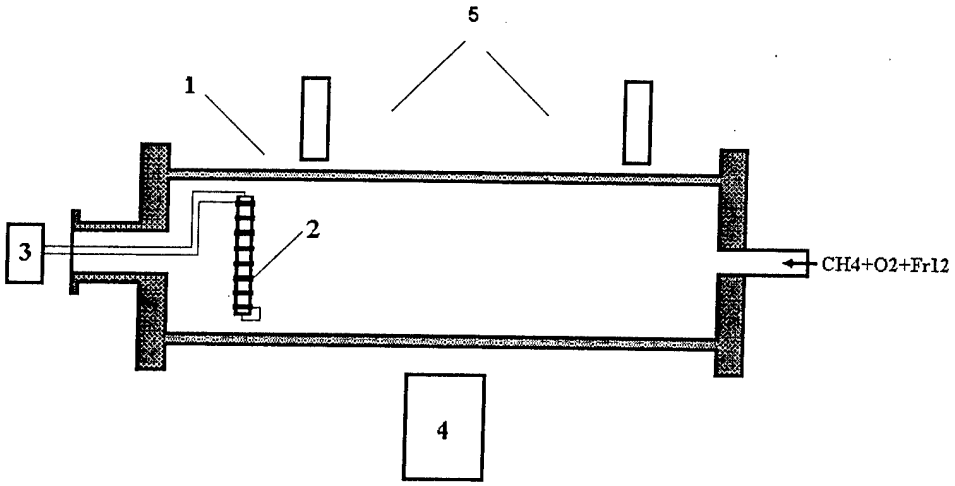

Fig.1. 1 – chamber of reactor; 2 – discharger; 3 – high voltage pulses generator; 4 – FER-7; 5 – photomultipliers.

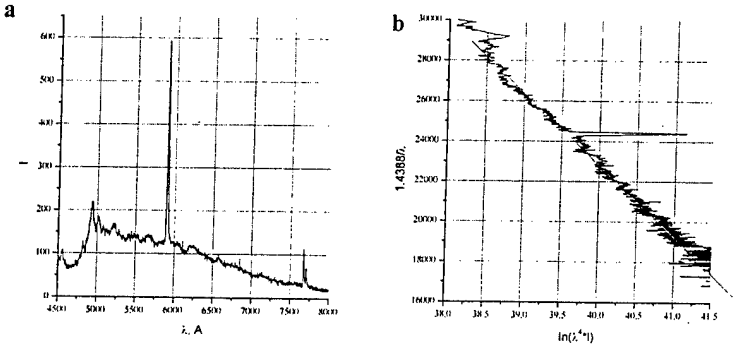

Fig.2. (a) – characteristic spectrum of burning CH_4+O_2 mixture radiation and (b) – result of this spectrum handling in accordance with (2).

INFLUENCE OF FUEL THERMAL DECOMPOSITION ON REACTION ACTIVITY OF A PROPANE/AIR MIXTURE

Yuriy Ya. Buriko, Viacheslav A. Vinogradov, Valentin F. Goltsev, Paul J. Waltrup***

**Central Institute of Aviation Motors, Moscow, Russia, 111116, 2 Aviamotornaya St.*
***Johns Hopkins University, Applied Physics Laboratory, Laurel, MD, USA*

Nomenclature

ABE = air breathing engine
C = concentration
FTDP = fuel thermal decomposition products
G = component mass fraction
M =Mach number
P = pressure
T = temperature
t = time
RC = radical concentration
Z = degree of fuel decomposition
ϕ = fuel/air equivalence ratio

Subscripts

a = air
c = combustion
d = decomposition
f = fuel
ind = induction
mix = mixture
q = maximum heat release rate

I Introduction

Numerous experimental investigations and computations show that there are serious difficulties with sustaining ignition and efficient combustion of hydrocarbon fuels in devices such as combustion chambers for ground power plants, gas turbine engines, and ramjet combustors [1-3,4].

The static pressure and temperature at the combustor entrance for typical flight trajectories of vehicles powered by air breathing ramjet engines from M=4-8 are in the range P=0.04-0.08 MPa and T=500-950K respectively. Flow velocities, V, are in the range $0.9\text{-}1.6\times10^3$ m/s. Consequently, residence times for air/fuel mixtures with combustor lengths of 1-2 m are not more than 1-2 ms.

For example, for stoichiometric (ϕ=1) hydrogen/air mixtures, the value of t_{ind} for the flow parameters listed above varies between 10-0.1 ms. It is therefore not possible to initiate combustion based on self-ignition of these fuel/air mixtures [5], particularly at the lower flight speeds. The addition of 20% by weight silane (SiH_4) in hydrogen decreases this value to t_{ind}=0.4-0.05 ms [10].

For hydrocarbon fuels, for example, kerosene, the values of t_{ind} increase to 10^2-10 ms, which is unacceptable for fuel self-ignition and efficient fuel/air combustion for these flight conditions. That is why for high-speed engines, special devices such as plasma jet generators [6] electric discharge spark plugs [7] and/or pilot flames using self-igniting components [8] are considered for application. As a rule, these devices only affect the flow locally, and so are installed in regions of flow recirculation (regions of combustion flame stabilization). The local velocity defines the dimensions of the flame stabilization zone along with other flow parameters such as pressure, P, temperature, T, fuel/air equivalence ratio, ϕ, and the physical dimensions of the flame holder. In this case, regimes of "residual flames" or "flame spreading" are realized [8]. Consequently, the results of this research could be applied not only to the whole flow in engine, but also to the flow in the flame stabilization zone.

Another ignition and combustion enhancement method is to use a gas generator to prepare the fuel for combustion. Definite success was achieved using gas generator schemes for the combustor operation of high speed ABE [6,10]. However, application of special initiators for ignition, especially with thermal fuel cracking in the presence of water, need to be

analyzed from the point of view of propulsion efficiency as a whole.

Along with the above, ignition and combustion intensification methods using the burning of fuel thermally decomposed (cracked) products (FTDP) is another possible ignition and combustion enhancement method since the fuel may be used for cooling of the airframe and engine structural elements. It is expected that these thermal decomposition products are more chemically active than the original fuel because of the increased fuel enthalpy, changing chemical composition, and the presence of active radicals, all of which would intensify the combustion process [4,11-13].

Another way to increase fuel reaction activity is to saturate the air/ fuel mixture with active radicals. This can be achieved, for example, by initiating an energetic discharge into one or both reactant streams. Other approaches include the injection of pre-combustion products containing high concentrations of radicals, or photochemical method of active-species injection when additional radicals are formed as a result of radiation-induced decomposition of a reagent.

The current analysis will be framed by the effect that these active radical species have on the ignition time delay, t_{ind}, without considering the details of how these active species are formed or the mechanism of their injection into the combustion system. In this paper, only one of these effects has been investigated numerically, namely, the impact of the radical concentration in the air/fuel mixture on the characteristic ignition delay time, which specifies the fuel reactivity. Currently, there is a lack of evidence for the matter in question and, therefore, further research is required.

The present research evaluates, within the framework of existing kinetic schemes, the possible intensification of the ignition and combustion processes by means of an increase in a hydrocarbon fuel's reactivity. The effects of fuel thermal decomposition and potential increases in radical concentration on the ignition-delay time (or other parameters, which characterize the combustion process) have been investigated. This includes the influence of the lifetime of the active radicals on the combustion.

Statement of work and method of study

Propane (C_3H_8) was chosen to represent the kerosene hydrocarbon fuel model. There is a large experience based on the combustion of C_3H_8, and propane's energetic (heat release) performance, in the first approximation, simulates most of the widely used kerosenes [14-16]. Detailed kinetic schemes of propane-air combustion are approbated well and can be found in many publications [17-21]. In this regard, the use of propane as the model fuel permits a methodical and nearly complete analysis of its reaction activity increase to be made when undergoing non-equilibrium thermal cracking. The results obtained will not only represent the individual performance of propane decomposition, but provide main tendencies for the thermal decomposition of the more complex hydrocarbons.

The time to reach the maximum rate of heat release, t_q, was chosen as the parameter for evaluation of the fuel and FTDP reaction ability. For this moment of time in a homogeneous combustion process, the maximum rate of temperature increase is calculated. Preliminary calculations of combustion show that the time of maximum heat release is, as expected, between the induction time t_{ind} and combustion time t_c. So, this parameter characterizes not only the possibility of self-ignition, but possibility to realize through the combustor (or residence time) intensive combustion.

Processes realized under the thermal decomposition and combustion of fuel and FTDP were calculated under the assumption of a one-dimensional model of the combustion process [22]. This model is based on the assumption that the mixing process (air with fuel and FTDP) is practically instantaneous. In such a way, the homogeneous combustion is modeled and,

for this case, all of the characteristic times, t_{ind}, t_q and t_c, are defined by only the kinetics of the chemical reactions.

Process of fuel thermal decomposition was calculated with use of mathematical model basing on free-radical mechanism. The presence of such a mechanism during the decomposition process has been demonstrated experimentally [14].

The following equations describe the combustion and decomposition processes, distribution of the reactant concentration and temperature along the reactor length:

$$U\frac{dC_i}{dx} = W_i \qquad (1)$$

$$U\frac{dH}{dx} = 0 \qquad (2)$$

where t=X/U - time, X - coordinate directed along the reactor length, C_i - i_{th} reactant concentration (i=1,...,n), W_i - i_{th} reactant formation (or consumption) rate, H – total mixture enthalpy, n – total number of reactants, and U - flow velocity.

Changing of the FTDP composition was calculated with Eq. (1) under the condition of reactant constant temperature (T_f=const). To simulate the combustion process for the original fuel/air mixture with and without additional radicals, the detailed kinetics scheme was applied for hydrocarbons oxidation based on Refs. 19-21, 23, and 24. The scheme comprises 303 reactions between 60 components, including atoms H, O, C, N and Ar. Constants of elementary reaction rates are adopted mainly from these references. Correction of the rate constants was conducted using the experimental data presented in Ref. 25.

It is assumed that the propane temperature T_f and pressure P_f are constant; the technical issues associated with defining the fuel state in heat-exchanger–reactor were not considered. The calculations show there is fuel decomposition at fixed values of T_f and P_f as the fuel heating time increases. This is manifested by a decreasing propane mass fraction in the mixture, the appearance of low molecular components, and a decrease in the mixture molecular weight [12].

Numerical research of the propane thermal decomposition process under parameters T=900-1400K and P=0.05-3MPa demonstrates [26]:

1. Thermal decomposition takes place at T≥900-950K with the products of composition consisting mainly of C_3H_6, C_2H_4, C_2H_2, CH_4 and H_2 depending on P, T and degree of decomposition Z. Increases in pressure provide an acceleration of the decomposition.

2. Mass fractions of more reactive H_2 specie and H radical, which are maximum among another radicals in the FTDP, do not exceed $(3\text{-}4)\times10^{-2}$ and 2×10^{-6}, respectively, for the considered values of Z≤95% and process parameters.

Effect of fuel thermal decomposition on enhancement of its reactive activity

Combustion of propane and thermal decomposition products were calculated with the use of the same mathematical model (1)–(2), which was given before.

It is known, that the reactive ability of air/fuel or air/FTDP mixtures is characterized by the level of energy activation of total combustion reaction. Definition of this parameter is based on calculation of the fuel ignition delay time. In this research, the time to obtain maximum rate of heat release, t_q, which was considered earlier was accepted as such a parameter.

In Fig.1, results of the t_q calculations for stoichiometric (ϕ=1) fuel/air mixtures at P=0.05 MPa versus the value of 1000/T are presented, where T is initial mixture temperature. The four regimes of decomposition given in Fig.1 were chosen to analyze the reactivity based on changes in the decomposition products for differing T_f and Z at constant P=1 MPa. It should be noted the dependence t_q (1000/T) is nearly linear and any incoherence of the activation energy for these limiting reactions does not vary by more than 20%. In the case of hydrogen combustion, the activation energy

is different for regions of low and high temperatures, with the main phase change at T≈1000K[5]. Data presented on the decomposition products shows the increase of reactive ability defined mainly by Z, but slightly with the decomposition process temperature as well.

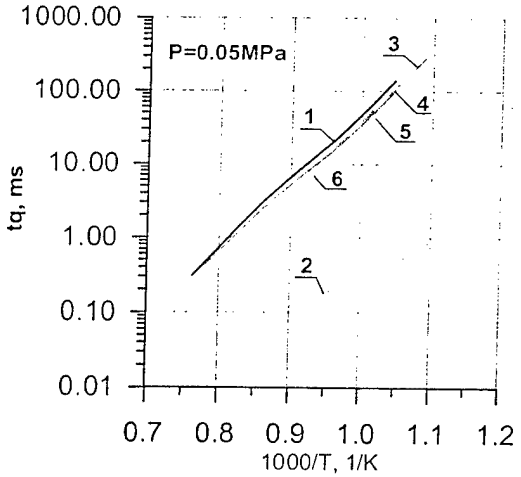

Fig. 1 Effect of stoichiometric air/fuel mixture temperature on time corresponding to maximal heat release rate at combustion.

1 – C_3H_8, 2 – H_2, 3-6 – products of fuel decomposition at P=1MPa and different T_f,

3 – T_f=1000K, Z=25%, 4 – T_f=1200K, Z=25%, 5 – T_f=1200K, Z=50%, 6 – T_f=1200K, Z=75%,

In Fig.1, results of the t_q calculations for stoichiometric (ϕ=1) fuel/air mixtures at P=0.05 MPa versus the value of 1000/T are presented, where T is initial mixture temperature. The four regimes of decomposition given in Fig.1 were chosen to analyze the reactivity based on changes in the decomposition products for differing T_f and Z at constant P=1 MPa. It should be noted the dependence t_q (1000/T) is nearly linear and any incoherence of the activation energy for these limiting reactions does not vary by more than 20%. In the case of hydrogen combustion, the activation energy is different for regions of low and high temperatures, with the main phase change at T≈1000K[5]. Data presented on the decomposition products shows the increase of reactive ability defined mainly by Z, but slightly with the decomposition process temperature as well.

Curves 1-4 in Fig.1 show decreases in the activation energy required under transition from propane to decomposed products of 3.2%, 4.9%, 9.4% and 12.2%, respectively, for the four example cases presented for a t_q of 1 ms. These are rather small in comparison with these same effects using hydrogen fuel. Increasing the FTDP reaction ability in comparison to when hydrogen is used, basing on average values of activation energy, is equal to 20-25%.

More computation verification of the reaction ability increase is given in Fig.2, where ratios of the t_q values for the initial hydrocarbon fuel and FTDP at combustion are presented. These data were obtained for the same regimes as given in Fig.1. The temperature of the mixture was changed by changing the air temperature, with the FTDP temperature being either T_f=1000 or 1200K.

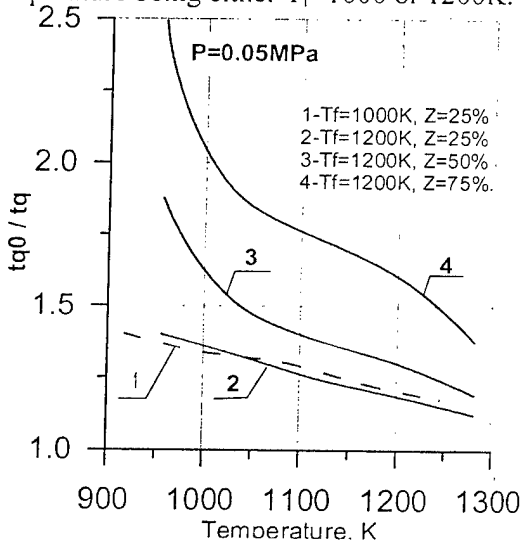

Fig. 2 Effect of air/fuel mixture temperature on decrease of time corresponding to maximal heat release rate at combustion of C_3H_8 decomposition products under P=1.0MPa

First, the effect of FTDP is more pronounced at low temperatures. For example, for T_{mix} < 1000K, the decrease in t_q is approximately 2.5-3 times that of the reference value. At T_{mix}>1300K this effect is less pronounced and, even at large Z, is not more than 20-30%. Also note that the effect of T_f on t_q is small. The data in Figs. 1

and 2 show that characteristics of t_q and t_{q0}/t_q are about the same versus mixture temperature, T_{mix} .

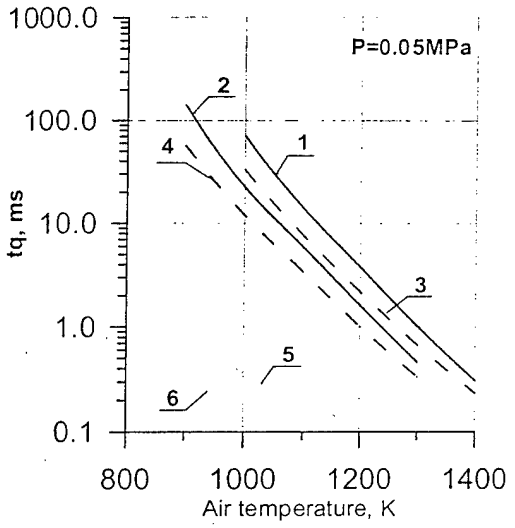

Fig.3 Effect of air temperature on time corresponding to maximal heat release rate at stoichiometric combustion of air/propane mixture, products of its decomposition and hydrogen.
1-2 Propane: 1 – T_f=900K, 2 – T_f=900K,
3-4 Products of C_3H_8 thermal decomposition at Z=75%: 3 – T_f=900K, 4 – T_f=1200K,
5-6 Hydrogen: 5 – T_f=900K 6 – T_f=1200K

Evaluations of the benefits of these ignition enhancements for high-speed air breathing engine performance were also done. In Fig.3, the effect of air and fuel temperatures T_a and T_f on the ignition time t_q under conditions P=0.05 MPa, T_f=900 and 1200K and Z=75% is presented. It could be concluded that the increase of T_a for all regimes results in decrease of t_q as T_{mix} is increased. It is also important to note a rather small decrease of t_q in the case of FTDP combustion. Here the data on hydrogen combustion are also presented for the same conditions as for the propane. Comparison of these t_q values show again small effect of FTDP application in comparison with the propane use.

So combustion organization under the self-ignition concept is possible only for a rather narrow region of referenced parameters (partly, at high T_a). Changing the propane to FTDP at low T_a does not permit effective combustion to be organized in the limits of the available fuel residence times.

However, increasing the hydrogen concentration in the FTDP, for example by fuel conversion in the presence of water [9,10], could provide combustion enhancement.

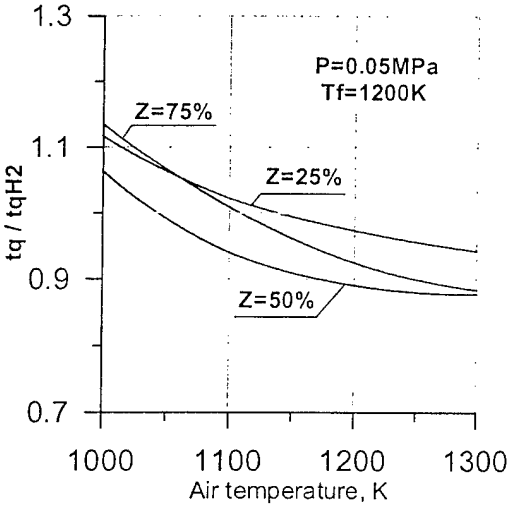

Fig. 4 Effect of air temperature on ratio of maximal heat release rate times at combustion of C_3H_8 thermal decomposition products (t_q) and of C_3H_8/H_2 mixture (t_qH_2)

Additional calculations were carried to determine the effects of the presence of hydrogen on the reactive ability of mixtures of gases, that is, for FTDP at P=0.05MPa and T_a=1000-1300K. The decomposition process was assumed to occur at P=1 MPa and T_f=1200K with Z=25%, 50% and 75%. The resulting values of t_q/t_{qH2} are shown in Fig. 4. The sense of these calculations is to find t_{qH2} values for FTDP, in which all of the hydrocarbon species are replaced by propane, but hydrogen is conserved. In each case (new mixture composition), the stoichiometric coefficient L, equal to its value in the initial mixture, was found by changing the nitrogen concentration. Based on the results shown in Fig. 4, it is possible to conclude that hydrogen presence does not explain the increase of the FTDP reactivity and so the values of t_q/t_{qH2} are <1. Nevertheless, for rough estimations, it is possible to use the hydrogen concentration in the FTDP to obtain the efficiency of thermal decomposition and to choose conditions under which the hydrogen concentration will be a maximum. Analysis

of data in Fig.4 shows a decrease in $t_q/t_{q|2}$ at T_a increases. This result can be explained by the behavior of $t_{q|2}$. At low T_a, the values of $t_{q|2}$ are less, but at high T_a, they are larger than the real values t_q. So, when we have an increase in T_a or T_{mix}, the concentration of radicals is increased during the pre-flame stage and their role becomes decisive during the combustion process.

It is useful to determine the increase in FTDP/air mixture specific efficiency with air temperature and Z increases. It is explained by the formation of low molecular components in mixture and by increasing equilibrium temperatures of FTDP/air combustion process. Data for these calculations are given in Table 1 for stoichiometric mixtures in a combustor with P=0.05 MPa and two values of T_a (T_f=1200K, P=1.0Mpa) with fixed thermal decomposition conditions of Z=25%, 50% and 75%.

Table 1. Relative value of FTDP specific efficiency $\Delta(RT)_d$ increase vs Z

Z, %	$((RT)_d - (RT)_0)/(RT)_0$, %	
	T_a=900 K	T_a=1200 K
25	0,642	0,581
50	1,418	1,280
75	2,238	2,024

Here, the propane specific efficiency $(RT)_0$ was taken as a base level. Note that the increase of FDTP is more for larger Z and for low Ta. In general, an increase of $(RT)_d$ does not surpass in 3% and mainly is explained by the hydrogen appearance during fuel decomposition.

Parametrical calculated data obtained of pressure, temperature T_a and equivalence ratio coefficient ϕ effects on operation process are summarized below as following:

1. An increase in air temperature effects much more on decreasing of combustion process time and enhances the organization of combustion based on self-ignition principles. The relative effect of FTDP use is more pronounced at low T_a.

2. An increase of pressure decreases the combustion process time and this fact is argued by numerical and experimental researches. It is explained by the second order of limited combustion reaction for the considered fuel. Process time dependence versus pressure is approximately the same when Z is varied. The effects of pressure on t_q for H_2 and C_3H_8 are different. For example, in case of hydrogen, $t_q \sim P^{-1}$, but for propane dependence $t_q(P)$ is also decreased when pressure increases and close to linear one. Another aspect of the pressure influence on fuel decomposition was discussed in the first section, which shows a favorable effect of pressure decrease on H_2 and H concentrations.

3. Decreasing the equivalence ratio ϕ from 1.0 down to 0.4 causes a decrease of t_q both for propane (30%) and FTDP (20%). This is confirmed qualitatively by the results[17] for the combustion of propane and n-butane.

Conclusions

The reactivity of C_3H_8 thermal decomposition products is more than for pure C_3H_8 and, for example, at T<1000K, the reference time t_q is less by 2-3 times in comparison with C_3H_8 fuel. Increases in specific efficiency $\Delta(RT)_d$ in the case of thermal decomposition products does not exceed 2-3%.

Acknowledgments

The authors are sincerely grateful to I. Gomzyakova for her help and assistance in preparation and processing the numerical data. This work was supported by the John Hopkins University Contract and Russian Fund of Fundamental Researches, Grant № 01-01-00910.

References

1. Vinogradov, V.A., Kobigsky, S.A., Petrov. M.D., "Experimental Investigation of Kerosene Fuel Combustion in Supersonic Flow," *Journal of Propulsion and Power*, Vol.11, No.1, 1995, pp.130-134.
2. Ortwerh, P., Vinogradov, V., Grin, V., Mathur, A., Goldfeld, M., Starov, A., "Experimental and Numerical Investigation of Hydrogen and Ethylene Combustion in a Mach 3-5 Channel with

a Single Injector," AIAA Paper 96-3245, 1996.
3. Kurziner, R.I., "Jet Engines for High Supersonic Speeds," *Mashinostroenie,* Moscow, 1989, pp.119-120 (in Russian).
4. Favorskiy, O.N., Kurziner, R.I., "The Development of Air-Breathing Engines for High Speed Aviation Is Synthesis of Different Brunches of Science and Techniques." *Journal of High Temperature Technique*, Vol. 29, No.4, 1990, pp.798-803 (in Russian).
5. Dimitrov, V.I., "Simple Kinetics," *Mashinostroenie,* Moscow, pp.117-120, 1989 (in Russian).
6. Waltrup, P., "Liquid Fueled Supersonic Combustion Ramjets: a Research Perspective of the Past, Present and Future," AIAA Paper 86-0158, 1986.
7. Yatsuyanagi, N., Chinzei, N., Mitani, N., Wakamatsu, Y., Masuya,G. et al, "Ramjet Engine Test Facility (RJTF) in NAL-KRC, Japan," AIAA Paper 98-1511, 1998.
8. Ogorodnikov, D.A., Vinogradov, V.A., Shikhman, Yu.M., Strokin, V.N., "Design and Research Russian Program of Experimental Hydrogen Fueled Dual Mode Scramjet: Choice of Conception and Results of Pre-Flight Tests," AIAA Paper 98-1586, 1998.
9. Hueter,U., "Rocket-Based Combined-Cycle Propulsion Technology for Access-to-Space Applications," AIAA Paper 99-4925, 1999.
10. Voloschenko, O.V., Mescheryakov, E.A., Ostras, V.N., Sermanov, V.N. "Analysis of Gas Generation Process and Conversion of Hydrocarbon Fuels in Dual Mode Scramjet," TsAGI Paper Collection, No. 2572, 1995. (in Russian).
11. Shikhman, Yu. M., Vinogradov, V.A., Yanovskiy, L.S. et al, "The Demonstrator of Technologies – Endothermic Hydrocarbon Fueled Dual Mode Scramjet," AIAA Paper 2001-1787, 2001.
12. Shigabiev, T.N., Yanovskiy, L.S., Galimov, F.M., Ivanov, V.F., "Endothermic Fuels and Working Mediums for Power- and Energetic Plants," *Kazan Sc. Center, Russian Acad. Sc. – Kazan State Tech. Univ.*, Kazan, 1996, 264p. (in Russian).
13. Ianovskiy, L.S., Ivanov, V.F., Sapgir, G.B., Sverdlov, E.D., Strokin, V.N., Vedeshkin, G.K., "Endothermic Fuels: Some Aspects of Fuel Decomposition and Combustion," AIAA Paper 99-7067, 1999.
14. Dubovkin, N.Pf., "Reference book on heat-physics properties of hydrocarbon fuels and its combustion products," *GosEnergoIzdat,* Moscow, 1962, 288p. (in Russian).
15. Dubovkin, N.Pf., Fedorov, E.P., "Physical-Chemical and Exploited Properties of Jet Fuels," *Nauka*, Moscow, 1985, 366p. (in Russian).
16. Schetinkov, E.S., "*Physics of gas combustion,*" *Nauka,* Moscow, 1965, pp.311-325
17. Starik, A.M., Titova, N.S. et al., "Kinetics Peculiarities of air/C_3H_8/n-C_4H_{10} Mixture Thermal Decomposition Products Oxidation," *Kinetics and Catalysis*, Vol.40, No.1, 1999, pp.11-26.
18. Jachimowski, C., "Chemical Kinetic Reaction Mechanisms for the Combustion of Propane", *Combustion and Flame*, Vol.55, No. 1, pp.213-224, 1984.
19. Warnatz, J., "Combustion Chemistry", *Jr. Springer Verlag,* New York, 1984.
20. Wilk, R.D., Cernansky, N.P., Pitz, W.J., Westbrook, C.K., "Propane Oxidation at Low and Intermediate Temperatures: A Detailed Chemical Kinetic Study," *Combustion and Flame*, Vol.77, 1989, pp.145-170.
21. Hoffman, J.S., Lee, W., Litzinger, T.A., Santavicca, D.A., Pitz, W.J., "Oxidation of Propane at Elevated Pressures: Experiments and modeling," Combustion Science and Technology, Vol.77, 1991, pp.95-125.
22. Volkov, D.V., Zaitsev, S.A., Goltsev, V.F., "Parametric Study of Nitrogen Oxides Formation at Combustion of

Premixed Methane-Air Mixture," *Fizika Gorenia i Vzriva*, Vol.35, No.2, 1999, pp.9-15 (in Russian).

23. Miller, J.A., Bowman, C.T., "Mechanism and Modeling of Nitrogen Chemistry in Combustion," *Progress in Energy and Combustion Science*, Vol.15, 1989, pp.287-338.
24. Kojima, S., "Detailed Modeling of n-Butan Autoignition Chemistry," *Combustion and Flame*," Vol.99, 1994, pp.87-136.
25. Burcot, A., Scheller, K., Lifshitz, "A. Shock-Tube Investigation of Comparative Ignition Delay Times for C_1-C_5 Alkanes," *Combustion and Flame*, Vol.16, No.1, 1971, pp.29-34.
26. Buriko, Ju., Vinogradov, V., Goltsev, V., Waltrup, P., "Influence of Active Radical Concentration on Self-Ignition of a Propane/Air Mixture", AIAA Paper 2001-3958, 2001.

APPLICATION OF ACTIVATED POROUS FUEL IN PROCESSES OF SUPERSONIC AND DETONATION COMBUSTION.

Bushmanov E.A., Velikodniy V.Yu., Timofeev I.B., Yanovskiy Yu.G., David M. Van Wie.*

Institute of Applied Mechanics RAS, Russia, Moscow, Leningradskiy pr-t. 7.
**The Johns Hopkins University, Applied Physics Laboratory, USA*

It is known that preliminary barbotage of liquid fuel with some oxidant (air, oxygen) or combustible gas (CH_4, H_2) dramatically improves characteristics of its sputter, mixturing decreases time of ignition delay and buildup of radicals may essentially decrease time of chain reactions induction with lower initial temperature of fuel-air mixture. All this effects improve the development of combustion processes and detonation. Our work considers methods and experimental test of devices producing activated porous fuel with mentioned above advantages. One of the ways includes barbotage using 40-100 microns pore diameter membranes, size separation of bubbles or without it if bubbles are small enough, cavitational processing of fuel-air mixture and then its sputtering into a supersonic flow or detonation chamber. It is known that cavitational processing essentially increases the speed of chemical reactions by buildup of radicals and ions, and interaction of micro-bubble media with shock-waves causes an intensive splitting up of micro-bubbles under high tangent tensions :

$$\tau = \frac{P_{//} - P_{\perp}}{2} \quad (1)$$

Its worth mentioning that with volume gas content of 15-20% in liquid fuel shock-wave modes appear in the cavitator at speeds of a flow V=20-30 m/s. This is caused by the value of the sound speed which is almost two powers less then the sonic speed in clear liquid and also one order less than it is in pure gas. To research the experimental achievement of shockwave modes in cavitator the following experiment was carried out: liquid (water in our case) was bubbled with gas (air) by glassceramic membrane with pour diameter 100 micron under pressure P=5 bar, specific content of gas was 10-30%, flow velocity reached the value of 40 m/s. Initial bubbles with diameter 200-500 micron were processed in the cavitator and then obtained mixture was injected into a glass cylinder. As a result we received a microbubble mixture with bubble diameter d<50 micron. Thus, microbubble media was created by a method allowing continuos operation. In earlier experiments such media was produced by dissolvation of gas in liquid under high pressure and then following appearance of microbubbles after abrupt pressure release. In that case only periodical process could be realized. Photo 1(a). shows volume with clear water, on photo number 1(b). you can see water with mucrobubble liquid "smoke" injected and on photo 1(c). same volume after some period of time when most bubbles have gone upper and an interface with clear water can be seen. Thus theory [7] and our experiment show that shock-wave processing of dispersion media can be obtained with up above mentioned parameters. Similar experiments were carried out for kerosene and glycerin. Appearance of "smoke" was observed in all cases. Besides collapse of microbubbles on the surface yield in vapor puffs. At present time experiments in research of content composition of this vapor are planned to be carried out. Theoretical research and analysis of literature show that beside splitting up of initial bubbles in cavitator the processes of vaporization and local heating are realized. Presence of some oxidant in bubbles may yield in partial combustion of fuel in the following scheme:

$$C_7H_{16} + X_1O_2 \rightarrow X_2CO_2 + X_3CO + X_4H_2 + X_5C + X_6H_2O + X_7C_\alpha H_\gamma \quad (2)$$

here X_j are stereometric coefficients. Products CO, H_2, $C_\alpha H_\gamma$ may intensify combustion when porous fuel is injected into a flow with oxidant and water vapor may work as a catalyst in chain reaction of fuel combustion. As a result of reactions taken place in cavitator bubbles start to pulsate then split up and vapor inside them is heated. Generated vapor, products of conversion, cracking and incomplete combustion, primary radicals and essentially improved sputter characteristics may provide steady-state combustion in supersonic flow and stable detonation. In order to research influence of barbotage and cavitation processes, previously bubbled liquid was let through the cavitator in our case working also as a sprayer. Experiments were carried out on the specially constructed setup which can be seen on the photo number 2. Photo 3. shows a jet of liquid spraying into an air media without using barbotage. On photo 4 we can see explosive widening of gas-dispersed jet. Interaction of liquid jet with supersonic flow of air presents photo number 5.

Resume:

1. With specific gas content in liquid equaled 10-20% intensive splitting up of bubbles in the cavitator is observed, conversion coefficient k=10-20.
2. Barbotage and cavitation essentially improve characteristics of gas-dispersed jet sputtering, mixture, decrease the diameter of drops and so on.
3. Devices and methods considered may be applied for better characteristics of engines with supersonic combustion and also detonation engines.

References

1. Avrashkov V., Baranovsky S., Levin V. Gasdynamic Features of Supersonic Kerosene Combustion.// AIAA-90-5268. P.8.
2. Vloshenko O.V., Korabelnikov A.V., Kuranov A.L., Features of methane and hydrogen barbotaged kerosene combustion in supersonic chamber.// Symposium. Thermochemical processes in plasma aerodynamics. St-Petersburg. 30.05.2000. P.35-36.
3. Velikodniy V.Yu. The structure of a shockwave in presence of physicochemical transformations.// Contemporary problems of aerohydromechanics. 1999. V.2.P.55-68.
4. Divakov O.G., Eremin A.V., Ziborov V.S., Fortov V.E. Nonequilibrium ignition of oxygen-hydrogen mixtures in shock front.// DAN. 2000. V.373.N4.P.487.
5. Yanovskiy L.S., Sapgir G.B., Sverdlov E.D. Baikov A.V. Comparison of combustion characteristics of thermochemical decomposition products of carbohydrated fuel in submerged tourch.// Symposium. Thermochemical processes in plasma aerodynamics. St-Petersburg. 30.05.2000. P.46-52.
6. Physical encyclopaedia.// Ed. Prohorov A.M. M.: Soviet encyclopaedia. 1983. P236.
7. Nigmatulin R.I. Basics of heterogeneous environment mechanics.// M.: Science. 1978. P.336.
8. Struminskiy V.V. Microbubbles gasliquids medium//Mechanica nonuniform medium and turbulent flows . M: Nayka. 1989. P 53-56.
9. Gyrentcov E. V., Divakov O.G., Eremin A.V. Experimental and numerical research of ignition of products of vapor methane conversion after shockwaves.// Symposium. Thermochemical processes in plasma aerodynamics. St-Petersburg. 30.05.2000. P.53-59.

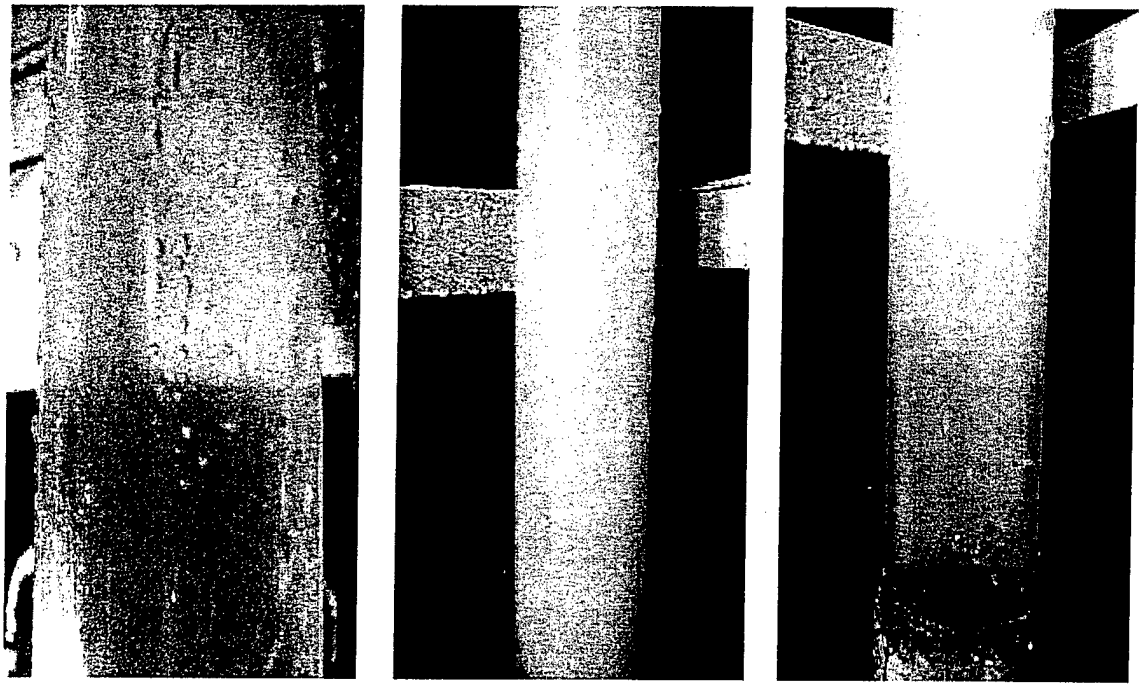

Photo 1. a) – clear water for comparison. b) – water with bubbled liquid injected. c) – an interface between bubbled water and clear one can be seen.

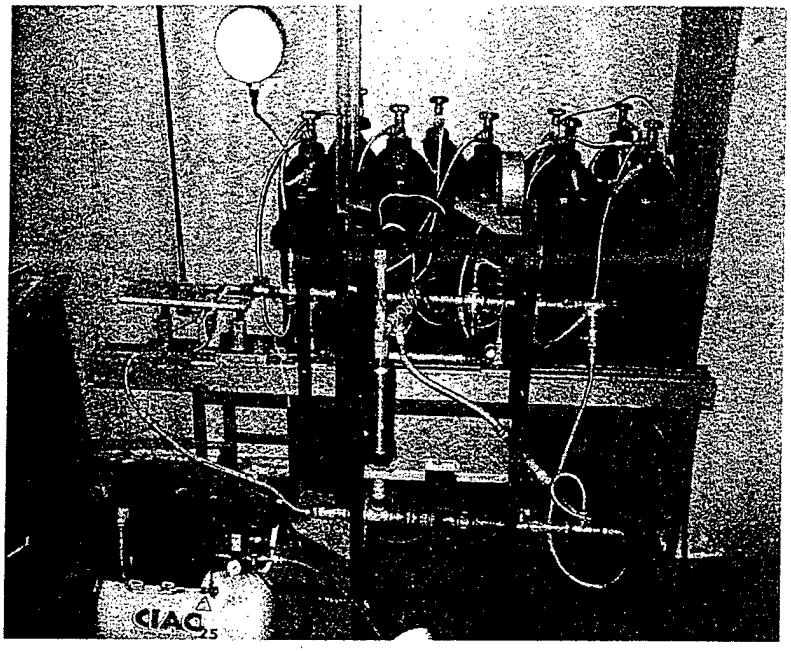

Photo 2. Experimental setup.

Photo 3. No barbotage is used.

Photo 4. A jet of barbotaged liquid.

Photo 5. Interaction with a supersonic flow of air.